



Durham E-Theses

Mars: a study of the burst spectrum in iron

Hansen, J. S.

How to cite:

Hansen, J. S. (1975) *Mars: a study of the burst spectrum in iron*, Durham theses, Durham University.
Available at Durham E-Theses Online: <http://etheses.dur.ac.uk/8211/>

Use policy

The full-text may be used and/or reproduced, and given to third parties in any format or medium, without prior permission or charge, for personal research or study, educational, or not-for-profit purposes provided that:

- a full bibliographic reference is made to the original source
- a link is made to the metadata record in Durham E-Theses
- the full-text is not changed in any way

The full-text must not be sold in any format or medium without the formal permission of the copyright holders.

Please consult the [full Durham E-Theses policy](#) for further details.

MARS: A STUDY OF THE BURST SPECTRUM IN IRON

BY

J. S. HANSEN, B.A.

The copyright of this thesis rests with the author.
No quotation from it should be published without
his prior written consent and information derived
from it should be acknowledged.



*Thesis Submitted to the University of Durham for the
Degree of Doctor of Philosophy*

September 1975

ABSTRACT

Using the Durham spectrograph, muon electromagnetic interactions have been studied both theoretically and experimentally.

The current best theoretical cross-sections for muon interaction processes in iron have been numerically calculated and tabulated. The muon burst probabilities and spectra have been determined for a 1000 gm cm^{-2} iron absorber.

Experimentally the study has been divided into two aspects of muon interactions. Firstly, a study using three different analysis techniques has been done to determine if positive or negative muons interact abnormally. No observable interaction charge asymmetry has been observed, the overall interaction charge ratio for bursts of > 2 particles being 1.020 ± 0.032 . Secondly, a study has been done to determine the differential muon burst spectra in a thick iron absorber over various muon energy ranges. A comparison has been made between the theoretical and experimental spectra. Over all energy ranges of this experiment (7 GeV to 1 TeV incident muon energy) no deviation has been observed between the two sets of spectra.

PREFACE

The work presented in this thesis represents work carried out during the period 1971 to 1974 while the author was a research student under the supervision of Dr. M. G. Thompson in the Cosmic Ray Group of the Department of Physics at the University of Durham.

When the author joined the group in 1971 the MARS spectrograph was physically complete and in the process of being put online to an IBM 1130 computer. The author helped in the general running and maintenance of the apparatus. The author also designed and built various electronic equipment for the spectrograph and the associated interaction experiment reported in this thesis.

The author was solely responsible for the interaction equipment, its running and the data collection, analysis and interpretation. All theoretical calculations used in comparison and interpretation are also the author's work. The spectrograph momentum analysis was provided by the group programmer, Dr. B. Daniels.

Some preliminary results from this work have been reported at the XVI International Cosmic Ray Conference in Munich, Germany (Hansen and Thompson 1975). The reports of further results are either in the press or are being prepared for publication.

ACKNOWLEDGEMENTS

Professor Haven E. Bergeson of the University of Utah is thanked for providing encouragement when the decision of whether or not to study for a Ph.D. had to be made. Thanks are extended to Dr. John L. Osborne who, while lecturing at the University of Utah, provided the idea of Durham, and to Professor Jack W. Keuffel and Professor Arnold W. Wolfendale, who encouraged and finalized the choice of the University of Durham for graduate study.

The author wishes to thank the University of Durham, Professor George D. Rochester and Professor Arnold W. Wolfendale for the provision of the working facilities. The author is grateful for the special attention of Professor Wolfendale.

The author's supervisor, Dr. Michael G. Thompson, is thanked for his interest at every stage of the work, his many hours of discussion, his many helpful ideas and suggestions, and his tolerance.

All members of the MARS group are thanked for their help in the building and running of the experiment. Special thanks go to Dr. Michael R. Whalley for the many discussions and helpful ideas, to Mr. John L. Piggott and Mr. John M. Baxendale whose help in the running of the experiment was invaluable, and to Dr. Brian Daniels for his continual assistance in data handling and analysis.

Dr. David A. Cooper is thanked for the useful discussions.

The Durham University Computer Unit and NUMAC Computing Centre are thanked for the provision of computing facilities and the many, many hours of computer time.

Mr. Ken Tindale, the MARS project technician, is thanked for his assistance in building, testing and operating the apparatus used in the interaction experiment.

Ms. Audry Gregory is thanked for the excellent preparation of the many diagrams in this thesis.

A special thanks is extended to the typist, Ms. Maya Jackson, for the beautiful typing of this thesis.

Finally, the United States Government, Box Elder County Bank, and the author's parents, Mr. and Ms. John W. Hansen, are thanked for providing a means for the author to undertake this study.

CONTENTS

	Page
CHAPTER 1. INTRODUCTION	
1.1 Introduction	1
1.2 Discussion of the Components of Cosmic Radiation	3
1.3 The Results of Previous Muon Interaction Experiments	6
1.3.1 Introduction	6
1.3.2 Previous Interaction Asymmetry Results	7
1.3.3 Previous Muon Interaction Cross- Section Results	8
1.4 Objectives	9
CHAPTER 2. INTERACTION PROCESSES - THEORETICAL CONSIDERATIONS	
2.1 Introduction	11
2.2 The Knock-On Process	12
2.2.1 Introduction	12
2.2.2 The Cross-Section for the Knock-On Process	13
2.2.3 The Results and Calculation of the Knock- On Cross-Section	14
2.3 The Bremsstrahlung Process	16
2.3.1 Introduction	16
2.3.2 The Cross-Section for the Bremsstrahlung Process	16
2.3.3 The Results and Calculations of the Bremsstrahlung Cross-Section	20
2.3.4 Errors in the Theoretical Treatment	20
2.4 The Direct Pair Production Process	21
2.4.1 Introduction	21
2.4.2 The Cross-Section for the Direct Pair Production Process	24
2.4.3 The Results and Calculations of the Direct Pair Production Cross-Section	28
2.4.4 Errors in the Theoretical Cross-Section	29
2.4.5 Considerations in the Calculations of the Cross-Section	30
2.5 The Photonuclear Interaction Process	31
2.5.1 Introduction	31
2.5.2 The Cross-Section for the Photonuclear Process	32
2.5.3 Results and Calculations of the Photo- Nuclear Cross-Section	36
2.5.4 Considerations in the Calculation	37
2.6 Results and Observations	38
2.6.1 Introduction	38
2.6.2 Comparison of the Interaction Cross- Sections	38

2.6.3	Comments on the Calculated Interaction Cross-Section	39
2.6.4	Conclusions	40

CHAPTER 3. THE MAGNETIC AUTOMATED RESEARCH SPECTROGRAPH (MARS)

3.1	Introduction	42
3.2	The Particle Detectors and Associated Systems	43
3.2.1	Introduction	43
3.2.2	The Momentum Selection System	44
3.2.2.1	The Momentum Selector Trays	45
3.2.2.2	The Momentum Selector	46
3.2.3	The Track Measuring System	48
3.2.3.1	The Measuring Trays	48
3.2.3.2	The Data Gathering System	49
3.2.4	The Scintillation Counters and Associated Electronics	50
3.2.4.1	The Scintillation Counters	51
3.2.4.2	The Scintillator Uniformity	52
3.2.4.3	The Amplification Systems	54
3.2.4.4	The Analogue to Digital Converter	55
3.2.4.5	The Multiparameter Pulse Analysis System	56
3.3	General Aspects of the Spectrograph	58
3.3.1	The Magnets	58
3.3.2	The Spectrograph Acceptance	59
3.3.3	The Data Handling	59
3.4	The Experimental Description	61
3.4.1	The Role of the Author	63

CHAPTER 4. THE GENERAL ANALYSIS OF THE DATA

4.1	Introduction	64
4.2	The Data	65
4.3	The General Analysis	67
4.3.1	Introduction	67
4.3.2	The Determination of the Muon Momentum	67
4.3.3	Estimation of the Burst Size in the Flash Tube Trays	69
4.3.4	Magnetic Field Effects on the Photo- Multipliers	72
4.3.5	Calibration of the Flash Tube Determined Burst Size	74

CHAPTER 5. THE INTERACTION CHARGE ASYMMETRY

5.1	Introduction	78
5.2	Method 1: The Interaction Charge Ratio	78
5.3	Method 2: The Ratio of the Mean Pulse Heights for Positive and Negative Events	79
5.4	Method 3: Comparison of the Pulse Height Distributions for Positive and Negative Events	80

5.5 Conclusions	84
5.5.1 Comparison with Previous Results	84

CHAPTER 6. THE THEORETICAL BURST SPECTRUM

6.1 Introduction	87
6.2 Considerations in the Calculation of the Burst Spectrum	88
6.2.1 Shower Development	88
6.2.2 Energy Loss in Iron	89
6.2.3 The Particle Probabilities	92
6.2.4 The Vertical Muon Spectrum	94
6.3 The Burst Spectrum	97
6.3.1 Fluctuations	100
6.4 Discussion of Errors	106

CHAPTER 7. THE EXPERIMENTAL BURST SPECTRUM

7.1 Introduction	112
7.2 The Uncorrected Burst Spectra	112
7.3 Corrections	114
7.3.1 Particle Number and Cell Width Corrections	114
7.3.2 The Knock-On in the Flash Tube Trays Correction	115
7.3.3 The Interaction Run Discriminator Correction	116
7.4 The Corrected Experimental Burst Spectra	118
7.5 The Comparisons of the Resultant Burst Spectra	127
7.6 Conclusions from the Burst Spectrum Study	129

CHAPTER 8. CONCLUSIONS	130
------------------------	-----

APPENDIX A. TABLES OF THE INTERACTION PROBABILITIES OF MUONS IN IRON	132
--	-----

Discussion of Units	133
---------------------	-----

APPENDIX B. THE FOUR-MOMENTUM TRANSFER SQUARED (q^2 OR t)	160
---	-----

REFERENCES	162
------------	-----

CHAPTER 1

INTRODUCTION

1.1 INTRODUCTION.

The objective of science, and particularly of Physics, is to seek explanations and understanding of the actions, motions and structures in the Universe and to learn how these fit into the fabric of logically consistent theories. From very early times, Man, being aware that he is separate from his environment, has sought knowledge in an effort to control or to successfully predict the events occurring around him. Early in history Man showed interest in the origins of the world, the nature of the Heavens, and the elemental make-up of physical objects. Of course, most of the early explanations and theories lay in the superstitious and the supernatural.

Before Man could obtain the intellectual and technological tools needed to study the extreme limits of space-time and to produce more than superficial explanations, it was necessary for men like Newton, Maxwell and others to develop a workable set of theories to explain the basic interactions in the classical universe. With an understanding of electricity, magnetism, and the motion of bodies, men began to search for the basic units of matter and for the forces that bind the Universe. Little did they know that to obtain an understanding of the atomic nucleus and all the associated sub-atomic particles, men would eventually look to the stars to seek the sources of extremely energetic (10^{18} - 10^{20} eV) particles and, in



turn, would use these particles as messengers bringing information from the distant parts of the Universe.

In August 1912, Victor Hess, a German physicist, conducted an experiment during a balloon flight to determine if the radiation present at ground level decreased with increasing altitude. Initially as he ascended the radiation did decrease; however, above altitudes of 700 m the radiation began to increase. At the flight's apogee (5000 m) the radiation present was four times the intensity at ground level. In the report of the experiment (Hess 1912), Hess concluded, '*The results of my observations are best explained by the assumption that a radiation of very great penetrating power enters our atmosphere from above.*' This penetrating radiation has become known as 'cosmic radiation'.

Originally cosmic rays were assumed to consist of γ -radiation because of their penetrating ability. Clay (1927) found a variation in intensity with geomagnetic latitude (the latitude effect) and Bothe and Kolhorster (1929) interpreted this effect in terms of the Earth's magnetic field to prove the existence of charged particles above the atmosphere. They also did experiments with various configurations of Geiger-Muller tubes to show the existence of charged particles at ground level. Johnson and Street (1933) discovered that the intensities from the eastward and westward directions were not equal (the East-West effect) showing not only that cosmic rays are charged but that there is a majority of positively charged particles.

With the discovery of the positron (Anderson 1932) it became possible to explain cosmic rays in terms of positive and negative electrons. The theories of energy loss by electrons were seriously questioned when it was found that cosmic radiation could be divided

into soft and hard components by using a 15 cm lead absorber (Rossi 1934, Auger and Ehrenfest 1934, Street et al. 1935). Bhabha (1938), in an effort to keep the energy loss theories, hypothesized the existence of 'heavy electrons' which would be both positively and negatively charged and have a mass intermediate between that of an electron and a proton.

Street and Stevenson (1937) and Anderson and Neddermeyer (1938) established the existence of a particle with a mass of about 200 electron masses. Originally named 'mu-meson', they are now called 'muons'. Unfortunately, due to its time of discovery, the muon was confused with the predicted quantum of the nuclear force (Yukawa 1935). It soon became apparent that the muon did not interact strongly with other nuclear active particles as was expected. In 1947, Lattes, Muirhead, Occhialini and Powell discovered the pi-meson (pion) which was found to decay into a muon and interacted strongly. The pion since has become identified as the Yukawa particle.

1.2 DISCUSSION OF THE COMPONENTS OF COSMIC RADIATION

Cosmic ray research can be divided into the study of primary cosmic rays, those incident at the top of the atmosphere, and the study of secondary cosmic rays, those seen in the atmosphere, at ground level, and underground. Primary cosmic rays have been studied by the use of balloons, satellites and even manned space flights. It has been found that these primaries consist mainly of protons (88%) and helium nuclei (11%), with a few heavier elements (1%). There are also some electrons, photons, and very likely large fluxes of neutrinos. A look at the abundances of elements in the Universe shows that there is an excess of light nuclei incident

on the atmosphere. This is believed to be due to fragmentation of heavier elements as they pass through the small quantities of matter in space ($\sim 4 \text{ g cm}^{-2}$).

Greisen (1965) produced an integral intensity spectrum for primary cosmic rays. Up to an energy of about $3 \times 10^{15} \text{ eV}$ his spectrum has a slope of -1.6. At $3 \times 10^{15} \text{ eV}$ the slope changes dramatically to -2.2. This change in slope is believed to be due to the inability of the galactic magnetic fields to contain the particles as their rigidity is exceeded. At about $3 \times 10^{18} \text{ eV}$ the slope again flattens to -1.6 due to an expected extra-galactic source. Greisen (1966) predicted a sharp cut-off in the spectrum at about 10^{20} eV due to the discovery of 2.7°K black body radiation in space (Roll and Wilkenson 1967) and the resultant expected photo-meson interactions.

Primary cosmic rays suffer a series of nuclear collisions with air nuclei as they pass through the atmosphere, resulting in a cascade of secondary particles known as extensive air showers (EAS). The mean depth of the first interaction of protons is about 18 km above the earth, the proton interaction length being 80 g cm^{-2} . In each collision the proton loses about 50% of its energy to the productions of charged and uncharged pions, with a small proportion of kaons and hyperons also being produced. The three charged states of pions are produced in almost equal quantities, but because of the different modes of decay of the charged and uncharged pions respectively different aspects of the EAS develop. Uncharged pions can decay electromagnetically and therefore do so quickly ($\sim 10^{-16} \text{ s}$) into two photons. These photons soon produce a pair of electrons (pair production) which produce more photons (bremsstrahlung) and a photon-electron cascade develops. The growth of the cascade is almost

exponential (Heitler 1948) until the average electron energy is less than the critical energy of the material (84 MeV in air). The ^{THE RATE OF} critical energy has been defined as the energy at which energy loss by ionization is equal to that ~~of~~ ^{by} bremsstrahlung. Beyond this point the shower slowly decreases in size because of the absorption of electrons.

Charged pions either undergo weak decay (2.6×10^{-8} s) into muons and neutrinos or they undergo further nuclear interactions producing more charged and uncharged pions. The muons which are produced and which constitute the most common single particle observed at sea level, will either decay (2.2×10^{-6} s) if they are of very low energy into an electron and neutrinos, or if they have an energy above a few GeV, will survive to be observed at the surface of the earth.

Extensive air showers from primaries of energies greater than 5×10^{13} eV will not be completely absorbed by the atmosphere and can be observed at sea level. Very energetic EAS may spread over several square kilometres. The study of EAS produces information about nuclear interactions occurring at energies many orders of magnitudes higher than man-made accelerators can attain.

If the observer is sufficiently far away from the shower core or if the electron-photon component has died away, it is possible to study individual particles, usually muons because of their abundance. Three aspects of muon physics are generally studied. Two of these are the muon momentum spectrum and the muon charge ratio. The study of these, like that of EAS, provides information about the parent particles and in turn about the nuclear interaction which produced these particles. The third aspect is to study how the muon interacts with matter. The study of muon interactions is essential to the understanding of what the muon is, where it fits into the classes of

particles and whether it obeys quantum electrodynamics (QED) as it is presently understood.

The study of muon interactions is not a new subject but a controversial one. Several previous experiments have been performed to compare the theoretically expected cross-sections of the interaction processes with the measured ones. Some of these experiments have yielded significant deviations from theory. Other experimenters have looked at the cross-sections of positive and negative muons separately with the result that some of these experiments have appeared to show that positive muons interact more readily than negative muons. If this is true, theories of muon physics and/or QED are in serious trouble. The experiment reported here has been done in an effort to determine whether or not the apparent anomalies exist. The next section will present a summary of previous interaction experiments. The last section of this chapter will discuss the objective of this experiment and experimental report.

1.3 THE RESULTS OF PREVIOUS MUON INTERACTION EXPERIMENTS

1.3.1 INTRODUCTION

This section will present briefly the result of previous interaction experiments, both from cosmic ray muons and accelerator muons. It is essential before embarking on an interaction experiment such as the one presented here to know the results of past experiments to justify the experiment being done and to know what the purpose of the experiment should be.

The experiments from which the results presented in this section are obtained will not be described in any detail, if at all. Discussion

and comparison of the previous results and the present results is presented in Chapter 5 (The Interaction Charge Asymmetry) and Chapter 7 (The Experimental Burst Spectrum). The previous results presented here are from comprehensive surveys compiled by Allkofer et al. (1971) and Grupen (1974).

1.3.2 PREVIOUS INTERACTION ASYMMETRY RESULTS

Neddermeyer et al. (1961), while using cloud chambers to study muon knock-on electron production, found an excess of events ~ 1 GeV energy transfer from muons of energy 5-50 GeV. They also examined the data with respect to the charge of the interacting muon and found an apparent interaction asymmetry which showed that positive muons interact more readily than negative muons. As would be expected, this result triggered a series of experiments to either support or disprove the Neddermeyer experiment. Unfortunately, these experiments have produced a variety of results (see Figure 1.1). About half of the experiments show an asymmetry and about half do not. Those showing support for an asymmetry are Neddermeyer et al. (1961, 1965, 1967) which obtained an asymmetry of 1.60 ± 0.30 , Allkofer et al. (1971) which obtained a result of 1.23 ± 0.11 , Ayre et al. (1971) which obtained a result of 1.32 ± 0.11 , and Sheldon et al. (1973) which obtained a result of 1.45 ± 0.19 . Two observations can be made from the figure. First, the accelerator results of Jain et al. (1970) and Kirk et al. (1968), quite surprisingly, have not produced very precise results. Neither experiment is inconsistent with there being quite a large asymmetry. Second, while it might be expected that some of the experiments deviate from the expected value, it is not expected that they should all have fluctuated to positive values.

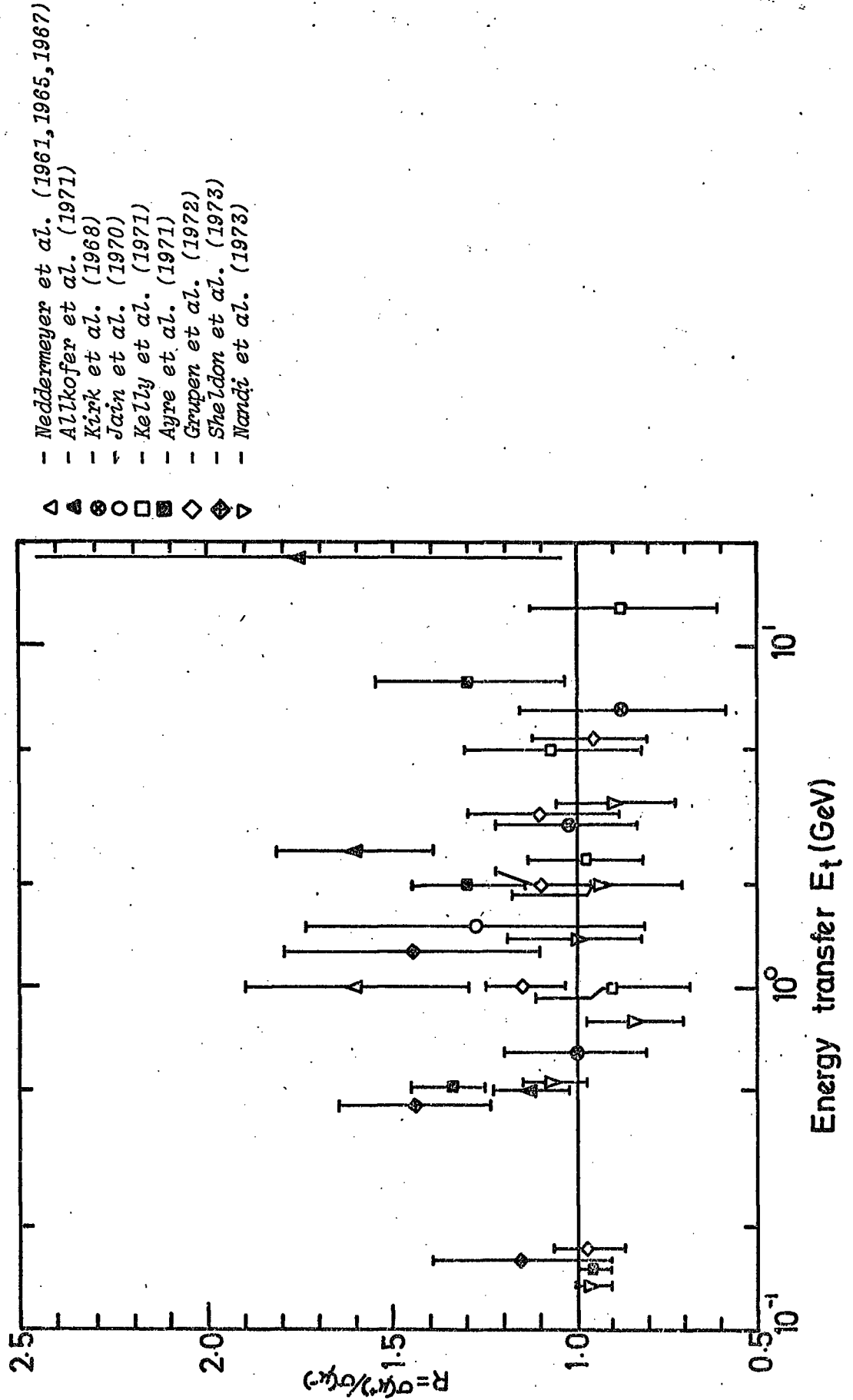


FIGURE 1.1. Previous results of interaction charge asymmetry experiments (after Grupen 1974).

It can be seen, based on these results, that it is still necessary for experimenters to look at this important problem. If no asymmetry is found in future experiments, it will also be necessary to attempt to provide plausible explanations as to why some experiments have obtained such marked asymmetries.

1.3.3 PREVIOUS MUON INTERACTION CROSS-SECTION RESULTS

These results are divided into the three electromagnetic processes and are presented graphically as a ratio of experimental cross-section to the theoretical cross-section as a function of energy transfer. In the comparison, Bhabha theory⁽¹⁹³⁸⁾ for the knock-on process, Christy and Kusaka theory⁽¹⁹⁴¹⁾ for the Bremsstrahlung process, ~~MURATA ET AL (MUT)~~⁽¹⁹⁵⁶⁾ and ~~MUT~~ theory for the direct pair production process, have been used. Knock-on, bremsstrahlung and direct pair production comparisons are presented in Figures 1.2, 1.3 and 1.4 respectively.

Figure 1.2 shows significant deviations from theory by the results of Neddermeyer et al. (1961), ~~Kearney~~^{KEARNEY} et al. (1965, 1972), and Allkofer et al. (1971) for the knock-on process. Their results also support an increasing deviation as a function of increasing energy transfer.

The bremsstrahlung results seem to agree to very large energy transfers for the majority of experiments, but deviate for a few experiments: Alexander et al. (1970), Matano et al. (1968) and Nagano et al. (1970).

The comparison of the direct pair production results shows a tendency for some of the experimental results to be low. In the next chapter, during the discussion of the direct pair production cross-section, it is pointed out that the theory of MUT probably

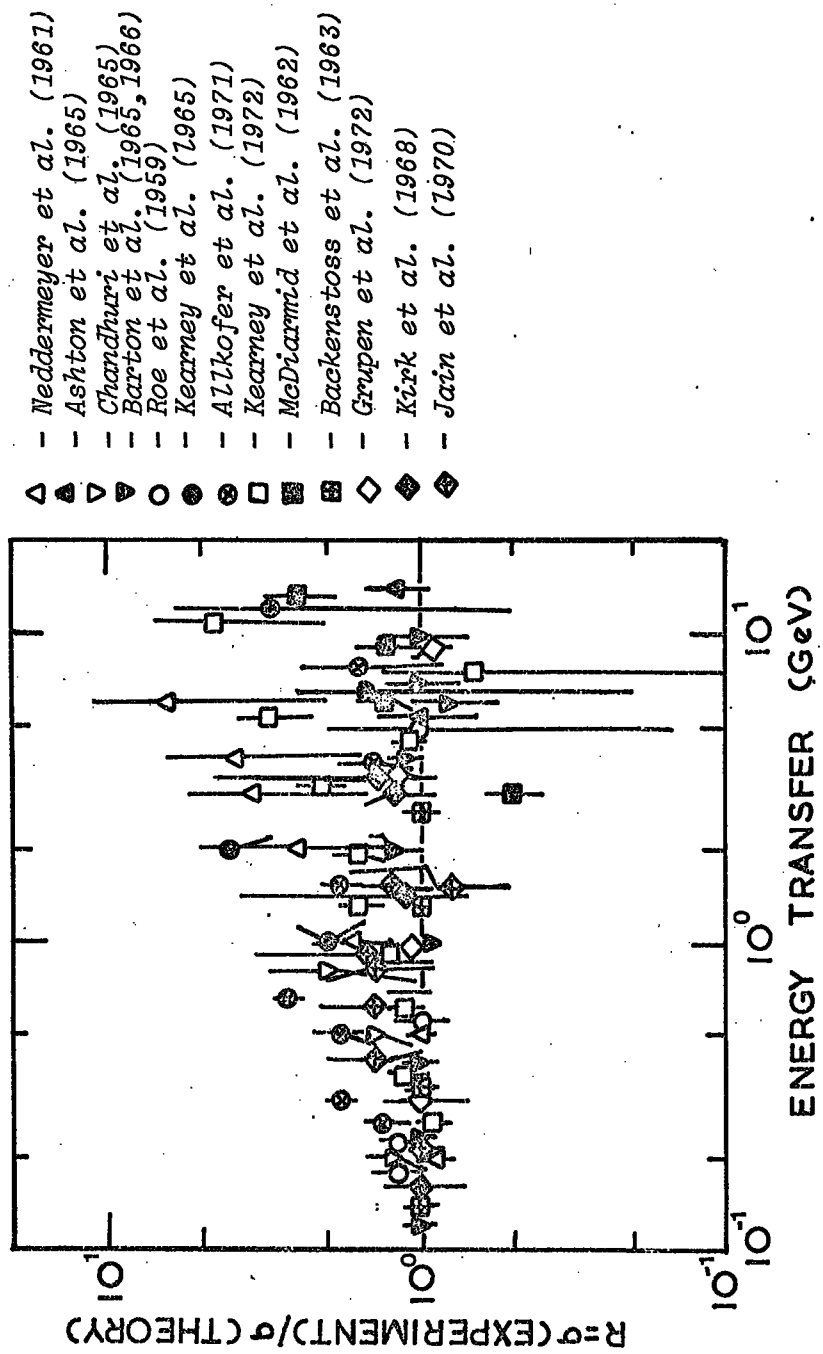


FIGURE 1.2. A comparison of the experimental and theoretical cross-section for the knock-on process as obtained by previous experiments (after Grupen 1974).

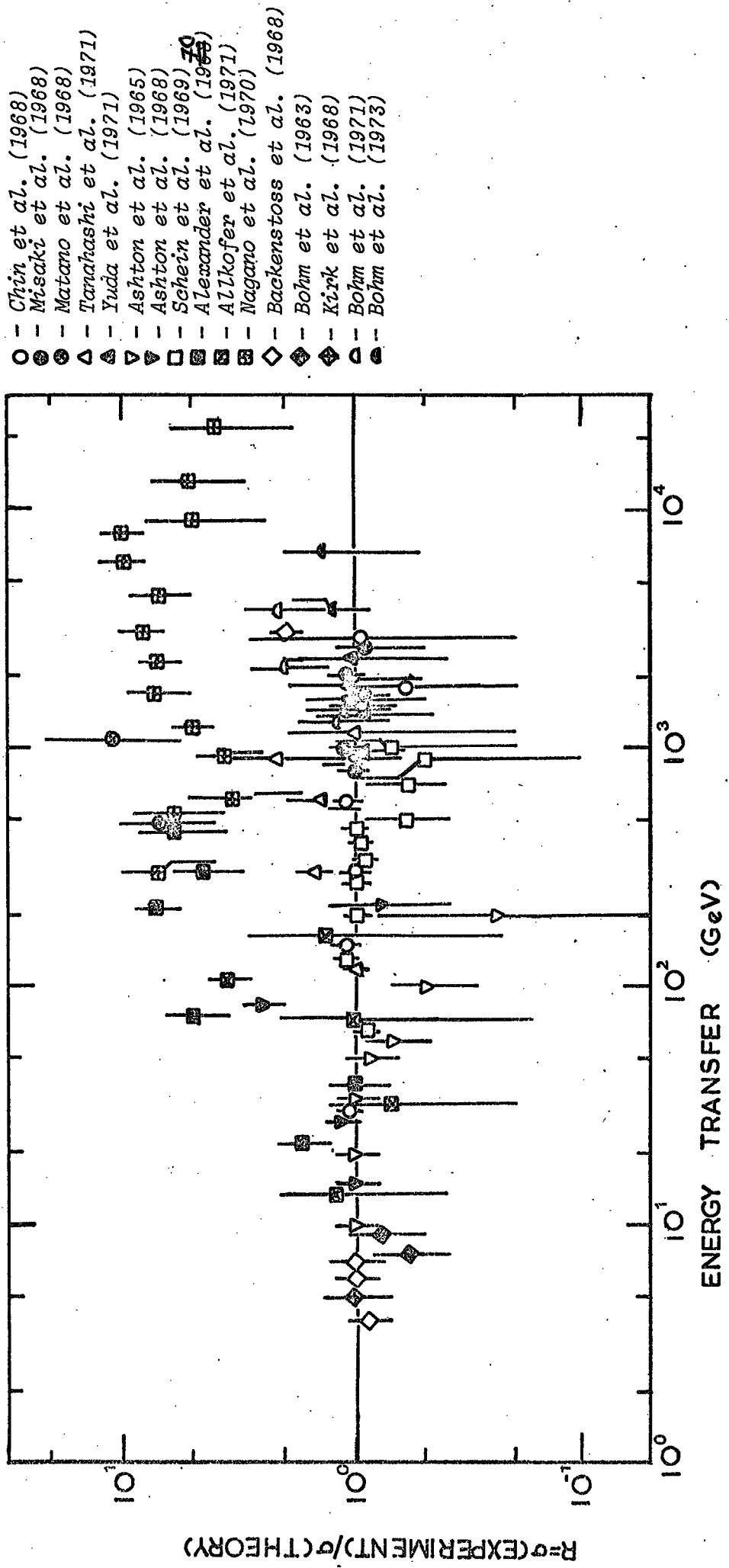


FIGURE 1.3. A comparison of the experimental and theoretical cross-sections for the bremsstrahlung process as obtained by previous workers (after Grupen 1974).

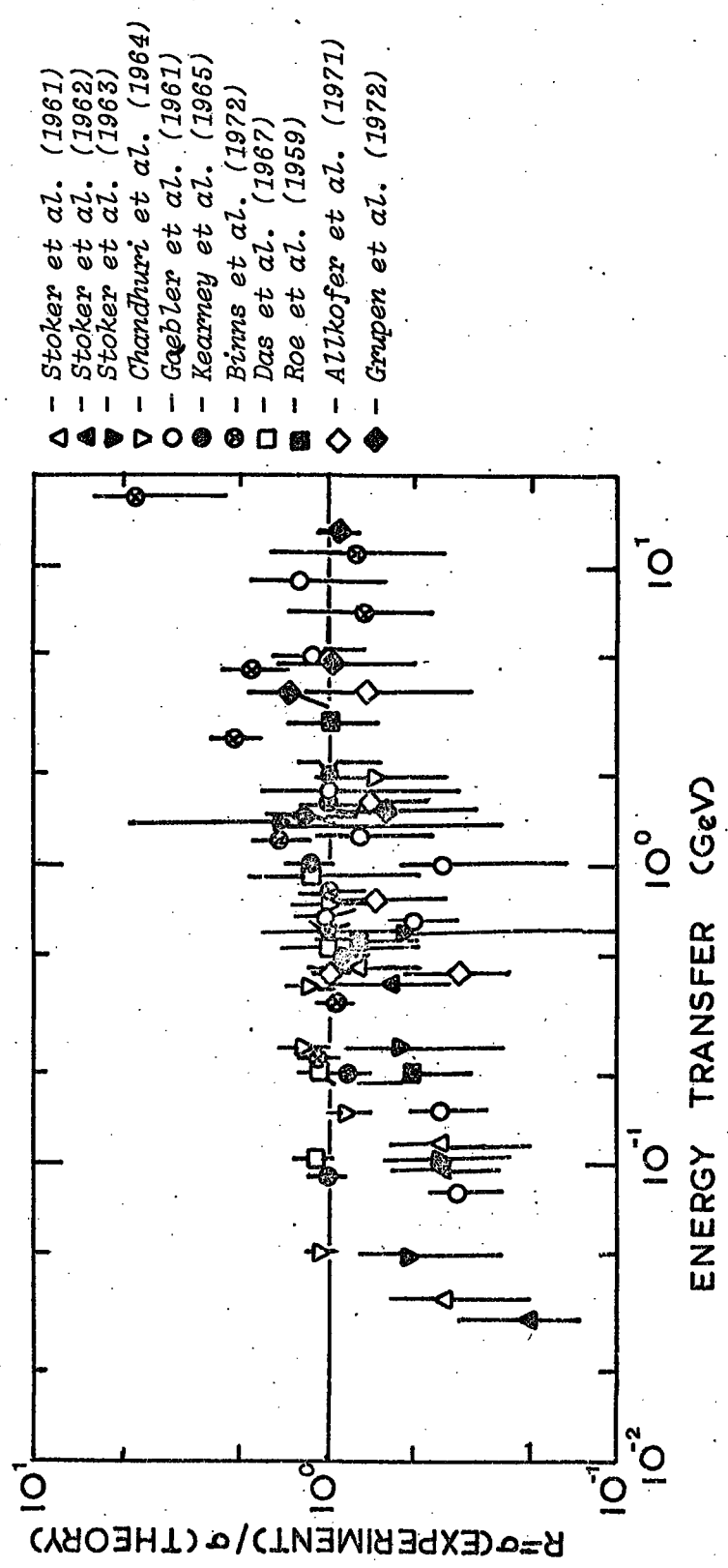


FIGURE 1.4. A comparison of the experimental and theoretical cross-section for the direct pair production process as obtained by previous experiments (after Grupen 1974).

over-estimates the cross-section by at least 20%. This could partly account for the apparently low results. A recent experiment (not shown in the figure) by Wright (1975) produced results in complete agreement with the direct pair production theory of ~~Petrukhin~~ and Kokoulin (1970, 1971).

All of these results have been presented as a function of energy transferred to the interaction, but not as a function of muon energy. While it is true theoretically (see Chapter 2) that knock-on and bremsstrahlung processes are virtually independent of muon energy, the direct pair production process is very energy dependent. The great majority of the past experiments have used relatively low energy muons, $\sim < 50$ GeV, with the exception of some underground work and some work using large spectrographs. All the accelerator experiments have used muon energies of less than 20 GeV. There is obviously a need to look at the high energy muon burst spectrum to determine if anomalies exist as a function of energy and large energy transfers, as well as a need to continue to look at lower energy muons to determine if the apparent discrepancies really exist.

High energy muons are so far only available in cosmic radiation, but due to the falling spectrum it is necessary to have an apparatus with a large acceptance. The MARS spectrograph has a large acceptance ($408 \pm 2 \text{ cm}^2 \text{ sr}$) and a good resolution (MDM ~ 5 TeV), and is in these respects ideal as a source of high energy muons.

1.4 OBJECTIVES

Using the MARS spectrograph it has been the author's intention to study the electromagnetic interactions of cosmic ray muons in iron. Muons are assumed to be the observed particles because they are the only

ARE

known charged particle which ~~is~~ able to penetrate $\sim 4000 \text{ gm cm}^{-2}$ of iron. The first objective of this experiment has been to look at the ratio of the interaction cross-section of positive muons to the interaction cross-section of negative muons, and to determine the magnitude of any variation from unity. The second objective has been to study the muon burst spectrum in iron both experimentally and theoretically and to compare the results to determine if the muon interaction probabilities vary from that predicted by quantum electrodynamics.

One note on terminology; throughout this thesis the terms energy and momentum have been used interchangeably. The error in doing so is 0.01% at 7 GeV and $6 \times 10^{-5}\%$ at 100 GeV.

CHAPTER 2

INTERACTION PROCESSES - THEORETICAL CONSIDERATIONS

2.1 INTRODUCTION

During the past forty years theoreticians have derived the muon interaction cross-sections assuming the muon to be electron-like but more massive. Each successive treatment has resulted in a more precise cross-section prediction. (At present all electromagnetic cross-sections are accurate to less than 3%.)

In this chapter the four known types of interactions by which muons can lose energy are discussed. The theories and predictions of various authors are considered and calculations have been made for the theories which appear to be the best. The four types of interactions are:

1. Excitation and Ionization (Knock-On)

Energy is transferred from the muon to an atomic electron via the coulomb fields involved.

2. Bremsstrahlung (Braking Radiation)

The emission of a photon (γ) as the muon is scattered by the nuclear coulomb field.

3. Direct Electron Pair Production

The materialization of a positron-electron pair from a virtual γ emission as the muon is scattered by the nuclear coulomb field.

4. Photonuclear

One of the virtual photons accompanying the muon interacts strongly with a nucleon in the atom.

2.2 THE KNOCK-ON PROCESS

2.2.1 INTRODUCTION

As a charged particle passes through matter its coulomb field, which may be extended relativistically, can interact with the field of an atomic electron. When this happens either the electron involved will be raised to a higher energy state (excitation) or, if it is given sufficient energy, it may be knocked out of its orbital (ionization). The approximate energy required for ionization is (see Rossi, 1952):

$$V_p = 13.6 Z \text{ eV} \quad (2.1)$$

V_p being the ionization potential and Z the atomic number of the material. For energy transfers $< V_p$ excitation occurs and for energy transfers $> V_p$ ionization occurs. If the energy transferred is $\gg V_p$, the electron can be considered as free and not bound to the nucleus. These electrons are called Knock-On (KO) electrons.

For iron, the material used in this experiment, $V_p = 281.2 \pm 0.8 \text{ eV}$ (Anderson et al., 1969). The present experiment is not concerned with energy transfers $< 1 \text{ MeV}$, therefore there is no need to consider excitation and all of the electrons can be described as free. Only the cross-section for the production of knock-on electrons will be discussed.

2.2.2 THE CROSS-SECTION FOR THE KNOCK-ON PROCESS

Bhabha (1938) has calculated the knock-on cross-section for particles of spin $\frac{1}{2}$ and mass M (i.e. the muon). In the present work, it is assumed that his expression (Equation 2.2) is valid up to muon energies of 10 TeV. Bhabha's derivation is

$$\sigma_{KO} (E \times E_t) dE_t = \frac{2\pi N_0 Z r_e^2 m_e c^2}{\beta^2 A} \frac{dE_t}{E_t^2} [1 - \beta^2 \frac{E_t}{E_{MAX}} + \frac{1}{2} (\frac{E_t}{E_t + Mc^2})^2] \quad (2.2)$$

where:

E_μ is the muon energy,

E_t is the energy transferred in the collision,

$m_e c^2$ is the electron rest mass,

Mc^2 is the muon rest mass,

β is $(E^2 - M^2 c^4)^{\frac{1}{2}}/E$,

N_0 is Avogadro's number - 6.02252×10^{23} mole $^{-1}$,

Z is the atomic charge (for iron Z = 26),

A is the atomic mass (for iron A = 55.85),

r_e is the classical electron radius - 2.8×10^{-13} cm.

Note that πr_e^2 is the projected area of an electron. Frequently the constant C is introduced in the expression for the cross-section where

$$C = \frac{\pi r_e^2 N_0 Z}{A} \quad (\text{units are electron cm}^2 \text{ gm}^{-1}) \quad (2.3)$$

which for any material reduces to

$$C = 0.148 Z/A \quad (2.4)$$

E_{MAX} is the maximum transferable energy and follows directly from the application of the law of conservation of energy and momentum to the

interaction. For the kinematics of the collision the energy transferred (E_t) to the electron as a function of the scattered angle (θ) is

$$E_t = \frac{2m_e^2 p_\mu^2 c^2 \cos^2 \theta}{((p_\mu^2 c^2 + M^2 c^4)^{\frac{1}{2}} + m_e^2)^2 - p_\mu^2 c^2 \cos^2 \theta} \quad (2.5)$$

p_μ is the momentum of the incoming muon. The maximum energy will occur when the electron is scattered forward (i.e. $\theta = 0$). This gives

$$E_{MAX} = \frac{2m_e^2 p_\mu^2 c^2}{M^2 c^4 + m_e^2 + 1m_e^2 (p_\mu^2 + M^2 c^4)^{\frac{1}{2}}} \quad (2.6)$$

or

$$E_{MAX} = \frac{2E_\mu^2 m_e^2 + M^2 c^4 m_e^2}{2E_\mu m_e^2 + M^2 c^4 + m_e^2} \quad (2.7)$$

Table 2.1 gives E_{MAX} and $(E_\mu - E_{MAX})$ as a function of E_μ . E_μ , E_{MAX} and $(E_\mu - E_{MAX})$ are plotted in Figure 2.1 as a function of E_μ . Note that for high energies (i.e. $E_\mu > 100$ GeV) $E_{MAX} \approx E_\mu - 11$ (GeV).

2.2.3 THE RESULTS AND CALCULATION OF THE KNOCK-ON CROSS-SECTION

In Equation 2.2, the final terms in the square bracket are a correction term for the maximum transferable energy ($\beta^2 E_t / E_{MAX}$) and a correction term for the muon magnetic moment ($\frac{1}{2} [E_t / (E + M^2 c^2)]^2$). The first correction term only becomes important as E_t approaches E_{MAX} . The second term is only important as E_t approaches E_μ and for $E_\mu \gg M^2 c^2$. In general, by the time the second correction begins to take effect the first term has reduced the cross-section significantly. It is also worth noting that because of the magnetic moment correction $E_t > E_{MAX}$ is a possibility.

TABLE 2.1

MAXIMUM TRANSFERABLE ENERGIES

E_{μ} (GeV)	E_{MAX} (GeV)	$E_{\mu} - E_{MAX}$ (GeV)
1.0×10^0	8.294×10^{-2}	9.171×10^{-1}
2.0×10^0	3.087×10^{-1}	1.690×10^0
4.0×10^0	1.071×10^0	2.929×10^0
7.0×10^0	2.733×10^0	4.267×10^0
1.0×10^1	4.774×10^0	5.256×10^0
2.0×10^1	1.294×10^1	7.06×10^0
4.0×10^1	3.142×10^1	8.58×10^0
7.0×10^1	6.055×10^1	9.45×10^0
1.0×10^2	9.015×10^1	9.85×10^0
2.0×10^2	1.896×10^2	1.04×10^1
4.0×10^2	3.894×10^2	1.06×10^1
7.0×10^2	6.892×10^2	1.08×10^1
1.0×10^3	9.890×10^2	1.10×10^1
2.0×10^3	1.989×10^3	1.10×10^1
4.0×10^3	3.989×10^3	1.10×10^1
7.0×10^3	6.989×10^3	1.10×10^1
1.0×10^4	9.989×10^3	1.10×10^1

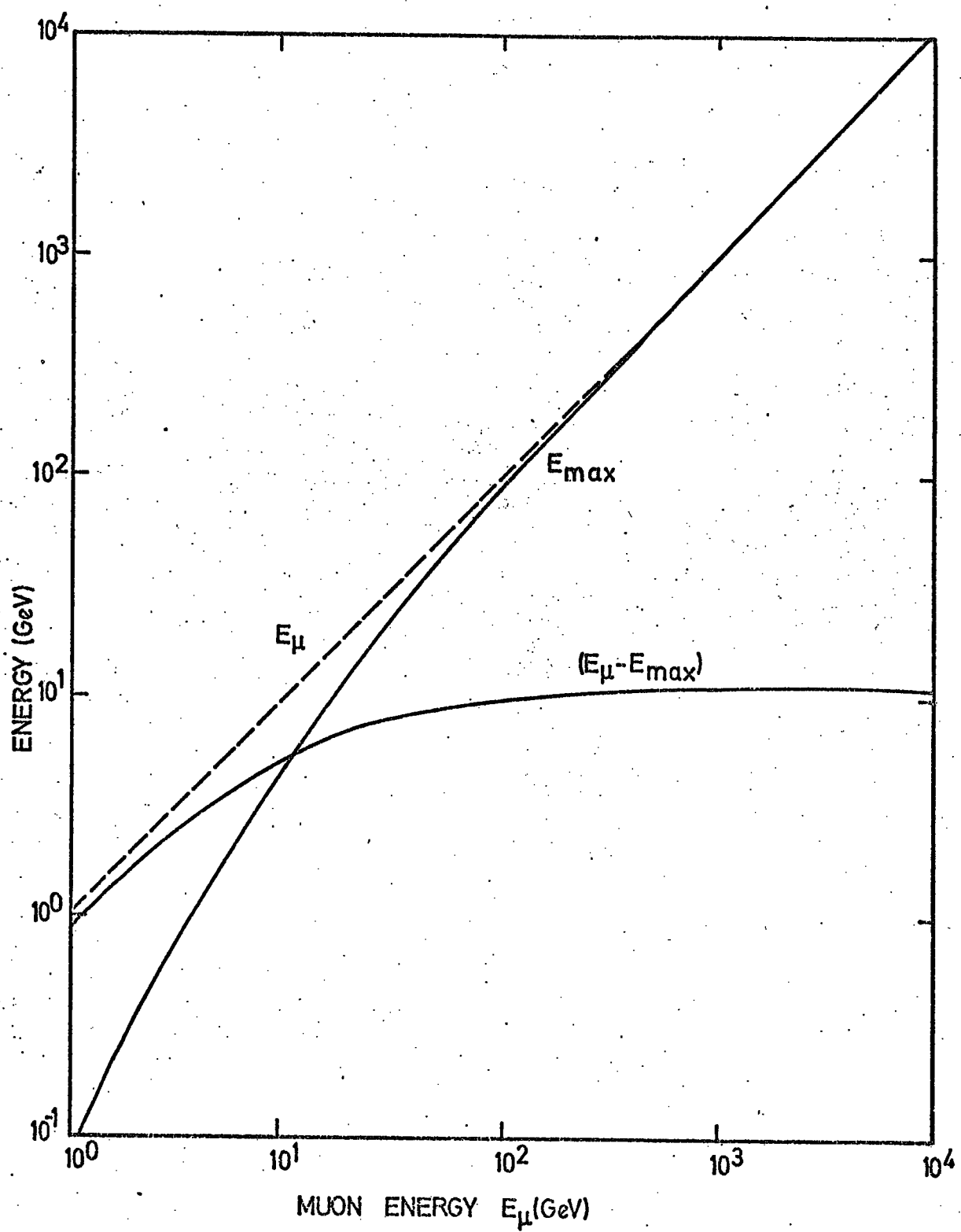


FIGURE 2.1. Plots of the maximum transferable energy for the knock-on process and the difference between the muon energy and the maximum transferable energy.

In Figure 2.2 the knock-on cross-section is plotted for five muon energies (1 GeV, 10 GeV, 100 GeV, 1 TeV and 10 TeV) and for $1 \text{ MeV} < E_t < E_{\text{MAX}}$. It can be seen from both Equation 2.2 and Figure 2.2 that until E_t ~~becomes~~ ^{APPROACHES} E_{MAX} , $\sigma_{\text{KO}} \propto 1/E_t^2$. The results of calculations for $1 \text{ GeV} < E_\mu < 10 \text{ TeV}$ and $10 \text{ MeV} < E_t < E_{\text{MAX}}$ are tabulated in Appendix A.

2.3 THE BREMSSTRAHLUNG PROCESS

2.3.1 INTRODUCTION

Whenever a force is applied to a charged particle it is accelerated and classically it must radiate energy in the form of electromagnetic radiation. As a particle radiates it must slow down, hence, the German name of Bremsstrahlung or braking radiation.

Bremsstrahlung occurs when a charged particle passes close to an atomic nucleus and is accelerated by the electric field present. This acceleration will occur over a very short time period $\sim 10^{-23} \text{ s}$; and results in the emission of a single photon. According to quantum mechanics this emitted photon is either a real photon or a virtual photon which may subsequently materialize as an electron-positron pair. The process which produces a single real photon is called the bremsstrahlung process. The materialization of a particle pair from the virtual photon is known as the direct pair production process and is discussed in Section 2.4.

2.3.2 THE CROSS-SECTION FOR THE BREMSSTRAHLUNG PROCESS

Bethe and Heitler (1934) carried out the initial theoretical treatment of this process. They derived a formula for spin $\frac{1}{2}$ particles

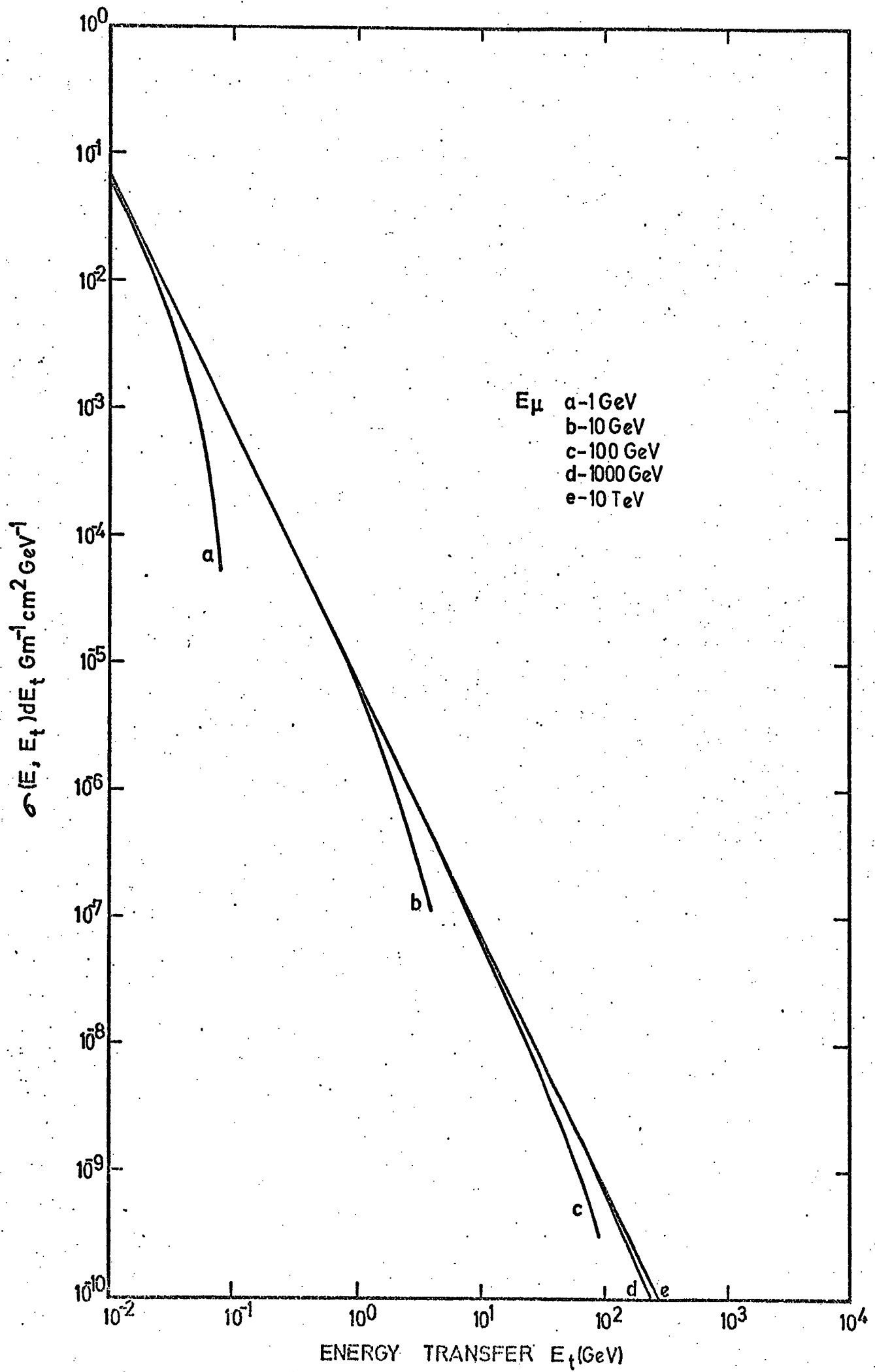


FIGURE 2.2. The knock-on cross-section for muons in iron.

by taking into account the effects of the atomic form factors (screening by atomic electrons).

Christy and Kusaka (1941) did calculations for particles of spin 1 and spin 0 and corrected the Bethe-Heitler spin $\frac{1}{2}$ formula for the finite size of the nucleus. In their calculations they made three assumptions about the interaction:

1. The kinetic energy of the particle is large compared to the electron mass.
2. The electric potential of the nucleus is that of a point charge for distance $> r_n$ (the nuclear radius) and constant for distances $< r_n$.
3. The screening by the atomic electrons is negligible.

Until recently the Christy-Kusaka spin $\frac{1}{2}$ formula has been the most widely used formula for muons. The Christy-Kusaka cross-section for the production of a photon of energy E_t from a particle (spin $\frac{1}{2}$) of energy E is given by

$$\sigma_{\text{BREM}}(E, E_t) \lambda = \frac{4\alpha N_0 Z^2}{A} r_e^2 \left(\frac{m_e c^2}{M c^2}\right) \frac{dE_t}{E_t} \left[1 + \left(\frac{E - E_t}{E}\right) - \frac{2}{3} \left(\frac{E - E_t}{E}\right)^2\right] \\ \times \left[\ln \left| \frac{2E_t(E - E_t)}{Mc^2 M c r_n E_t} \right| + \frac{1}{2} \right] \quad (2.8)$$

where

α is the fine structure constant - 1/137,

N_0 is Avagadro's number - 6.02252×10^{23} mole $^{-1}$,

Z is the electronic charge of the medium,

A is the atomic molar weight,

r_e is the classical electron radius - 2.8×10^{-13} cm,

r_n is the nuclear radius = $1.38 \times 10^{-13} A^{1/3}$ cm,

$m_e c^2$ is the electron rest mass,

M_c^2 is the muon rest mass,

\hbar is Planck's constant (\hbar) / 2π = 6.5820×10^{-22} MeV s.

Petrukhin and Shestakov (1966, 1968) suggest that for $Z \sim 25$, Christy and Kusaka have underestimated the nuclear form factor (i.e. nucleon screening) by a factor ~ 2 . They also suggest that this is one of the reasons why Ashton and Coats (1966) found for muon energies > 100 GeV, where bremsstrahlung is the dominant process, some disagreement between their calculations and their experimental data, the theoretical calculations being overestimates.

Rossi (1952) says that the Christy-Kusaka formula is probably correct to

$$E \leq \frac{M_c^2}{m_e c^2} \frac{137}{Z^{1/3}} \approx 1 \text{ TeV} \quad (2.9)$$

above which energy screening of the nuclear electric field by the atomic electrons becomes important. Petrukhin and Shestakov (1968) believe that at $E \sim 100$ GeV screening is very important.

In 1966 Petrukhin and Shestakov, using the original work of Bethe and Heitler (1934), derived a single analytical expression to take into account any degree of atomic screening. In 1968 they made a correction to the 1966 expression for the nuclear screening. For their work they made two assumptions

1. The energy of the muon is much larger than the muon mass.
2. For distances $> r_n$ (the nuclear radius), the nucleus is a point charge and for distances $< r_n$, they assumed a Fermi charge distribution.

They began with the following Bethe-Heitler derivation:

$$\begin{aligned} \sigma_{\text{BREM}}(E, E_t) dE_t &= \alpha \left(\frac{2Zr_e m_e c^2}{EMc^2} \right)^2 \\ &\times [(2 - 2EE_t + E_t^2)\phi_1(\delta) - \frac{2}{3}(E - E_t)\phi_2(\delta)] \frac{dE_t}{E_t} \quad (2.10) \end{aligned}$$

where all terms are as defined earlier and where

$$\delta = \frac{M^2 c^4}{2E} \frac{E_t}{E - E_t} \quad (2.11)$$

(the least momentum transferred to the nucleus). $\phi_1(\delta)$ and $\phi_2(\delta)$ are functions that were shown by Bethe and Heitler to be very nearly equal. For the case of no screening $\phi_1(\delta) = \phi_2(\delta)$ and for the case of complete screening $\phi_1(\delta) = \phi_2(\delta) = 1/6$. In their derivation, Petrukhin and Shestakov assumed $\phi_1(\delta) = \phi_2(\delta) = \Phi(\delta)$ where

$$\Phi(\delta) = \int_{\delta}^{q_{\text{MAX}}} [F_n(q) - F_a(q)]^2 \phi(q, \delta) \frac{dq}{q^3} \quad (2.12)$$

F_n , F_a are the functions of the nuclear and atomic form factors respectively. $\phi(q, \delta)$ is a function of the kinematics of the interaction. They obtained the following expression for $\Phi(\delta)$ which takes into account both nuclear and atomic screening:

$$\Phi(\delta) = \ln \left| \frac{126Mc^2}{z^{2/3} (m_e c^2 + 189\sqrt{e} \delta z^{-1/3})} \right| \quad (2.13)$$

Combining Equations 2.10, 2.11 and 2.13

$$\begin{aligned} \sigma_{\text{BREM}}(E, E_t) dE_t &= \alpha \left(\frac{2Zr_e m_e c^2}{Mc^2 E} \right)^2 \left(\frac{4}{3} E^2 - \frac{4}{3} EE_t + E_t^2 \right) \frac{dE_t}{E_t} \\ &\times \ln \left| \frac{126Mc^2}{z^{2/3} (m_e c^2 + \frac{94.5\sqrt{e} Mc^2 E_t}{E(E - E_t) z^{1/3}})} \right| \quad (2.14) \end{aligned}$$

This cross-section goes to zero for

$$E_t = E_{MAX} = E - \frac{3}{4}\sqrt{e} Mc^2 Z^{1/3} \approx E - 0.387 \text{ (GeV)} . \quad (2.15)$$

The maximum energy transferred to the nucleus is

$$\delta_{MAX} = \frac{2Mc^2}{3\sqrt{e}} Z^{-1/3} \approx 0.404 Z^{-1/3} Mc^2 \quad (2.16)$$

and for iron $\delta_{MAX} = 14.42 \text{ MeV}$.

2.3.3 THE RESULTS AND CALCULATIONS OF THE BREMSSTRAHLUNG CROSS-SECTION

For the present experiment the expression by Petrukhin and Shestakov (1968) is considered to be the best and to take into account the most recent information about the nuclear size. Calculations have been done for $1 \text{ GeV} < E_\mu < 10 \text{ TeV}$ and $10 \text{ MeV} < E_t < E_{MAX}$ (see Equation 2.15) and are presented in Appendix A. The results are also presented in Figure 2.3, where it can be seen for $E_t \ll E_\mu$ that $\sigma_{BREM}(E_\mu, E_t) \propto 1/E_t$. From a comparison between Figures 2.3 and 2.2 it can be seen that for muon energies greater than 100 GeV and for all energy transfers greater than 4 GeV that bremsstrahlung is the dominant process.

2.3.4 ERRORS IN THE THEORETICAL TREATMENT

Rozental' (1968) has analyzed the errors in the Petrukhin-Shestakov derivation and has concluded that the overall accuracy of the continuous formula is about 2%. At an energy of 1 TeV he estimates the radiative correction necessary to be $\sim -5\%$. The use of the Born approximation in the treatment introduces a further 1% error. If

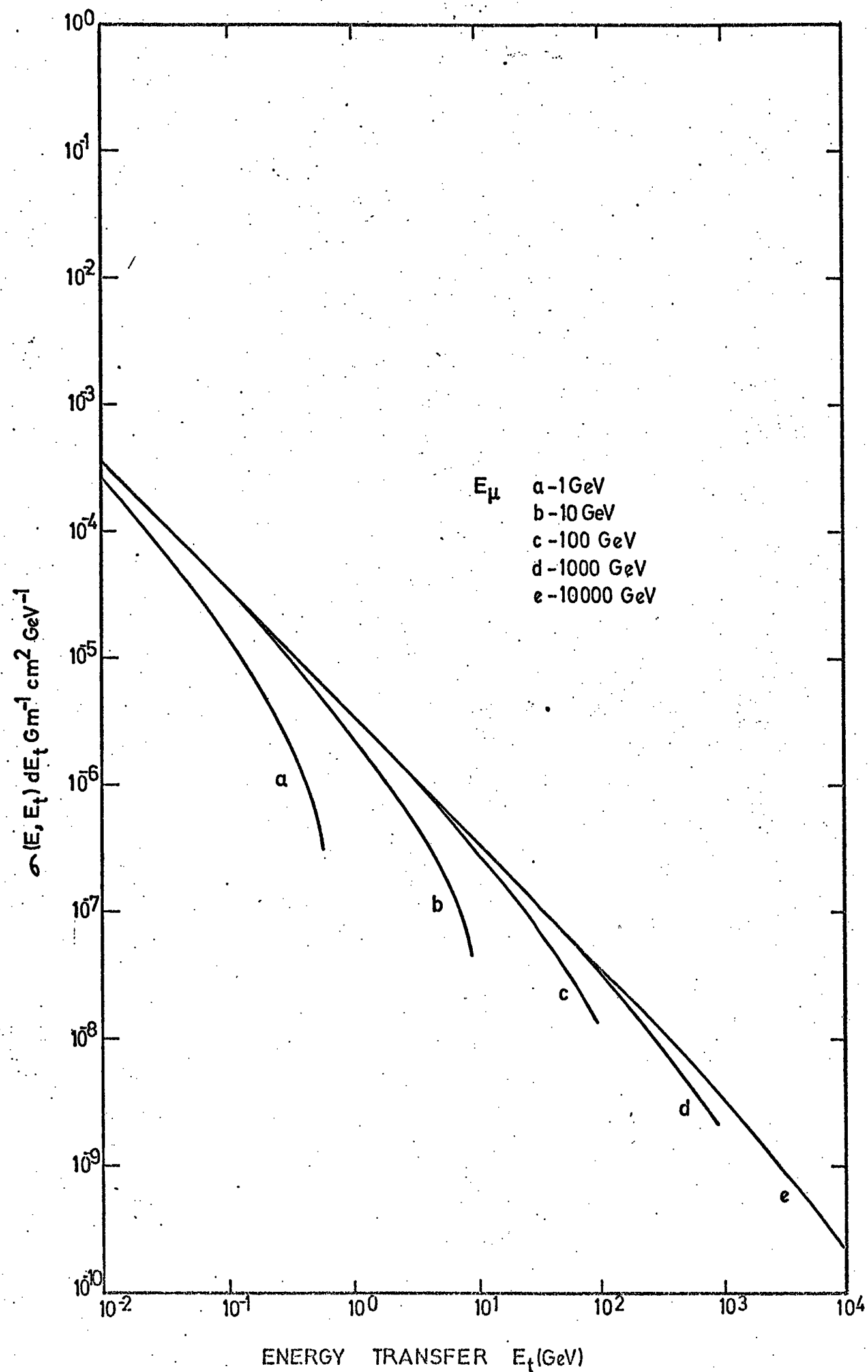


FIGURE 2.3. The bremsstrahlung cross-section for muons in iron.

bremsstrahlung in the atomic electrons' coulomb field is considered it has the effect of raising the Z^2 term to $Z(Z + \zeta)$ where $\zeta \approx 1$. Kel'ner (1968) has estimated $1 < \zeta < 1.23$ for iron as the cross-section varies from the non-screened to the screened case. The effect of making allowance for the atomic electrons is to raise the cross-section by about 5%. The radiative correction and the electron bremsstrahlung correction tend to cancel one another. The net error in the formula used is about 3%.

2.4 THE DIRECT PAIR PRODUCTION PROCESS

2.4.1 INTRODUCTION

As described in Section 2.3, as a muon passes close to an atomic nucleus it will be scattered and in the process radiate energy. Classically, this radiation would always be electromagnetic and only bremsstrahlung would occur. With the advent of quantum mechanics, electromagnetic waves could be described in terms of quanta ~~of the electromagnetic field~~ (i.e. photons). A further implication is that a photon with sufficient energy will spend some of its time as a virtual particle-antiparticle pair. To take the process one step further it is possible for a virtual photon accompanying a charged particle to spend some of its time as a virtual pair. The pair that a photon will usually assume is an electron-positron pair, because such a pair has the smallest mass (energy). Figure 2.4 shows the Feynman diagram representing a photon which breaks into an electron and a positron which, in turn, recombines into the photon again.

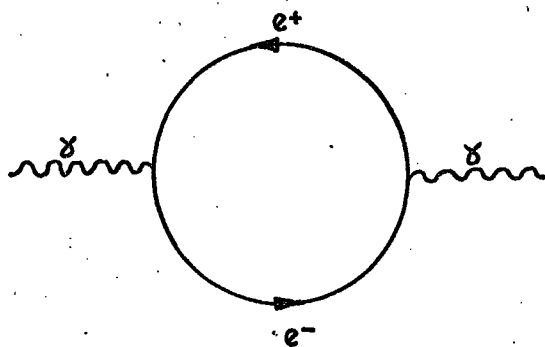


FIGURE 2.4. Diagram of a virtual particle-antiparticle pair

It is not immediately apparent why, when the photon is in the particle-antiparticle state, that it will not remain so, or why $\gamma \rightarrow e^- + e^+$ is not a valid decay mode of the photon. (All quantum numbers are conserved.) However, when the kinematics of such a system are considered it becomes evident that it is necessary for some momentum to be exchanged with another particle before the momentum of the system can be conserved.

Figure 2.5 is the diagram for γ pair production where the momentum q is exchanged with a nucleus or other particle. Figure 2.5 is Figure 2.4 opened out. It is apparent ~~in~~ ⁱⁿ Figure 2.6, which is electron bremsstrahlung, is compared with Figure 2.5 that pair production is simply reverse bremsstrahlung.

Direct pair production, as opposed to photon pair production, is when a muon (or other particle) is scattered in the atomic electric field and the photon which is emitted materializes as an electron-positron pair, the momentum being conserved by a single γ exchange with a nucleus by one of the particles (muon or electrons) involved. Figures 2.7a,b show the four diagrams for direct pair production by muons. Figure 2.7a is the 'second order' processes, when the γ exchange is done with one of the leaving electrons. Figure 2.7b is the 'first

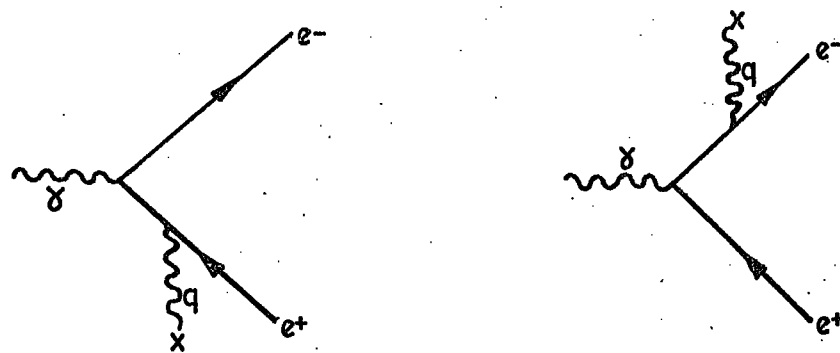


FIGURE 2.5. *Feynman* diagrams of photon pair production of electrons

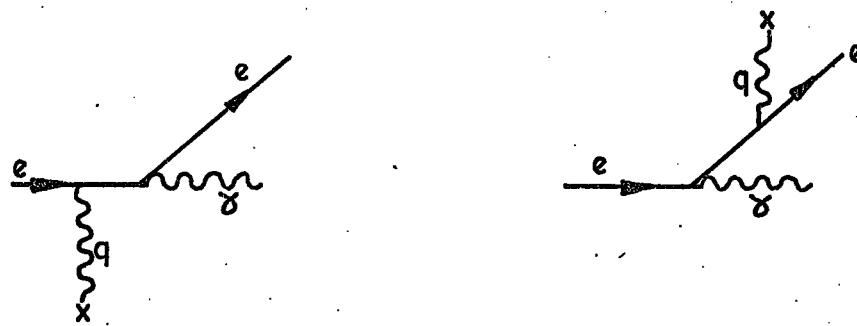
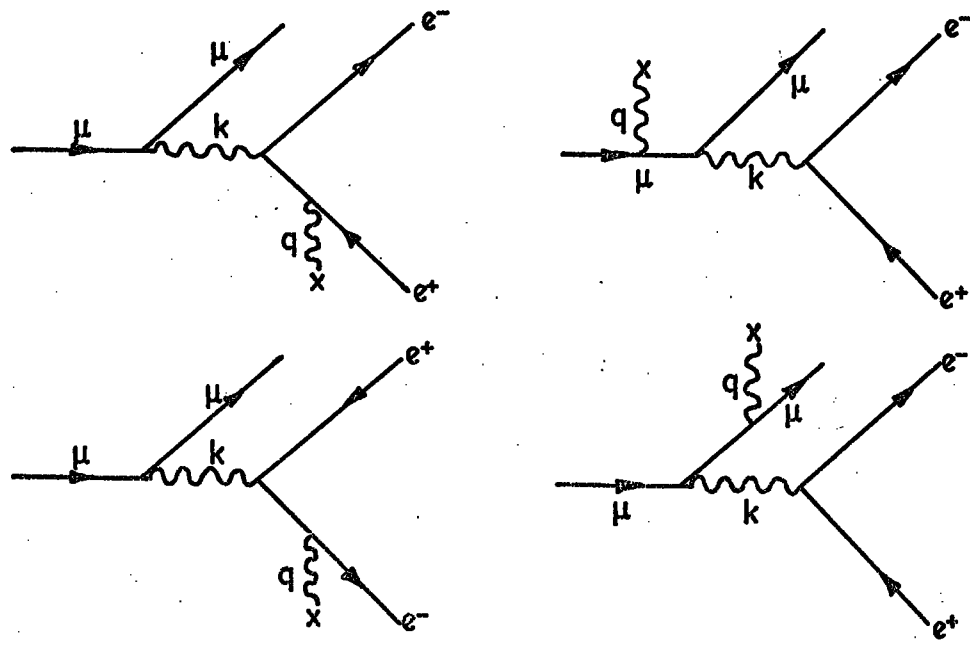


FIGURE 2.6. *Feynman* diagrams of electron bremsstrahlung.



(a)

(b)

FIGURE 2.7. *Feynman* diagrams of muon direct pair production of electrons. (a) Second order processes. (b) First order processes.

'order' processes, when the γ exchange is done with the muon. The terminology, first and second order, is not strictly correct and is misleading since the dominant process for muons over most energy transfers is the second order process. For the sake of clarity, the notation of Petrukhin and Kokoulin (1970) has been adopted. The first order diagram will be referred to as ' μ ', and the second order diagram as 'e'. Strictly speaking there are six diagrams as pointed out by Kel'ner (1967). The last two (not shown) are interference diagrams and follow from the Feynman-Dyson method of analysis. It turns out, however, that when all the states of the system are considered, these diagrams make no contribution to the cross-section.

2.4.2 THE CROSS-SECTION FOR THE DIRECT PAIR PRODUCTION PROCESS

For the discussion of the cross-section it is useful to define regions of interest. Figure 2.8 shows the regions as defined by various workers (after Wright, 1972). The discussion here shall only concern itself with relativistic particles ($E_\mu > 1$ GeV and $E_t > 10$ MeV). Therefore, the regions labelled A, B and C will not be considered. The remainder of the figure is divided into four areas labelled IN, IS, IIN, IIS. I denotes small energy transfers ($E_t < 0.005 E$), II denotes large energy transfers ($E_t > 0.005 E$). N, S denote the non-screening and screening of the atomic electrons. N, S regions are defined by $\gamma > 1$ and $\gamma < 1$ respectively, where

$$\gamma = \frac{189(2m_e^2 c^4 + M^2 c^4 v^2(1 - \rho^2))}{4E_\mu v(1 - \rho^2)m_e^2 c^2(1 - v)} \quad (2.17)$$

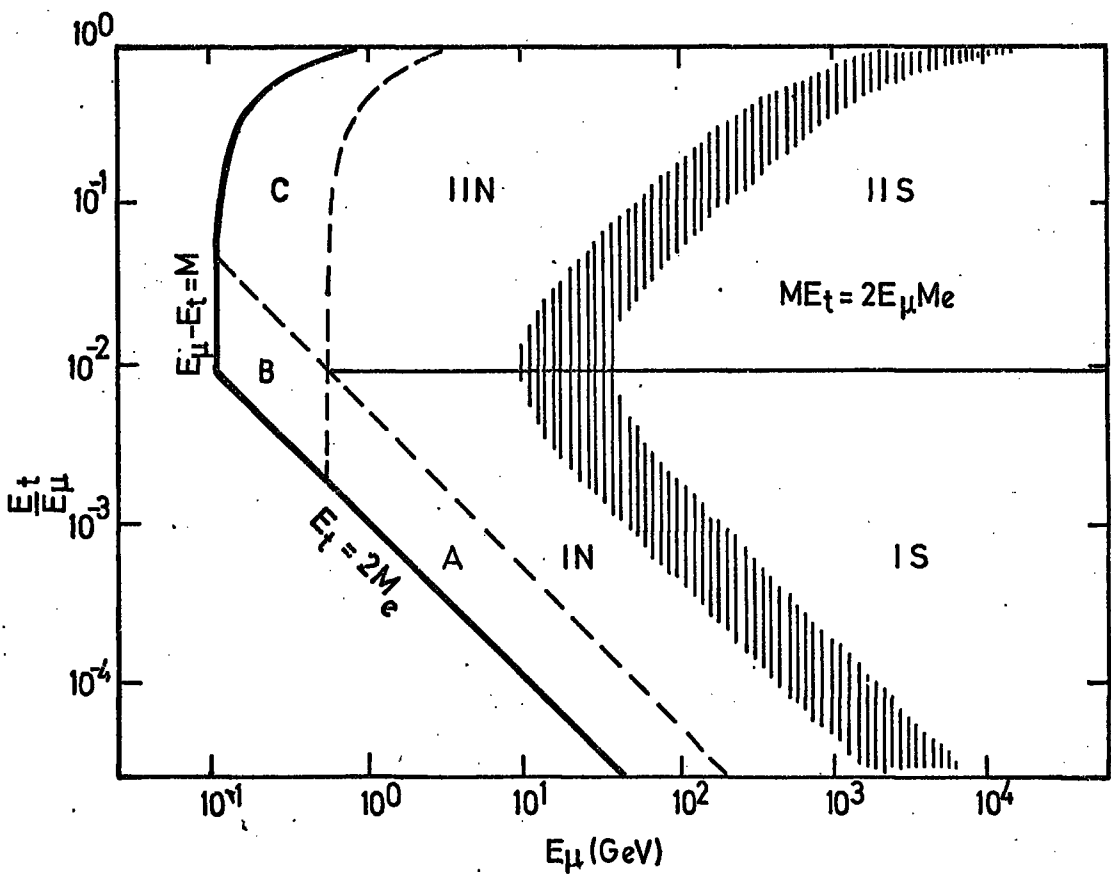


FIGURE 2.8. Direct pair production regions of interest (after Wright, 1972). N, S are the non-screened and screened regions respectively. I, II are the regions of small energy transfers ($E_t < 0.006E_\mu$) and large energy transfers ($E_t > 0.010E_\mu$) respectively. The thick solid line represents the physical limit. The dashed line separates the relativistic (right) and non-relativistic (left) regions.

where

E_μ is the muon energy,

v is the fraction energy transferred,

$m_e c^2$ is the electron rest mass.

$M c^2$ is the muon rest mass,

ρ is the asymmetry coefficient of the energy distribution of the produced pair.

Carlson and Furry (1933), shortly after the discovery of the positron, were the first to attempt to calculate the direct pair production cross-section in the IN region. More exact cross-sections were calculated by Landau and Lifshitz (1934), Bhabha (1935), Nishina et al. (1935), and Racah (1937). They all considered the fields involved classically and as such their work is only valid for small energy transfers (i.e. regions IN and IS). To obtain correct results in the IIN and IIS regions the Feynman-Dyson formalism should be used. All workers using this method only considered the case when $E \gg M c^2$ (relativistic particles). Murota, Ueda and Tanaka (MUT) (1956) were the first to use the Feynman method. They claimed that their calculations have shown that only the e diagram ^{IN} ~~NEEDED~~ to be considered. Until recently, the MUT theory has been the most popularly used set of formulae. Its main drawback in calculation is the constant α which is of the order of unity. It is usually accepted that $\alpha = 2$. If the MUT formulae are compared with the later work of Ternovsky (1959) and Kel'ner (1967), it appears more likely that $1.36 < \alpha < 1.65$ ($e/2 < \alpha < e^{1/2}$).

It is very probable that the MUT cross-section is an overestimation of the correct one. MUT, themselves, have suggested that the method they used may overestimate the cross-section by as much as 20%. Comparison of the calculation of Thompson (private communication, 1971) and

Allkofer et al. (1971) with the Allkofer experimental results (total cross-section) and the more recent cross-section calculations reported here (see Figures 2.9 and 2.10) suggest that MUT do indeed overestimate the cross-section by at least 20%.

Kel'ner (1967) and Kel'ner and Kutov (1968) have done the most definitive work to the present date. These workers not only considered the four diagrams in Figure 2.7, but also took into account the interference process. Kel'ner found that after the integration over all the final states, the interference term was zero. Kel'ner-Kutov (1968) corrected the original Kel'ner equations taking into account the nuclear form factors in a similar fashion to the method used by Petrukhin and Shestakov (1968) for the bremsstrahlung process. Kel'ner's equations for the IN and IS regions are the same as the Bhabha formulae as updated and presented by Davidson in Rossi (1952). ~~His EQUATIONS IN THE IN AND IS REGIONS~~ These equations also show contrary to the results of MUT that for very large energy transfers the μ diagram becomes dominant and should be taken into account. However, if only the energy loss is important the μ diagram contributes less than 0.1% to the total.

1970
Kokoulin and Petrukhin (1969, 1971) used the work of Kel'ner and developed a single analytical formula for both the e and μ diagrams which for the extreme cases of screening and non-screening gives results identical to those of Kel'ner. Their results are

$$\sigma_{DPP}(E_\mu, v, \rho) dv d\rho = \frac{2}{3\pi} (Z \alpha e)^2 \frac{1-v}{v} (\phi_e + \frac{m_e c^2}{Mc^2} \phi_\mu) dv d\rho \quad (2.18)$$

$$\phi_e = \{ [(2 + \rho^2)(1 + \beta) + \zeta(3 + \rho^2)] \ln(1 + \frac{1}{\zeta}) + \frac{1 - \rho^2 - \beta}{1 + \zeta} - (3 + \rho^2) \} L_e \quad (2.19)$$

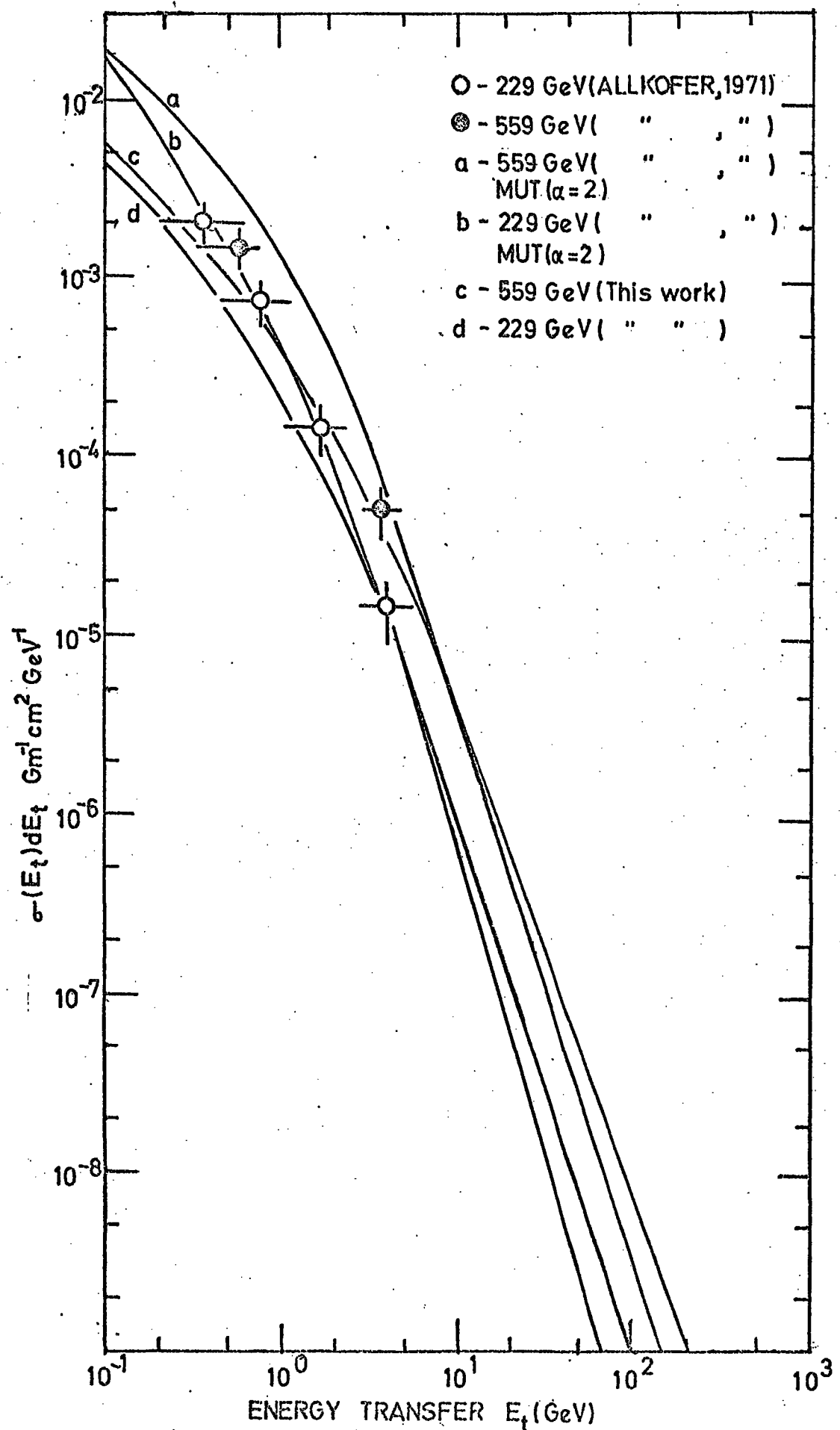


FIGURE 2.9. Comparison of experiment of Allkofer et al. (1971) with direct pair production cross-sections in iron.

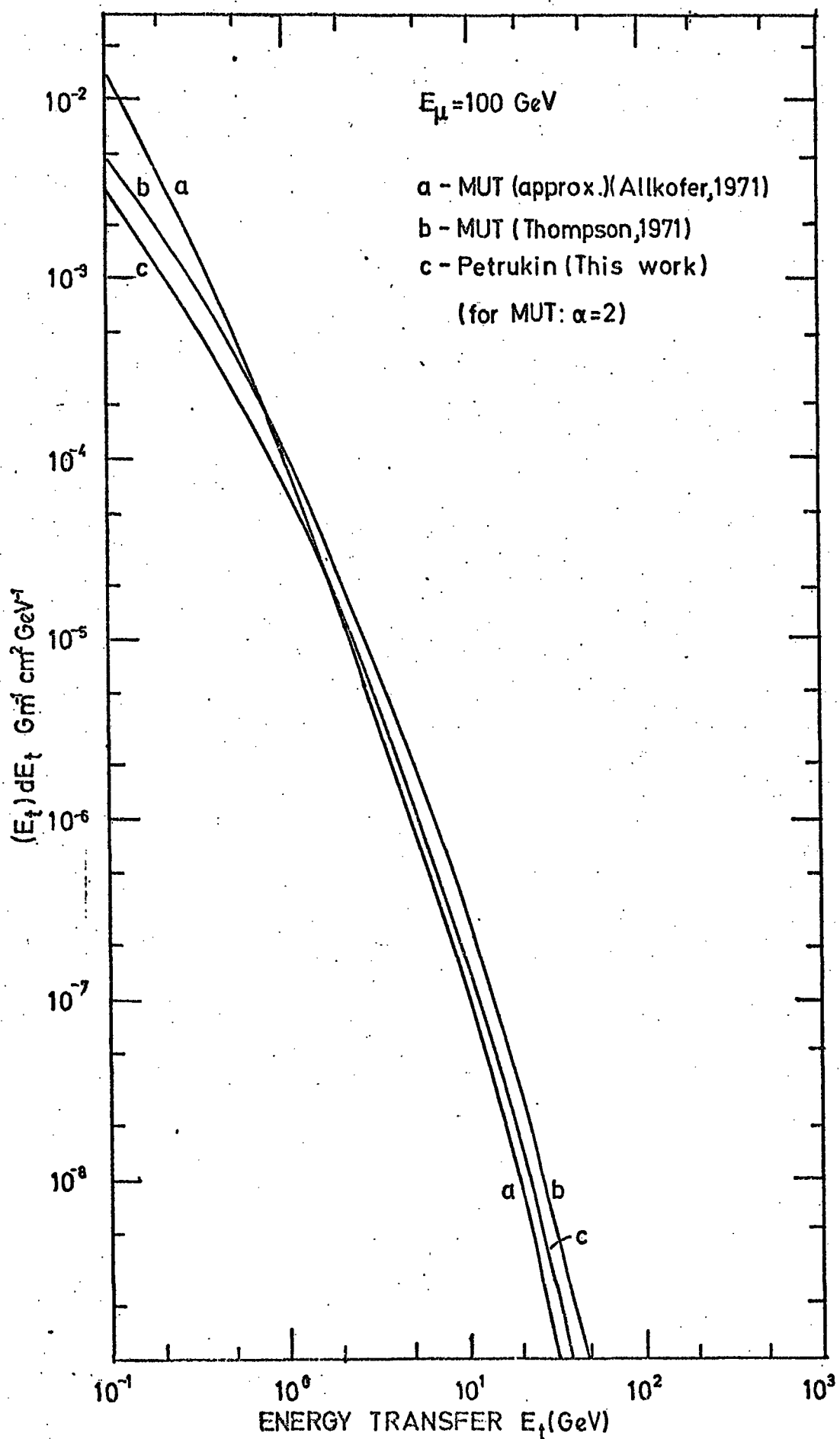


FIGURE 2.10. Comparison of various direct pair production cross-sections at 100 GeV muon energy in iron.

$$\phi_{\mu} = \left\{ \left[(1 + \rho^2) \left(1 + \frac{3}{2} \beta \right) - \frac{1}{\zeta} (1 + 2\beta) (1 - \rho^2) \right] \ln(1 + \zeta) + \frac{\zeta (1 - \rho^2 - \beta)}{1 + \zeta} + (1 + 2\beta) (1 - \rho^2) \right\} L_{\mu} \quad (2.20)$$

$$L_e = \ln \left\{ A Z^{-1/3} \left[(1 + \zeta) (1 + Y_e) \right]^{\frac{1}{2}} / 1 + \left[\frac{2 m_e c^2 e^{\frac{1}{2}} A Z^{-1/3} (1 + \zeta) (1 + Y_e)}{E v (1 - \rho^2)} \right] \right\} - \frac{1}{2} \ln \left[1 + \left(\frac{3}{2} \frac{m_e c^2}{M c^2} Z^{1/3} \right)^2 (1 + \zeta) (1 + Y_e) \right] \quad (2.21)$$

$$L_{\mu} = \ln \left\{ \frac{2}{3} \frac{M c^2}{m_e c^2} A Z^{-2/3} / 1 + \frac{2 m_e c^2 e^{\frac{1}{2}} A Z^{-1/3} (1 + \zeta) (1 + Y_e)}{E v (1 - \rho^2)} \right\} \quad (2.22)$$

$$Y_e = \frac{5 - \rho^2 + 4\beta(1 + \rho^2)}{2(1 + 3\beta) \ln(3 + \frac{1}{\zeta}) - \rho^2 - 2\beta(2 - \rho^2)} \quad (2.23)$$

$$Y_{\mu} = \frac{4 + \rho^2 + 3\beta(1 + \rho^2)}{(1 + \rho^2) (\frac{3}{2} + 2\beta) \ln(3 + \zeta) + 1 - \frac{2}{3} \rho^2} \quad (2.24)$$

$$\zeta = \left(\frac{M c^2 v}{2 m_e c^2} \right) \frac{1 - \rho^2}{1 - v} \quad (2.25)$$

$$\beta = \frac{v^2}{2(1 - v)} \quad (2.26)$$

where

E is the muon energy (E_{μ}),

E_+ (E_-) is the positron (electron) energy,

E_t is the energy transferred to the pair - $E_t = E_+ + E_-$,

v is the fractional energy transferred to the pair - $v = E_t/E$,

ρ is the asymmetry coefficient of the energy distribution of the pair - $\rho = (E_+ - E_-)/E_t$,

Z is the electronic charge of the material,

α is the fine structure constant - $\alpha = 1/137$,

A is the constant determining the value of the radiation logarithm - $A = 189$,

r_e is the classical electron radius - $r_e = 2.8 \times 10^{-13}$ cm,

$m_e c^2$ is the electron (positron) rest mass,

M_c^2 is the muon rest mass.

The indices e and μ represent the contribution from the two diagrams.

The cross-section is non-negative for

$$\frac{4m_e c^2}{E_\mu} \leq v \leq 1 - \frac{3}{4} e^{\frac{1}{2}} \frac{M_c^2}{E_\mu} Z^{\frac{1}{2}} \quad (2.27)$$

$$2.041 \text{ MeV} \leq E_t \leq E_\mu - 0.387 \text{ GeV} \quad (2.28)$$

and

$$0 \leq p \leq \left(1 - \frac{6M_c^2}{E_\mu^2(1-v)}\right) \left(1 - \frac{4m_e c^2}{E_\mu v}\right)^{\frac{1}{2}} \quad (2.29)$$

According to calculations and comparisons done by Petrukhin and Kokoulin, their cross-section varies an average of 1% from that of Kel'ner. Because of the simplicity of calculation (as compared to others) and its agreement with Kel'ner's derivations, the formulae of Petrukhin have been used in this work.

2.4.3 THE RESULTS AND CALCULATIONS OF THE DIRECT PAIR PRODUCTION CROSS-SECTION

It is important to know how the energy transferred to a pair of particles is divided between the two particles. Figure 2.11a,b,c,d shows the probability $P(\epsilon'/\epsilon)$ of one of the pair receiving a fraction of the energy transfer ϵ'/ϵ for various muon energies and energy transfers. ϵ' is the energy transferred to one of the pair, ϵ is the total

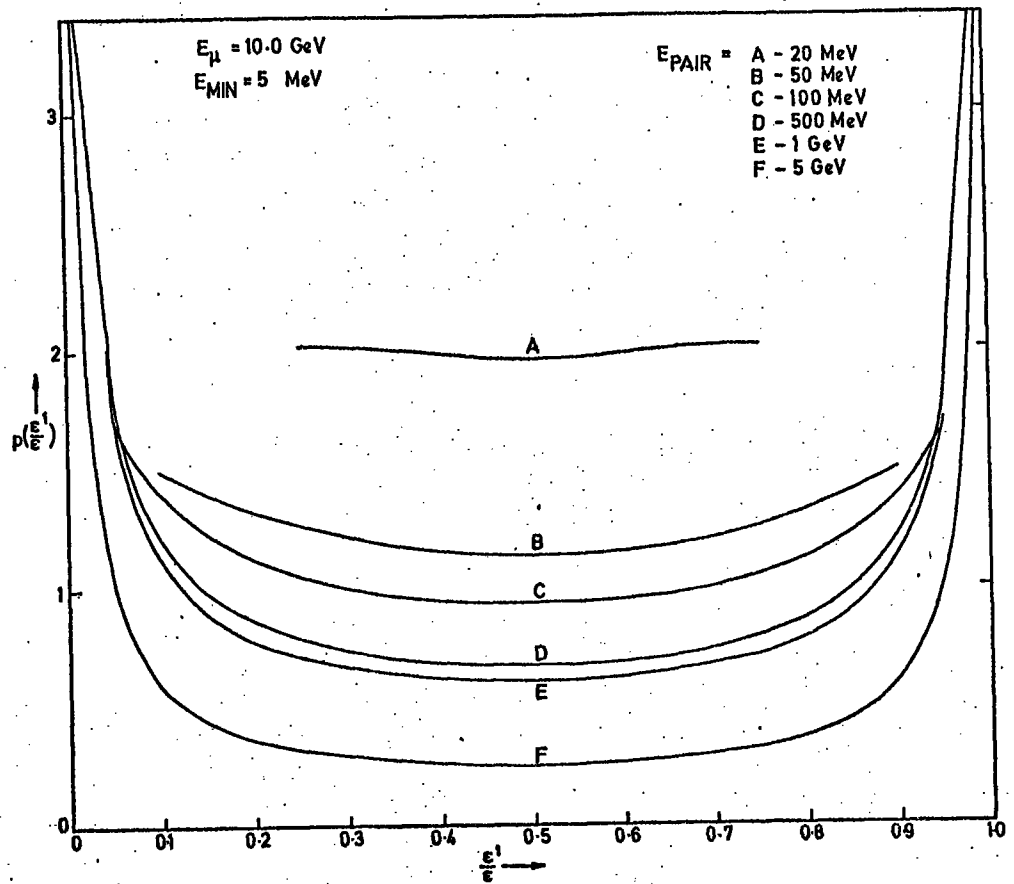


FIGURE 2.11(a). Division of energy to produced pair .

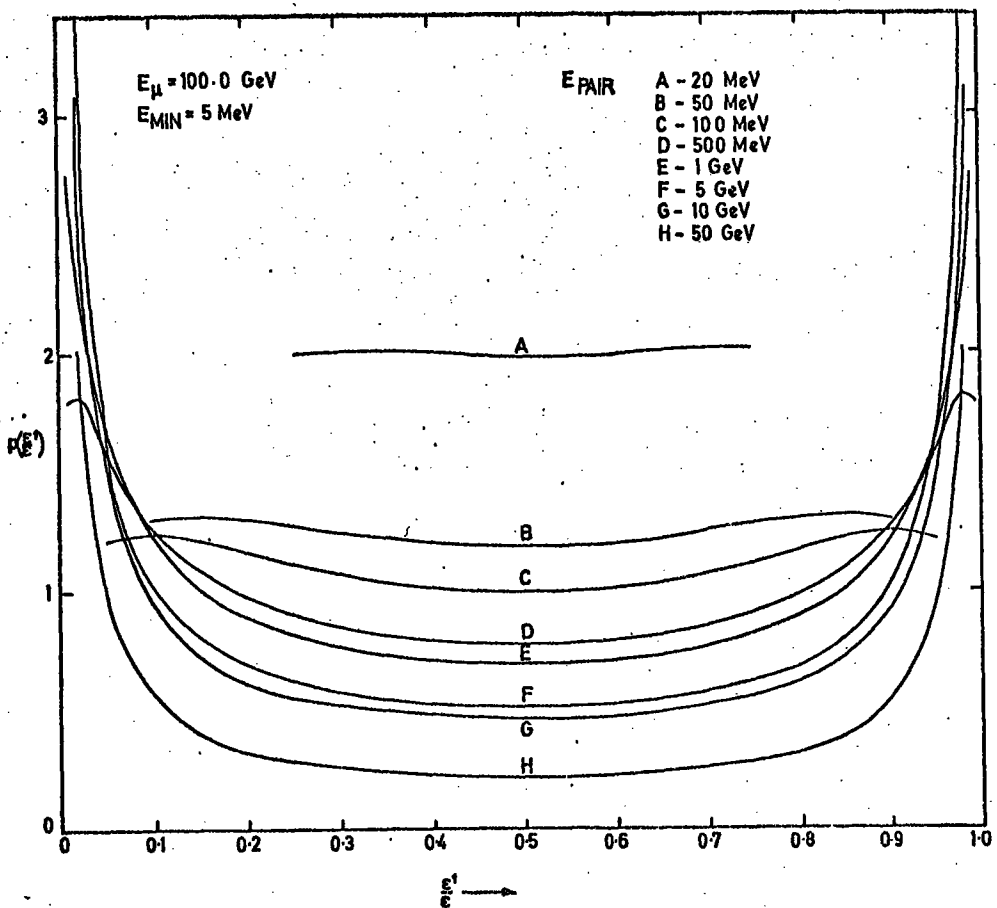


FIGURE 2.11(b). Division of energy to produced pair .

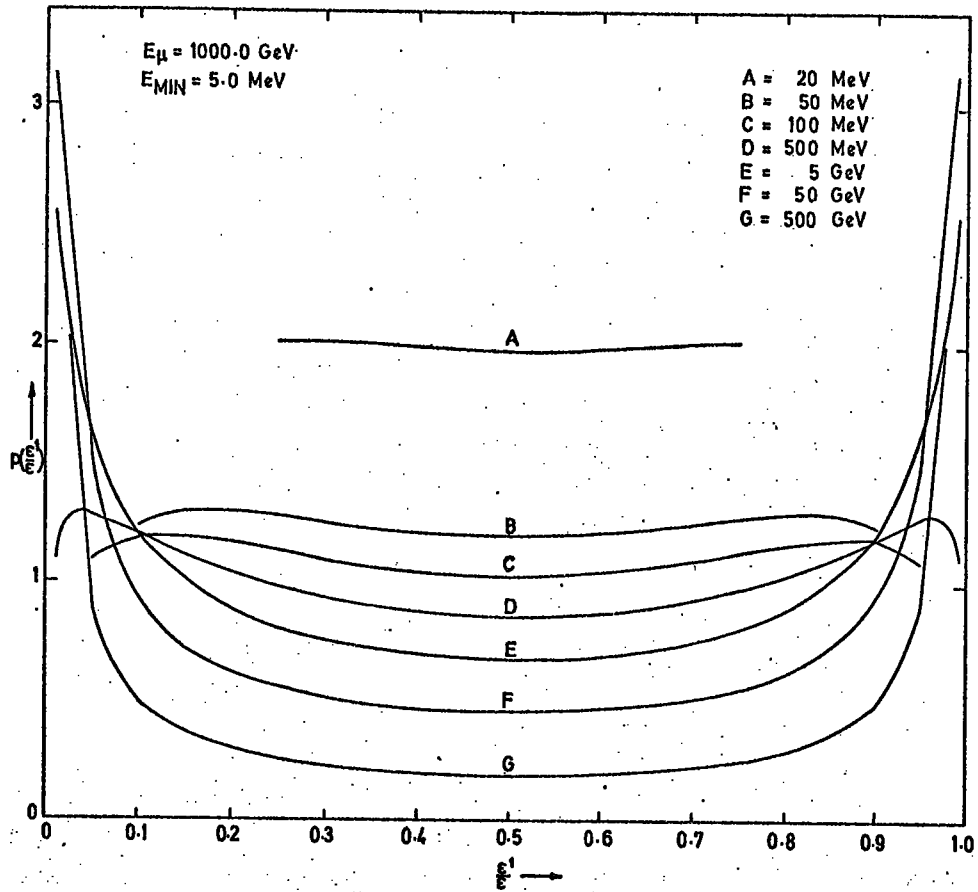


FIGURE 2.11(c). Division of energy to produced pair.

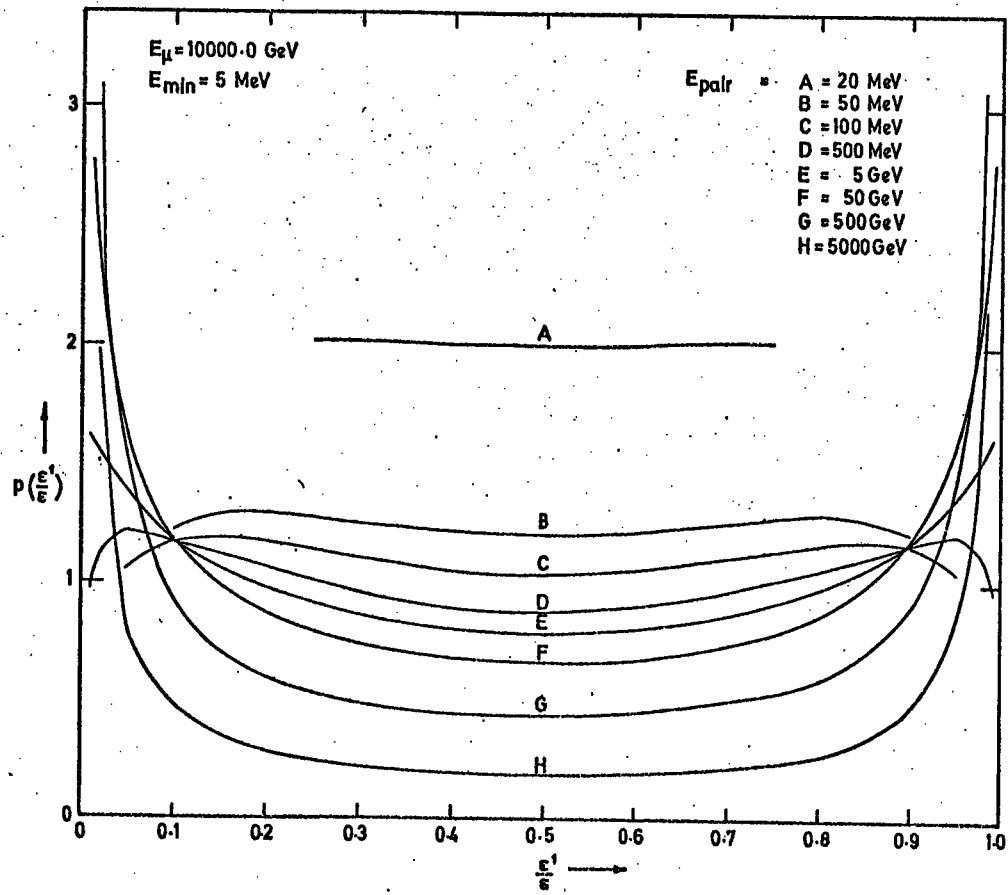


FIGURE 2.11(d). Division of energy to produced pair.

energy transferred to the pair (elsewhere called E_t) and $P(\epsilon'/\epsilon)$ is

$$P\left(\frac{\epsilon'}{\epsilon}\right) = \sigma_{DPP}(E_\mu, \epsilon, \frac{\epsilon'}{\epsilon}) d\epsilon / \int_{(\epsilon'/\epsilon)_\text{min}}^{(\epsilon'/\epsilon)_\text{max}} (\sigma_{DPP}(E_\mu, \epsilon, \frac{\epsilon'}{\epsilon}) d\epsilon) d\left(\frac{\epsilon'}{\epsilon}\right). \quad (2.30)$$

In the calculation it was required that each particle in the pair has a minimum energy of 5 MeV. It is apparent that except for small energy transfers $E_t < 0.01 E$, it is very likely that one of the particles of the pair will carry away most of the energy transferred to the pair.

As stated in the last section, Kel'ner in his work found it necessary to include the μ diagram and its contributions for high energy transfers. In Figure 2.12 the cross-section contributions from the e and μ diagrams are presented for $E_\mu = 100$ GeV. This plot is typical of other energies. For energy transfers of $\sim 0.5 E_\mu$ the μ contribution is significant and becomes dominant for very high energy transfers. The direct pair production cross-section $\sigma_{DPP}(E_\mu, E_t) dE_t$ was calculated for $1 \text{ GeV} \leq E_\mu \leq 10 \text{ TeV}$ and $10 \text{ MeV} < E_t < E_{\text{MAX}}$ (see Equation 2.29). The results are tabulated in Appendix A and presented in Figure 2.13. In the two previous discussions on cross-section it is shown that $\sigma_{KO} \propto 1/E_t^2$ and $\sigma_{BREM} \propto 1/E_t$ over certain regions. Unfortunately σ_{DPP} shows no such simplicity in any of the regions of interest, nor can it be represented by a single power law. Also contrary to the knock-on and bremsstrahlung cross-sections, the direct pair production cross-section is very sensitive to muon energy. Because of this dependence it would be expected that for high energies, pair production should be the dominant process.

2.4.4 ERRORS IN THE THEORETICAL CROSS-SECTION

Since the direct pair production process is very similar to the bremsstrahlung process, the errors involved will be equally similar

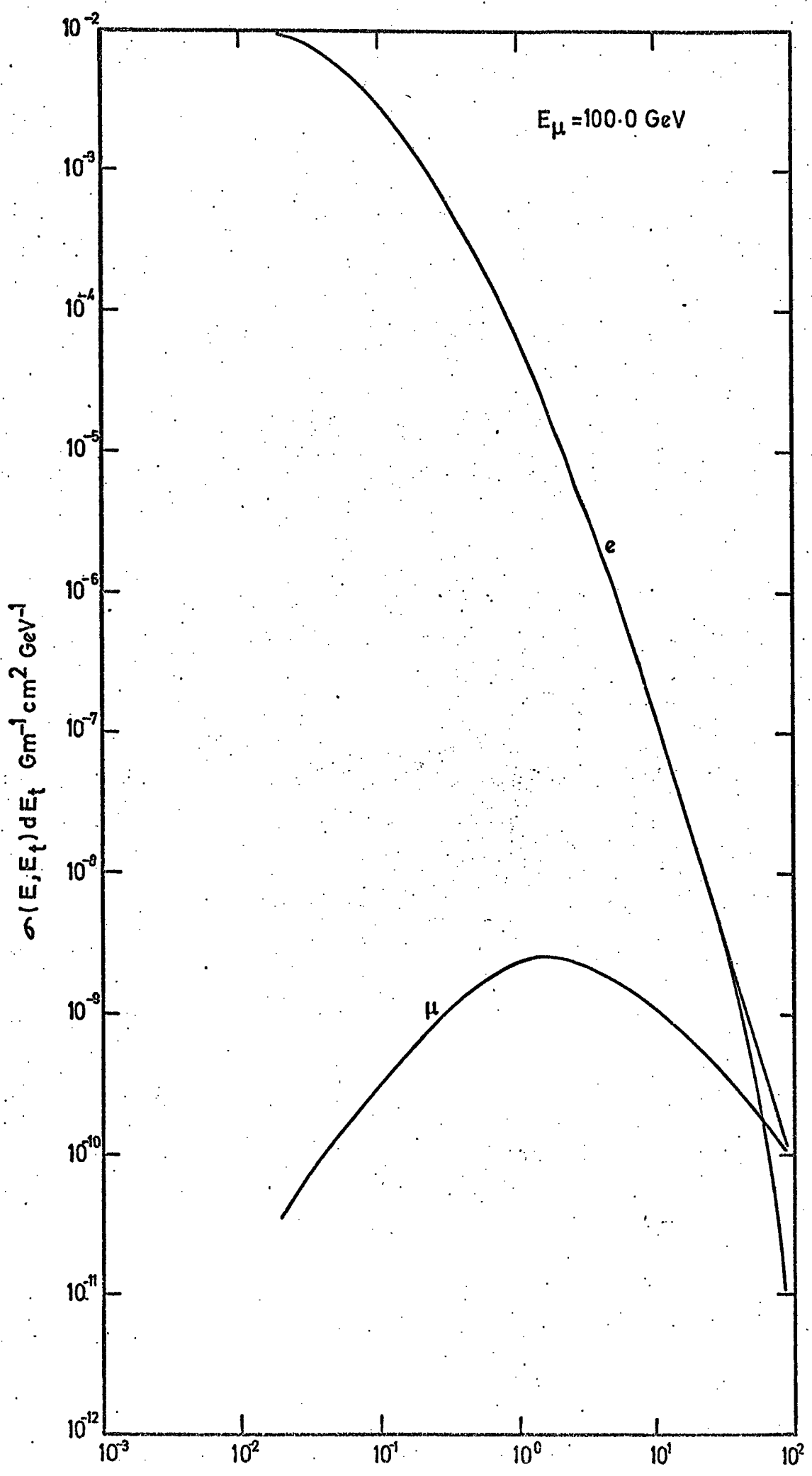


FIGURE 2.12. e and μ components of the direct pair production cross-section in iron for a 100 GeV muon.

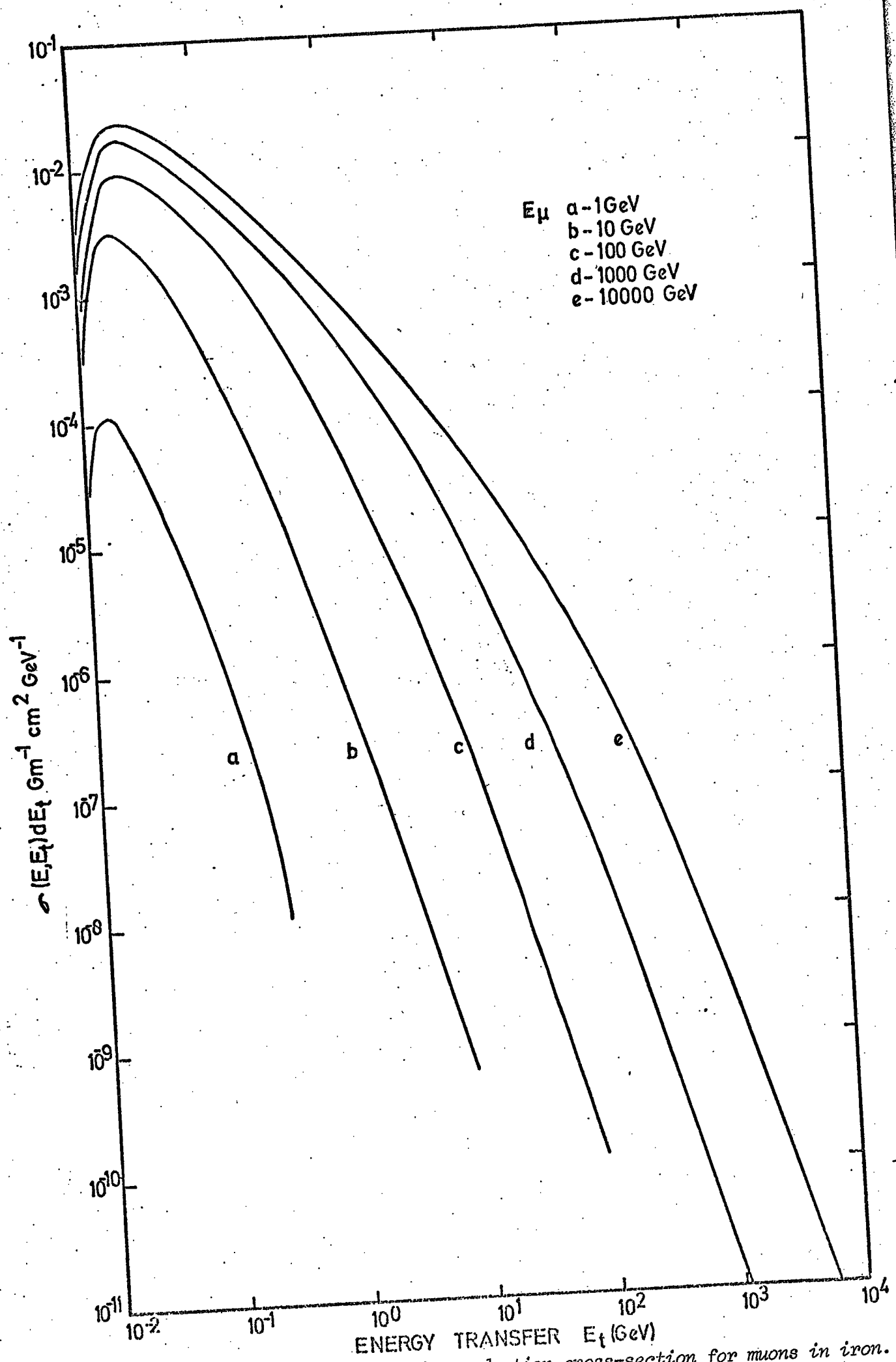


FIGURE 2.13. The direct pair production cross-section for muons in iron.

(Rozental', 1968). The corrections due to radiation and the pair production in the electron shells should cancel out. Petrukhin and Kokoulin estimate the errors in their interpolation formula to be 1 to 2%. The approximation in Kel'ner's formulae should introduce an error of $\sim 1\%$. The overall cross-section for pair production therefore should be accurate to about 3%.

2.4.5. CONSIDERATIONS IN THE CALCULATIONS OF THE CROSS-SECTION

To calculate $\sigma_{DPP}(E_\mu, E_t) dE_t$ the formulae given in Section 2.4.3 (Equations 2.18 to 2.26) must be integrated numerically over the coefficient of asymmetry in the energy of the pair, ρ , where

$$\rho = (E_+ - E_-)/E_t . \quad (2.31)$$

Figures 2.11a,b,c,d show how the cross-section varies with ρ . (Note that ρ can be expressed as

$$\rho = \frac{2e'}{\varepsilon} - 1 . \quad (2.32)$$

Two observations can be made. First, the cross-section is symmetric about $\rho = 0$. This implies that

$$\int_{\rho_{\min}}^{\rho_{\max}} \sigma_{DPP} d\rho = 2 \int_0^{\rho_{\max}} \sigma_{DPP} d\rho . \quad (2.33)$$

Second, as the energy transfers increase the cross-section varies more rapidly as $\rho \rightarrow \rho_{\max}$. In this area the integration error can be great if the integration steps taken are too large.

The integration over the variable ρ , has been performed on the Northumberland Universities Multi-Access Computer (NUMAC, IBM 360/67)

using Simpson's method. The formulae, though lengthy, are straightforward and easily used. To eliminate errors that can be caused by using integration intervals that are large in the region where the differential cross-section is varying rapidly, each successive point was checked. If the difference between any two consecutive points was $\gtrsim 10\%$ the interval size was reduced. This procedure, although taking considerable computer time, should have minimized the integration error $\ll 1\%$.

2.5 THE PHOTONUCLEAR INTERACTION PROCESS

2.5.1 INTRODUCTION

As has been mentioned before, when a charged particle is in motion, it is accompanied by an electromagnetic field, which can be described as a cloud of virtual photons. As a muon passes very close to a nucleon, possibly through a nucleus, one of the photons with sufficient energy can interact strongly producing one or more hadrons, usually pions. Figure 2.14 is a Feynman diagram for the photonuclear process. The muon (μ) as it passes the nucleon (N) emits a photon (γ) which is absorbed at Θ and a group of hadrons move away. It is not completely clear what happens at Θ , how the photon couples with nucleon. Because of this lack of understanding, the diagram and cross-section calculations are divided into two parts.

1. $\mu \rightarrow \mu + \gamma$

2. $\gamma + N \rightarrow N + \text{ANYTHING}$.

The first process is very well understood from the Feynman formalism and QED, but the second is still open to speculation.

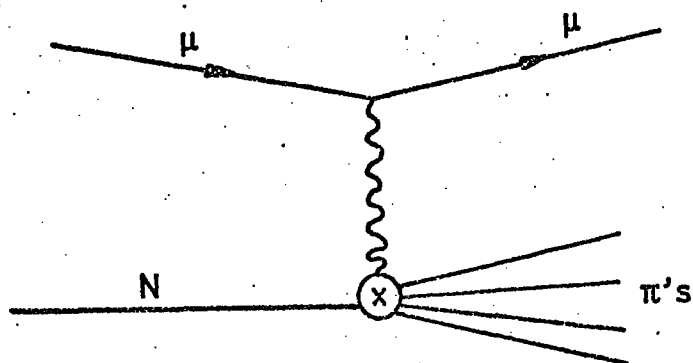


FIGURE 2.14. Feynman diagram of the photonuclear process

2.5.2 THE CROSS-SECTION FOR THE PHOTONUCLEAR PROCESS

In the past the cross-section has been calculated by estimating the virtual photon flux and then coupling this to the real photon-nucleon (γ -N) cross-section. Weizacker (1934) and Williams (1935) were the first workers. They divided the virtual photon flux into frequency components and multiplied it by a constant γ -N cross-section (σ_γ). Later Kessler-Kessler (1956) carried out a treatment using QED, but only considered the case when the four-momentum transfer to the nucleon squared (q^2 or t) was zero. (For a definition and derivation of q^2 see Appendix B.)

The most recent approach to the cross-section has been to split the virtual photon flux into longitudinally and transversely polarized components and to assume that the total cross-section (σ_{PN}) is equal to the sum of the two fluxes multiplied by their respective nucleon cross-sections.

$$\sigma_{PN} = \phi_T \sigma_T + \phi_L \sigma_L \quad (2.34)$$

ϕ_T , ϕ_L are photon fluxes for the transverse and longitudinal components respectively; σ_T , σ_L are the corresponding cross-sections for the two fluxes.

Diayasu et al. (1962) used this approach and obtained

$$\begin{aligned} \phi_T(E_\mu, E_t, t) \sigma_T(E_t, t) dE_t dt &= K \{ (E_\mu^2 + (E_\mu - E_t)^2) t \\ &\quad - 2Mc^2 E_t - \frac{t^2}{2} \} L(E_t, t) dE_t dt \end{aligned} \quad (2.35)$$

$$\phi_L(E_\mu, E_t, t) \sigma_T(E_t, t) dE_t dt = K \{ (2M^2 c^4 - t) t \} L'(E_t, t) dE_t dt \quad (2.36)$$

$$K = \frac{\alpha}{8\pi} \frac{1}{(E_\mu^2 - M^2 c^4)} \frac{1}{t^2} \quad (2.37)$$

where

E_μ is the muon initial energy,

E_t is the energy transferred (the energy of the γ),

Mc^2 is the muon rest mass,

$t = |q^2|$ is the four-momentum transfer squared,

L and L' are nucleon structure functions. Diayasu made two possible assumptions for L and L' :

$$\underline{\text{assumption a:}} \quad L(E_t, t) = \frac{4\pi\sigma}{E_t} \quad L'(E_t, t) = 0 \quad (2.38)$$

$$\underline{\text{assumption b:}} \quad L(E_t, t) = \frac{4\pi\sigma}{E_t} \left(\frac{\Lambda^2}{\Lambda^2 + t} \right)^2 \quad L'(E_t, t) = 0 \quad (2.39)$$

where $\Lambda^2 = 0.365 \text{ GeV}^2$.

In assuming $L' = 0$, he has also assumed that the longitudinal cross-section is zero. Assumption a is the 'point-like assumption' which describes a nucleon with no structure (a point nucleon). Assumption b is the 'cloud-like assumption' which describes the nucleon structure as a function of t . The structure function as defined by Diayasu is essentially the exponential charge distribution of a proton with a

radius 1.4×10^{-13} cm. Based on the cloud chamber experiment of Higashi et al. (1965), the best fit to t suggests that their data is 10% point-like and 90% cloud-like.

The most recent work has been done by Dreiss and Walecka (1964), Perl et al. (1969) and Cassiday (1971). The work of Perl and Cassiday is the basis of the calculations done here.

Writing again Equation 2.34

$$\sigma_{PN}(E_\mu, K, t) dK dt = \phi_T(E_\mu, K, t) \sigma_T(E_t, t) dK dt + \phi_L(E_\mu, K, t) \sigma_L(E_t, t) dK dt$$

(EQUATION 2.39a)

where $K = E_t - t/2M_p c^2$ ($M_p c^2$ is the proton rest mass.)

K is the photon energy in the c.m. system of the final-state hadrons. K has been preferred by many authors because it is invariant.

The muon-photon vertex ($\mu \rightarrow \mu + \gamma$) is well understood by theoreticians with the result (Cassiday, private communication, 1972)

$$\phi_T(E_\mu, K, t) = \frac{\alpha}{2\pi t} \left(\frac{K}{E_\mu^2 - M_p^2 c^4} \right) \left(1 - \frac{2M_p^2 c^4}{t} + \frac{2E_\mu(E_\mu - E_t) - \frac{1}{2}t}{E_t^2 + t} \right) \quad (2.40)$$

$$\phi_L(E_\mu, K, t) = \frac{\alpha}{2\pi t} \left(\frac{K}{E_\mu^2 - M_p^2 c^4} \right) \left(\frac{2E_\mu(E_\mu - E_t) - \frac{1}{2}t}{E_t^2 + t} \right) \quad (2.41)$$

where

α is the fine structure constant - 1/137,

E_μ is the muon energy,

E_t is the energy transferred.

The problem as before is the lack of a model for σ_T and σ_L . Models based on regge poles (Fowler, 1964), partons and vector dominance (Perl et al., 1969) have met with only limited success. Vector dominance will be considered here.

The vector dominance theory assumes that the γ -N coupling is done via one of the vector mesons (ρ, ω, ϕ). The ρ meson is considered to be the dominant coupling and to a first approximation the ω, ϕ mesons are not considered.

Sakurai (1969) used vector dominance to predict

$$\sigma_T(K, t) = \left(1 + \frac{t}{M_p^2 c^4}\right) \sigma_T(K, t=0) \quad (2.42)$$

$$R = \frac{\sigma_L(K, t)}{\sigma_T(K, t)} = \left(\frac{t}{M_p^2 c^4}\right) \left(\frac{K}{K + t/2M_p^2 c^2}\right)^2 \zeta(K) \quad (2.43)$$

where

$M_p c^2$ is the proton rest mass,

$M_\rho c^2$ is the ρ -meson mass - ~ 275 MeV,

$$\sigma_T(K, t=0) = \sigma_\gamma(E_t),$$

$\zeta(K)$ is the ratio of ρ -N total cross-section for various helicity states. $\zeta(K) \approx 1$. (Perl et al. obtained $\zeta(K) = 1.2 \pm 0.2$.)

There is now sufficient information to calculate a cross-section.

$$\begin{aligned} \sigma_{PN}(E_\mu, E_t) dE_t &= \int_{t_{\min}}^{t_{\max}} A * \left\{ \frac{\phi_T(E_\mu, E_t, t)}{(1 + t/M_p^2 c^4)^2} \right. \\ &\quad \left. + R \frac{\phi_L(E_\mu, E_t, t)}{(1 + t/M_p^2 c^4)^2} \right\} \sigma_\gamma(E_t) \frac{\partial K}{\partial E_t} dt dE_t. \end{aligned} \quad (2.44)$$

From Equation 2.37 2.39a

$$\frac{\partial K}{\partial E_t} = 1 + \frac{E_\mu}{M_p^2 c^2} - \left\{ \frac{(E_\mu^2 - M_p^2 c^4)^{\frac{1}{2}}}{((E_\mu - E_t)^2 - M_p^2 c^4)^{\frac{1}{2}}} \right\} \left(\frac{E_\mu - E_t}{M_p^2 c^2} \right) \quad (2.45)$$

with

$$t_{\min} = \frac{M_p^2 c^4 E_t}{E_\mu (E_\mu - E_t)}. \quad (2.46)$$

This comes from forward scattering, in Equation b.4 set $\theta = 0$, simplify assuming

$$\frac{(E_\mu - E_t)^2}{M_p^2 c^2} \gg 1. \quad (2.47)$$

$$t_{\max} = 2M_p^2 c^2 E_t. \quad (2.48)$$

2.39a

This comes from Equation 2.37 when $K = 0$, i.e. all of the energy transfer is given to the nucleon; or the energy of the photon in the c.m. system

of the final-state hadrons is zero.

$\sigma_{\gamma}(E_t)$ is shown in Figure 2.15. This is a survey of γ -P cross-section data from Daresbury, SLAC and DESY compiled by Lewis (1973). For this work a constant cross-section of $\sigma_{\gamma} = 125 \mu\text{b}$ has been assumed. The implications of this are discussed in the next section (Section 2.5.3).

A^* is a factor to account for the number of nucleons that the γ can interact with in a given nucleus. A is the atomic mass number. (For iron $A = 55.85 \text{ gm}^{-1}$ mole.) Gottfried and Yennie (1969) and Stodolsky (1967) discussed the A dependence of the cross-section. There are two opposing views. First, if the mean free path of the photon is large relative to the nucleus then the optical theorem applies and

$\sigma_{\text{nucleus}} = A^1 \sigma_{\text{nucleon}}$. Second, if vector dominance is completely correct, and the vector meson's mean free path is small compared to the size of the nucleus, then $\sigma_{\text{nucleus}} = A^{2/3} \sigma_{\text{nucleon}}$. The results vary, Caldwell et al. (1969) found $\sigma_{\text{PN}} \propto A^{0.9}$, while Engler et al. (1968) claim an $A^{2/3}$ dependence. A recent survey done by Cassiday (private communication, 1973) shows that at present the best estimate of the exponent is 0.8, i.e. $\sigma_{\text{nucleus}} = A^{0.8} \sigma_{\text{nucleon}}$. A value of 0.8 was used in these calculations.

The minimum energy transfer is the mass of the pion ($M_{\pi} c^2$). As Figure 2.15 implies $\sigma_{\gamma}(< M_{\pi} c^2) = 0$. The maximum transferable energy is given by the kinematics of a head-on collision:

$$E_{\text{MAX}} \approx E_{\mu} - \frac{M_{\pi} c^2}{2} \left(1 + \frac{M_{\pi}^2 c^4}{M_{\rho}^2 c^4}\right) = E_{\mu} - 0.4635 \text{ GeV} . \quad (2.49)$$

2.5.3 RESULTS AND CALCULATIONS OF THE PHOTONUCLEAR CROSS-SECTION

The calculations were performed using Equation 2.42 and assuming $\sigma_{\gamma}(E_t) = 125 \mu\text{b}$. From Figure 2.15, it can be seen that this is a good approximation for energy transfers $> 1 \text{ GeV}$. It was assumed that the

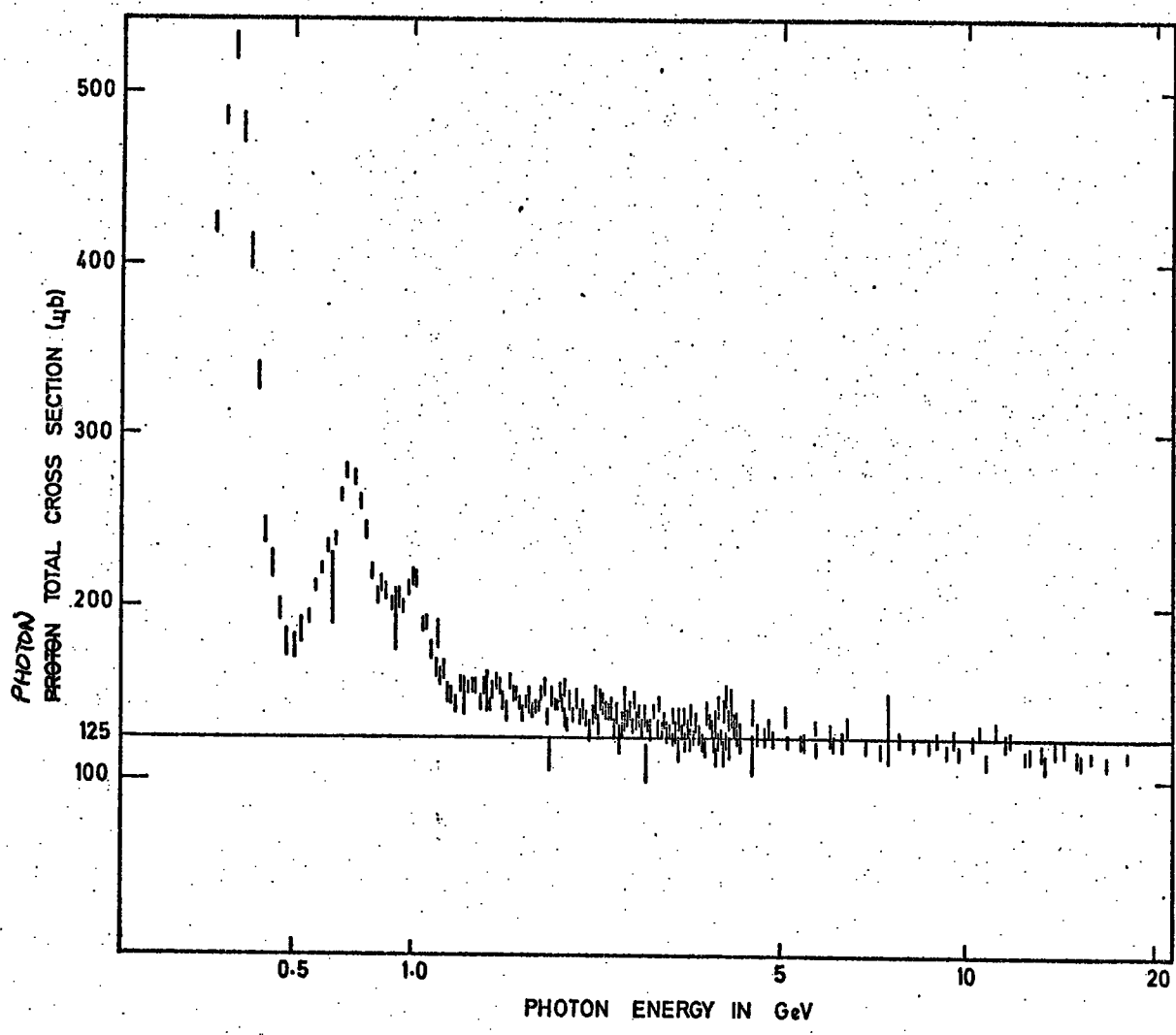


FIGURE 2.15. Photon-proton cross-section after Lewis (1973).

cross-section, $\sigma_\gamma(E_t)$, remained constant for $E_t > 20$ GeV, although it looks as though the cross-section may be falling slowly. For $E_t \leq 1$ GeV, the discrepancy becomes very great, a maximum of 400%. In Figure 2.16, the results of the calculations are presented. Figure 2.17 shows the same results with a correction (dashed line) for resonances in the γ -P cross-section. It is believed that the assumption of $\sigma_\gamma = \text{constant}$ is justifiable since in the region where the resonance peaks occur, the cross-section for the knock-on and the direct pair production processes are orders of magnitude larger. The present experiment is only looking at the total cross-section. Any error in the photonuclear cross-section in this region is unimportant. If the cross-section for photo-production alone was being studied then it would have been important. Tables of calculated results are presented in Appendix A.

The errors involved are hard to estimate, due to the lack of knowledge about the γ -N vertex and the lack of experimental results. Fortunately, the cross-section is nowhere dominant, except possibly at extreme high energy transfers.

2.5.4 CONSIDERATIONS IN THE CALCULATION

As in the case of direct pair production, the photonuclear cross-section must be integrated numerically, Figure 2.18 shows how $\sigma_{PN} dt$ varies with t for a 100 GeV muon. The curves are everywhere, except at the peak, steep. Care should be taken particularly at the t_{\min} end to ensure that the cross-section is not under- or over-estimated. As in the direct pair production integration, the difference between two successive integration points was monitored and not allowed to vary more than 10%. This ensures an accuracy in integration of $\ll 1\%$.

If σ_γ is taken as a constant (125 μb) the cross-section is continuous and non-negative to energy transfers $< M_\pi c^2$. As is shown in Figure 2.15,

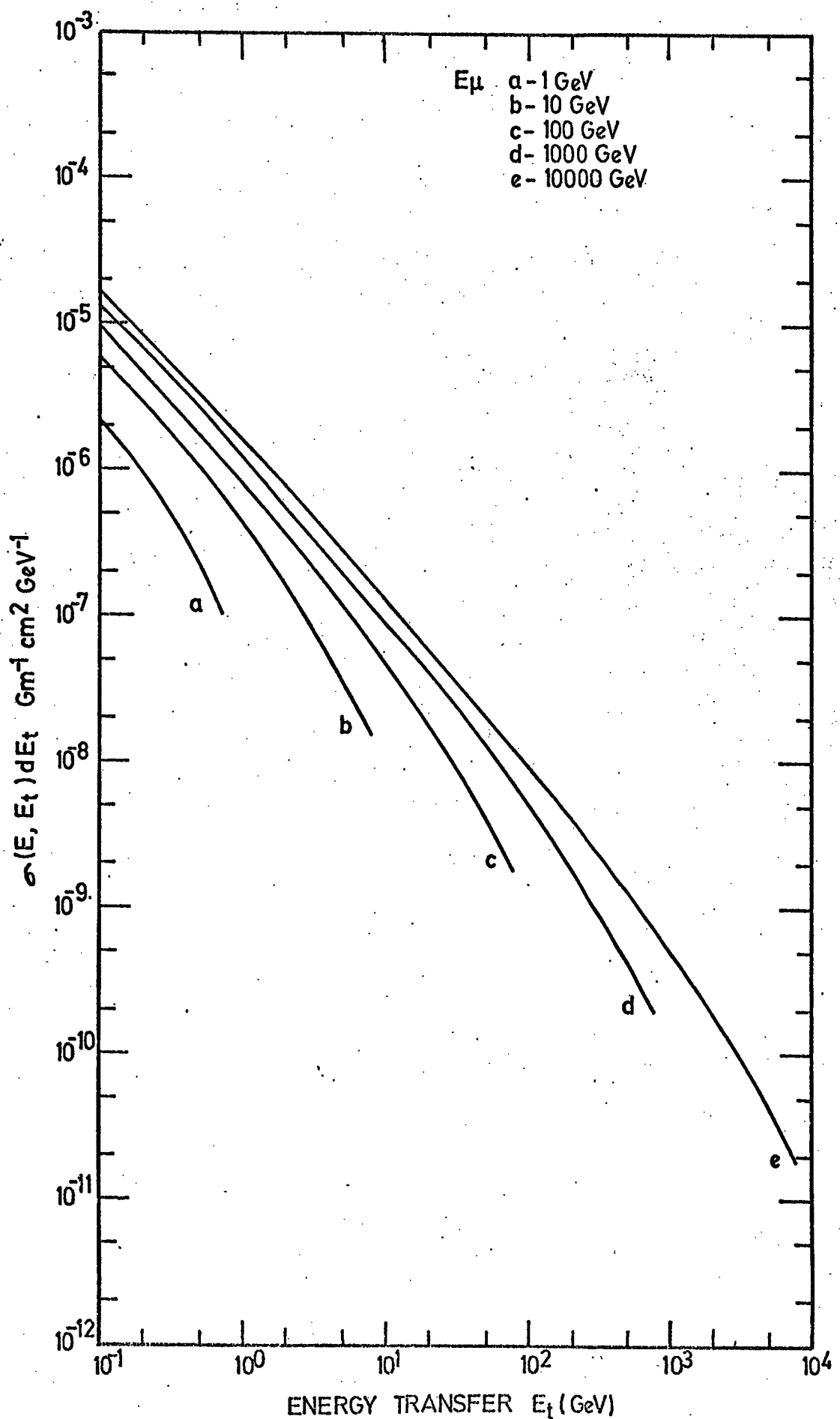


FIGURE 2.16. The photonuclear cross-section for muons in iron assuming constant photon-nucleon cross-section (125 μb)

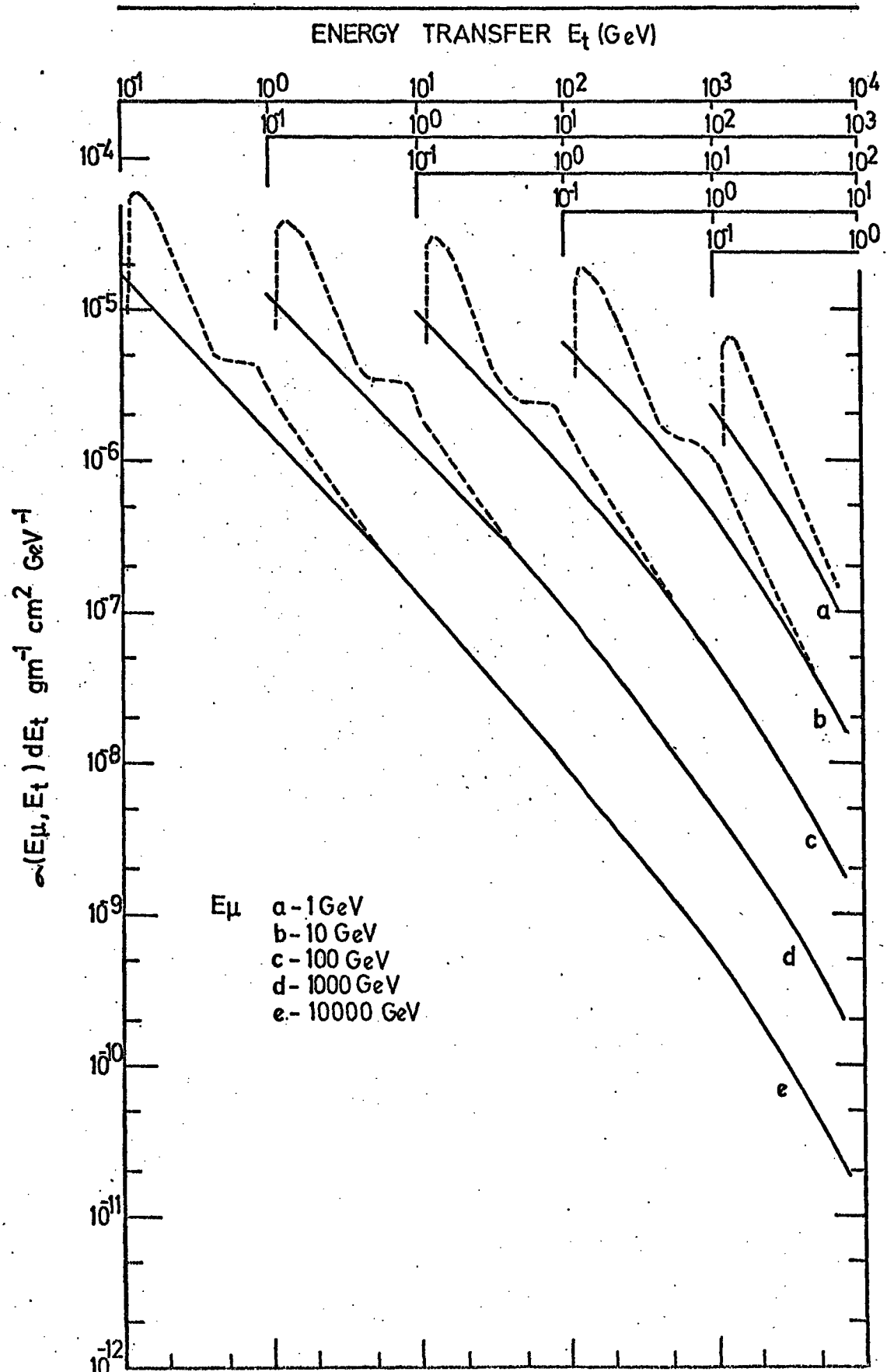


FIGURE 2.17. The photonuclear cross-sections. Dashed line is cross-section taking into account the resonant peak in photon-nucleon cross-section.

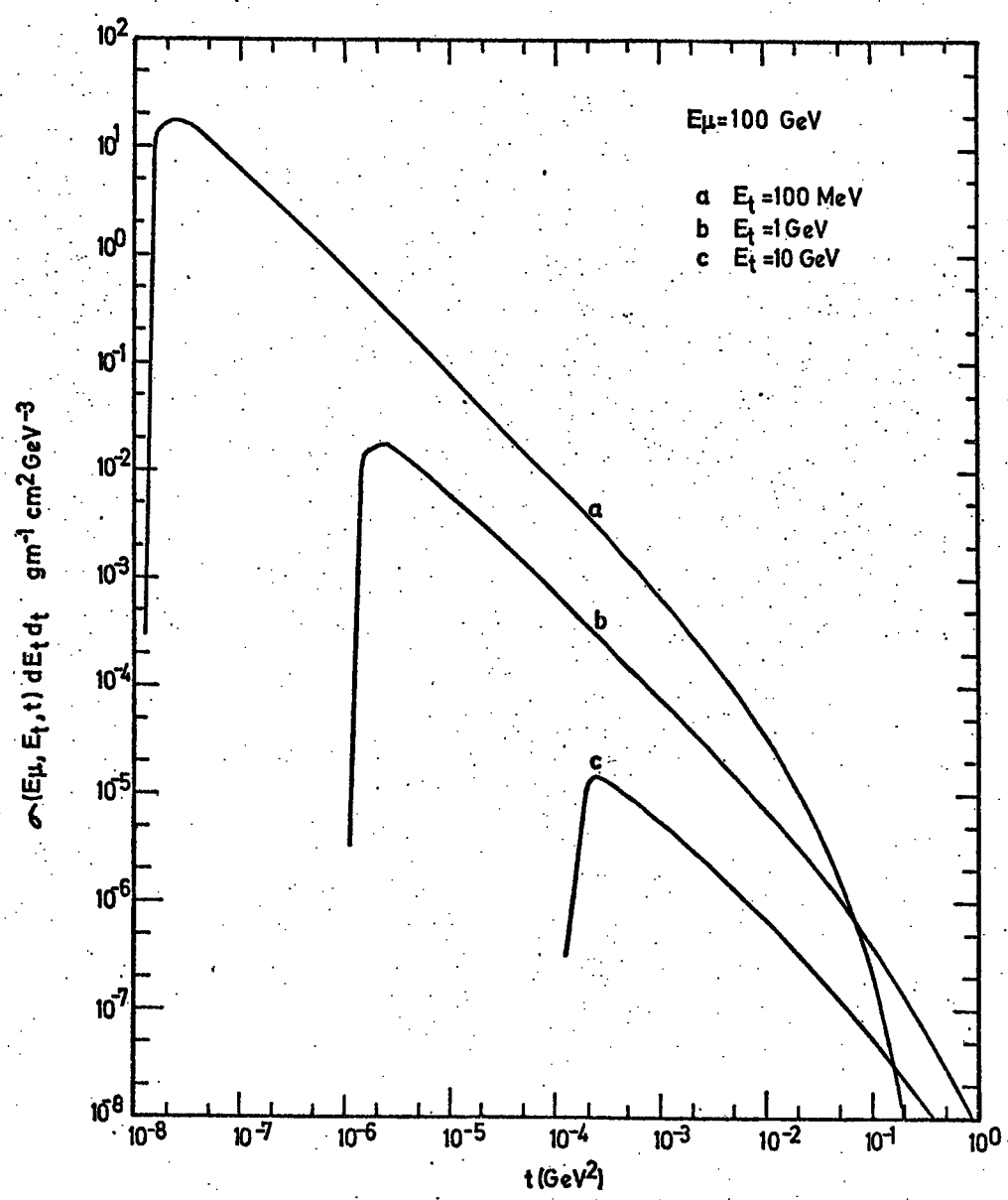


FIGURE 2.18. The differential cross-section as a function of four-momentum transfer squared.

the cross-section $\sigma_{\gamma}(E_t) = 0$ for $E_t < M_{\pi}c^2$. Therefore, although calculations for $E_t < M_{\pi}c^2$ can be carried out (using a constant σ_{γ}) they are not meaningful.

2.6 RESULTS AND OBSERVATIONS

2.6.1 INTRODUCTION

As mentioned earlier in this chapter the theoretical calculations reported in this thesis are based on the knock-on (KO) cross-section of Bhabha (Section 2.2), the bremsstrahlung (BREM) cross-section of Petrukhin and Shestakov (Section 2.3), the direct pair production (DPP) cross-section of Petrukhin and Kokoulin (Section 2.4), and the photonuclear (PN) cross-section derived on the basis of the work done by Cassiday and Perl (Section 2.5). The results of the calculations are presented graphically in this section followed by some comments and observations on the results. (Complete numerical tables or the calculations are presented in Appendix A.)

2.6.2 COMPARISON OF THE INTERACTION CROSS-SECTIONS

In Figures 2.19 to 2.23 the differential cross-sections as a function of energy transfer for the four processes at five muon energies are plotted. Two plots of the photonuclear cross-section are shown; one (solid line) is the result assuming that the photon-nucleon cross-section remains constant, and the other (dashed line) is the result when the cross-section is corrected for the resonances in the γ -N cross-section.

The critical energies for each process as a function of muon energy are presented in Figure 2.24. The critical energy is defined as the

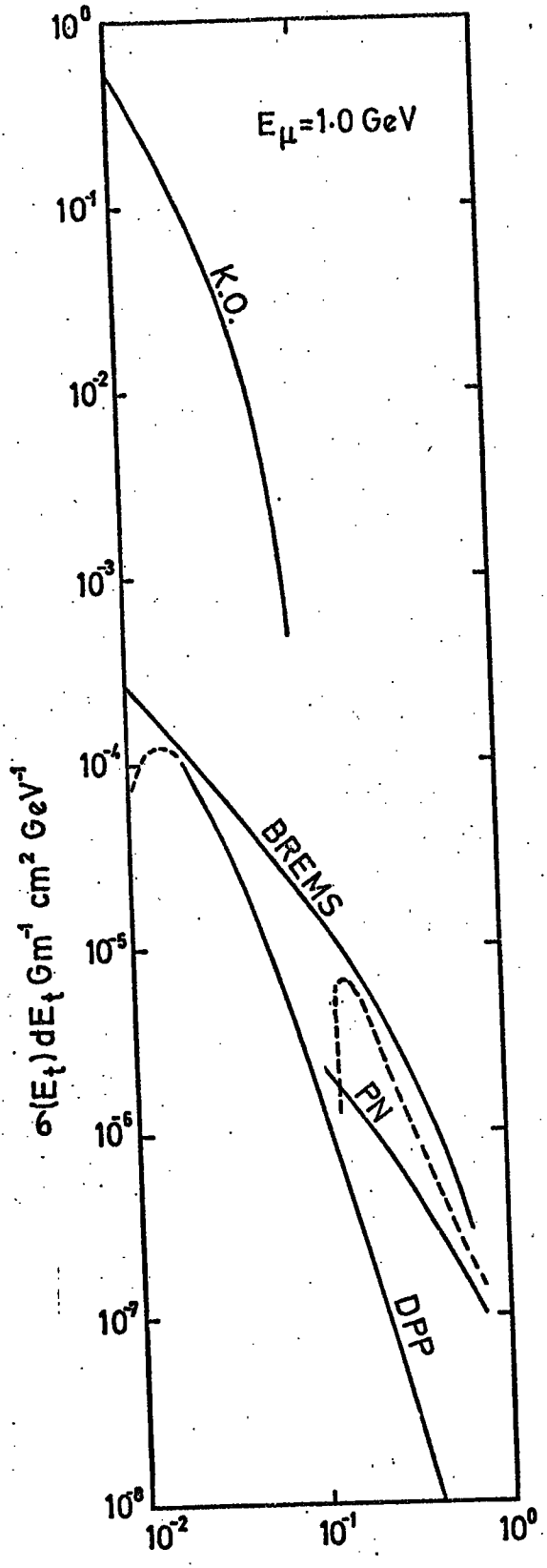


FIGURE 2.19.

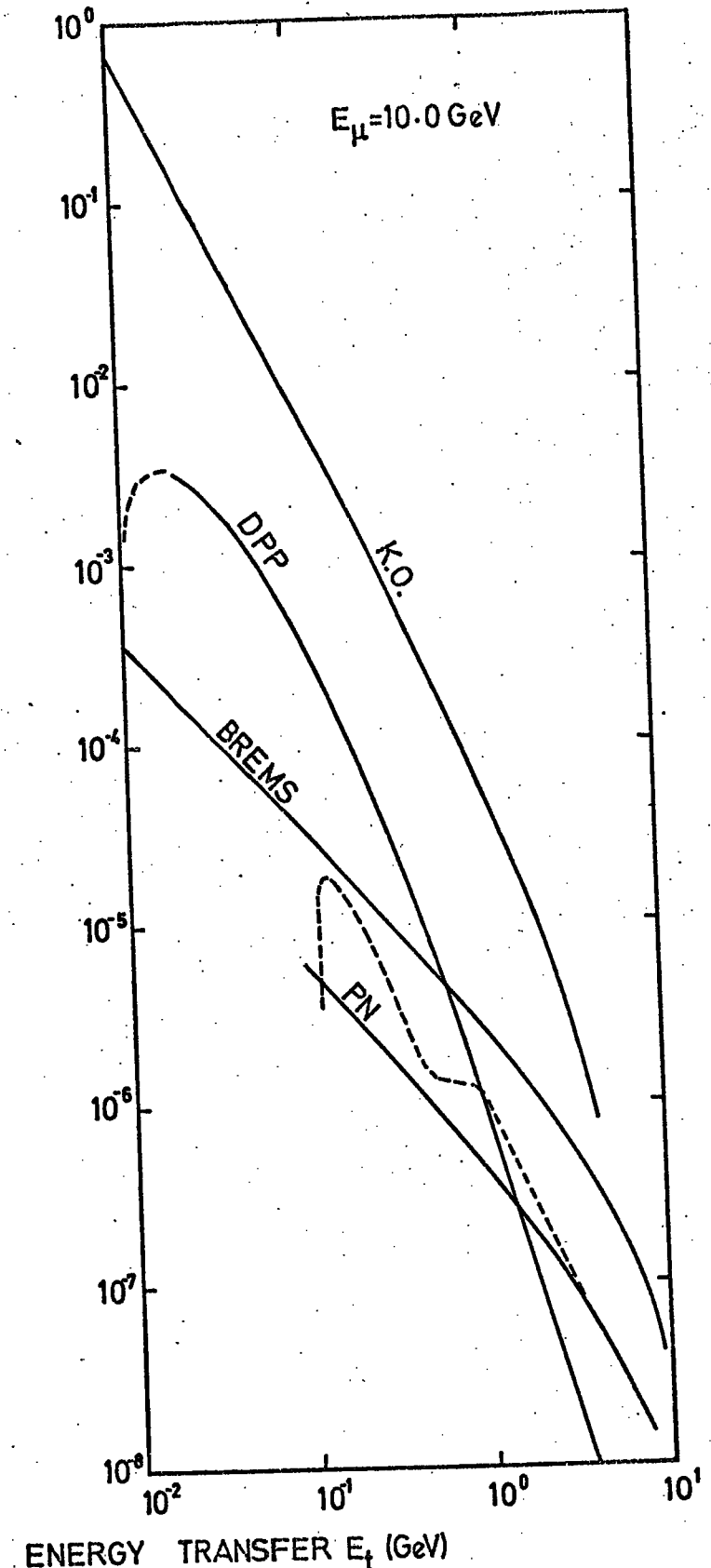


FIGURE 2.20

The differential cross-sections for the interaction processes of muons in iron ((knock-on (KO), bremsstrahlung (BREMS), direct pair production (DPP), photonuclear (PN)).

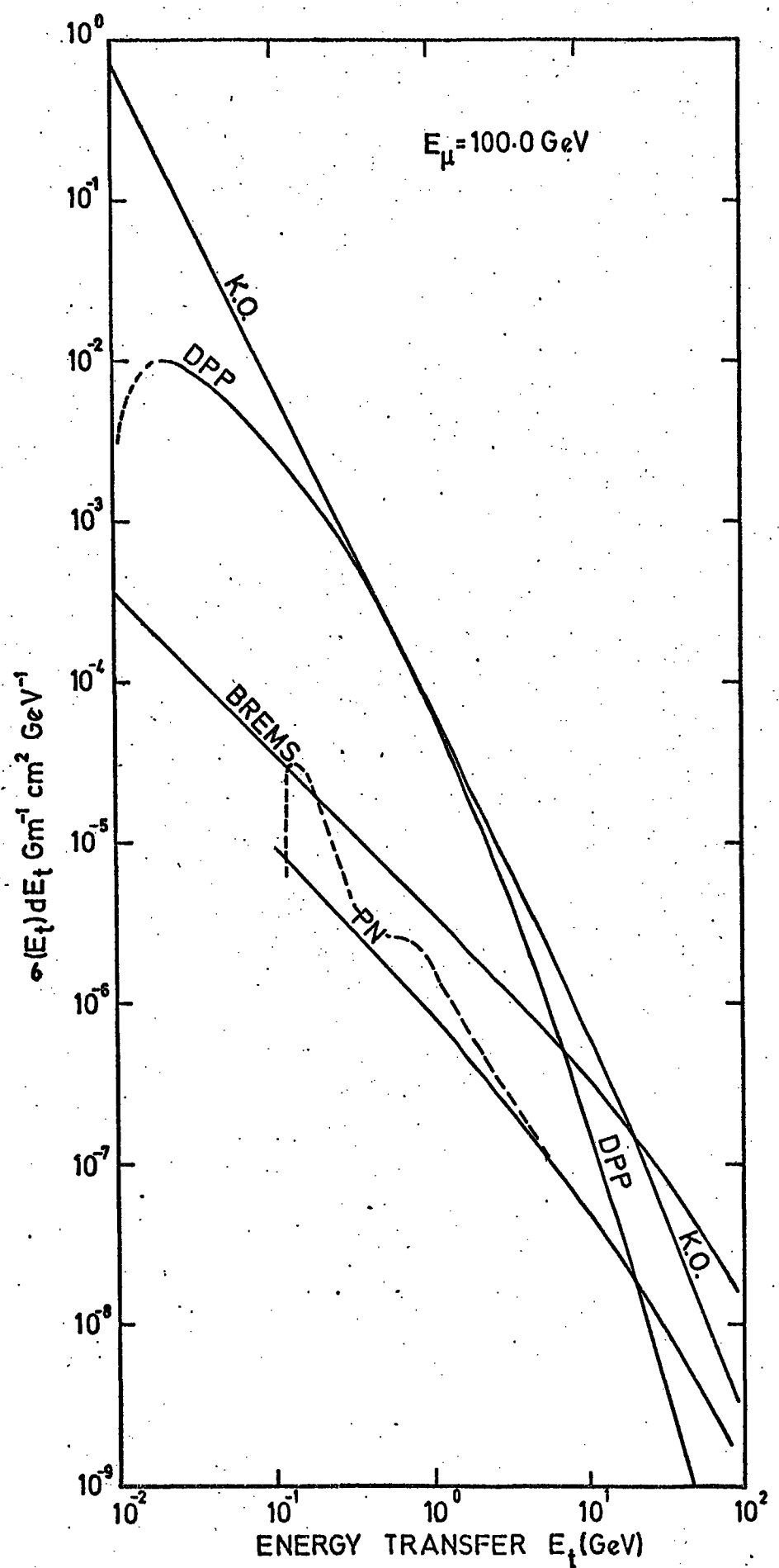


FIGURE 2.21. The differential cross-sections for the interaction processes of muons in iron ((knock-on (KO), bremsstrahlung (BREMS), direct pair production (DPP), photonuclear (PN)).

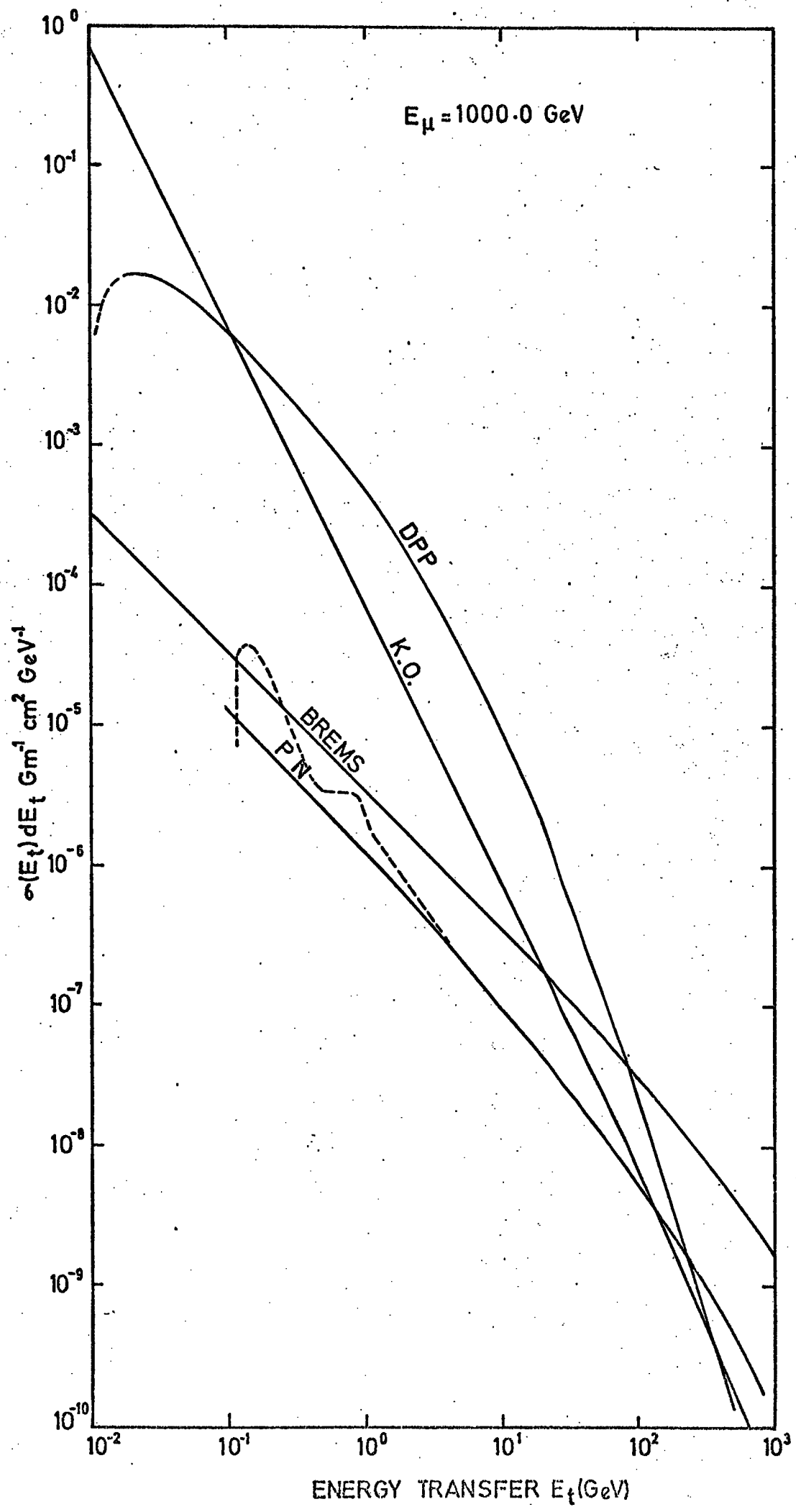


FIGURE 2.22. The differential cross-sections for the interaction processes of muons in iron (knock-on (KO), bremsstrahlung (BREMS), direct pair production (DPP), photonuclear (PN)).

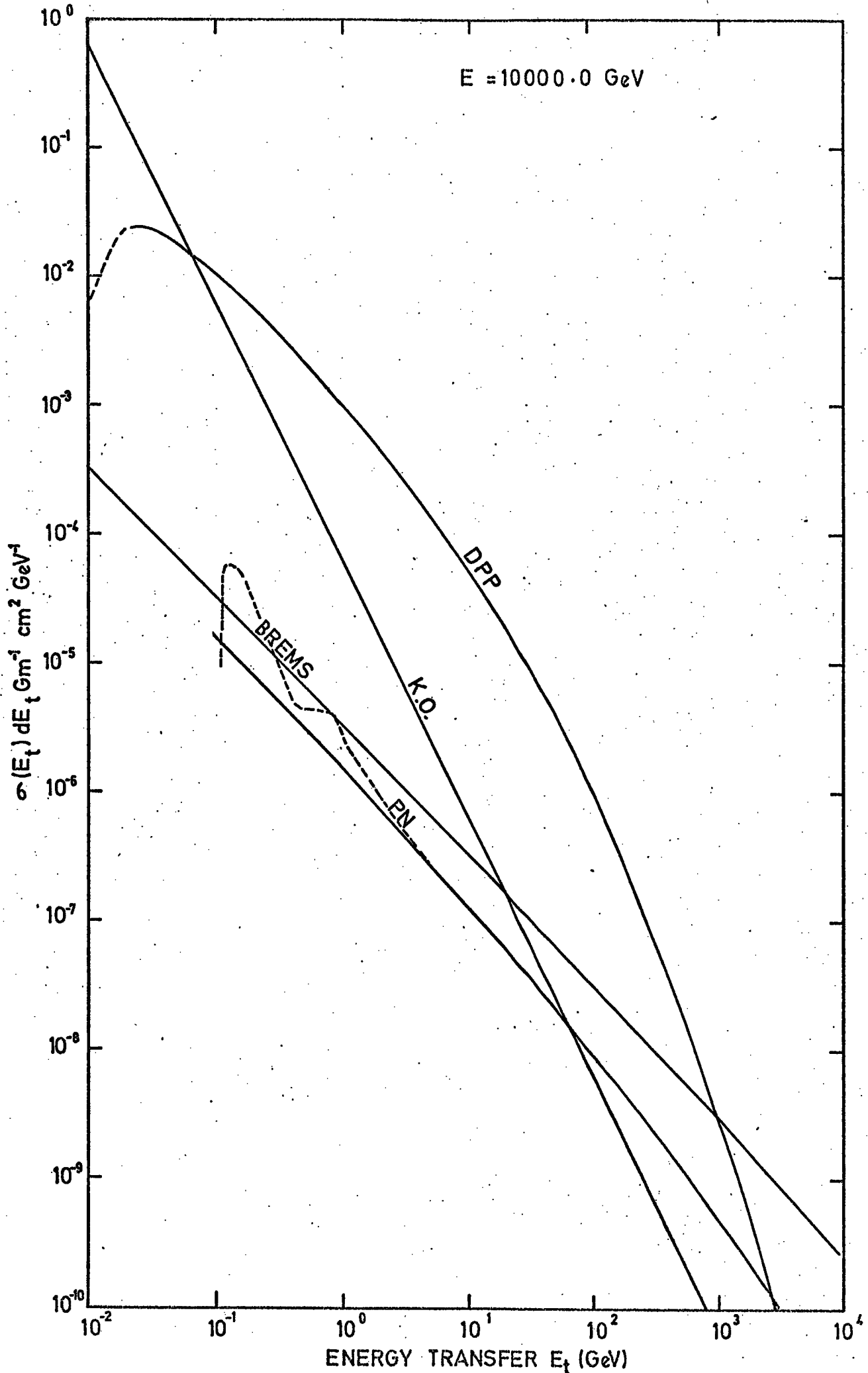


FIGURE 2.23. The critical energies for the interaction processes of muons in iron. THE DIFFERENTIAL CROSS-SECTION OF MUONS IN IRON.

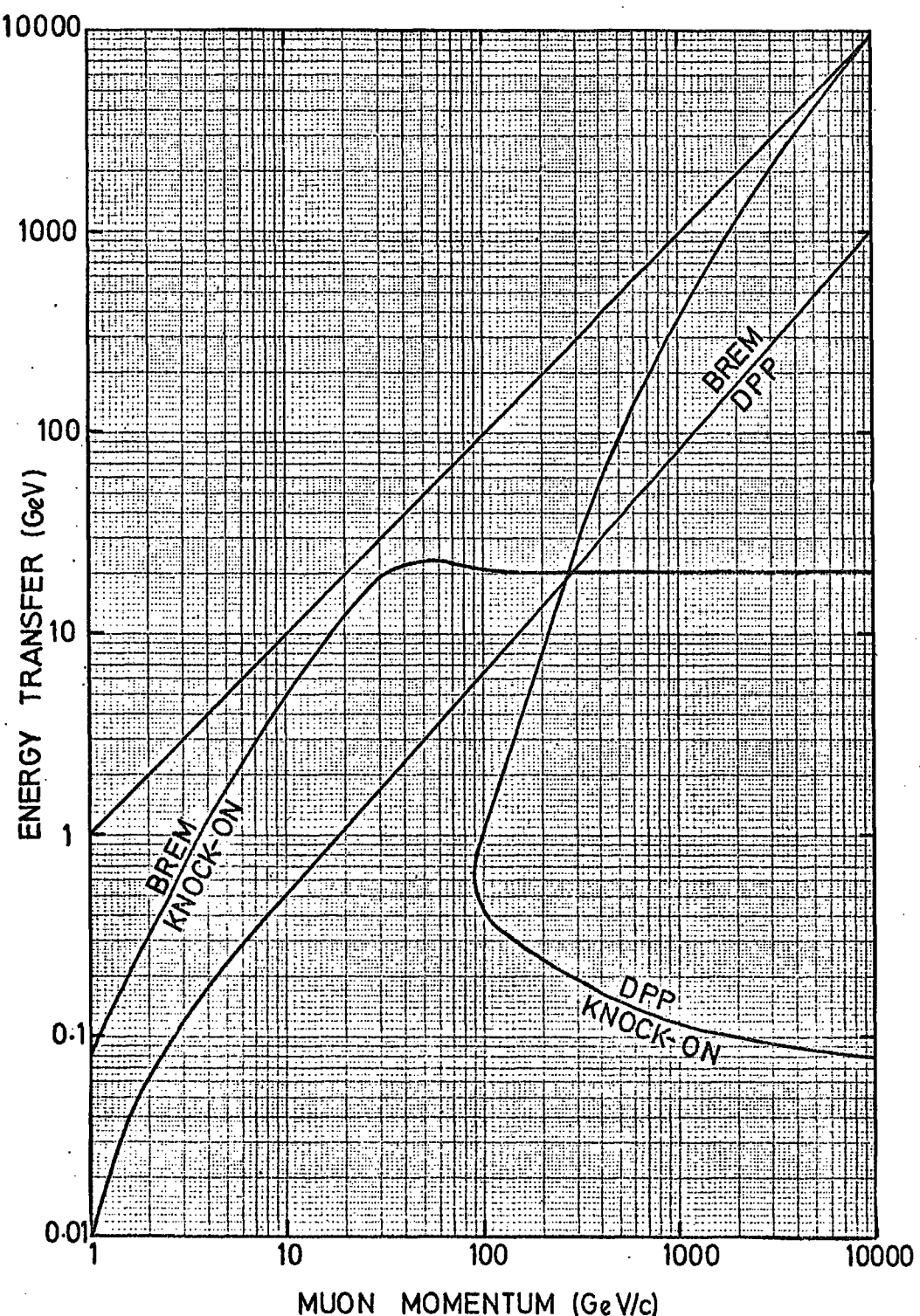


FIGURE 2.24. The differential cross-sections for the interaction processes of muons in iron (knock-on (KO), bremsstrahlung (BREMS), direct pair production (DPP), photonuclear (PN)).

THE CRITICAL ENERGIES FOR THE INTERACTION
PROCESSES OF MUONS IN IRON

energy transfer when the cross-sections for two competing processes are equal. This means that the curve labelled BREM/KNOCK-ON is where

$\sigma_{\text{BREM}}/\sigma_{\text{KO}} = 1$; the curve labelled BREM/DPP is where $\sigma_{\text{BREM}}/\sigma_{\text{DPP}} = 1$; the curve labelled DPP/KNOCK-ON is where $\sigma_{\text{DPP}}/\sigma_{\text{KNOCK-ON}} = 1$. The photonuclear cross-section is not included because it is nowhere important except possibly at $E_\mu \sim 1$ GeV and as E_t approaches E_μ , it can be seen in Figure 2.22. One point of interest is where

$\sigma_{\text{BREM}}/\sigma_{\text{DPP}} = \sigma_{\text{BREM}}/\sigma_{\text{KO}} = \sigma_{\text{DPP}}/\sigma_{\text{KO}} = 1$, this occurs at $E_\mu \approx 280$ GeV and $E_t \approx 20$ GeV.

Figure 2.25 uses the critical energies in Figure 2.24 as the demarcation for regions (shown shaded) in which the labelled process is dominant. If photoproduction were included, it might be expected to occupy the region immediately next to the $E_t = E_\mu$ line.

Figures 2.26a,b,c,d show which process is dominant for a given muon energy and energy transfer.

Figures 2.27a,b,c,d,e,f present the integral cross-section for a minimum energy transfer as a function of muon energy, i.e.

$$\sigma(E_\mu, E_t > E_{\min}) = \int_{E_{\min}}^{E_{\max}} \sigma(E_\mu, E_t) dE_t . \quad (2.50)$$

2.6.3 COMMENTS ON THE CALCULATED INTERACTION CROSS-SECTION

The following is a summary of important points which can be seen from the graphical results.

1. The only apparent region where the photonuclear process can be successfully studied corresponds to muon energies ~ 1 GeV and large fractional energy transfers ($> 10\%$). For fractional energy transfers $> 10\%$ the contribution from the photonuclear process $\sim 33\%$. For energy transfers $E_t > 0.8 E_\mu$ photoproduction may be the dominant process.

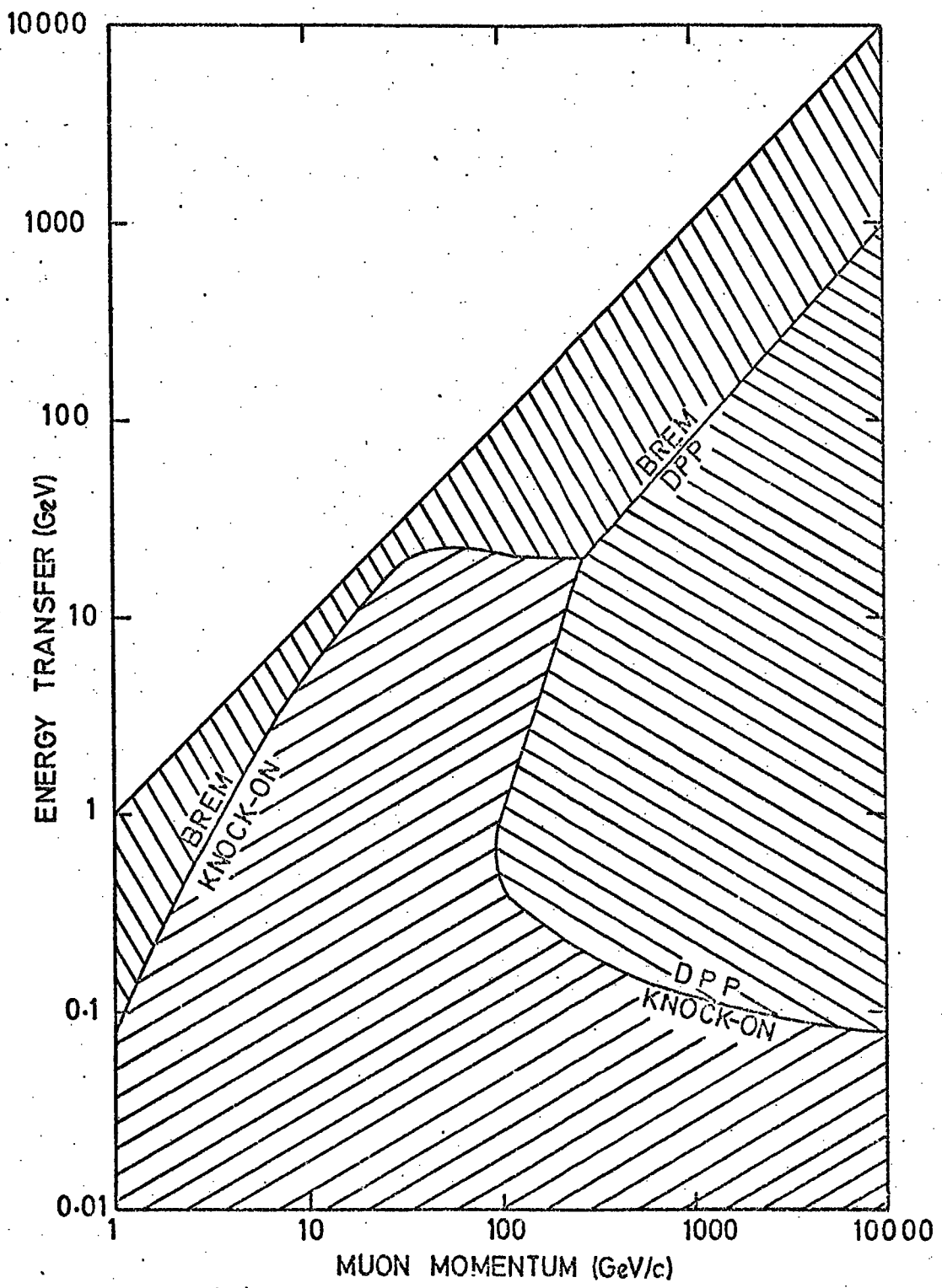


FIGURE 2.25. Regions of dominance for the interaction processes of muons in iron.

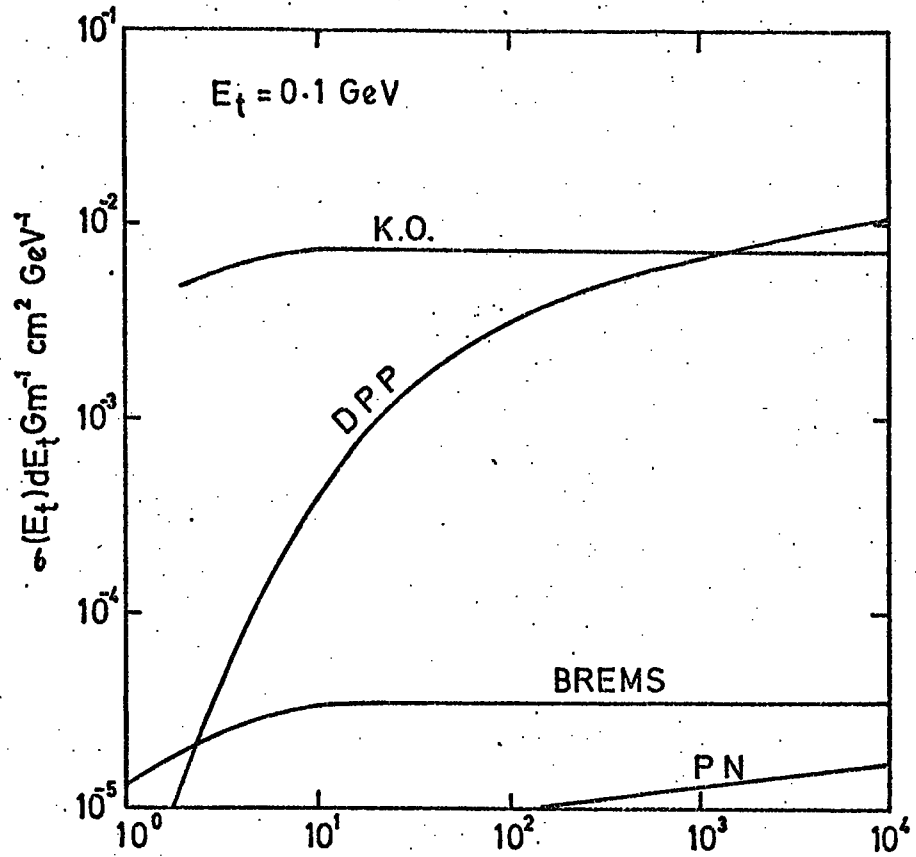


FIGURE 2.26(a). The cross-sections for a given energy transfer

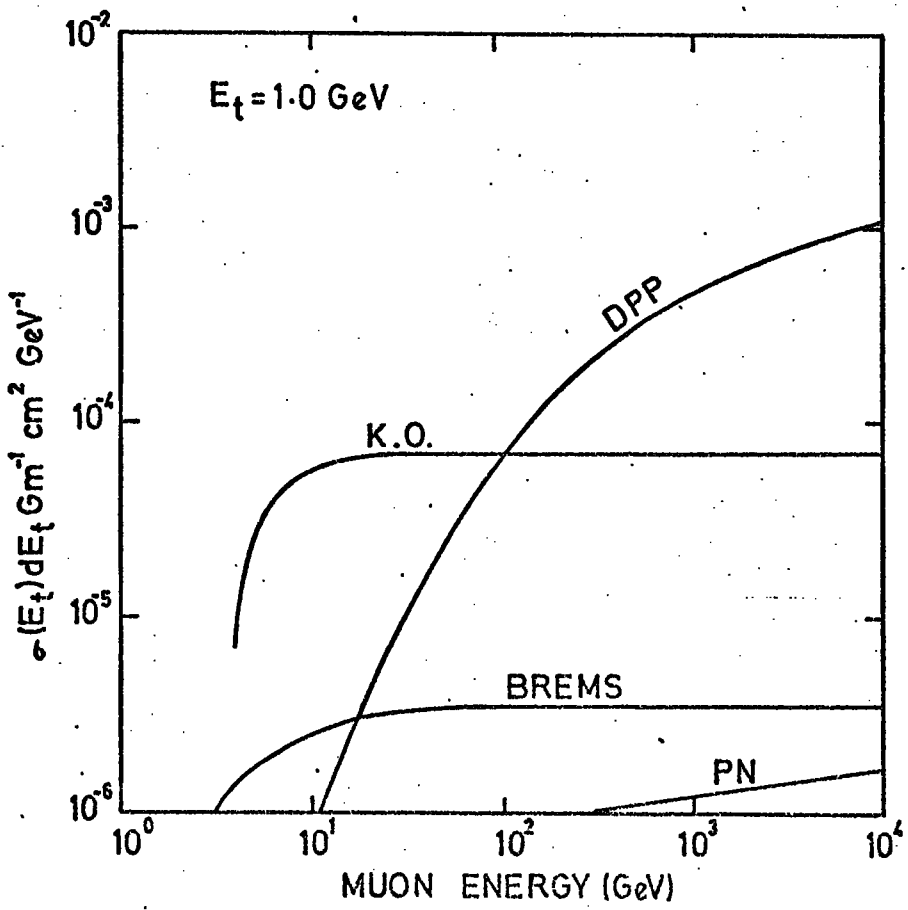


FIGURE 2.26(b). The cross-sections for a given energy transfer.

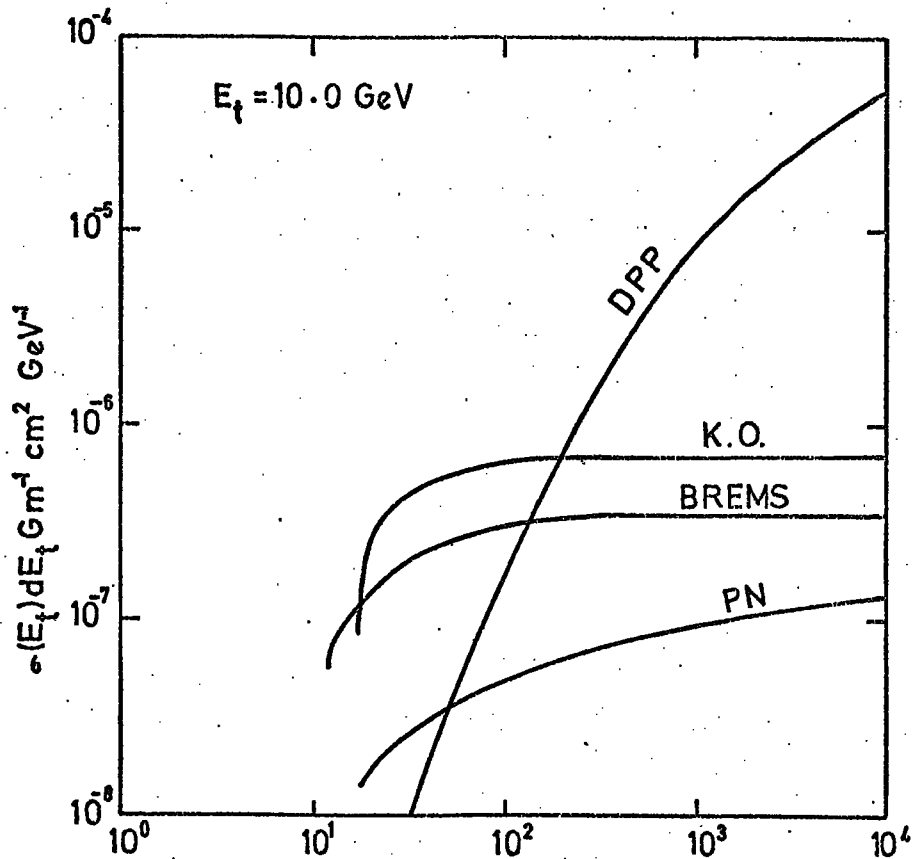


FIGURE 2.26(c). The cross-sections for a given energy transfer

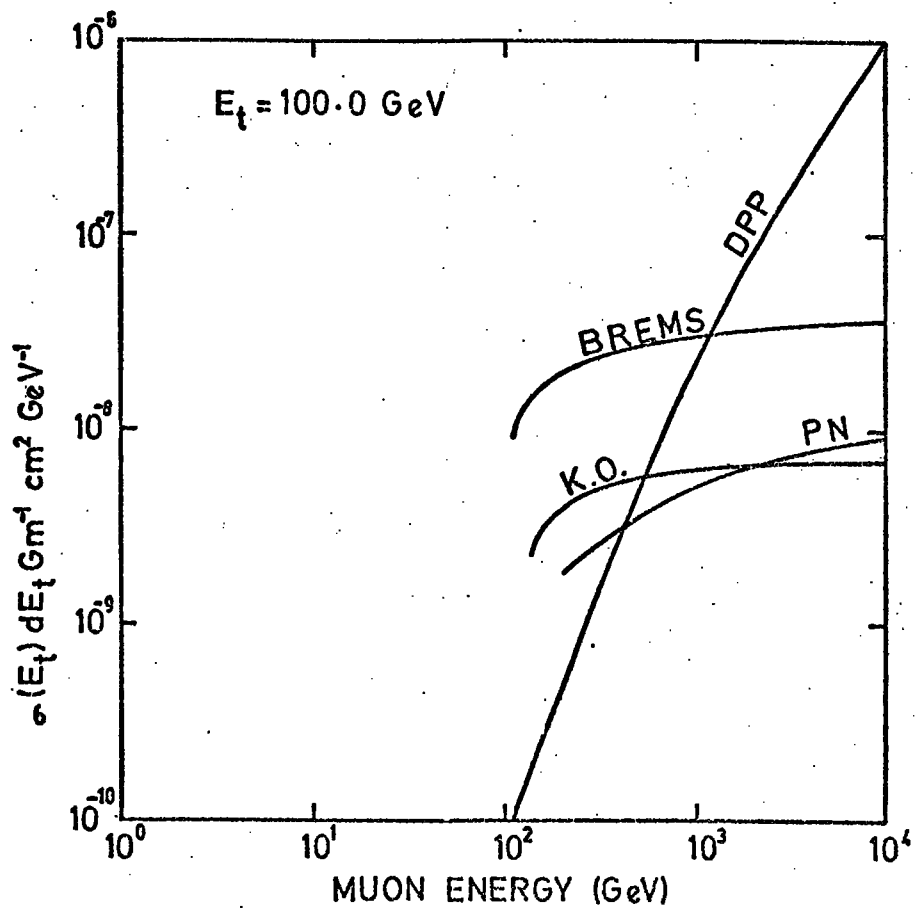


FIGURE 2.26(d). The cross-sections for a given energy transfer.

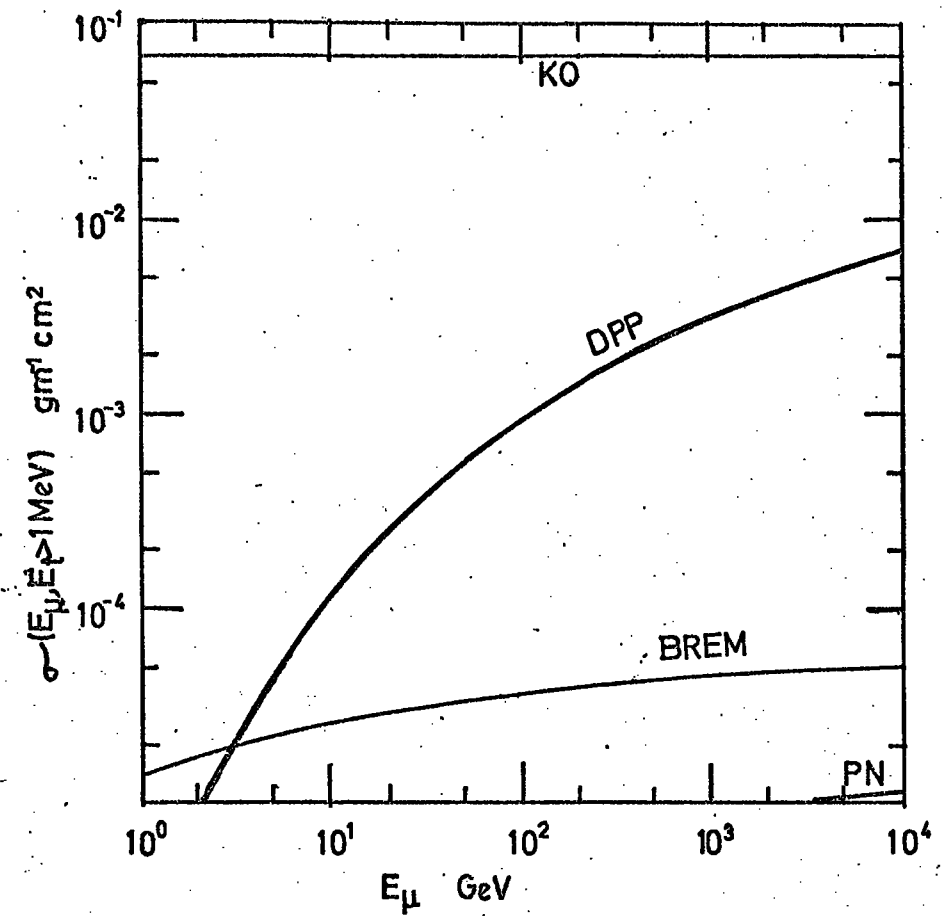


FIGURE 2.27(a). The integral cross-section greater than a given energy transfer.

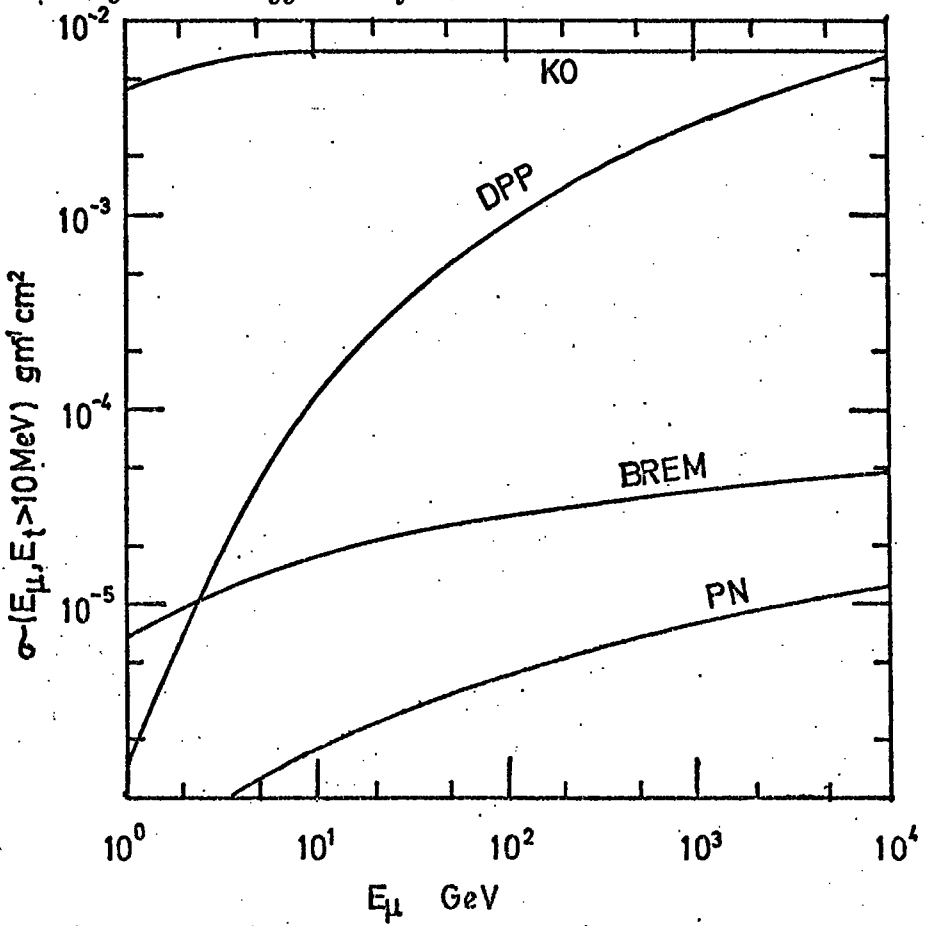


FIGURE 2.27(b). The integral cross-section greater than a given energy transfer.

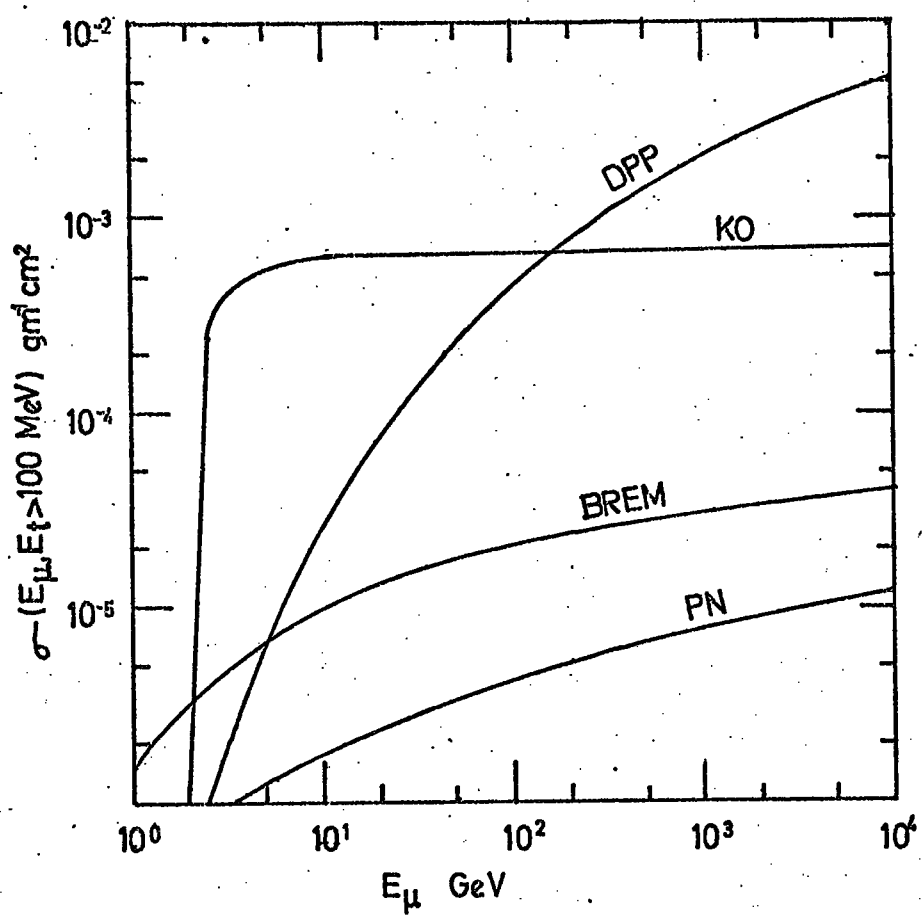


FIGURE 2.27(c). The integral cross-section greater than a given energy transfer.

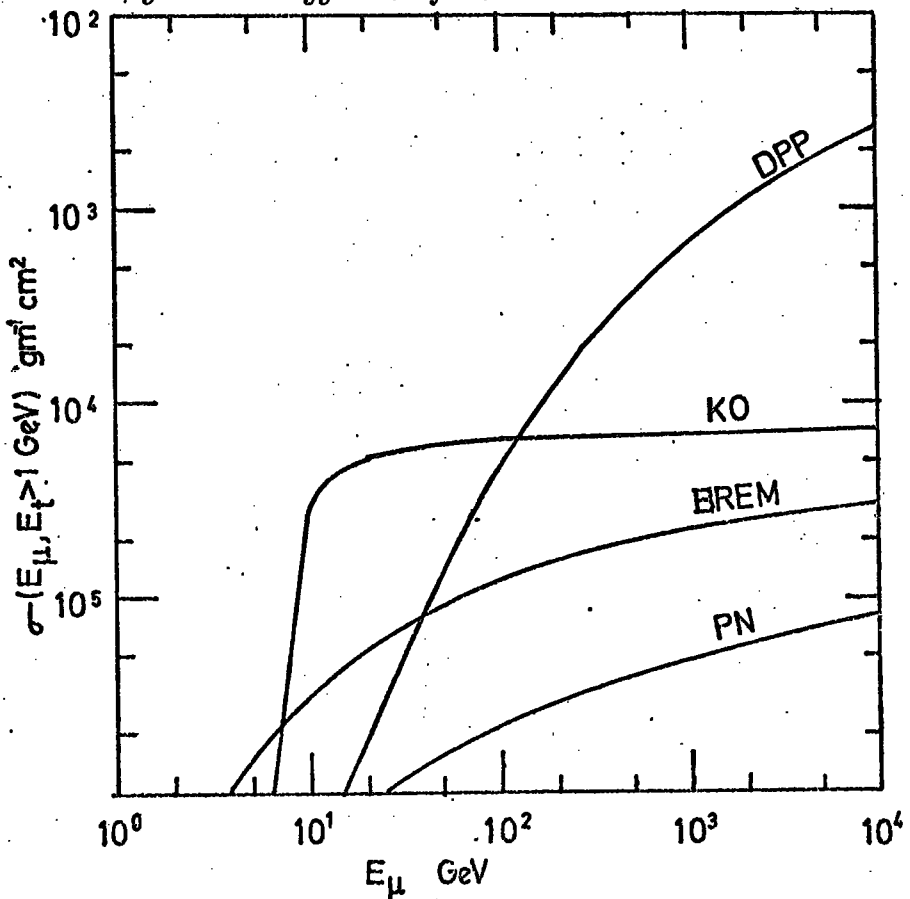


FIGURE 2.27(d). The integral cross-section greater than a given energy transfer.

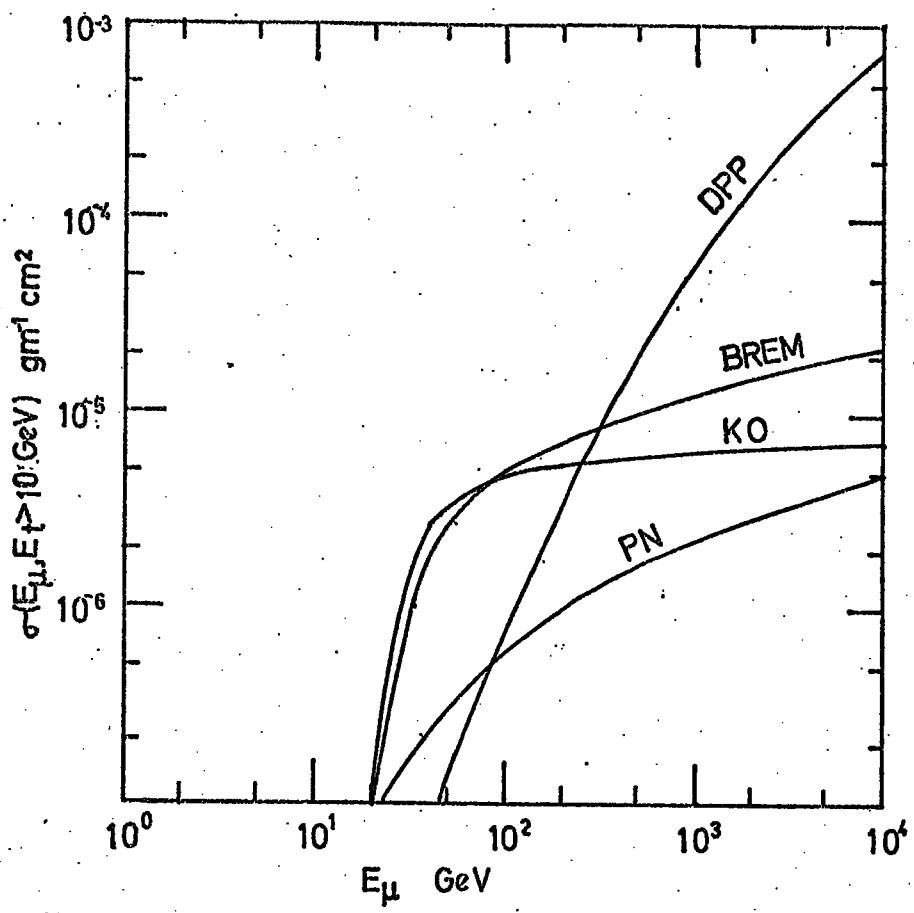


FIGURE 2.27(e). The integral cross-section greater than a given energy transfer.

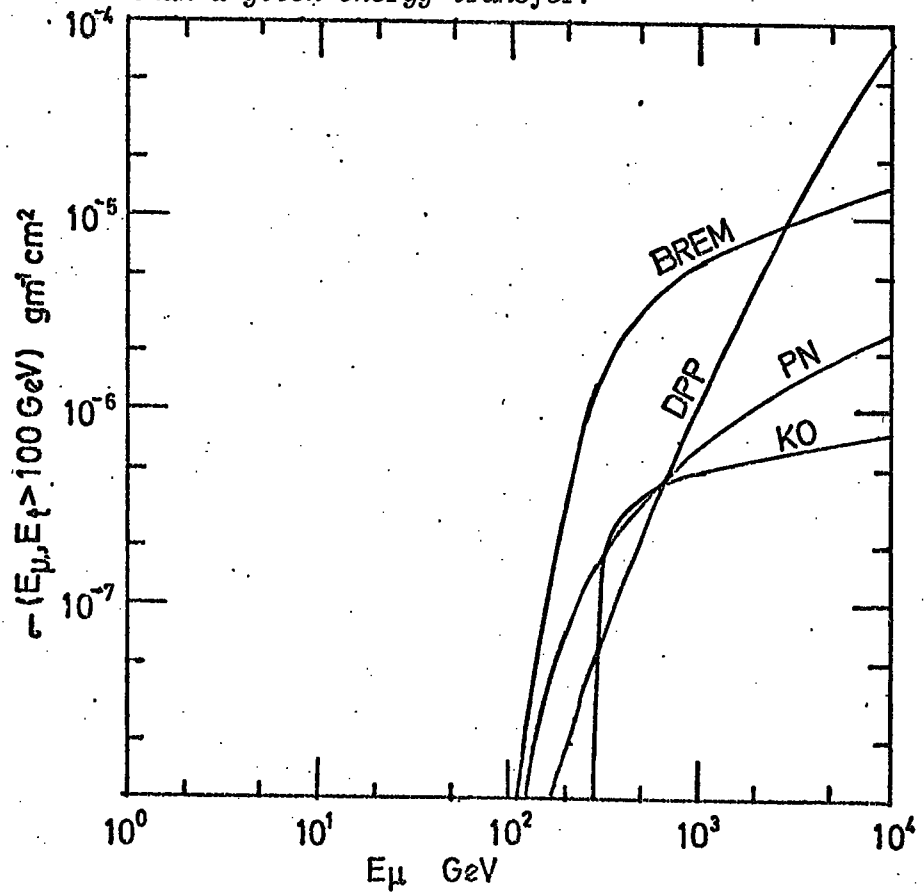


FIGURE 2.27(f). The integral cross-section greater than a given energy transfer.

2. For muon energies to 10 TeV, all energy transfers < 80 MeV will be via the knock-on process.

3. The knock-on process will never dominate for energy transfers > 20 GeV. Direct pair production will be dominant to $E_t \approx 0.1 E_\mu$ and bremsstrahlung will be dominant to $\sim E_\mu$.

4. All very large fraction energy transfers ($E_t/E_\mu \gtrsim 0.1$) are via the bremsstrahlung process.

5. For $E_\mu > 280$ GeV, the DPP-BREM critical energy is approximately proportional to E ($E_c \approx 0.1 E_\mu$).

6. Although direct pair production for muon energies > 400 GeV is not dominant over the entire E_t range, it is very probable that if a muon of energy > 400 GeV does interact, it will do so via the direct pair production process.

7. For muons with $E_\mu < 100$ GeV, direct pair production makes no significant contribution to the energy loss.

8. At $E = 280$ GeV and $E_t = 20$ GeV, all three electromagnetic cross-sections are equal.

2.6.4 CONCLUSIONS

From the results three general conclusions can be drawn with respect to muon energy. Firstly, for $E_\mu \sim 1$ GeV it should be possible, by studying a very narrow energy transfer range ($E_t \gtrsim 0.1 E$), to investigate the photonuclear process.

Secondly, for moderate muon energies (10 GeV $< E_\mu < 400$ GeV), the knock-on and bremsstrahlung processes can be studied. The knock-on process will be the main means of energy loss, but for energy transfers greater than the knock-on maximum transferable energy (Equations 2.5, 2.6), the bremsstrahlung process will dominate.

Thirdly, for high energy muons ($E_\mu > 400$ GeV), although low energy transfers will be via the knock-on process, direct pair production will be the dominant process and easily studied over a very large region of energy transfers. Very large energy transfers will be via the bremsstrahlung process.

CHAPTER 3

THE MAGNETIC AUTOMATED RESEARCH SPECTROGRAPH (MARS)

3.1 INTRODUCTION

MARS has been in operation for four years, being used to study the muon charge ratio (Hume 1975), the interaction asymmetry (Hamdan 1972), the absolute rate of energy loss by muons in iron (Wells 1972), and the muon energy spectrum to 800 GeV (Whalley 1974). As a consequence, the MARS spectrograph has been described in detail in several publications (Ayre et al. 1969, 1972(a),(b) and Thompson and Wells 1972) and in several unpublished works. Therefore, the description given here is brief with attention being given to those aspects of the apparatus which are unique or of particular importance to this experiment.

MARS is a 7.3 m tall muon spectrograph consisting of four 71 ton solid iron magnet blocks with particle detectors placed above and below each block (see Figures 3.1 and 3.2). Scintillation counters (SC) are placed at levels 1, 3 and 5 (level 1 is the lowest measuring level, Figure 3.2). The scintillators provide a three-fold coincidence for a main trigger of the apparatus. The scintillators also provide pulse height information for this experiment. Momentum selector trays (MST), which consist of four layers of ~ 1.5 cm diameter neon flash tubes, are also placed at levels 1, 3 and 5. Information from tracks in these three trays is used to determine whether the particle is of high momentum ($P_\mu \gtrsim 100$ GeV). At each of the levels 1, 2, 3, 4 and 5 are placed measuring trays (MT) which each consist of eight layers of ~ 0.55 cm internal diameter neon flash tubes.

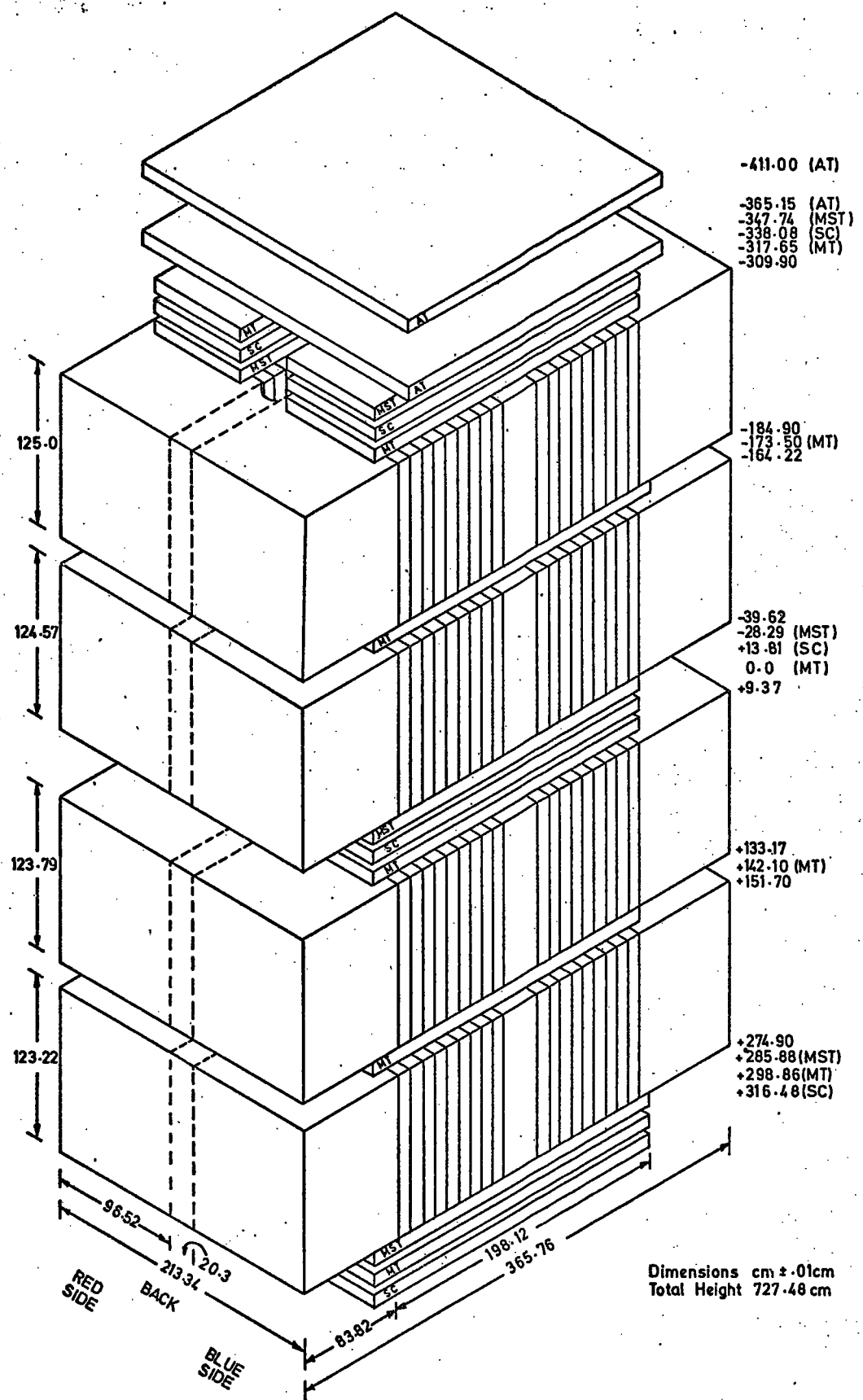
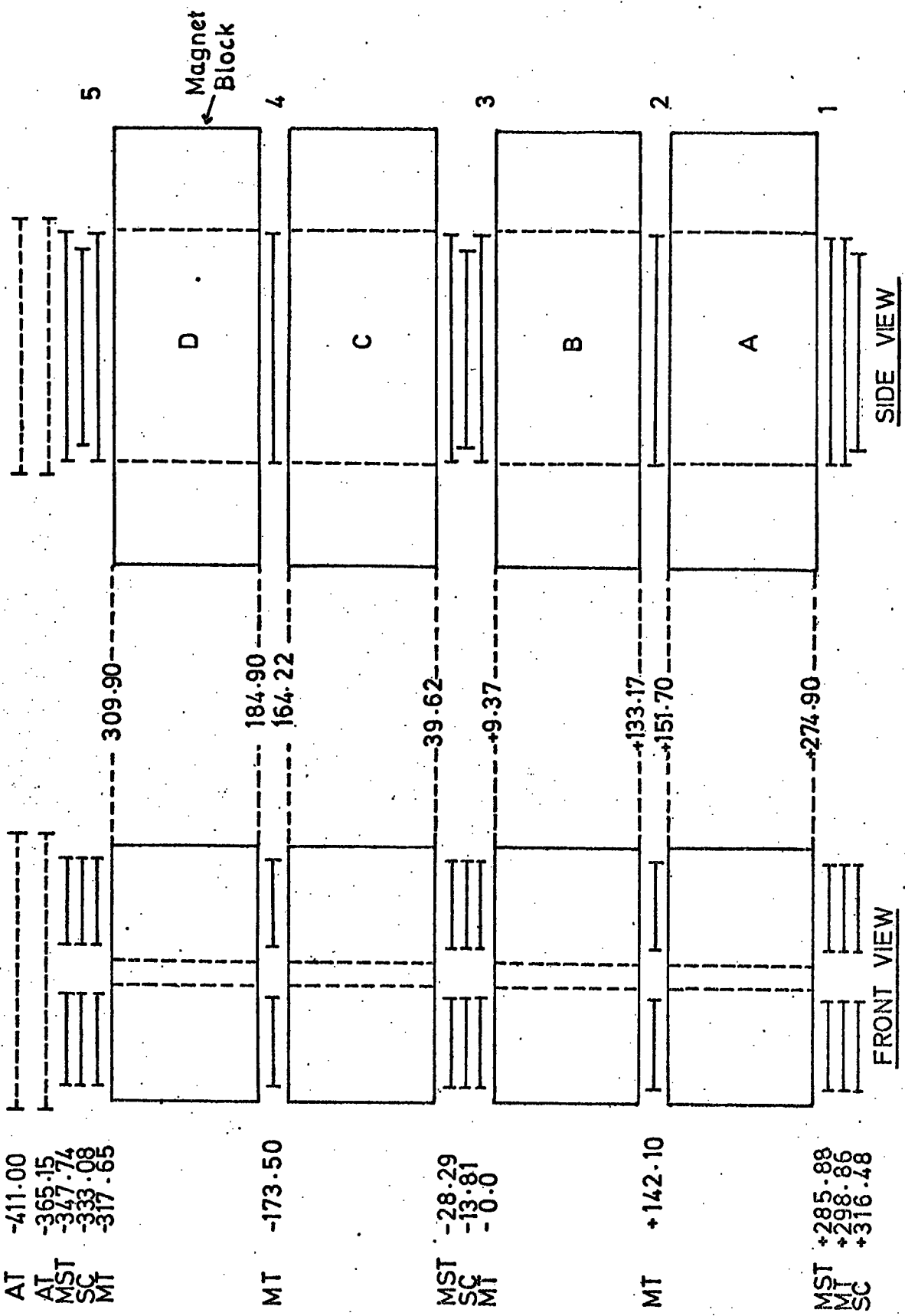


FIGURE 3.1. The muon automated research spectrograph (MARS).



MST Momentum Selector Tray
 MT Measuring Tray
 SC Scintillation Counter

All dimensions are given in cm. and are accurate to 0.1cm.

FIGURE 3.2. The front and side view of MARS.

These high resolution tubes give a particle trajectory location with an accuracy of 0.3 mm^{1N} up to five measuring levels, three being the necessary minimum required to determine the momentum of the particle. The over-definition is to allow for electron shower accompaniment which becomes very probable for high energy muons ($E_\mu \gtrsim 1$ TeV). Both the measuring tray data and the pulse height information from the scintillators are digitized and are stored on a magnetic disk via the on-line IBM 1130 computing system which is shared with the High Energy Nuclear Physics Group (HENPG).

When the spectrograph becomes completely operational two azimuthal trays (levels 6 and 7) will also be digitized and will provide directional information in the back plane of the spectrograph. As can be seen in the figures, the spectrograph is divided into two halves known as the 'red side' (western side) and the 'blue side' (eastern side). The blue side has been completely digitized and has been used in this experiment.

The discussion in this chapter will be divided into three general parts: the particle detectors and the associated systems, the general aspects of the spectrograph, and the experimental description.

3.2 THE PARTICLE DETECTORS AND ASSOCIATED SYSTEMS

3.2.1 INTRODUCTION

In the operation of the spectrograph three types of particle detector have been used:

- (a) Neon flash tubes first introduced by Conversi and Gozzini (1935) are the main bulk of the detectors. Each flash tube is a 2 m long tube filled with neon gas. A charged particle

ionizes the gas as it passes through the tube and on the application of a high voltage pulse (~ 6 kV for ~ 3 μ s) the tube will discharge and will give an optical flash. Fortunately, the flash tube will also give a voltage pulse on a capacitance probe placed close to the end of the tube. This pulse has been made compatible with conventional DTL and TTL logic and consequently the systems using these flash tubes have been digitized (see Ayre et al. 1972, Ayre and Thompson 1969).

- (b) Plastic (NE102a) scintillation counters are used to initially detect the passage of a muon through the spectrograph and via a coincidence system to trigger the high voltage to the momentum selector trays and the measuring trays, as well as to trigger the data analysis and storage systems. For this experiment the pulse heights from the scintillators have been digitized and stored with the flash tube information.
- (c) Geiger-Muller counters have been placed above and below the spectrograph and have been used to give some locational information as to where the muon traversed the spectrograph in the back plane. This information has been used to line-up the trays in the spectrograph and, in this experiment, to check the uniformity of the scintillation counters.

3.2.2 THE MOMENTUM SELECTION SYSTEM

Any spectrograph which is built to study high momentum (> 100 GeV) muons must be able to cope with the enormous flux of low momentum (~ 10 GeV) muons. The rate through MARS of muons

$10 \text{ GeV}/c < P_\mu < 100 \text{ GeV}/c$ is ~ 18 particles/minute while the rate of muons $P_\mu \gtrsim 100 \text{ GeV}/c$ is ~ 19 particles/hour. This means that for every high momentum event $\gtrsim 100 \text{ GeV}/c$ the spectrograph will also have the passage of ~ 60 low momentum events. To eliminate the low momentum events the MARS spectrograph uses a low resolution momentum selecting system. The momentum selecting system consists of two parts: the momentum selector trays (MST) and the momentum selector, an electronic device which uses the information from the momentum selector trays to select high momentum events and to trigger the data storage systems. The minimum detectable momentum of the momentum selecting system is $\sim 220 \text{ GeV}/c$ and it is 100% efficient at $\sim 560 \text{ GeV}/c$. For a complete and detailed description see Ayre (1971).

3.2.2.1 THE MOMENTUM SELECTOR TRAYS

At levels 1, 3 and 5 of the spectrograph are placed momentum selector trays, each consisting of four layers of large diameter ($\sim 1.5 \text{ cm}$) flash tubes with 39 flash tubes in layers 1, 2 and 4, and 38 flash tubes in layer 3 (the measuring layer). Figure 3.3 shows the tube pattern as seen from the front of a tray on the blue side.

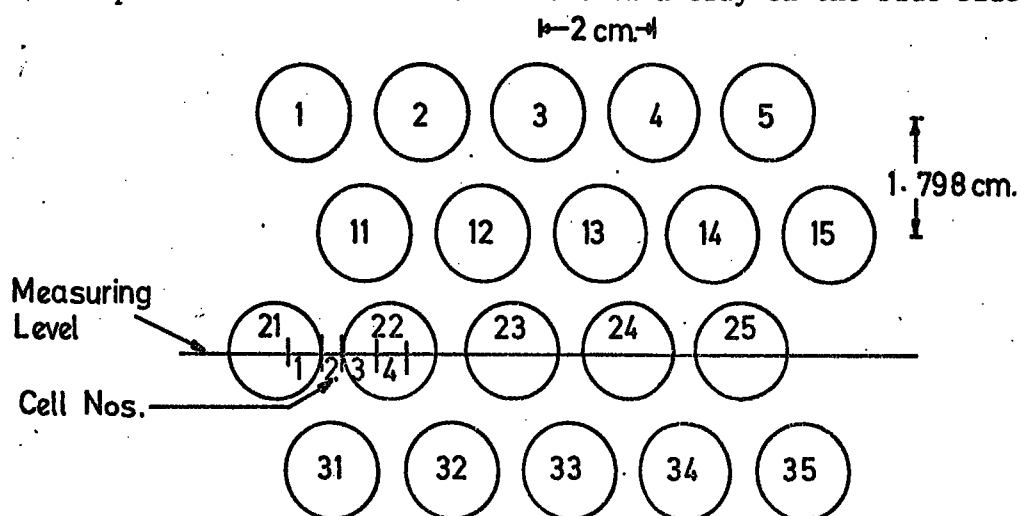


FIGURE 3.3. Momentum tray flash tube pattern.

The tubes have been digitized according to the method developed by Ayre and Thompson (1969) and each tube's output is fed into DTL latching circuits. Within $\sim 12 \mu\text{s}$ after an event has been recognized in MARS, the tray front electronics have allocated the tube configuration set off by the traversing particle to a 0.5 cm cell as defined at layer 3, the measuring layer (see Figure 3.3). There are 152 0.5 cm cells across each tray.

3.2.2.2 THE MOMENTUM SELECTOR

The momentum selector is an electronic device which uses the cells that have been allocated by the tray fronts to determine if the event was a possible high momentum event. A high momentum event has been defined as a muon which appears to have passed through the magnetic fields of the spectrograph with no deflection. The momentum selector finds high momentum events by searching for straight-line combinations of the cells set by the trays. To do this the momentum selector puts the cell information into a corresponding bit in a shift register. There are three shift registers, shift register A for level 5, B for level 3 and C for level 1. The information in each register is shifted and the shifts counted until a set bit is shifted off the end. Let N_a , N_b and N_c be the number of shifts in A, B and C respectively for a given event. A straight line (and hence a high momentum event) corresponds to $N_a + N_c = 2N_b$. Since it is possible for a muon to be allocated a wrong or slightly misplaced cell (Ayre 1971), the straight-line definition is relaxed to ± 2 cells, i.e. $|N_a + N_c - 2N_b| \leq 2$. Figure 3.4(a) shows the ceiling of a high momentum event.

There are two cases in which a low momentum event may be classified as a high momentum event by mistake. The first, as the most

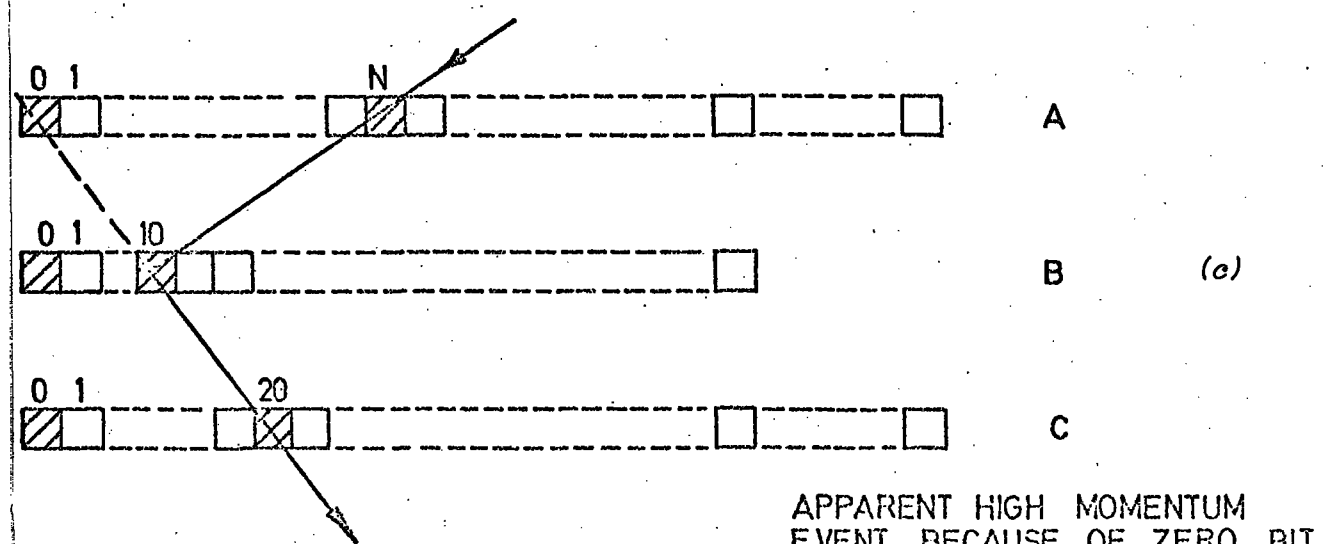
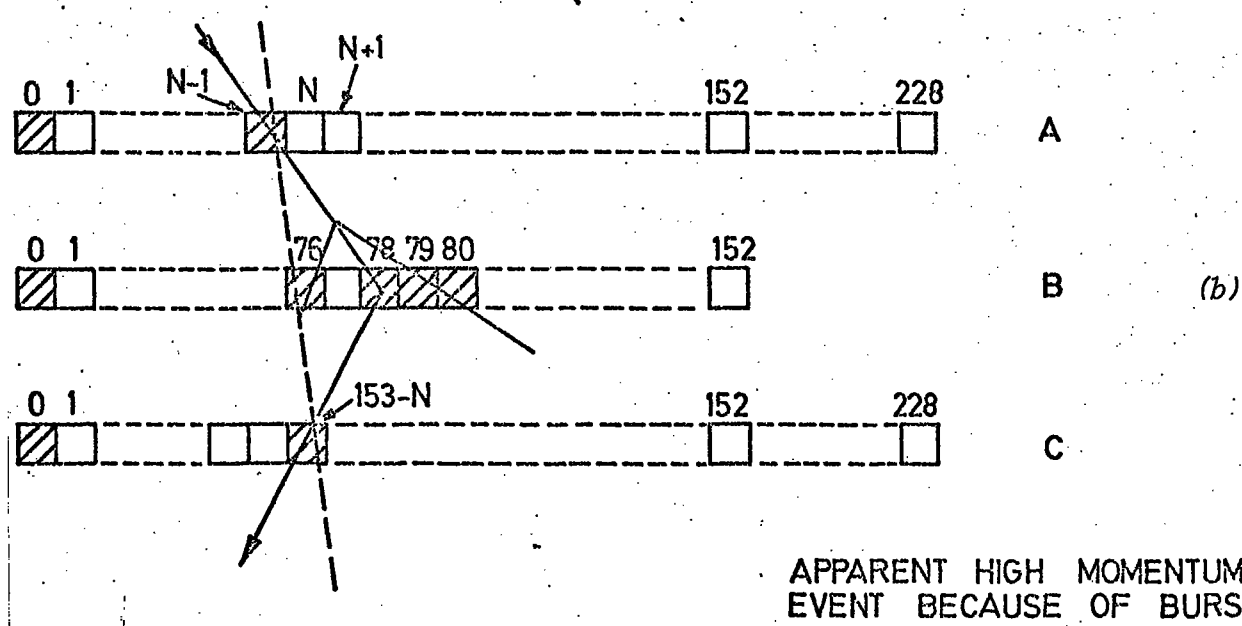
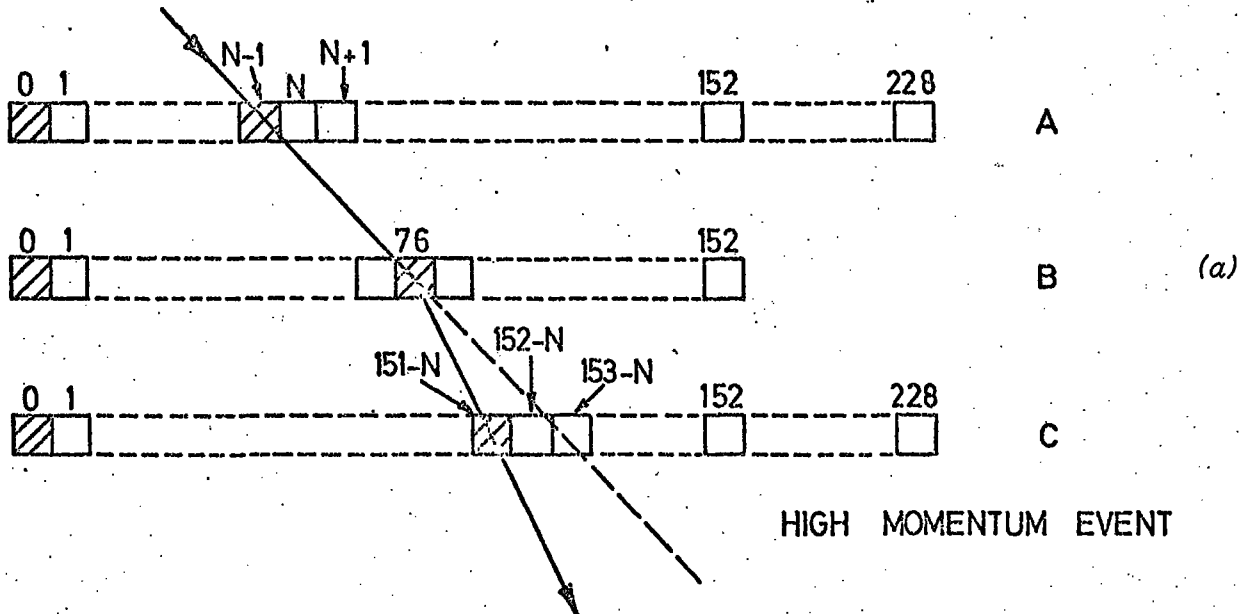


FIGURE 3.4. The momentum selector ceiling of possible accepted events.

obvious case, is when the muon is accompanied out of a magnet block by one or more electrons. When this happens the tray front electronics will allocate more than one cell to the event. Therefore, it becomes more likely that one of the extra cells will lie in a straight line with cells in the other two levels. Figure 3.4(b) shows diagrammatically how a burst event may appear to the momentum selector as a high momentum event.

The second case in which a low momentum event may be selected is that of the 'zero' bits line-up with cells on two other levels. The zero bit does not correspond to a cell in the tray front but is set at the beginning of each event and is used as a continual check that the shift registers are working. A monitoring system checks to make sure that this bit is shifted completely across the register. However, frequently this bit will also line-up with the track of a low momentum event and cause a high momentum trigger. Figure 3.4(c) illustrates how this could occur.

The most important attribute of the momentum selector is that although it may accept some low momentum events, it will always accept all high momentum events. Since the low momentum contamination is relatively small, the main analysis programs can identify these events with no major problems.

The momentum selector must produce a 'deflection' for every event in the spectrograph to determine if it is or is not a high momentum event. It is, therefore, useful to use that deflection to study the low momentum (7 GeV/c to 500 GeV/c) end of the spectrum. For this purpose RUDI (Restricted Use Digital Instrument) has been built and has been functioning for several years. For a complete description and results see Whalley (1974).

3.2.3 THE TRACK MEASURING SYSTEM

The track measuring system is the most fundamental system of the spectrograph. From the data gathered by this system the muon event can be reconstructed, the muon momentum found, and the event studied for bursts, double muons, showers, etc. This system consists of the measuring trays (MS) with special tray front electronics, a data gathering and assembling system, and an on-line IBM 1130 computer for data storage and analysis. This system can locate the position of the muon track to ± 0.3 mm in each tray and it has a momentum resolution in excess of $5 \text{ TeV}/c$, if good tracks are available in five trays (Wells 1972).

3.2.3.1 THE MEASURING TRAYS

At levels 1, 2, 3, 4 and 5 are placed measuring trays (see Figures 3.1 and 3.2) which each consist of eight layers of small diameter (~ 0.55 cm) flash tubes. Figure 3.5 shows the flash tube pattern as seen from the front on the blue side. Each layer contains 89 flash tubes (a total of 712 per tray). The columns are labelled 2 to 90 for convenience in data processing. The flash tubes have been digitized using the method developed by Ayre and Thompson (1969). The tray front electronics prepare the data in such a fashion that it is read into the data gathering system in the form of two one byte words (one byte is two hexadecimal digits). The first word of data contains the column number and the second contains the tube configuration. Each tube in a particular column is assigned a '1' if it has discharged and a '0' if it has not. It is, therefore, possible to specify every tube configuration (i.e. 2^8 combinations) in two

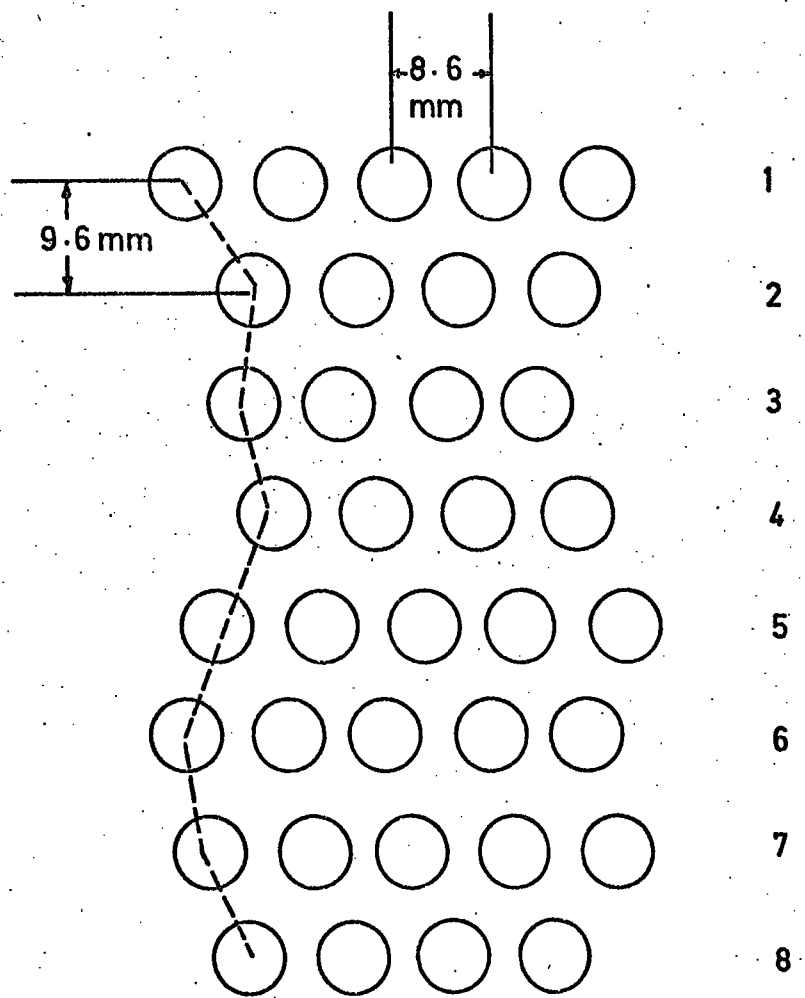


FIGURE 3.5. The measuring tray flash tube pattern on the blue side of the spectrograph.

hexadecimal digits. Figure 3.6 shows a section of a tray with a muon event accompanied through the tray by a knock-on electron. On the diagram are also given the data for the event. The first piece of data is '6276', which interpreted means that the data are for column 62 with 76 being the tube pattern. ^{HEXIDECLIMAL} Seventy-six in ~~binary~~ is '01110110'. This binary number corresponds exactly to the pattern in column 62 if the right-most digit (0) applies to the tube in layer 1 and the left-most digit (0) applies to the tube in layer 8. By the same argument the second piece of data '6491' corresponds to the pattern '10010001' in column 64. As can be seen, it is very easy to reconstruct the track left by the muon at each level. Ayre (1971) gives a description in detail of the trays and digital logic used.

3.2.3.2 THE DATA GATHERING SYSTEM

The data gathering and assembling system can be operated in one of two modes. Either it will only come into operation when the momentum selector signals that the event is a high momentum event (high momentum mode) or it can be operated to gather and store the data from every event (all events mode).

The data gathering and assembling system consists of a 'tray steerage unit' and a 1024 8-bit (1 byte) word core store. When this system receives a store event pulse, the core store system puts together a 'header' which contains vital information about the event (i.e. event number, time and date of the event, atmospheric pressure, magnetic field direction, magnetic current, geiger counter information and trigger mode). The core store unit then notifies the tray steerage that it is ready for the data. The tray steerage unit then transfers the data from the tray fronts to the core store, one tray at a time, starting at level 1. When all the data are gathered in the

PATTERN DATA: 6276 6491
 COLUMN TUBE PATTERN

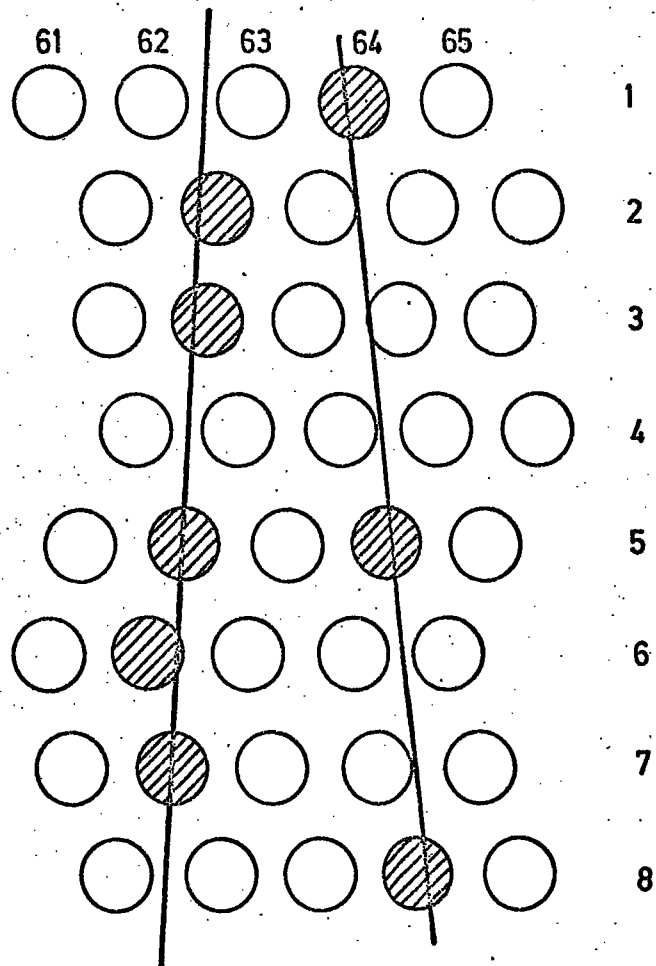


FIGURE 3.6. A muon event with an accompanying electron in a measuring tray presented with the computer pattern data.

core store, it notifies the on-line IBM 1130 that it has an event to store on disk. When the computer finds time (within 2 s) it transfers the data to a data storage disk.

During the day-time the 1130 is shared with the High Energy Nuclear Physics (HENP) Group which uses it for scanning bubble chamber films. When operating in this mode the MARS data is simply stored on a satellite disk drive. During the night-time the 1130 computing system is used exclusively by the MARS project. When running in this mode the computer is used to analyze data which has been gathered and at the same time is used to store data as it is gathered. For a more complete description of the tray steerable unit see Ayre (1971). For a complete description of the core store unit, the data format and the on-line system see Wells (1972).

3.2.4 THE SCINTILLATION COUNTERS AND ASSOCIATED ELECTRONICS

The scintillation counters have been used for two purposes in this experiment. The first use has been to determine when a muon has traversed MARS by providing a three-fold coincidence to the spectrograph systems. The other use has been to obtain pulse height information which could be associated and identified with individual events in the spectrograph. In particular, it can be used to study bursts.

This system consists of scintillation counters viewed by two photomultipliers at each end looking through a triangular perspex light guide. The outputs of the photomultipliers are added and mixed in specially designed head amplifier units which give two kinds of output. One type is from two $\sim X50$ amplifiers, which is used to generate the spectrograph coincidence (the coincidence system is described in Ayre 1971). The other type is from an $\sim X1$ amplifier to be used in the burst analysis system. The $\sim X1$ output is inverted in a linear

amplifier of gain -0.75 and is fed into an analogue to digital converter (ADC) which assigns a digital value to a certain pulse height. The digital data are then read into a core storage system and eventually transferred to magnetic disks with the flash tube data for later analysis. Figure 3.7 gives a diagrammatic representation of the system from photomultiplier to computer.

3.2.4.1 THE SCINTILLATION COUNTERS

At levels 1, 3 and 5 are ~ 176 cm \times 75 cm \times 5 cm type NE102a plastic scintillators. Each scintillator is observed by four Mullard type 53AVP photomultipliers. At each end two of these photomultipliers are attached, via optical cement, to triangular perspex light guides. Figure 3.8 shows a scintillator with light guides and photomultipliers. The scintillator and light guides are wrapped in aluminium foil in order to help reduce light loss and sheets of black opaque plastic are wrapped round the aluminium foil to prevent light from getting into the system. The scintillator and photomultipliers are sealed in a light-tight box.

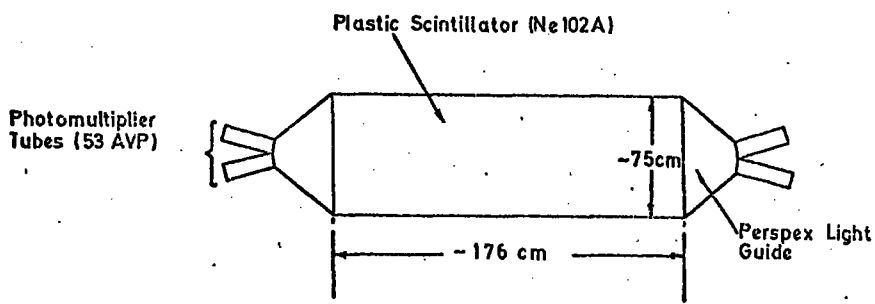


FIGURE 3.8. A MARS scintillation counter.

Since the gain of the photomultipliers is affected by the presence of a magnetic field, it is essential that when the scintillation counters are placed in the spectrograph that the photomultipliers are protected from the stray magnetic fields which exist between the

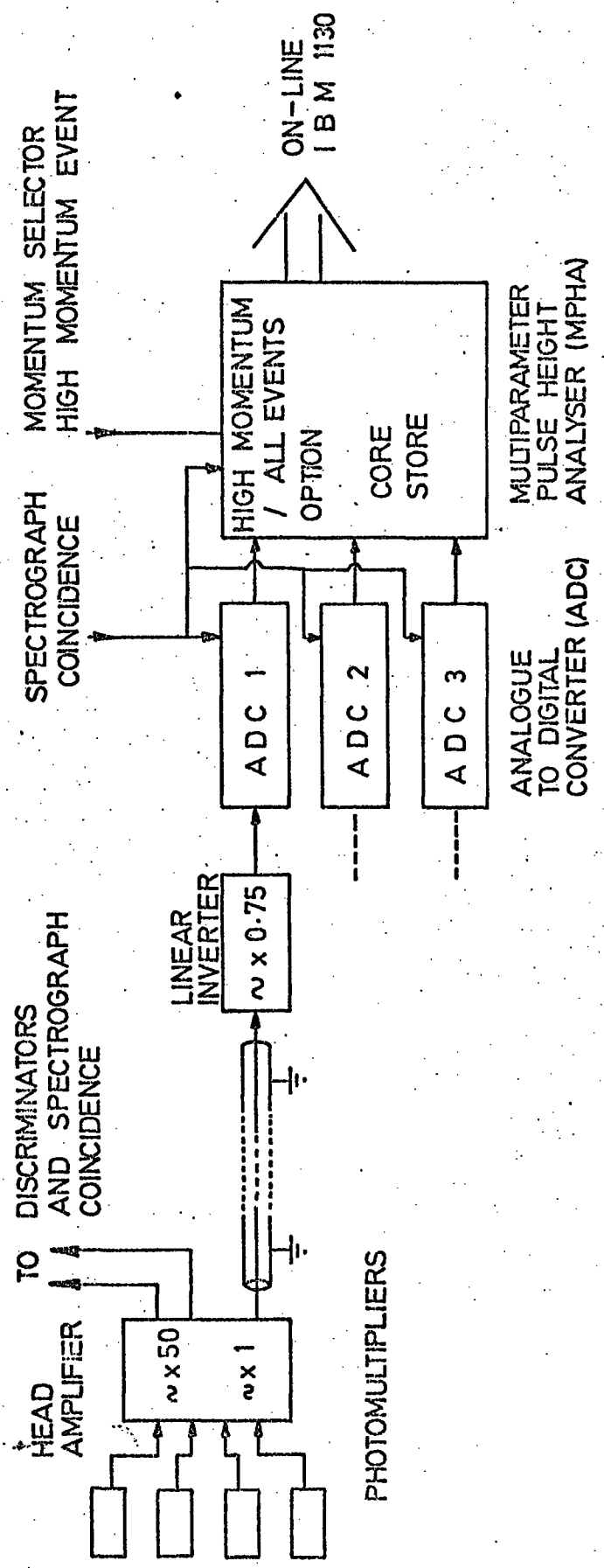


FIGURE 3.7. A diagrammatic view of the pulse height analysis system.

magnetic blocks. Hamdan (1972) investigated how best to shield the photomultipliers and his work yielded the current shielding technique of placing an inner mu-metal cylinder and an outer soft core iron cylinder over each photomultiplier.

The voltages (EHT) on the photomultipliers were adjusted to give the same gain for each photomultiplier. ~~This~~ ~~that~~ was achieved while the scintillators were in the spectrograph by using two of the three scintillation counters as telescopes to provide coincidence with one of the four photomultipliers of the third scintillation counter in a 400 channel PHA. The EHT on each tube was adjusted until the desired gain was obtained. This procedure was then repeated for all the photomultipliers in the spectrograph.

3.2.4.2 THE SCINTILLATOR UNIFORMITY

A study of one of the scintillators using two 9 inch (23 cm) square scintillation telescopes has been done to obtain the uniformity as a function of the distance from the light guide. The study was done using only one photomultiplier. The telescope was placed successively at three positions laterally across the scintillator at intervals of 15 cm from the light guide (see Figure 3.9). The output from the photomultiplier was analyzed in coincidence with the telescope by a 400 channel PHA. The collected data were transferred to cards and analyzed via the NUMAC IBM 360/67 computer by fitting a third order polynomial using the least squares method in the region of the statistical mode. The form of the fitted equation was

$$y = ax^3 + bx^2 + cx + d . \quad (3.1)$$

The maximum and minimum can be found by setting the first derivative

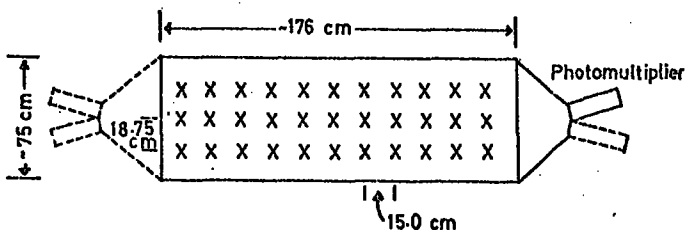


FIGURE 3.9. A scintillation counter with telescope measuring positions marked (X).

of the equation (3.1) to zero.

$$\frac{dy}{dx} = 3ax^2 + 2bx + c = 0 . \quad (3.2)$$

It has two solutions (generally real)

$$x_{1,2} = \frac{-b \pm \sqrt{b^2 - 3ac}}{3a} . \quad (3.3)$$

The mode is the solution (x_1 or x_2) at which the second derivative of equation (3.1) is negative.

$$\frac{d^2y}{dx^2} = 6ax + 2b < 0 . \quad (3.4)$$

This method of locating the mode is accurate to $\sim 5\%$. The result of the uniformity is presented in Figure 3.10. The curve shown is a least squares fit of an equation of the form $y = e^{ax + b}$ to the data at distances > 30 cm from the light guide. It was decided to fit the curve to the last nine points only because of a special geiger counter spectrograph run used to determine whether or not the scintillators at levels 1 and 3 have similar uniformity to the one used in the uniformity study. The results of the run which used four geiger counter trays, two at the top, front and back of the spectrograph, and two similarly at the bottom, are presented in Figures 3.11(a), (b). The geiger counters were used to determine the general position of the

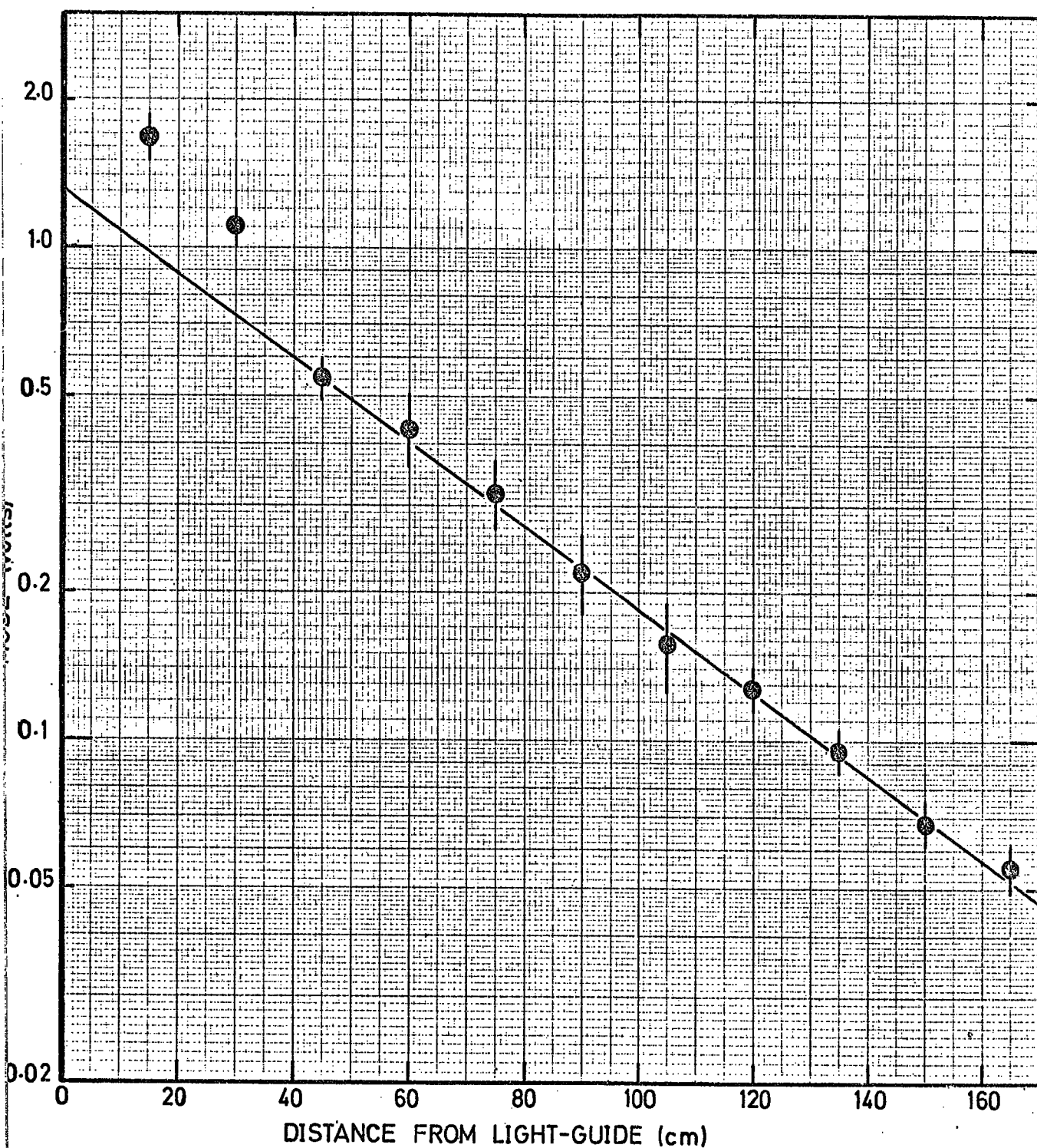


FIGURE 3.10. The scintillator uniformity as viewed from one end presented with an exponential fit to the experimental point > 30 cm from the light guide.

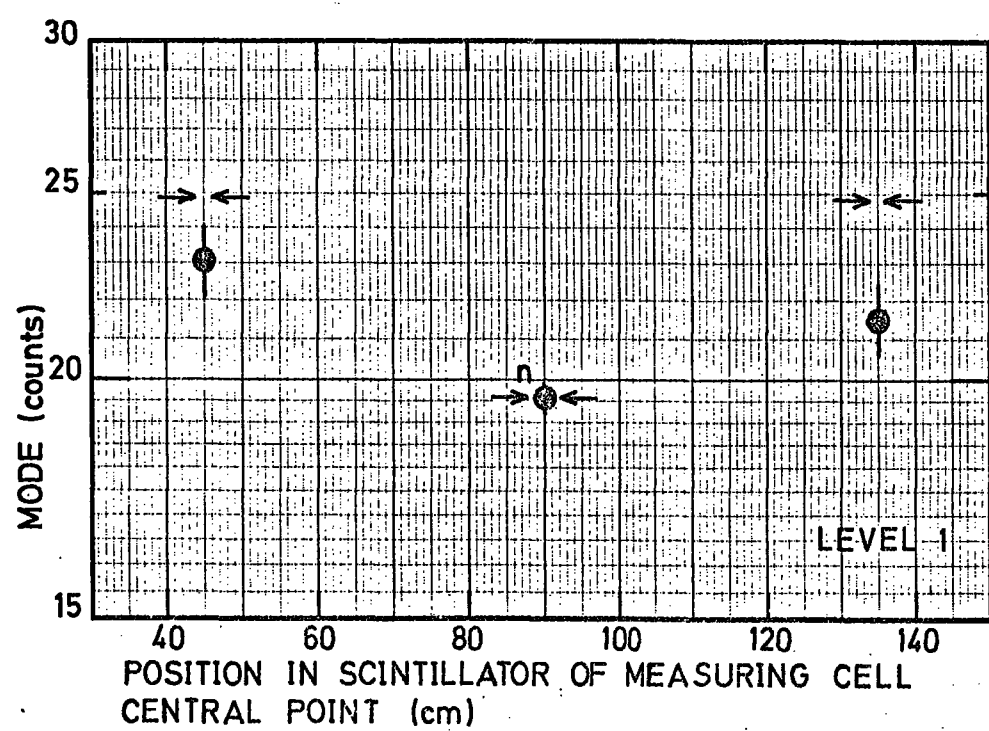
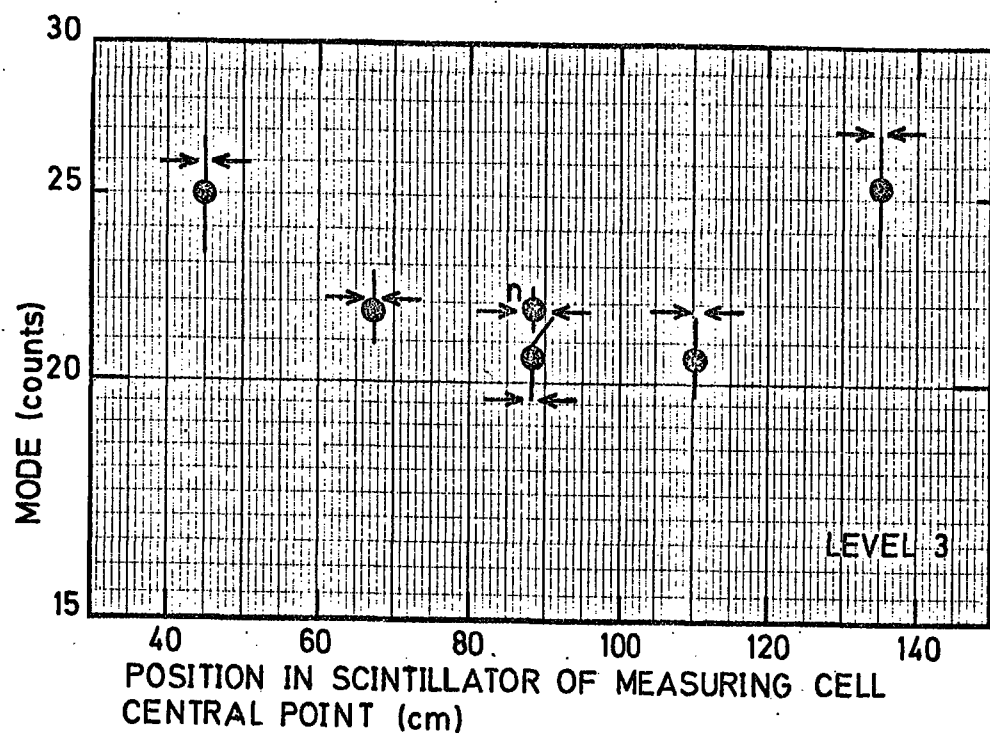


FIGURE 3.11. The experimental uniformity results (●) with the theoretical predictions (+ -) normalized at the point labelled n.

particle as it traversed MARS. The experimental points (•) are presented with the theoretically predicted points (↔). The theoretical values are based on the fit in Figure 3.10 and are normalized to the point labelled 'n'. Figure 3.11(a) is the result for level 3 and Figure 3.11(b) is the result for level 1. The reason why level 3 has six experimental points while level 1 has only three is that at level 3 it is possible to locate six regions of particle traversal due to particles crossing front to back and vice versa.

As can be seen the level 3 uniformity agrees very well with the expected result. However, the results for level 1 suggest that the scintillator is more uniform by a small amount than the scintillator at level 3.

Figure 3.12 presents the normalized non-uniformity curve based on the Figure 3.9 fit. Curve (a) is the curve obtained if viewing the scintillator from one end only. Curve (b) is the expected curve if the scintillator is viewed with the photomultipliers at both ends. The curve shows about 60% non-uniformity from the end to the centre; for the scintillators in MARS.

3.2.4.3 THE AMPLIFICATION SYSTEMS

Each photomultiplier has identical base circuits (shown in Figure 3.13). The pulse out of these bases is of length $\sim 20 \mu s$, being solely determined by the load resistance ($10 K\Omega$) and the capacitance of the circuit. The output from each photomultiplier is fed into a specially designed head unit. Figure 3.14 presents a circuit diagram for these units. Each unit has four inputs (A, B, C, D) which correspond to the four photomultipliers at each level. Three amplifiers are contained in the head unit; these consist of one $\sim x1$ amplifier and two $\sim x50$ amplifiers. Each of the $\sim x50$ amplifiers add

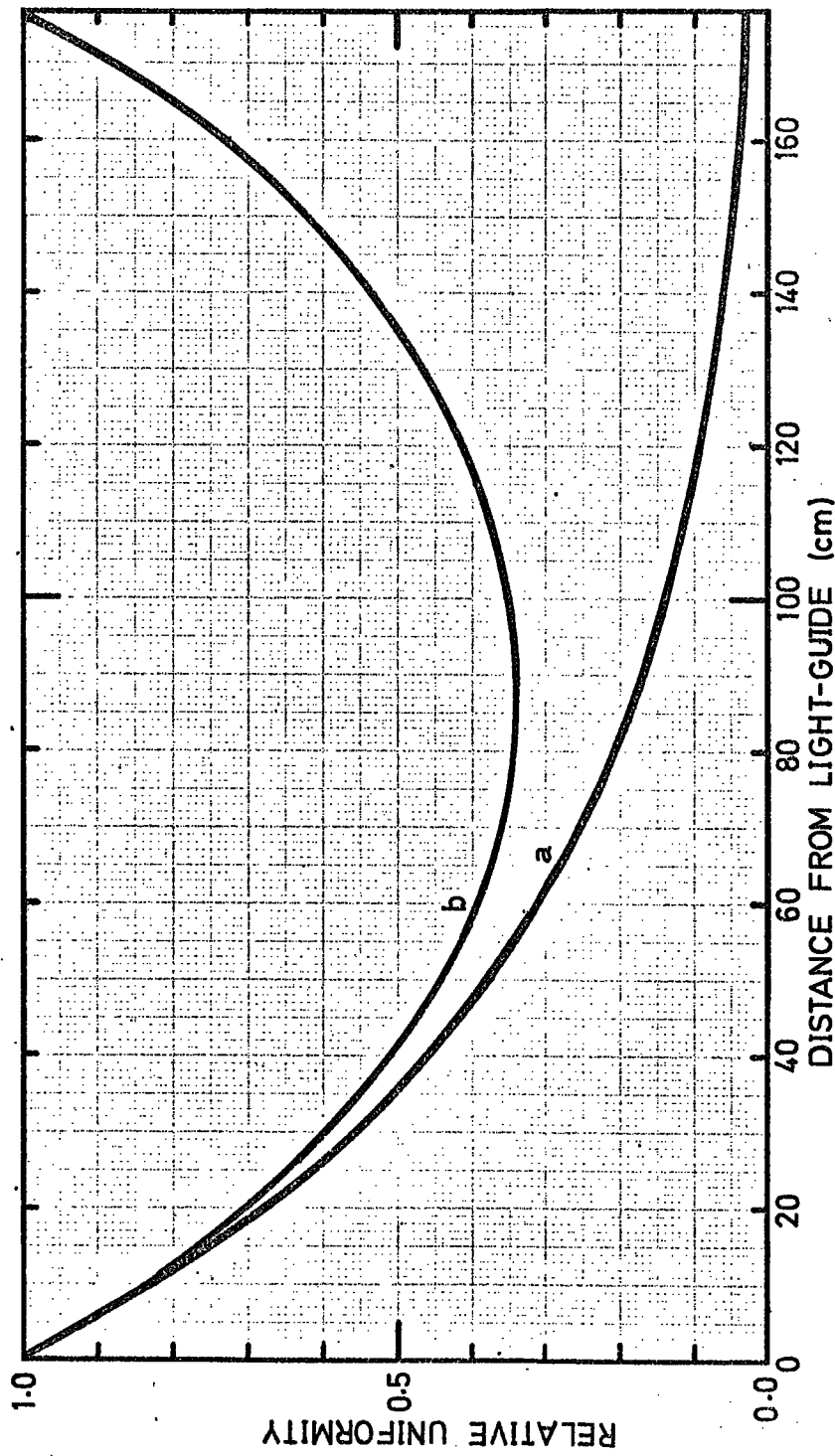


FIGURE 3.12. The relative scintillator uniformity as (a) viewed from one end only, (b) viewed from both ends.

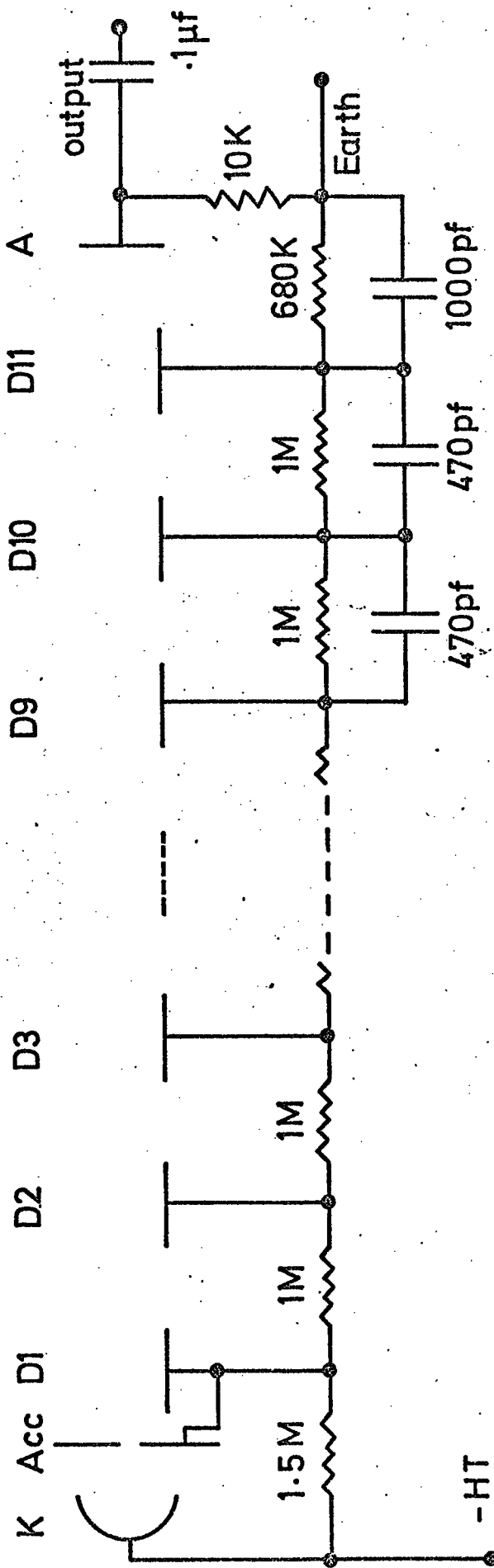


FIGURE 3.13. The photomultiplier base circuit diagram.

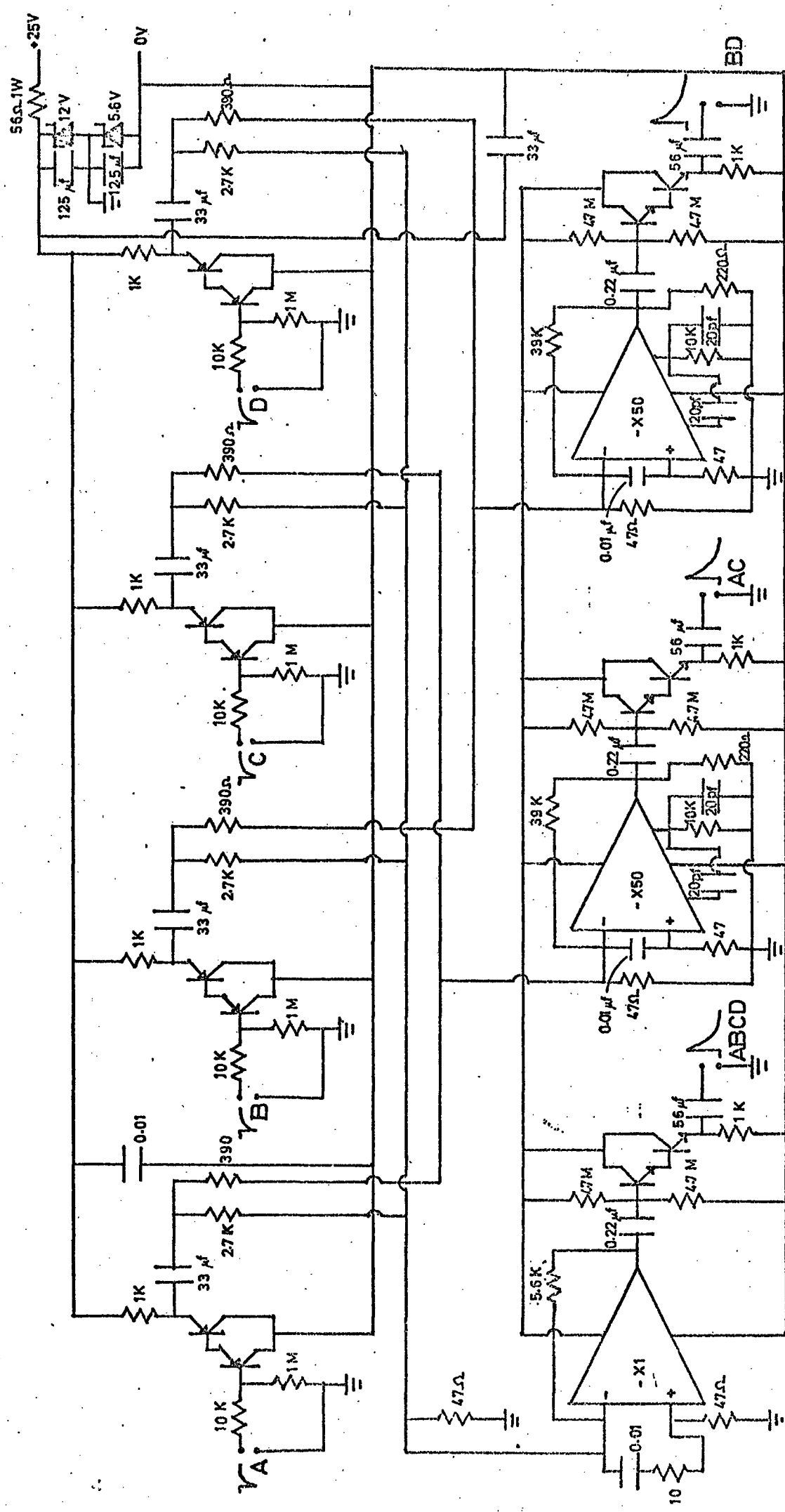


FIGURE 3.14. The photomultiplier head amplifier circuit diagram.

two diagonally opposing photomultiplier outputs together (see Figure 3.8). The output of the two $\sim \times 50$ amplifiers is sent to a discriminator and then to the coincidence unit to provide the main trigger for the spectrograph. The $\sim \times 1$ amplifier adds all four ($A + B + C + D$) inputs together, and the output has been used in the experiment reported here.

Figures 3.15 and 3.16 show the linearity of the $\sim \times 50$ and $\sim \times 1$ amplifiers respectively. Also shown are the curves when various inputs are added together. The linearity is considered to be good since the analogue to digital converters (ADC) attached to the $\sim \times 1$ amplifier saturate at 4 to 5 V.

A study was done to determine the variation of the gain as a function of temperature. This is useful to know, since the temperature varies a number of degrees from the top to the bottom of the spectrograph. The results of this study (Rada, private communication) are presented in Figure 3.17. The gain variation over the temperature range used (20°C to 30°C) is $\sim 2\text{-}3\%$.

The output of the $\sim \times 1$ amplifier is fed into an inverting amplifier of gain -0.75 via an ~ 10 m cable. The circuit diagram can be seen in Figure 3.18 and the linearity is shown in Figure 3.19.

3.2.4.4 THE ANALOGUE TO DIGITAL CONVERTER

The analogue to digital converter is a device which converts the height of an input pulse into a series of digital pulses whose number is a measure of the height. The ADC's which were used in this experiment were designed by Dr. E. Bateman based on the Wilkenson principle of charging a capacitor up to the peak voltage of the input pulse via an emitter follower, and then discharging it with a constant current source and detecting the time length of the linear ramp produced

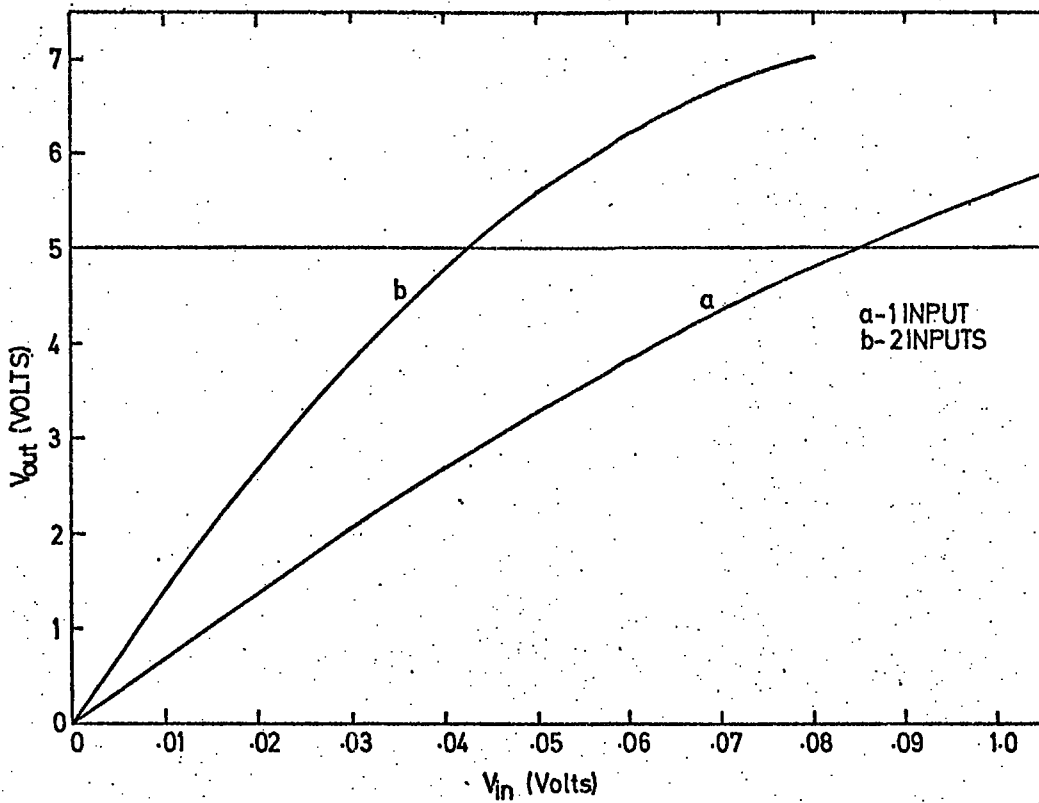


FIGURE 3.15. The linearity plot for the $\sim \times 50$ head amplifier.

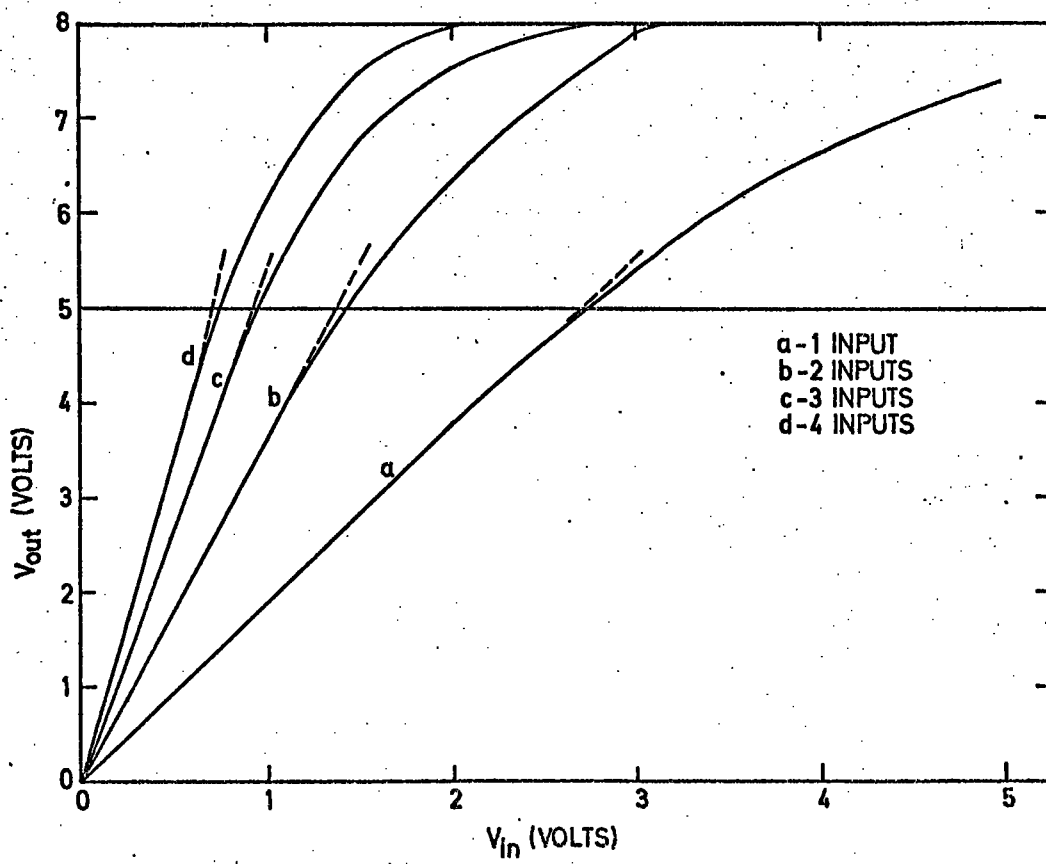


FIGURE 3.16. The linearity plot for the $\sim \times 1$ head amplifier.

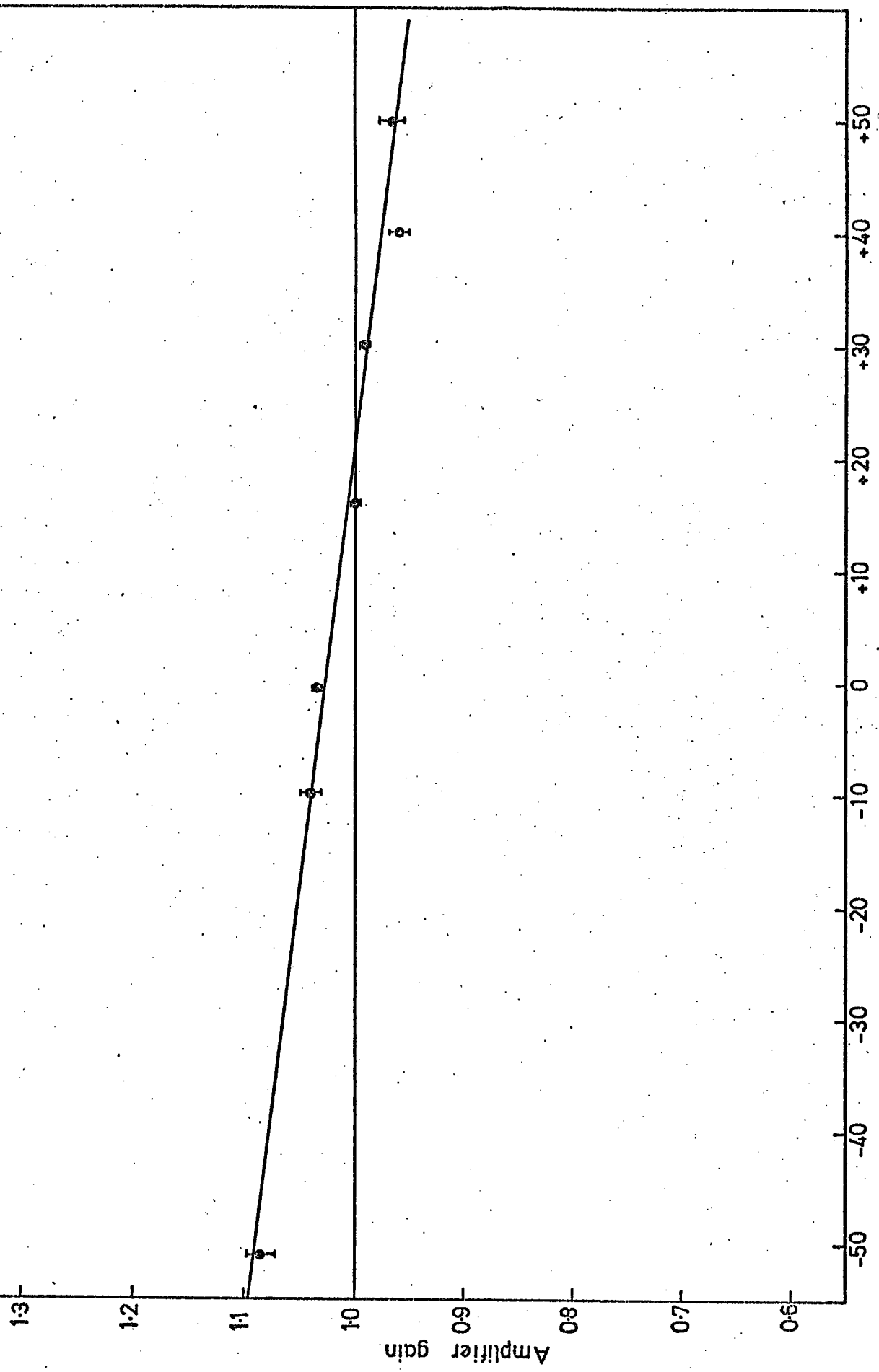


FIGURE 3.17. The gain temperature dependence of the head amplifier.

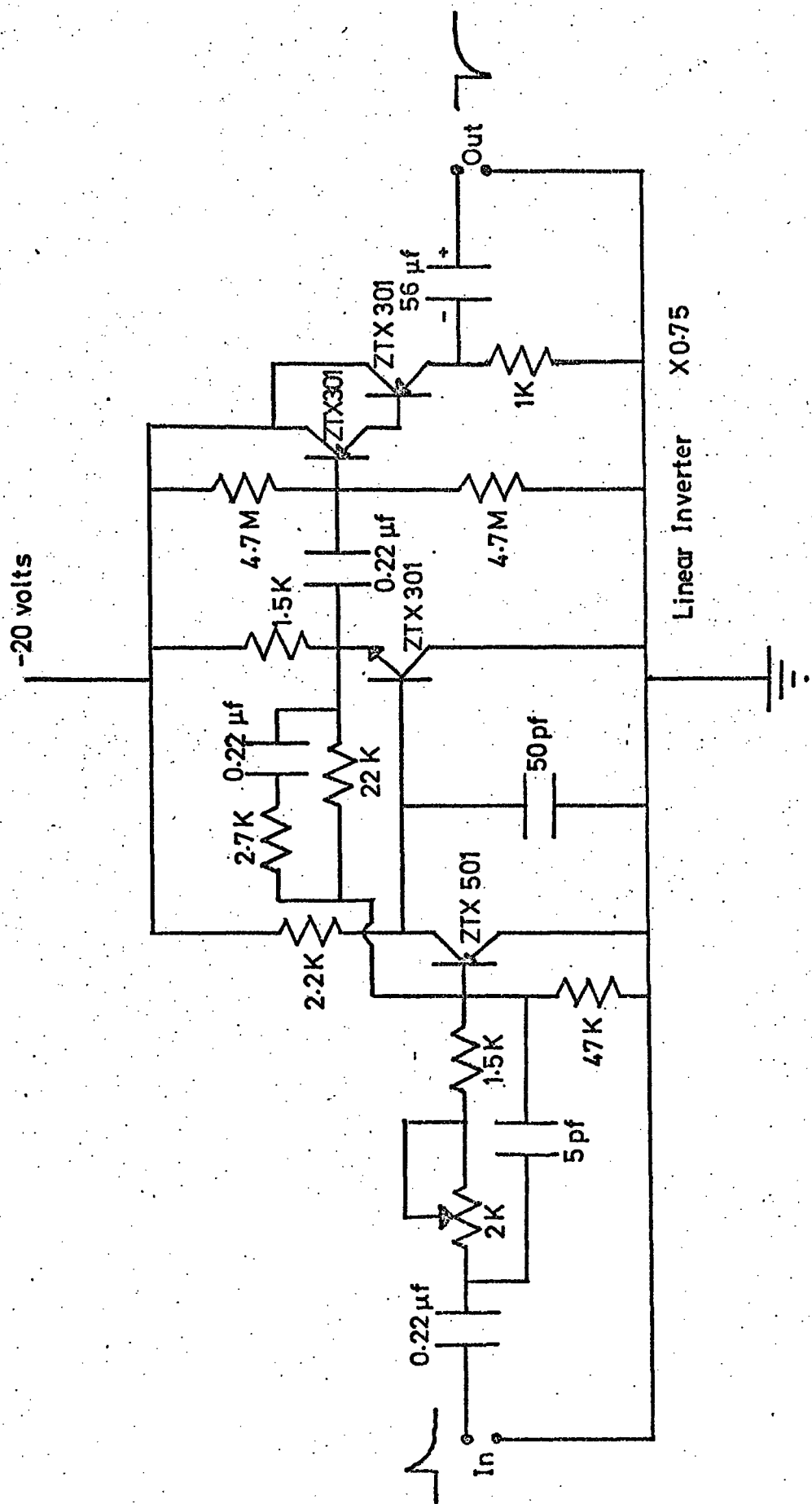


FIGURE 3.18. The linear inverting amplifier circuit.

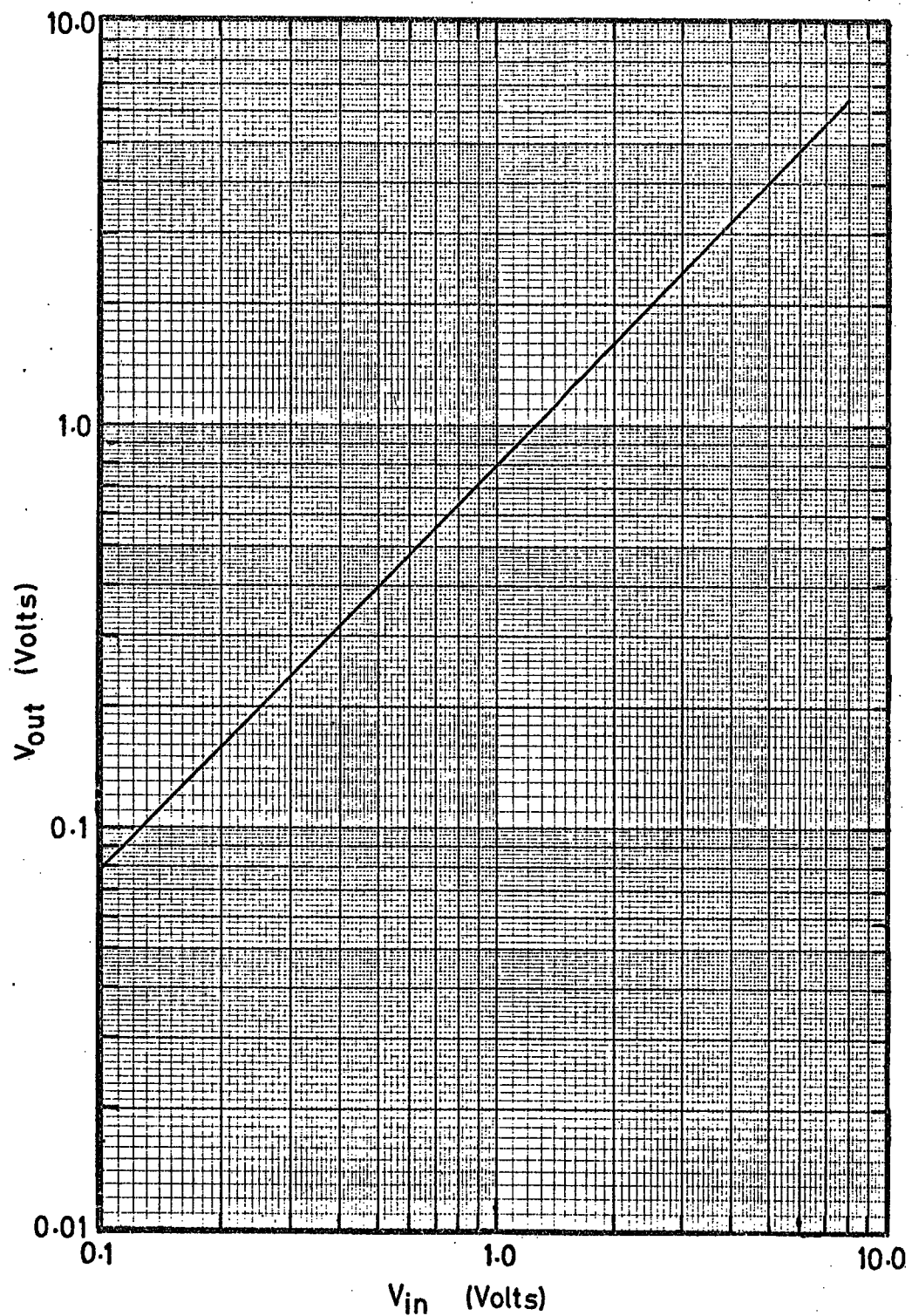


FIGURE 3.19. The linearity plot for the inverting amplifier.

by a Schmitt trigger. The width-modulated pulse is used to gate a constant frequency astable, and the number of counts is counted on a scalar to give a numerical measure of the pulse height.

Figure 3.20 gives circuit and block diagrams of the working ADC. Figure 3.21 presents the progressive change of the input pulse as it passes through the ADC until it is a string of digital pulses. A detailed description of the ADC's is given in an unpublished work by Whalley (1972).

In an analysis of the errors in the ADC system, it has been found that the fluctuation in counts for a given pulse height is $\lesssim 1\%$ over the entire range (0-1024 counts). Figure 3.22 shows this result for one of the ADC's used in this experiment. The linearity of the ADC's used has been checked using a precision pulse generator. In Figures 3.23(a), (b) are the results of this test for level 1 and level 3 respectively. It was decided when the ADC's were calibrated that it would be best to have a negative threshold, so that no pulse, or a pulse of zero height, gave a count of +2 at each level. This makes it easy to determine the spectrum's starting cell. It is also this threshold which makes the data points appear to be non-linear at the low end. The data are presented with a least squares linear fit. The ADC's are very linear and the apparent curvature of the linear fit is due to plotting a straight line that has a non-zero intercept on a log-log scale.

3.2.4.5 THE MULTIPARAMETER PULSE ANALYSIS SYSTEM

The multiparameter pulse analysis system (MPHA) consisted of six ADC's (described in the previous section) and a magnetic core store system similar to the core store system associated with the flash tube measuring trays. The MPHA, as with the track measuring system, could

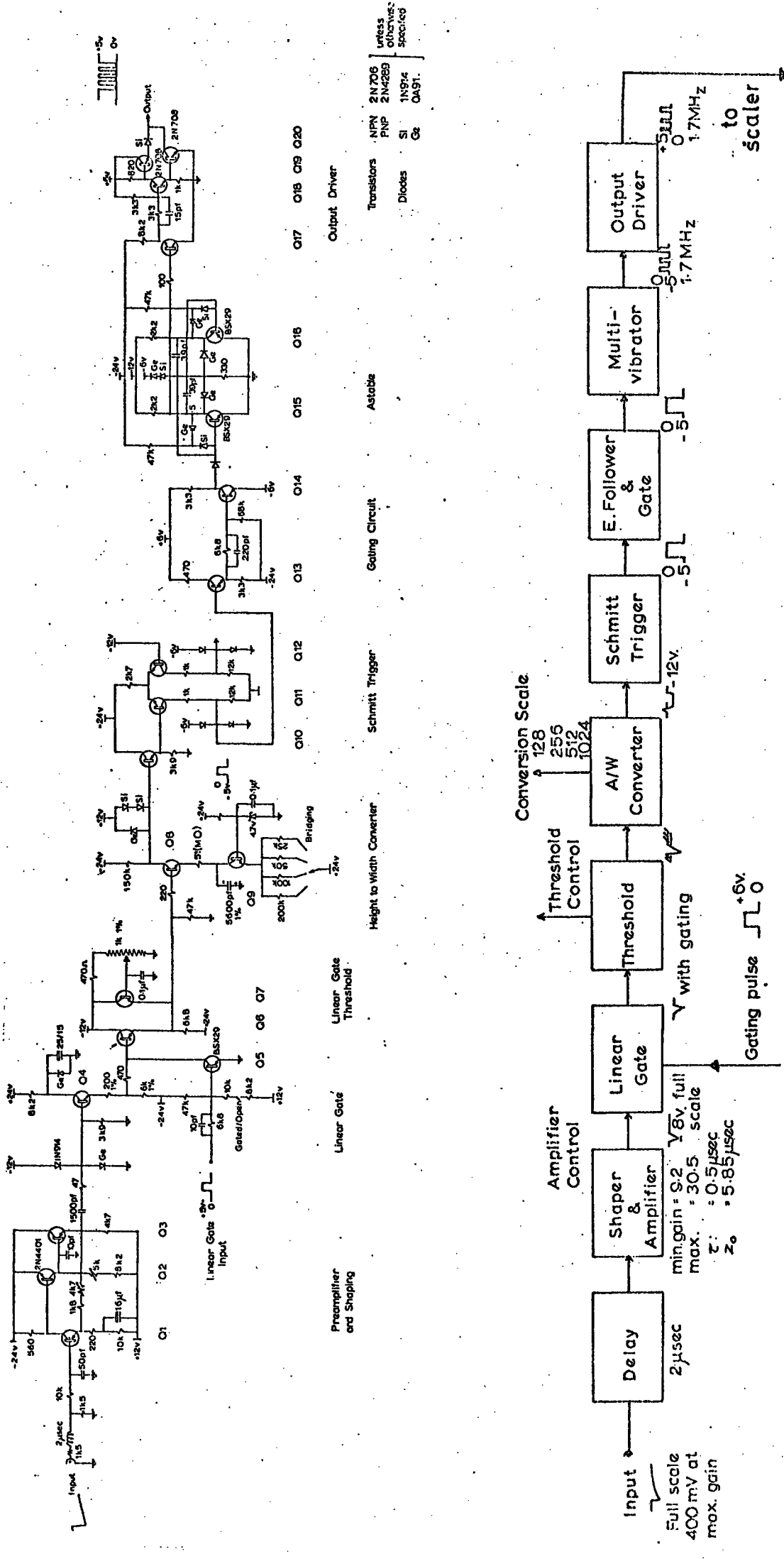


FIGURE 3.20. The analogue to digital (ADC) circuit diagram (top) and block diagram (bottom).

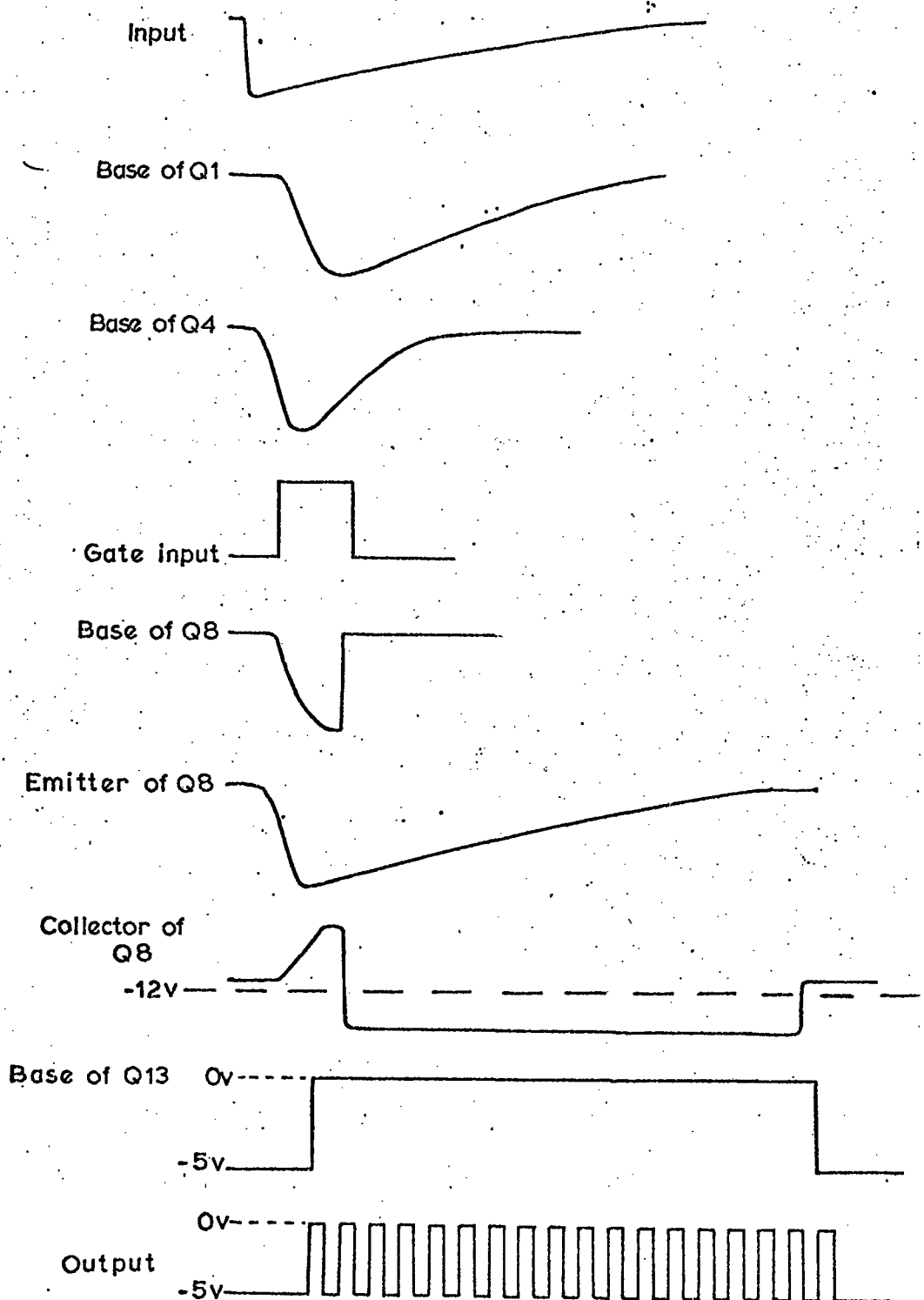


FIGURE 3.21. The progressive changes to a photomultiplier pulse as it passes through an ADC.

Serial No. 3

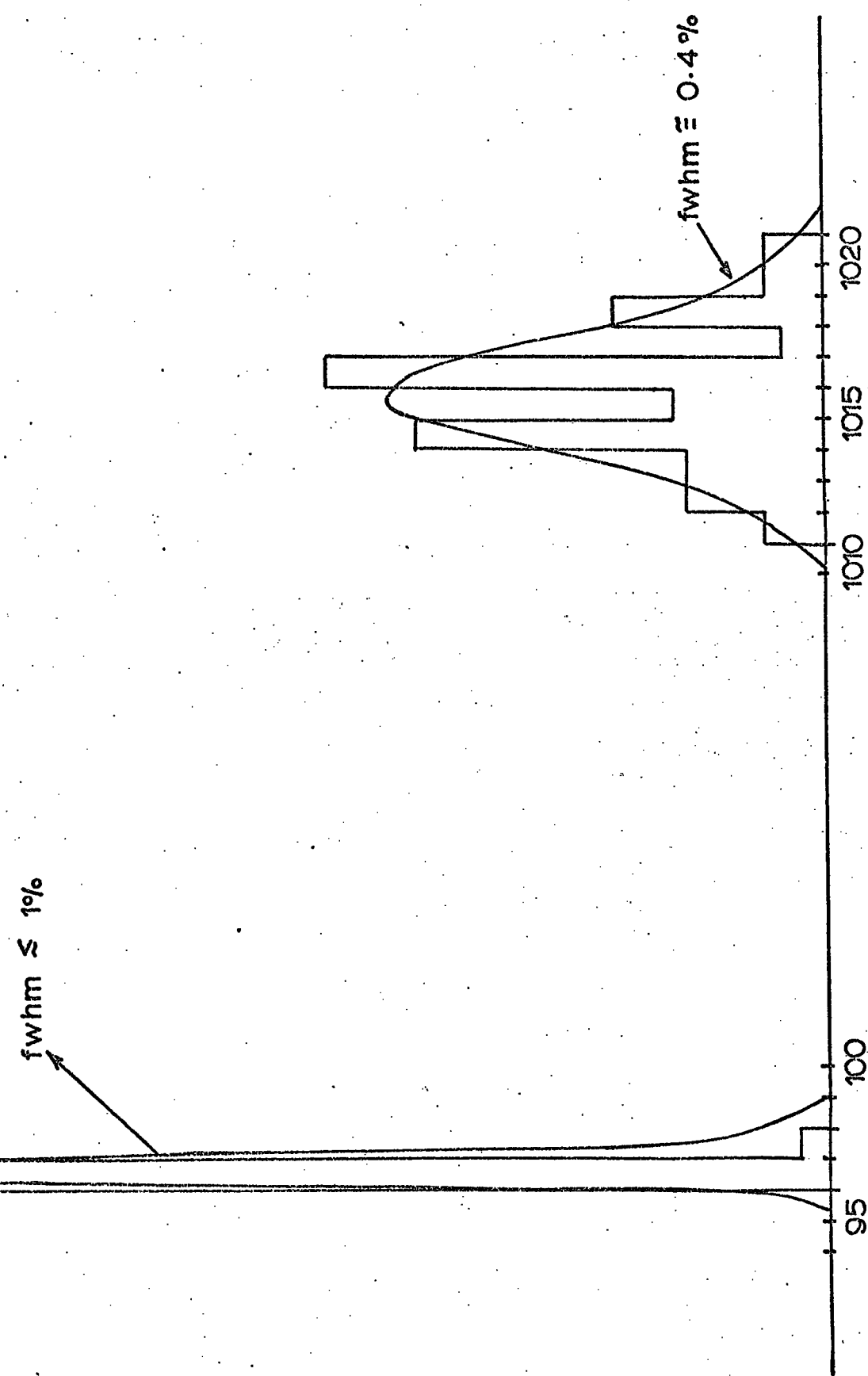


FIGURE 3.22. Fluctuations in ADC digital conversion (after Whalley 1972).

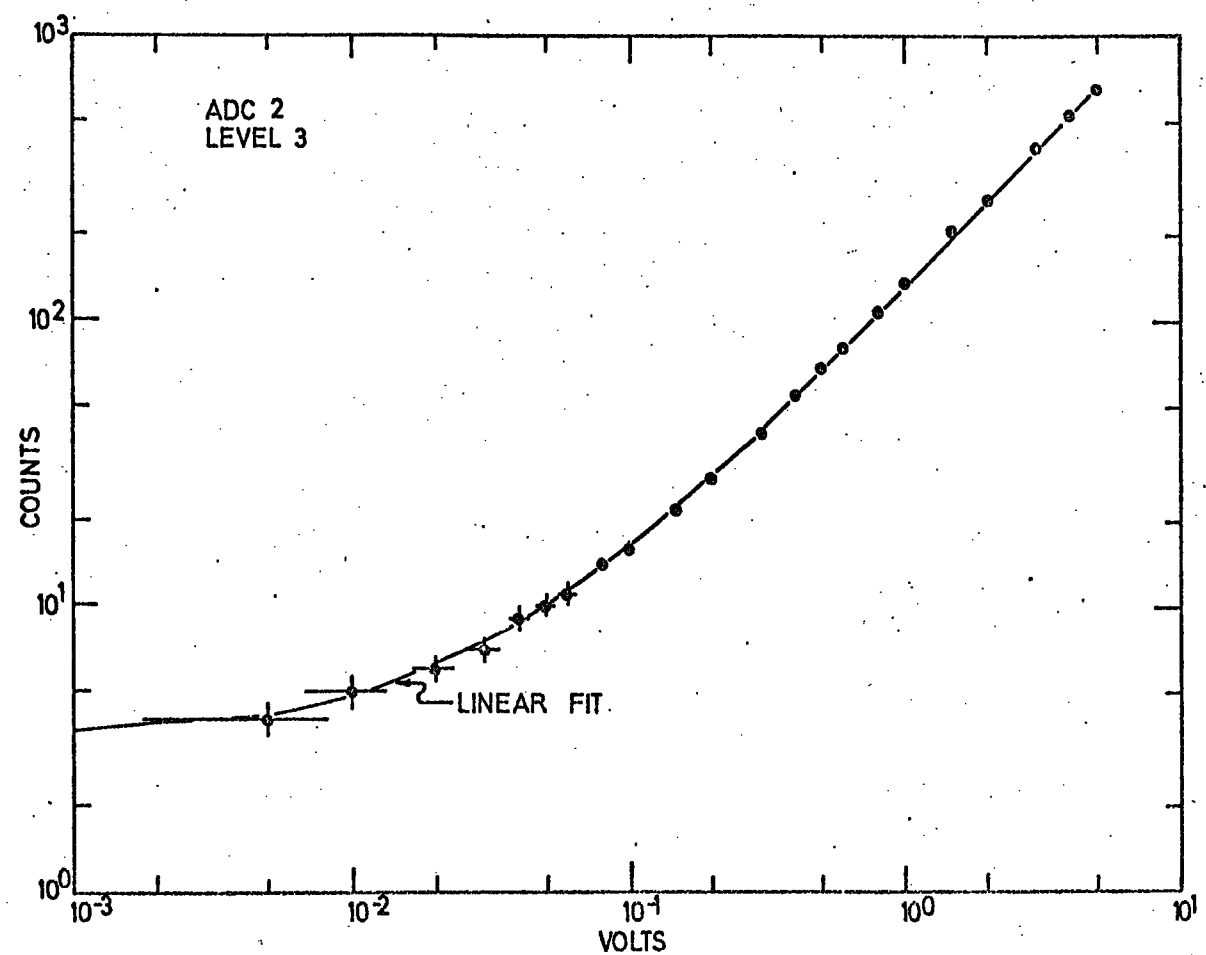
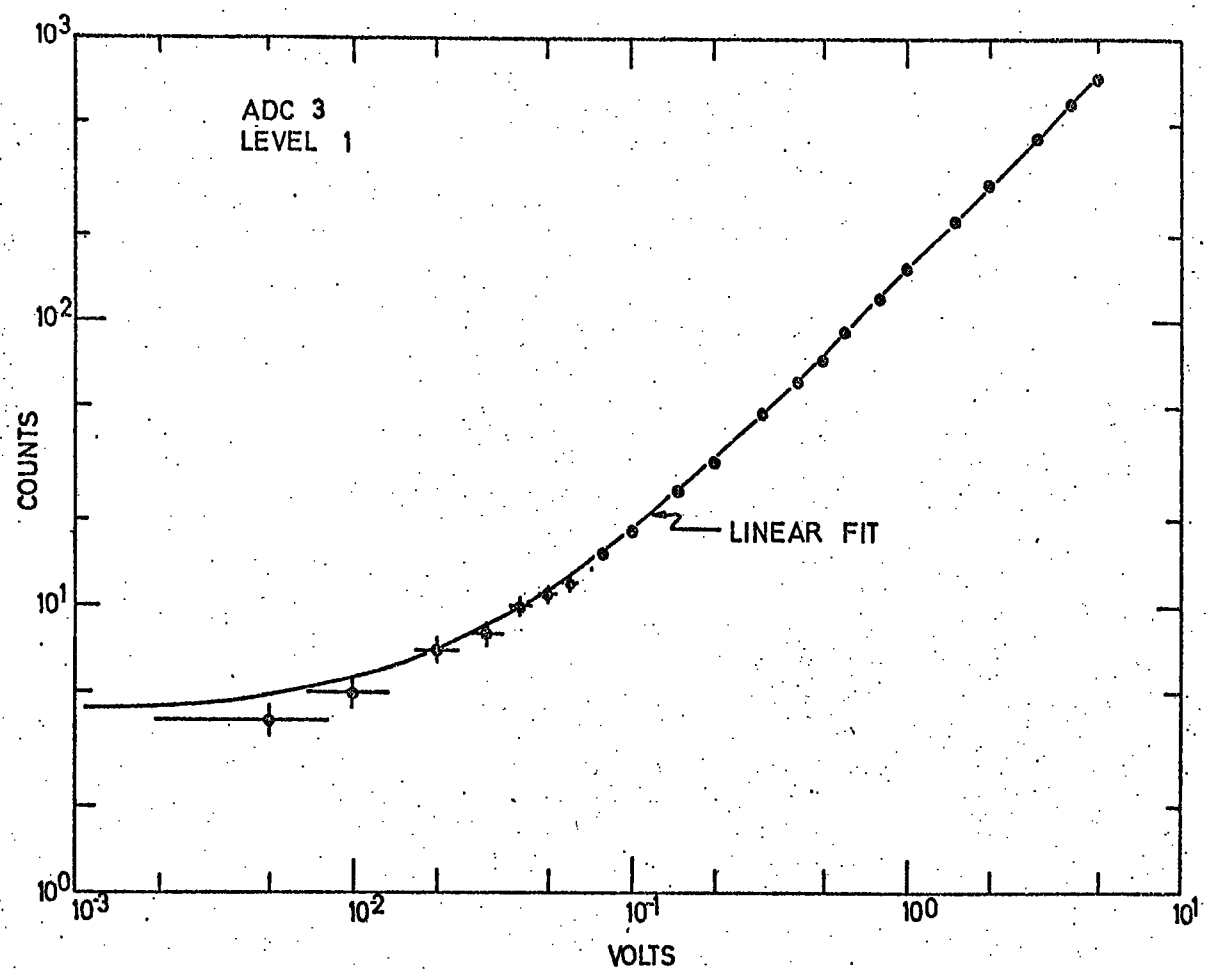


FIGURE 3.23. Analogue to digital conversion of ADC's with linear fit.

be operated in either a high-momentum mode or an all-events mode. When a three-fold coincidence occurred the ADC's were triggered to analyze the scintillator pulses associated with the event. If the momentum selector flagged the event as a possible high-momentum event, or if the operation mode was all events, the data from the ADC's plus event information (i.e. event number, run flags and magnetic field flags) were stored in a 1024 8-bit word ferromagnetic core store.

Each event in the core store consisted of:

- (a) a two word event 'start' identifier (FFF1)
- (b) a three word event number (0-FFFFF)
- (c) one word of geiger counter information associated with the event (if available)
- (d) one word for series number (0-F) and magnetic field (0 for zero field, 1 for '+' field and 2 for '-' field)
- (e) one word for run number (0-FF)
- (f) twelve words (two each) for the six ADC's
- (g) a two word event 'end' identifier (FFF2).

Each event used a total of 22 words, and as a result the core store unit stored 46 events (1012 words plus 4 word core store identifier (00 00 FF FF)) before it dumped the data to the disk storage via the IBM 1130 computer. Figure 3.24 shows a diagram of the logic circuitry for the control section of the core store unit. Figure 3.25 is a schematic of the MPHA system. In this figure data gates 1 and 2 correspond to the start and end identifiers respectively, data gates 3 and 4 receive the event number and geiger information, and with the manual flag, the series number, run number, and magnetic field were

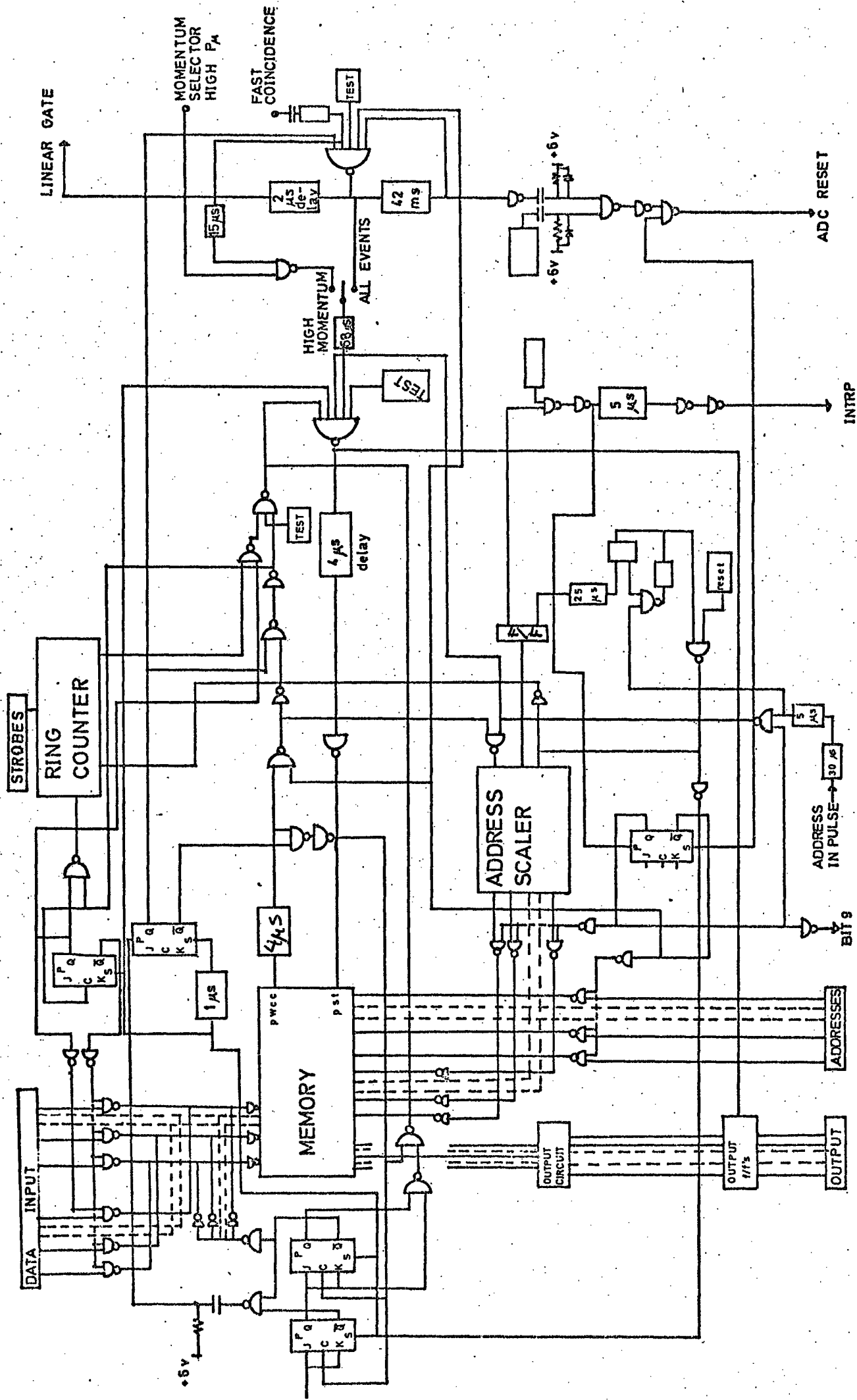


FIGURE 3.24. Logic diagram for the multiparameter pulse height analyzer (MPHA) control.

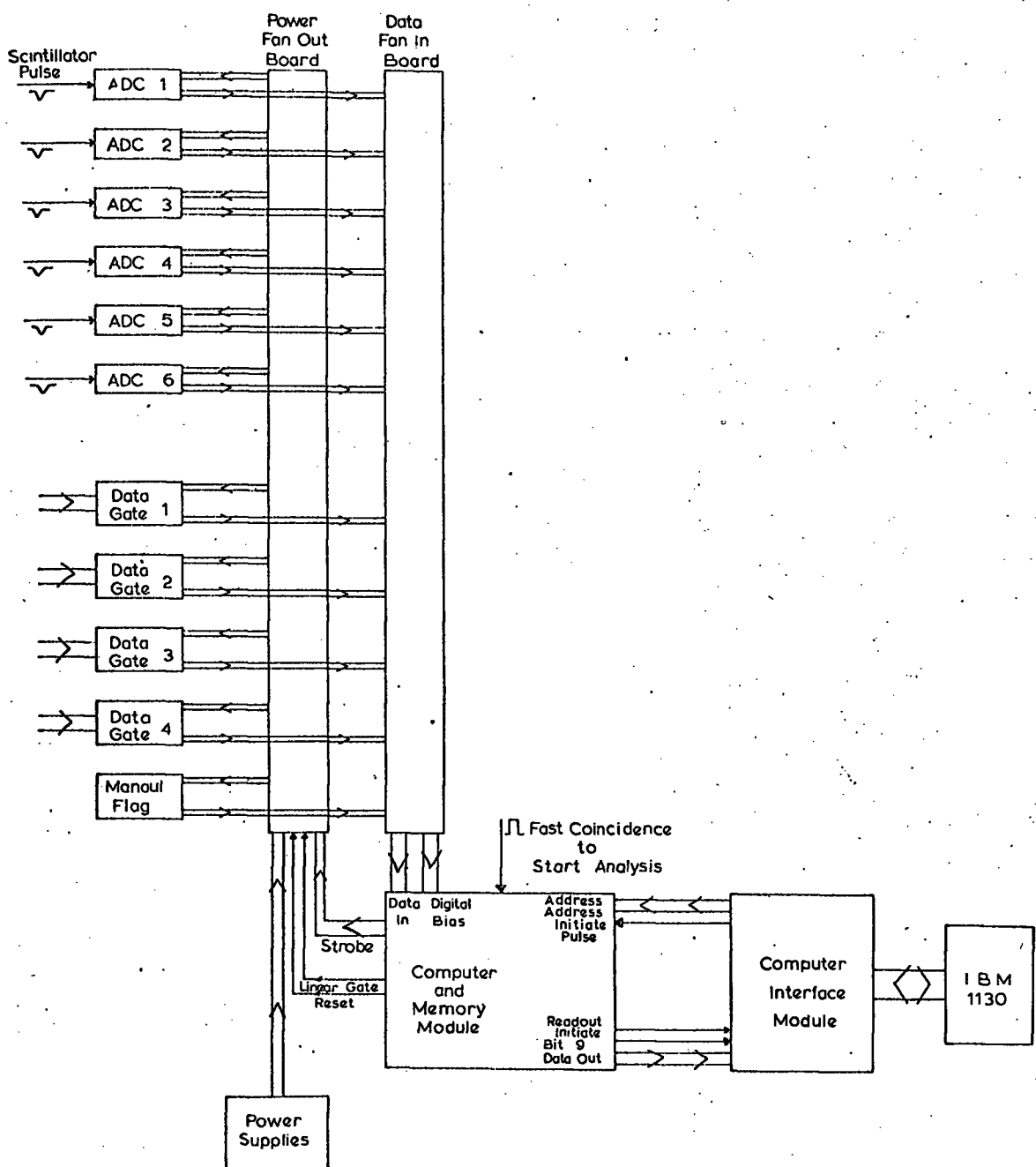


FIGURE 3.25. Block diagram of the MPHA from data input to computer.

set. For a complete and detailed description of the MPHA see Whalley (1972).

3.3 GENERAL ASPECTS OF THE SPECTROGRAPH

3.3.1 THE MAGNETS

The main physical bulk of the spectrograph consists of four solid iron magnet blocks (size: 1.24 m x 3.66 m x 2.13 m) (see Figures 3.1 and 3.12). Each block is made from 78 5/8 inch (1.59 cm) iron plates and is constructed as a toroid to contain a maximum amount of the field. The magnets, being toroidal, conveniently divide the spectrograph into two halves (the red or west side and the blue or east side) with fields in opposing directions. The field direction is defined such that a positive muon will be deflected towards the centre of the magnet in a positive field (i.e. a positive field is into the blue side and out of the red side when standing at the front, electronics end, of the spectrograph).

Each energizing coil has a resistance $\sim 1 \Omega$. Magnets A and C, B and D (as labelled in Figure 3.2) are wired in series and the two series circuits then wired in parallel giving the entire circuit also a resistance of $\sim 1 \Omega$. The coils are energized by a 100 V DC power supply to 100 Amp. During operation the magnets dissipate ~ 10 kW. The magnetic field inside each block is 16.3 ± 0.1 kG with a variation of only 4% over the sensitive areas of the blocks (Ayre 1971 and Whalley 1974).

3.3.2 THE SPECTROGRAPH ACCEPTANCE

The geometrical arrangement of the scintillators determines the acceptance of the spectrograph. An infinite momentum particle traverses the spectrograph in a straight line and determines the maximum acceptance. Whalley (1974) studied the acceptance in detail using numerical and Monte Carlo methods. The maximum acceptance is $408 \pm 2 \text{ cm}^2 \text{ sr}$. He considered the effects of magnetic field, coulomb scattering and muon energy. It was found that at the energies studied ($E > 7.2 \text{ GeV}$, the spectrograph threshold) coulomb scattering could be neglected. As a consequence the zero field acceptance is a step function (i.e. $A(E) = 0$ for $E < 7.2 \text{ GeV}$ and $A(E) = 408 \text{ cm}^2 \text{ sr}$ for $E \geq 7.2 \text{ GeV}$).

When the magnetic fields are considered, it can be seen that the more curvature the trajectory of the particle has, the more likely it is to pass outside the acceptance volume. Consequently the lower the momentum the more particles are lost. For energies $\gtrsim 7.2 \text{ GeV}$ the acceptance starts at zero and rises almost exponentially until at $\geq 100 \text{ GeV}$ the acceptance becomes equal to $408 \text{ cm}^2 \text{ sr}$. Figure 3.26 presents both the zero field acceptance and the field acceptance as a function of energy. Table 3.1 is a table of the magnetic field acceptance versus energy (after Whalley 1974).

3.3.3 THE DATA HANDLING

The analysis and data handling programs for the IBM 1130 have been developed by Wells ^{AND} Thompson (1972) and Daniels (private communication). These programs determine for each event the charge and momentum and, also, flag trays which may contain bursts. They also put the data into a useable form for further analysis on the NUMAC IBM 360/67.

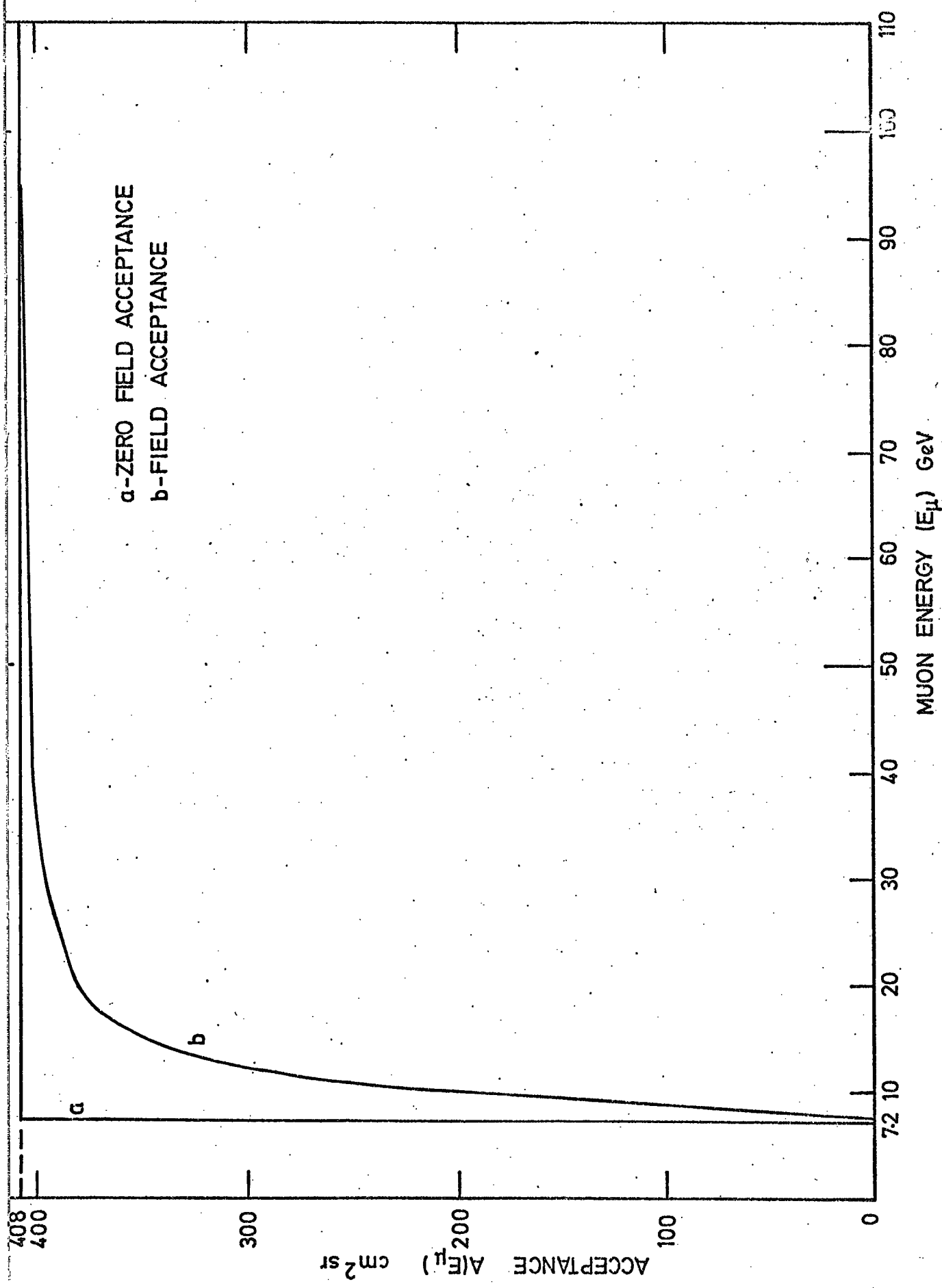


FIGURE 3.26. The spectrograph acceptance as a function of muon energy with and without the magnetic field.

TABLE 3.1

THE ACCEPTANCE AND RELATIVE ACCEPTANCE OF THE SPECTROGRAPH

Incident Energy (GeV)	Relative Acceptance	Absolute Acceptance (cm ² sr)
7.8	0.014	5.71
8.0	0.055	22.44
8.5	0.177	72.22
9.0	0.298	121.58
9.5	0.408	166.46
10.0	0.500	204.00
12.5	0.764	311.71
15.0	0.862	351.70
20.0	0.935	381.48
40.0	0.987	402.70
80.0	0.996	406.37
100.0	1.000	408.00

Since the flash tube data are collected and put on disk with each event and the pulse height data are saved until it has a block of 46 events and then stored on disk, the data end up in blocks of \sim 46 events of each of the two types of data. The initial handling programs separate the data into the different types. This separation is done to save program steps in the MARS analysis program.

The data in this divided form are then analyzed by the main MARS program to determine, if possible, the momentum, charge and other information. If an event fails in the analysis it is flagged, but saved. Later it is given special attention and is analyzed by a more sophisticated program on the IBM 360 (Daniels, private communication). For a description of the analysis programs see Wells (1972).

The analyzed data are then put into 80 column card image format and are transferred from the IBM 1130 via disk to tape and disk on the IBM 360 for further analysis and general access to any member of the MARS group.

Figure 3.27 shows the general handling procedure. The upper half of the diagram is the on-line data handling system and is under the direction of the MARS group programmer. This part of the diagram has been described briefly above. The second half is the IBM 360 data handling system as developed and used by the group programmer and by the author.

3.4 THE EXPERIMENTAL DESCRIPTION

The short term interaction experiment was set-up to run alongside and in conjunction with the long term measurement of the high energy muon spectrum. The MPFA and its associated electronics were built to operate in either of the two operational modes of the spectrograph; the object being to have pulse height information associated with each

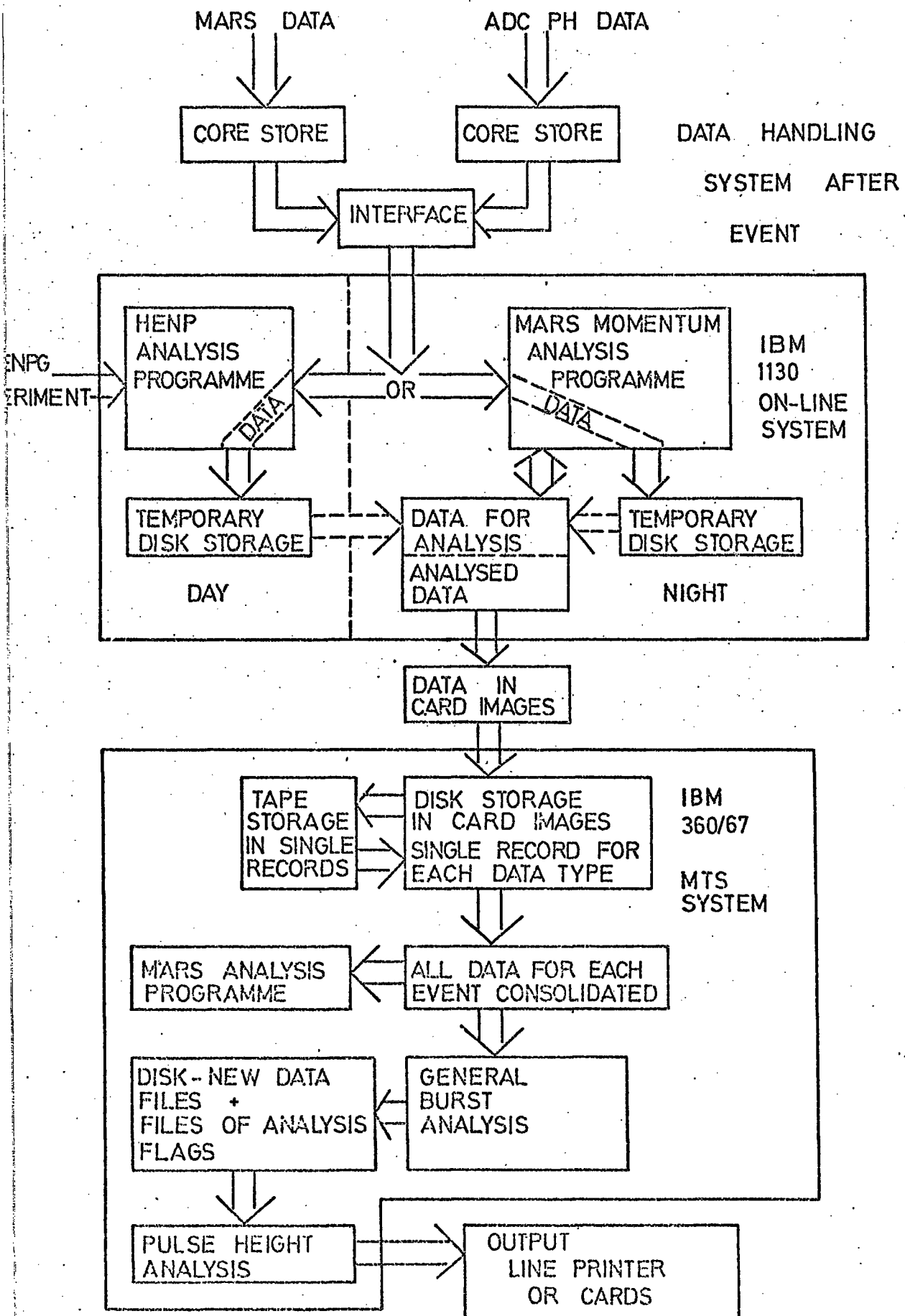


FIGURE 3.27. The MARS and interaction experiment data handling procedure.

event stored along with the flash tube data. Figure 3.28 shows diagrammatically how the experimental arrangements are operationally interconnected.

The method of using flash tubes and scintillation counters in conjunction is a powerful experimental tool, particularly for cross-calibration. The flash tubes can be used to select the single particle pulse height distribution in the scintillators. This distribution can, in turn, be used to calibrate the method used to determine the number of particles in the flash tube trays to obtain an accurate burst spectrum. Details of this method will be discussed in the next chapter.

The interaction experiment was performed in a six-month period between the 19 December 1973 and the 11 June 1974. In the first five months two types of data corresponding to the two operational modes of the spectrograph were collected. There were 4175 useable events in the 'All Events Data' and 5203 useable events in the 'High Momentum Data'.

It was decided that for about 1 month (8 May to 11 June 1974) the spectrograph could be used exclusively by the interaction experiment for a special interaction run, the object being to bias the triggering of MARS in favour of events which are accompanied out of a magnetic block by an electron shower. To do this the coincidence system was altered to trigger on large pulse heights in the scintillators at either level 1 or level 3. Figure 3.29 shows the modification to the coincidence system. The level 1 discriminator was set to a pulse height equivalent to about 3.5 particles and the level 3 discriminator was set to an equivalent pulse height of about 5.5 particles. This collection of data (called the 'Interaction Data') yielded 13349 useable events. The analysis and data handling of these three different kinds of data will be discussed in Chapters 4,5, and 7.

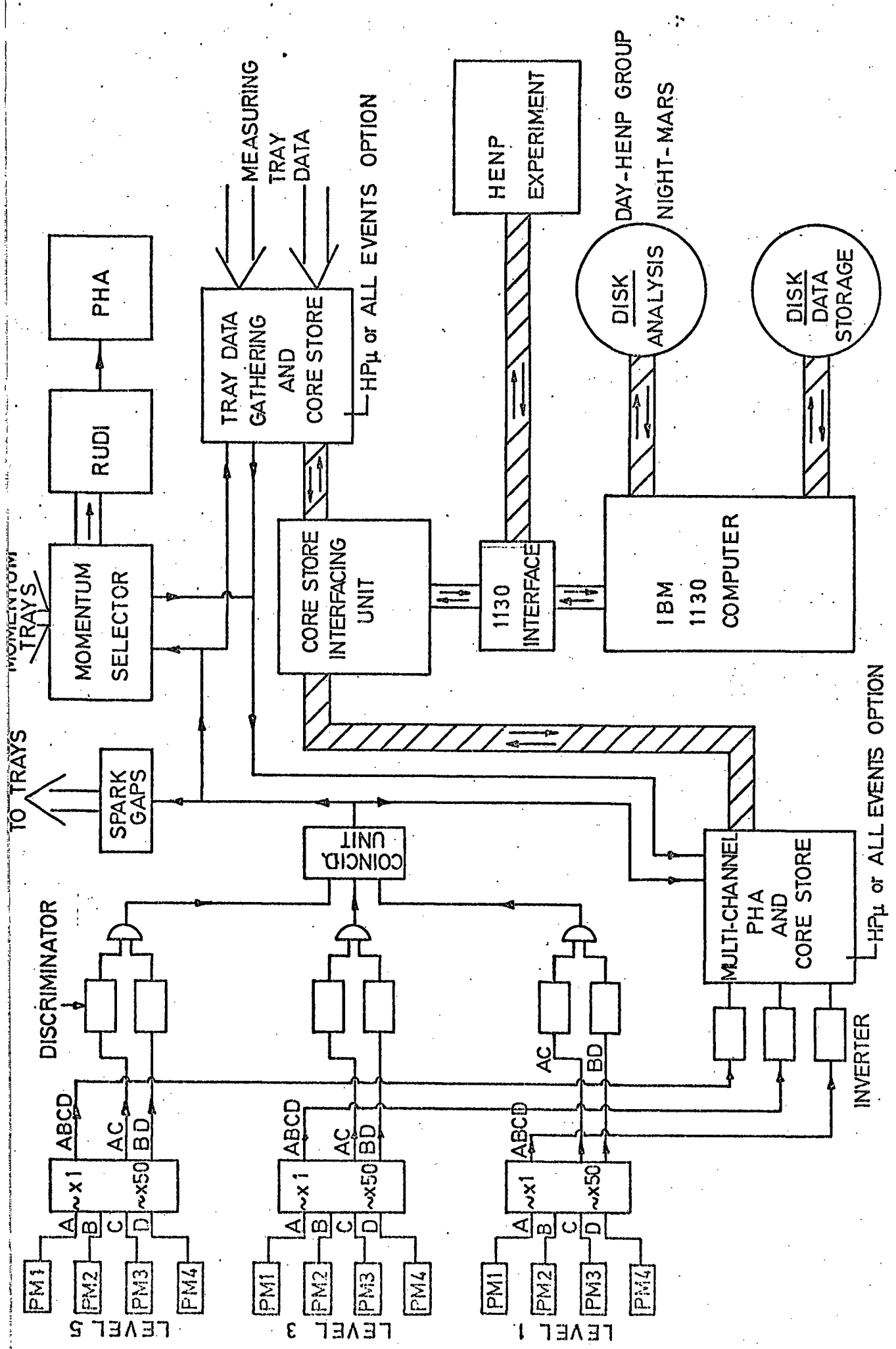


FIGURE 3.28. The MARS/interaction experiment on-line operational system.

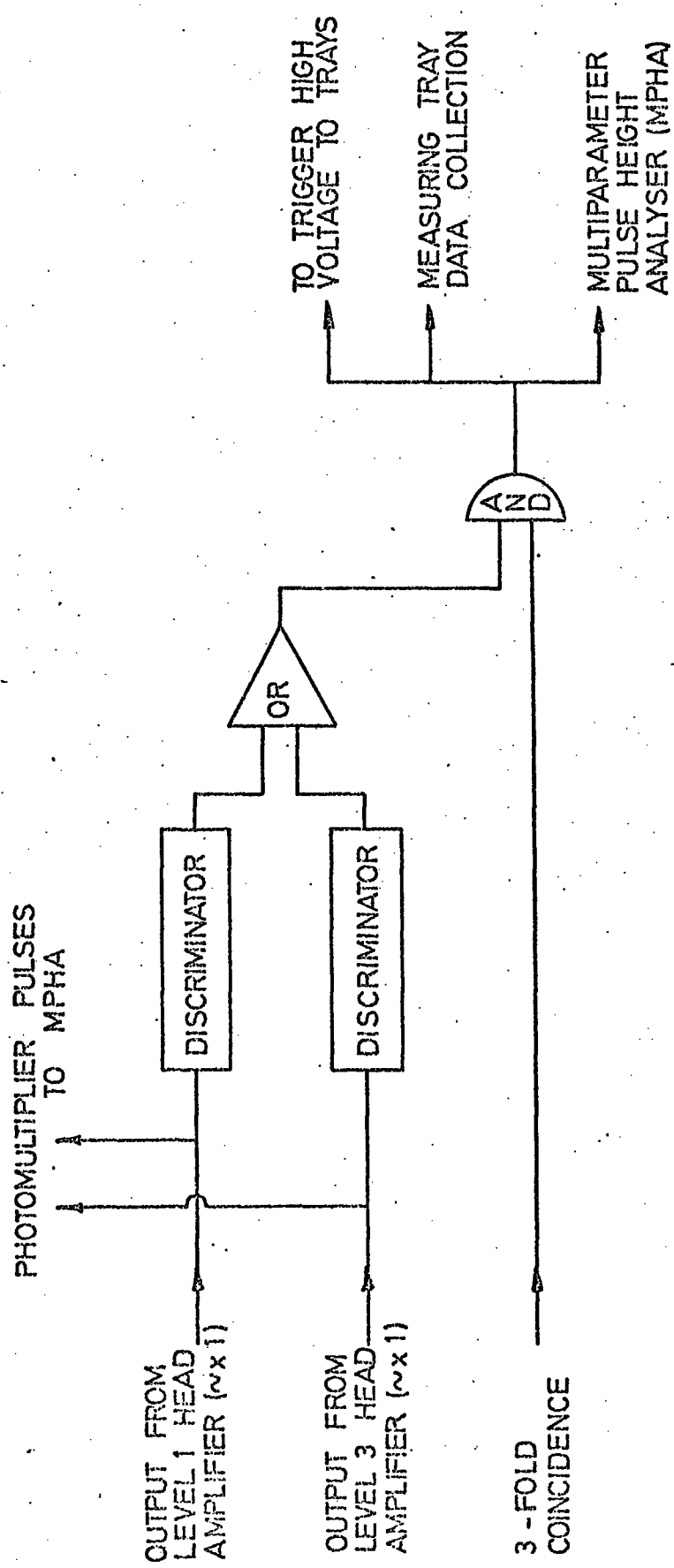


FIGURE 3.29. The special interaction run coincidence system.

3.4.1 THE ROLE OF THE AUTHOR

With an experimental project of the size and complexity of MARS, it cannot be the work of one person, but rather the work of a group. When the author joined the group in 1971, the spectrograph and the bulk of the electronics had been completed. Even part of the equipment for the interaction experiment had been built, though not operational with the spectrograph. On arrival, the author was involved in scanning and analysis of the previous interaction experiment (Hamdan 1972). This work resulted in two papers: 'Electromagnetic Interactions of Cosmic Ray Muons in Iron I: Search for a Charge Asymmetry' (Grupen et al. 1972(a)) and 'Electromagnetic Interactions of Cosmic Ray Muons in Iron II: Momentum Dependence of the Interaction Probabilities' (Grupen 1972(b)). The conclusions were that it appeared that there is no charge asymmetry, although a previous experiment by Hamdan (1972) exhibited a slight asymmetry, and that the experiment was in good agreement with the cross-section probabilities for knock-on and pair production. Since that experiment the author has been mainly concerned with setting up and operating this interaction experiment which has included the scintillator uniformity study, the development of the special photomultiplier head amplifiers, the design and building of the core store interfacing unit (built to handle the orderly passage of data from one to three core stores to the IBM 1130), the installation of the MPHA into the spectrograph system, and the production of data handling and analysis programs for the IBM 360/67. The actual running of the apparatus was carried out by the author assisted by other members of the group.

The theoretical calculations and predictions are presented in Chapter 2 and Chapter 6. The data analysis and results are presented in Chapters 4, 5 and 7.

CHAPTER 4

THE GENERAL ANALYSIS OF THE DATA

4.1 INTRODUCTION

The purpose of this experiment was to study two aspects of muon physics in iron: (1) whether or not there is an interaction charge asymmetry as observed by some experimenters, and (2) does the muon follow the predictions of quantum electrodynamics with the assumption that the muon is just a heavy electron. As a result the data analysis has been divided into three parts. This chapter discusses the general analysis of all the data. Chapter 5 discusses the interaction charge asymmetry analysis and results, and Chapter 7 discusses the burst spectra analysis and results.

As would be expected with an apparatus the size and complexity of MARS, there are systematic effects which must be taken into account. In an attempt to eliminate the effects of the magnetic field, the fields of the magnets were reversed approximately every 24 hours and the total run times under each field direction were made equal. While this eliminated field dependent effects in the acceptance and flash tube patterns, the field reversal was found to introduce a systematic effect on the gains of the photomultipliers. The correction is discussed in Section 4.3.3.

It is essential in the development of any analysis by computer to have some form of visual display to determine what the analysis ~~has~~ done and what, if any, details or errors have been missed. ~~Wm~~

In Section 3.2.3.1 the rebuilding of events in a tray has been discussed as a result and as an aid to analysis a simple program has been written to display the trays of the spectrograph for each event. Figures 4.1 to 4.7 show examples of burst events which occurred in the spectrograph. Each display also gives vital information about the event.

As can be seen from the figures, there were six ADC's recording pulse height information, two for each scintillator. This was done in case of system failures during experimental runs, of which there were none. This experiment used only levels 1 and 3 and for this analysis only ADC 3 and ADC 2, respectively, have been used.

4.2 THE DATA

In the six-month run of this experiment three classifications of data were collected (the all events data, the high momentum data and the interaction run data), each with its own distinctive attributes. Each class of data contained air shower events, events without flash tube or pulse height data, and events to which the main MARS analysis program could not assign a momentum or charge. Each event was classified as an useable or unuseable event for the analysis using the following criteria.

1. Each useable event must have had both flash tube and pulse height information associated with it.
2. It also had to have been assigned a momentum by the main analysis programs.

Of these useable events some may have been partly or completely disqualified for other reasons during subsequent analysis (i.e. no data

EVENT: 535927 DATE: 280574 TIME: 31414 FIELD: -

SERIES: 5 RUN: 10

MOMENTUM: -8.5710E 01

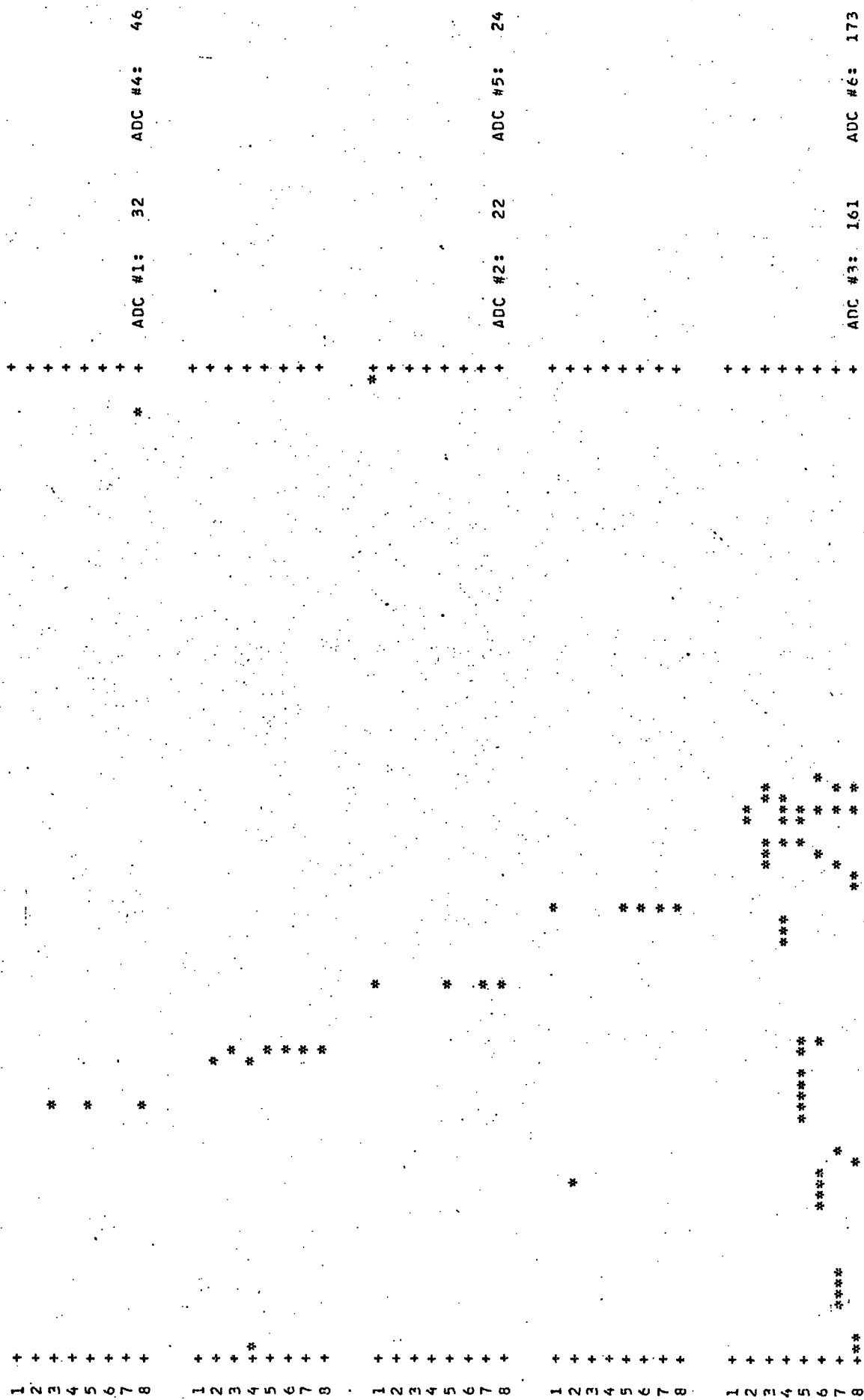


FIGURE 4.1. A muon event in MARS with a burst at level 1.

EVENT: 562920 DATE: 90674 TIME: 20139 FIELD: + SERIES: 5 FIELD: + MOMENTUM: 1.9850E 04

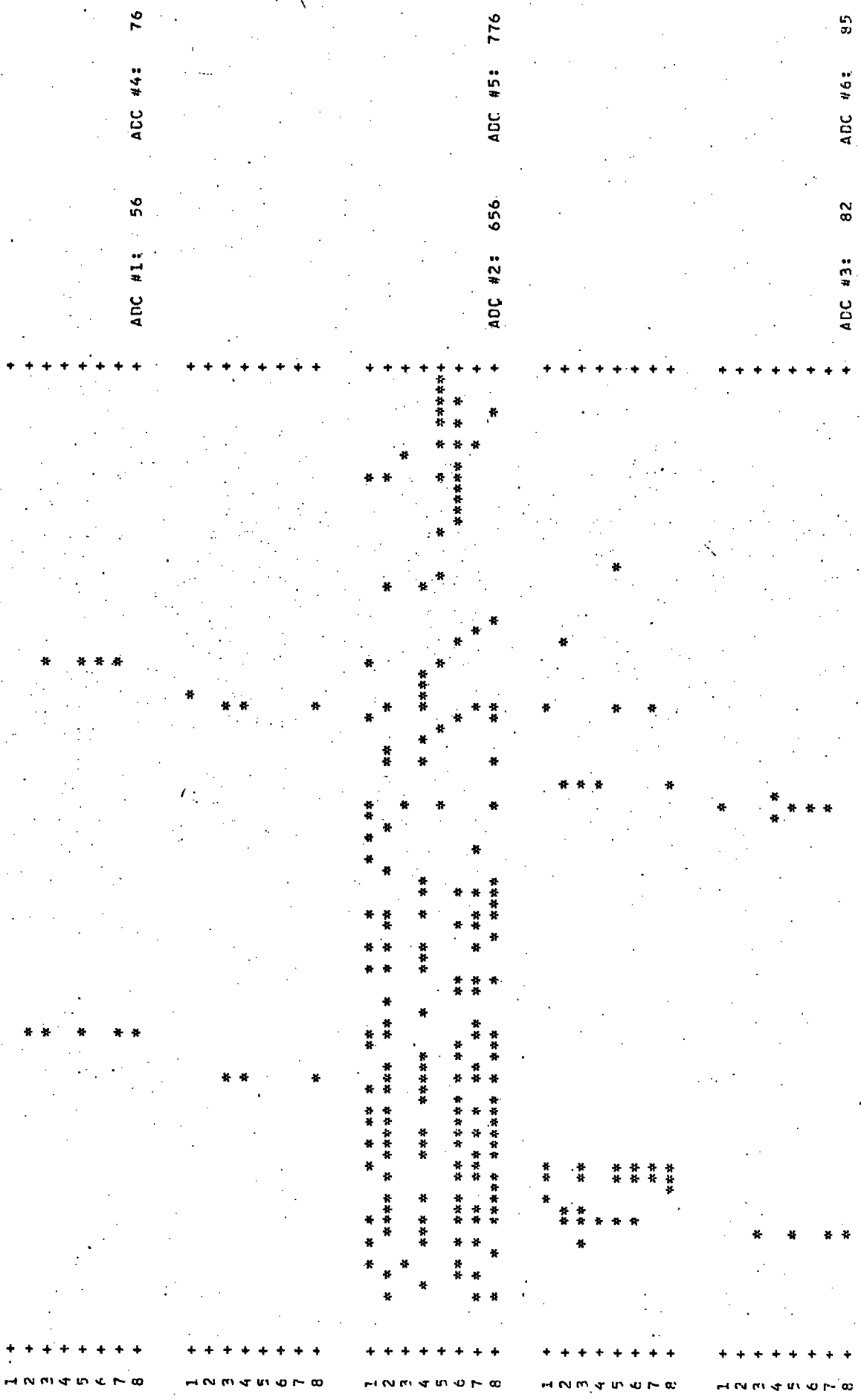


FIGURE 4.2. A double muon event in MARS with a very large burst in level 3. The left-most muon had an energy in excess of the MDM of the spectrograph.

EVENT: 495282 DATE: 200574 TIME: 185502 FIELD: + SERIES: 5 RUN: 09 MEMENTUM: 6.9000E 01

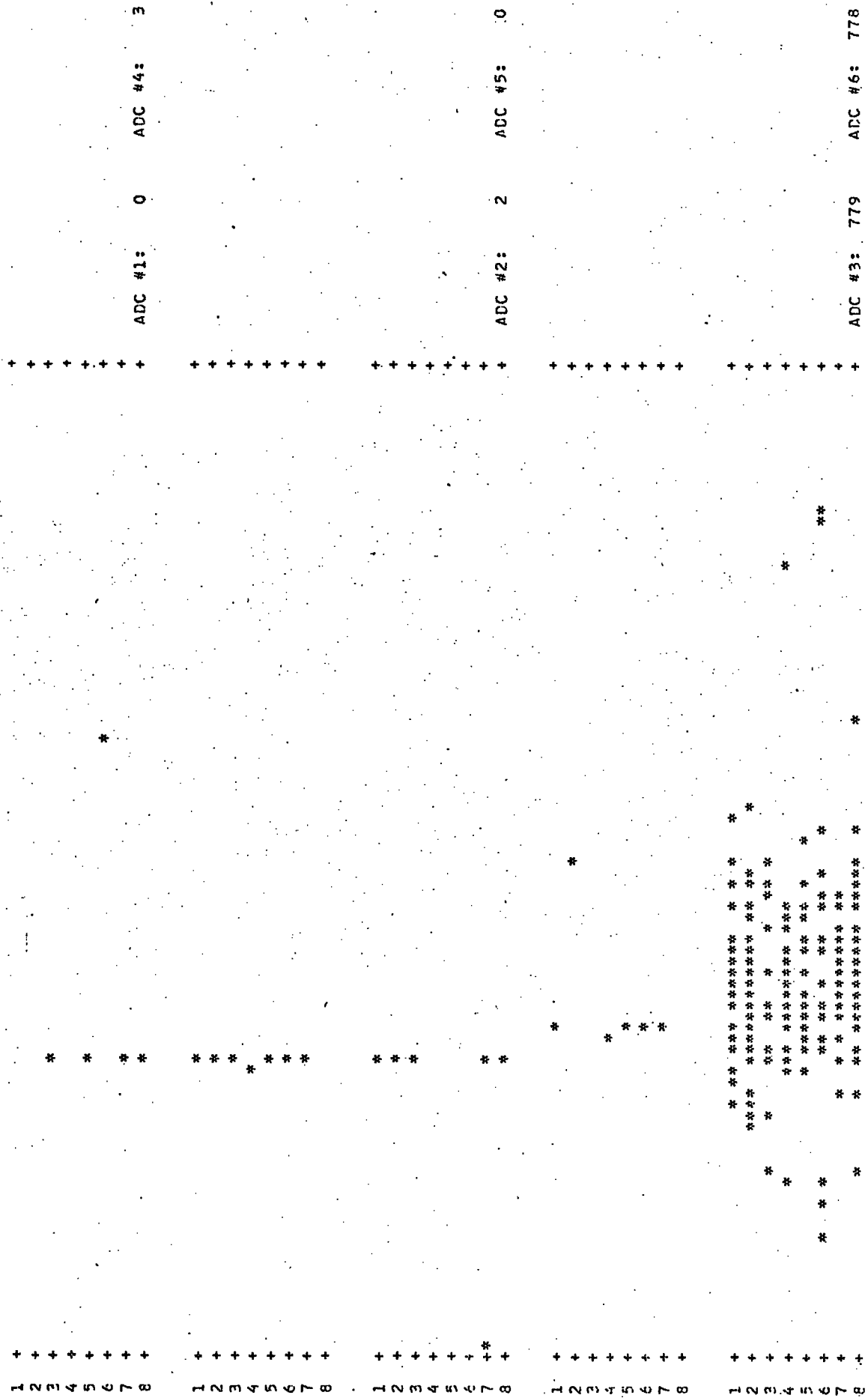


FIGURE 4.3. A muon event in MARS with a large burst at level 7.

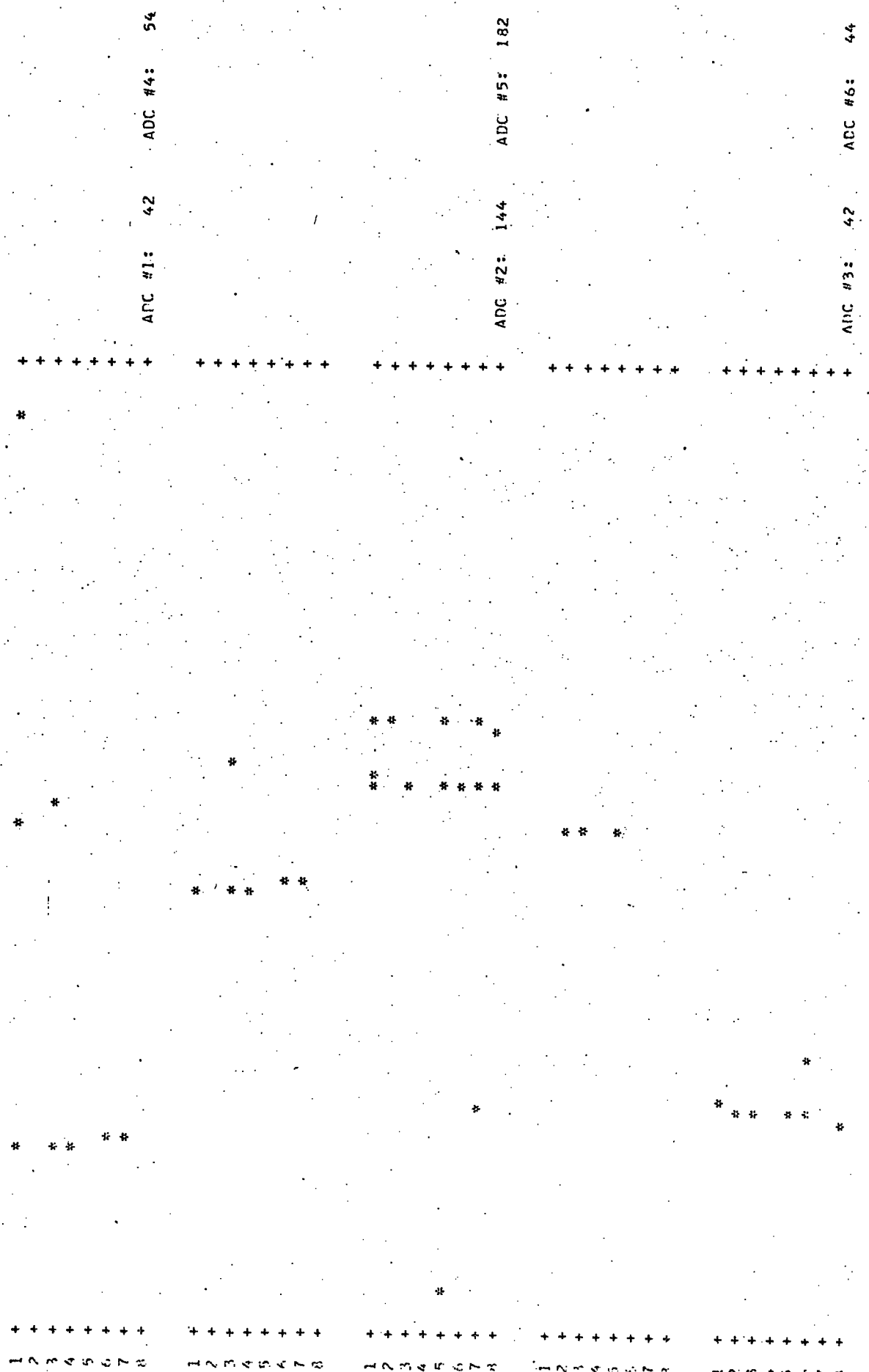


FIGURE 4.4. A muon event in MARS with a single particle accompaniment at Level 3.

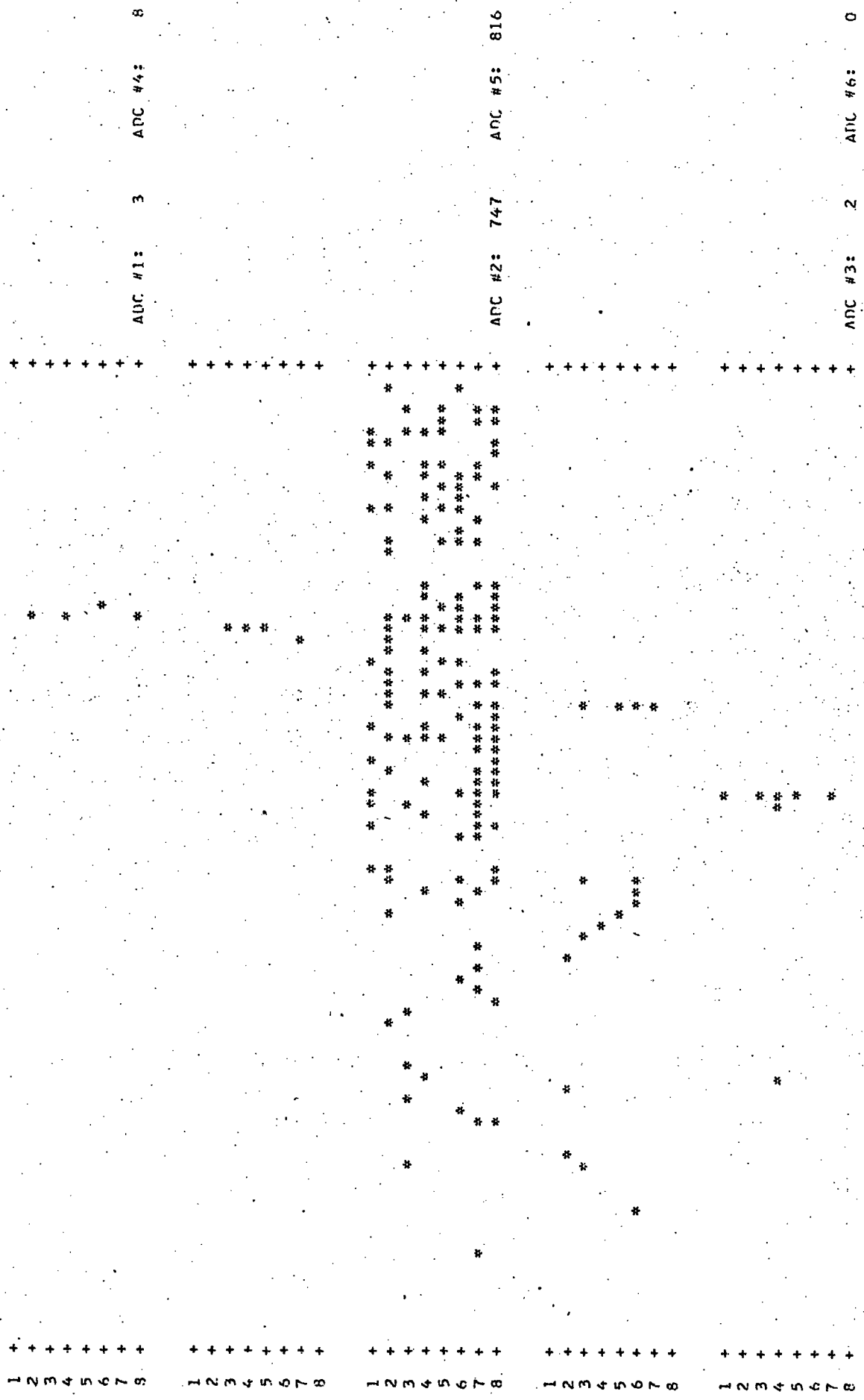


FIGURE 4.5. A muon event in MARS with a very large burst at level 3.

DATE: 210574. TIME: 135727 FIELD: - SERIES: 5 RUN: OA
MOMENTUM: -8.1070E-01
EVENT: 496339

FIGURE 4.6. A muon event in MARS with a large burst at level 3.

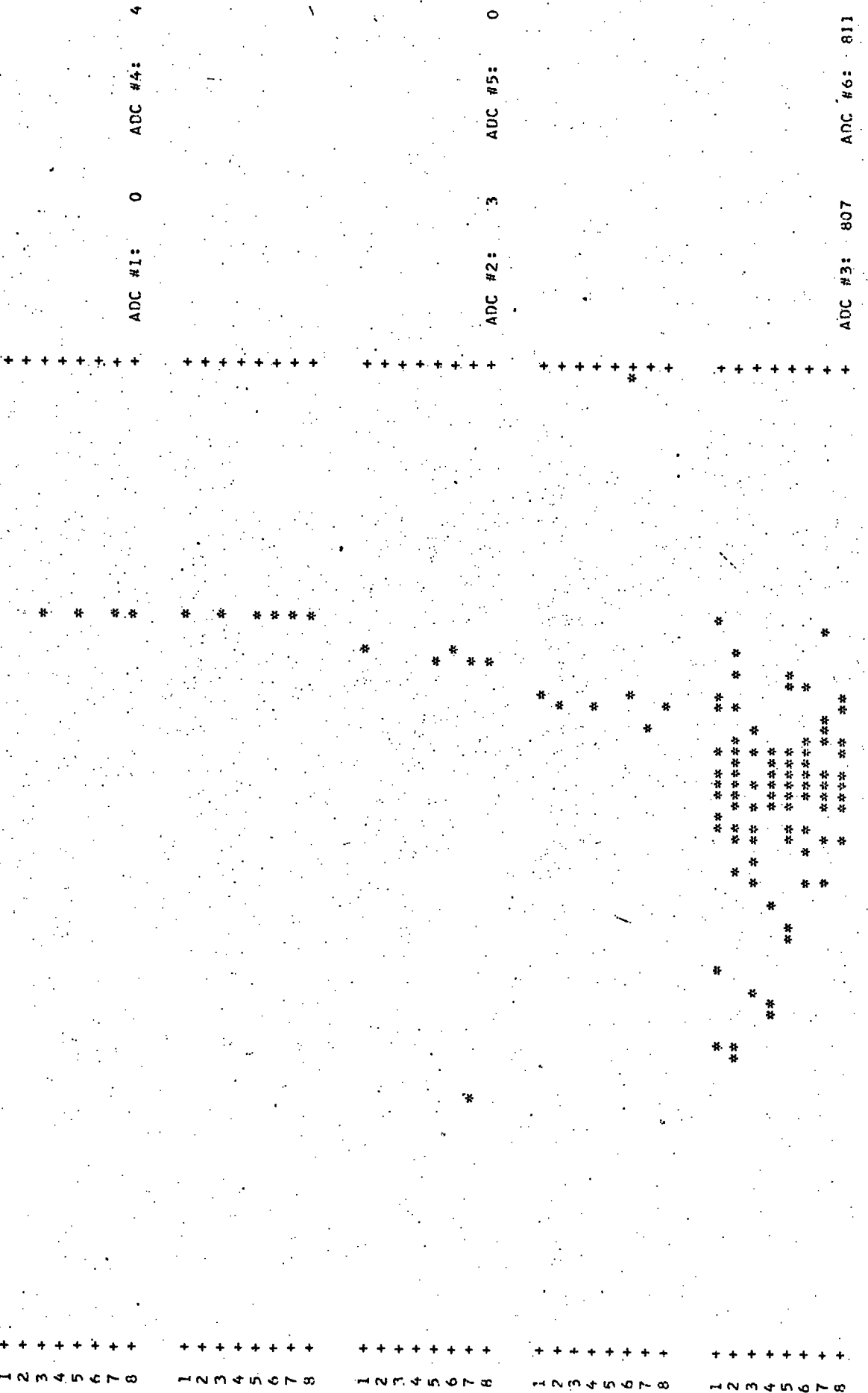


FIGURE 4.7. A muon event in MARS with a burst at level 1.

or abnormal data for a tray, or possible multiple muons traversing the spectrograph). For example, the event shown in Figure 4.2, which had three interactions, was also a double muon and was excluded.

The 'All Events' data, as the name implies, is a collection of 4175 useable events in which any event within the spectrograph acceptance is included. As would be expected the bulk of this data is low momentum. This data contains the least systematic effects and can be used as a basis to correct the other data. This data has been used for both the interaction charge asymmetry analysis and the burst spectra analysis.

The 'High Momentum' data was collected using the momentum selector described in Section 3.2.2.2. This set of data, which contains 5203 useable events, is severely biased by the momentum selector. Not only does it bias the muon spectrum but it is biased in such a way as to have a tendency to accept burst events. As a consequence this data has not been used for the burst spectra measurements, but has been used for the charge asymmetry experiment, where the muon spectrum biases should cancel one another. A benefit of this is that the bias towards bursts should amplify an asymmetry, if it exists.

The 'Interaction Run' data was collected, as described in Section 3.4, by biasing the triggering of the spectrograph towards bursts. This resulted in 13349 useable events, most of which contain bursts at levels 1 or 3. This data was biased by the triggering criteria, but by the use of the single particle distribution obtained from the All Events data, this data has been corrected (see Sections 4.3.4 and 7.3.3).

Due to the logical 'or' in the triggering circuits, there is cross-contamination of the two levels (that is, a burst event at level 1 is not likely to be a burst event at level 3). To eliminate this contamination, any events having a pulse height of less than 75 (MPHA cell) has been excluded for that level. The cut at cell 75 was chosen after comparing the pulse height distributions for the Interaction Run data at both measuring levels. This data, like the All Events data, has been used in both types of analysis. Because of the number of events, it contains the most statistically significant results.

4.3 THE GENERAL ANALYSIS

4.3.1 INTRODUCTION

The next three sections present the analyses performed on, or results obtained from, all three classes of data. These preparatory analyses and results are necessary for both the asymmetry and burst spectra measurements.

4.3.2 THE DETERMINATION OF THE MUON MOMENTUM

The momentum P (eV/c) of a particle moving in a uniform magnetic field B (gauss) with a radius of curvature r (cm) is given by

$$P = 300Br \quad (4.1)$$

The magnetic field in MARS is 16.5 kG. The radius of curvature is determined by fitting a parabola by the least squares method

to a set of from three to five co-ordinates along the track observed in the flash tube trays of the spectrograph. A parabola has been used instead of a circle to take into account energy loss. The method has been developed by Wells (1972), Wells and Thompson (1972), and Daniels (private communication, 1974).

It has been shown by Wells that the radius of curvature (r) is directly related to a parabola of the form $ax^2 + bx + c = y$ by its first coefficient

$$r = \frac{1}{2a} \quad . \quad (4.2)$$

Wells also took into account the effects of the gaps between the magnet blocks which lower the momentum predicted by equation (4.1) by about 20%. The result is that the mean spectrograph momentum in GeV/c is given by

$$p = \frac{0.196}{a} \quad (4.3)$$

a being in m^{-1} .

Wells also gives the correction required to convert the mean spectrograph momenta to incident momenta. On average, the difference is about 4 GeV/c. The momenta quoted in this report are incident momenta.

The maximum detectable momentum (MDM) is dependent on which trays are used for the fit and on the accuracy of particle location. A five-tray fit with a location of 0.3 mm gives an MDM of 5427 GeV/c. Above this momentum less than 10 muons per year are expected to pass through the spectrograph.

4.3.3 ESTIMATION OF THE BURST SIZE IN THE FLASH TUBE TRAYS

All of the data at levels 1 and 3 have been divided into particle number bins by estimating the number of particles in the flash tube trays from the flash tube pattern. This was done in the first instance to study the charge asymmetry as a function of burst size, and in the second instance to determine the burst spectra. It was therefore necessary to develop a consistent and realistic method of estimating the burst size.

The data for each tray were divided into 'groups'. A group has been defined as a cluster of discharged flash tubes lying in adjacent columns such that the number of flash tubes (> 3) discharged is greater than the number of adjacent columns. This criterion eliminates spuriously discharged flash tubes lying in adjacent columns. Because of the tube ^{PATTERN} patters (see Figure 3.5), it is very unlikely that a muon will pass through a tray without setting off at least three flash tubes. If a tray had no defined groups the data for that level have been rejected.

In most cases it was easy to determine when a single unaccompanied muon passed through a tray. Most unaccompanied muons were selected by defining a single muon event as an event with only one group of 3-8 tubes, if: (a) there was only one column of data, or (b) there were less than two tubes that lined up with other tubes in the same layer. This included all events with three or four discharged flash tubes and all other events with less than eight discharged flash tubes where there were less than 1.25 discharged flash tubes per layer.

For any other tube configuration the analysis was more complex and has been based on previous work done by Rogers (1965), modified

by the author to be useable with the present apparatus. It is based on binomial statistics and assumes that within the boundary of the shower the shower particles are uniformly distributed.

Consider K adjacent counters each of area $S \text{ m}^2$. The probability (P) of L of the K counters being triggered by a shower of uniform density Δ particles m^{-2} is given by

$$P(K, L, \Delta) = \frac{K!}{K!(K-L)!} (1 - e^{-\Delta S})^L (e^{-\Delta S})^{K-L} \quad (4.4)$$

where $1 - e^{-\Delta S}$ is the probability of at least one particle passing through any single counter.

The most likely density for triggering L of K counters can be obtained by maximizing equation (4.4)

$$\frac{\partial P(K, L, \Delta)}{\partial \Delta} = 0 = \frac{(K-L)}{K} e^{-\Delta S} \quad (4.5)$$

and solving for Δ (particles m^{-2})

$$= \frac{1}{S} \ln \left| \frac{K}{K-L} \right| \quad (4.6)$$

To obtain the burst size it is only necessary to multiply by the physical shower size. The shower size was assumed to be KS (the area of one detector times the number of detectors triggered), and therefore

$$N = QK \ln \left| \frac{K}{K-L} \right| \quad (4.7)$$

where N is the shower size and Q is an enhancement constant introduced to take into account: (1) the non-uniform density of shower particles, and (2) particles which may have passed through the gaps between the flash tubes.

Equation (4.7) was applied to the trays in the following way.

It was said

$$N = \text{integral part of } (1.78K \ln \left| \frac{K}{K-L} \right|) \quad (4.8)$$

where

N is the number of particles in the burst, if one of the special cases below does not apply,

1.78 is the arbitrary enhancement constant Q,

K is the number of adjacent columns with at least one flash tube discharged,

L is the average number of discharged tubes per layer, i.e.

$$L = \frac{\sum \text{ tubes}}{8} \quad (4.9)$$

There are three special cases.

1. If $K - L = 0$, then it was assumed that

$$\ln \left| \frac{K}{K-L} \right| = 1 \quad (4.10)$$

2. If the result of equation (4.8) yielded $N = 0$ then N was set equal to 1.

3. If N from equation (4.8) was less than the number of groups then N was set equal to the number of groups.

When an event with more than one group was analyzed, it was assumed to be one large group with the empty columns between the groups not included. The value of N includes the muon so that the burst size was $N - 1$.

As an example of how this method has been used, consider the burst event at level 1 in Figure 4.3. This event contains three groups, where there are 31 adjacent columns of data ($K = 31$) and there are 124 tubes discharged in the three groups ($L = 124/8 = 15.5$ (tubes/layer)). From equation (4.7)

$$N = \text{integral part of} (1.78 \times 31 \times \ln \frac{31}{15.5}) = 38 \text{ particles.}$$

(4.11)

Due to the arbitrariness of the constant and the unknown effect of the non-uniform density, it is essential that this method be calibrated. The calibration is discussed in Section 4.3.5.

4.3.4 MAGNETIC FIELD EFFECTS ON THE PHOTOMULTIPLIERS

To eliminate the effect of the magnetic field on the acceptance, the fields in the magnet blocks were reversed every 24 hours. However, it was discovered while comparing the pulse height distributions with respect to field that despite the precautions taken to shield the photomultipliers from the fields, there was a noticeable effect on the photomultiplier gains.

A study has been carried out to look at the effect on the scintillation counter pulse heights at levels 1 and 3 as a function of lateral position of the event track in the flash tube trays and as a function of magnetic field. Each tray was divided into nine ten-flash-tube column cells. The mean pulse height of unaccompanied muons passing through each cell was determined.

Figure 4.8 presents the results of this study along with third-order polynomials fitted to the statistical results by the least squares method. It can be seen from this figure that there is

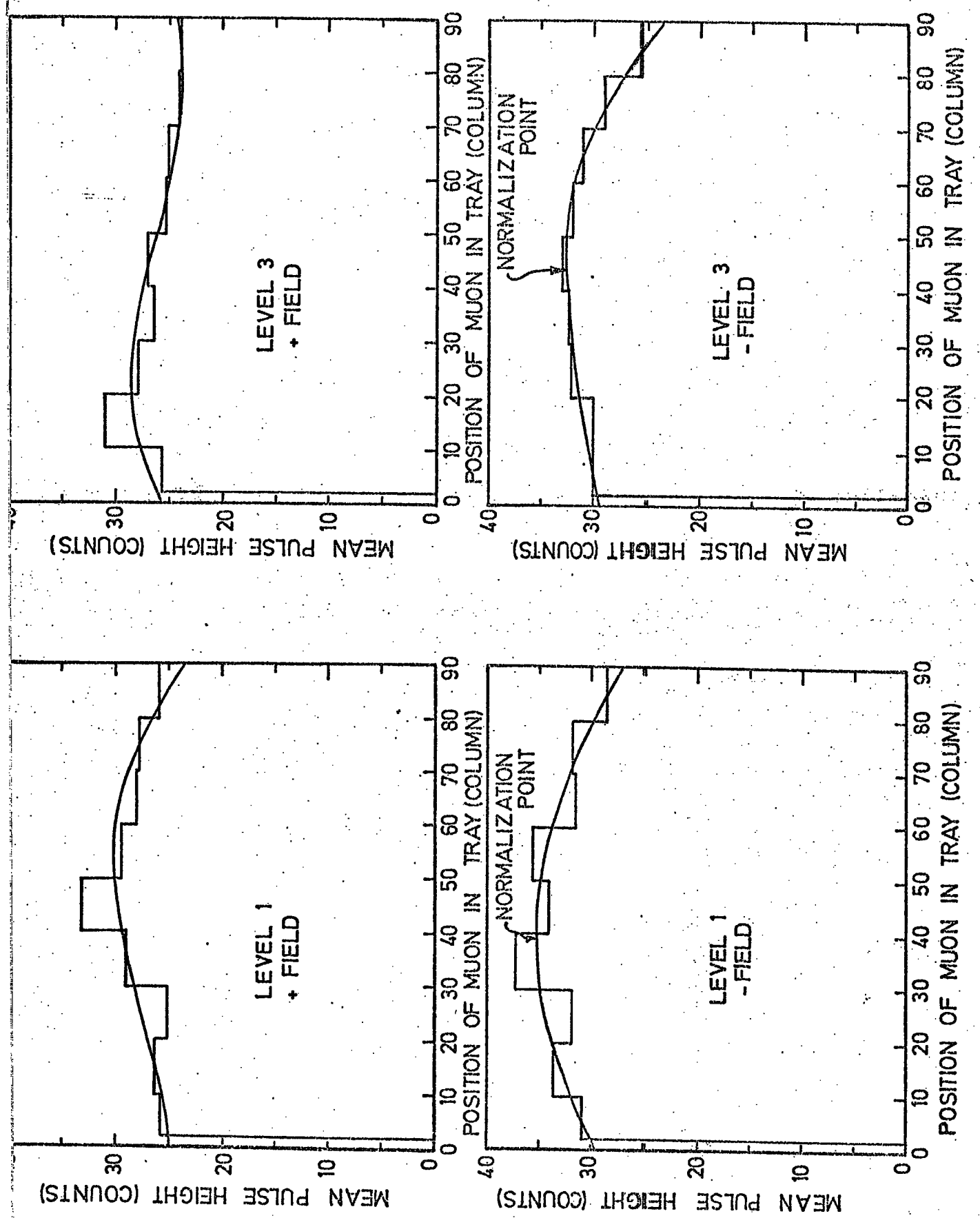


FIGURE 4.8. The photomultiplier mean pulse height as a function of tray position, magnetic field and level presented with third order polynomial fits.

an effect of both position and field. The negative field pulse heights were generally larger than the positive field pulse heights. Figure 4.9 compares the polynomial fits at each level.

Using the polynomials the pulse heights of all the events were corrected so that the means of the pulse height distributions were equal to the normalization point shown in both figures. The normalization point was arbitrarily selected to be the maximum value at each level.

The polynomial fit was of the form

$$Y = aX^3 + bX^2 + cX + d \quad (4.12)$$

where X is the position of the tray determined by taking the mid-point in the group or groups,

Y is the mean pulse height expected from equation (4.12).

The correction was then

$$PH_N = \frac{Z}{Y} PH_o \quad (4.13)$$

where

PH_N is the corrected pulse height

PH_o is the measured pulse height

Y is as defined above

Z is the normalization point: for level 1 $Z = 35.18$, for level 3 $Z = 32.65$.

The error in the correction is estimated at about 5%.

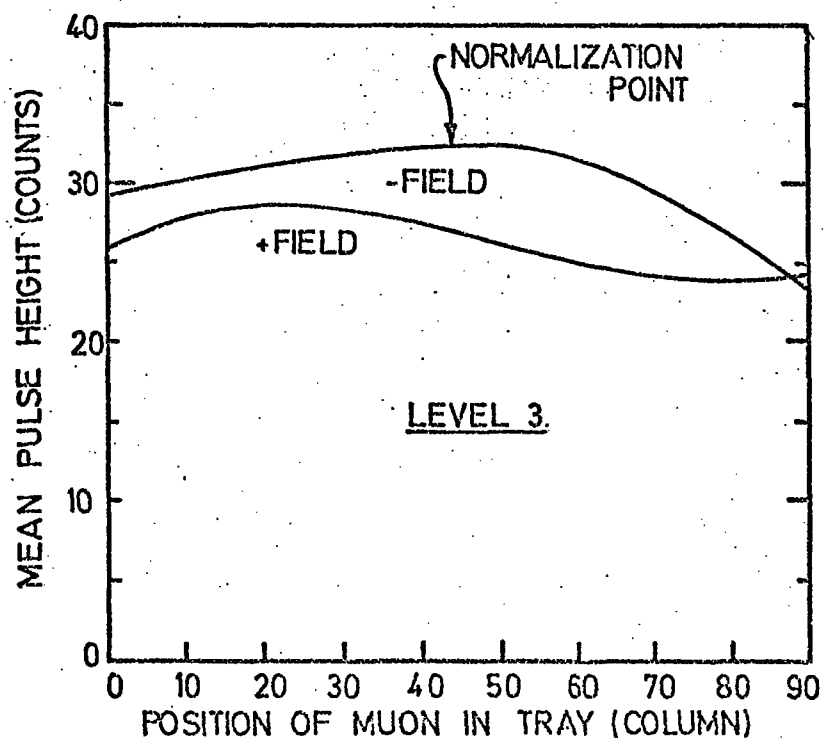
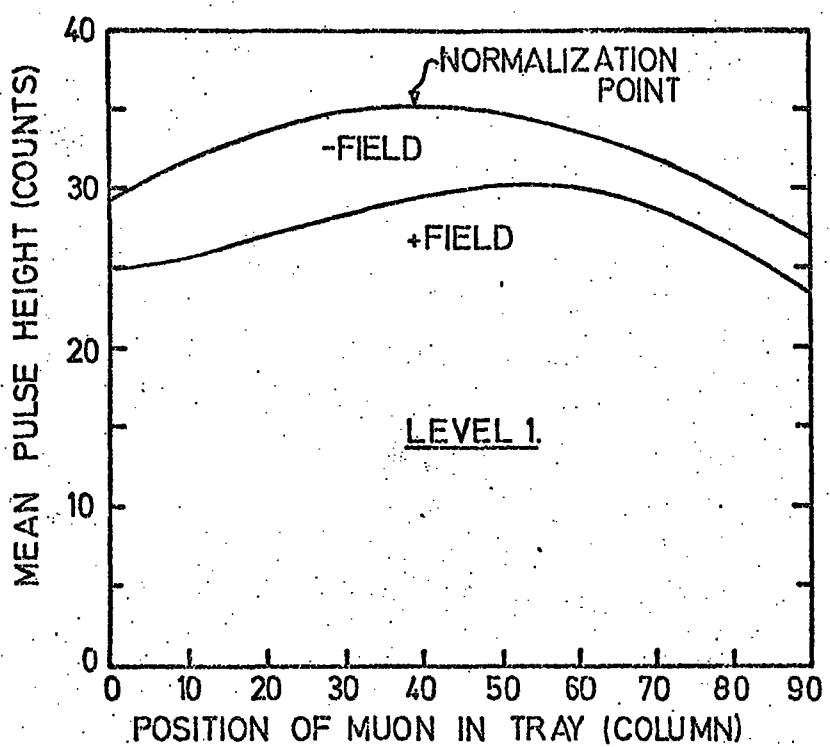


FIGURE 4.9. The polynomial fits to the mean pulse height as a function of lateral tray position and magnetic field.

TABLE 4.1

COEFFICIENTS OF POLYNOMIALS FITTED (EQUATION (4.12))

	a	b	c	d
Level 1:	+ Field -4.21×10^{-5}	2.74×10^{-3}	7.51×10^{-2}	24.72
	- Field 1.84×10^{-6}	-3.70×10^{-3}	2.90×10^{-1}	29.39
Level 2:	+ Field 5.84×10^{-5}	-8.60×10^{-3}	2.92×10^{-1}	25.58
	- Field 13.21×10^{-5}	1.10×10^{-3}	9.28×10^{-2}	29.17

4.3.5 CALIBRATION OF THE FLASH TUBE DETERMINED BURST SIZE

Using the definition of unaccompanied particles, the single particle pulse height distribution in the scintillation counters has been determined by selecting the pulse heights associated with these single muons only. Figures 4.10 and 4.11 are the single particle distributions at the experimental levels. In this section they will be used to calibrate the flash tube trays. In a later section they will be used to correct the interaction run data.

All the pulse height data has been divided into particle number cells according to the flash tube method described in Section 4.3.3. The means of these distributions were then divided by the mean of the single particle distribution to determine the mean number of particles in the cell (including the muon).

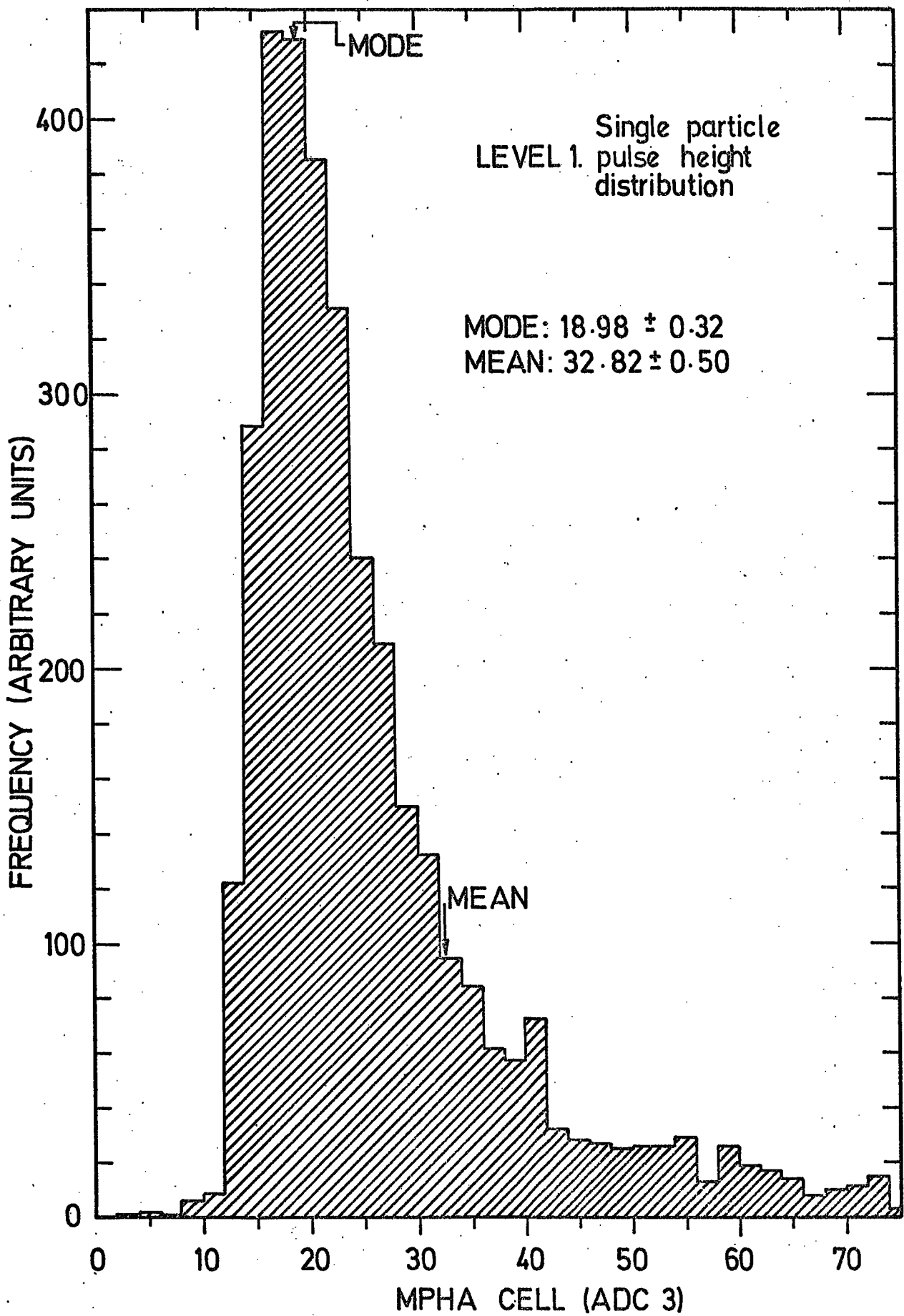


FIGURE 4.10. The single particle pulse height distribution at level 1.

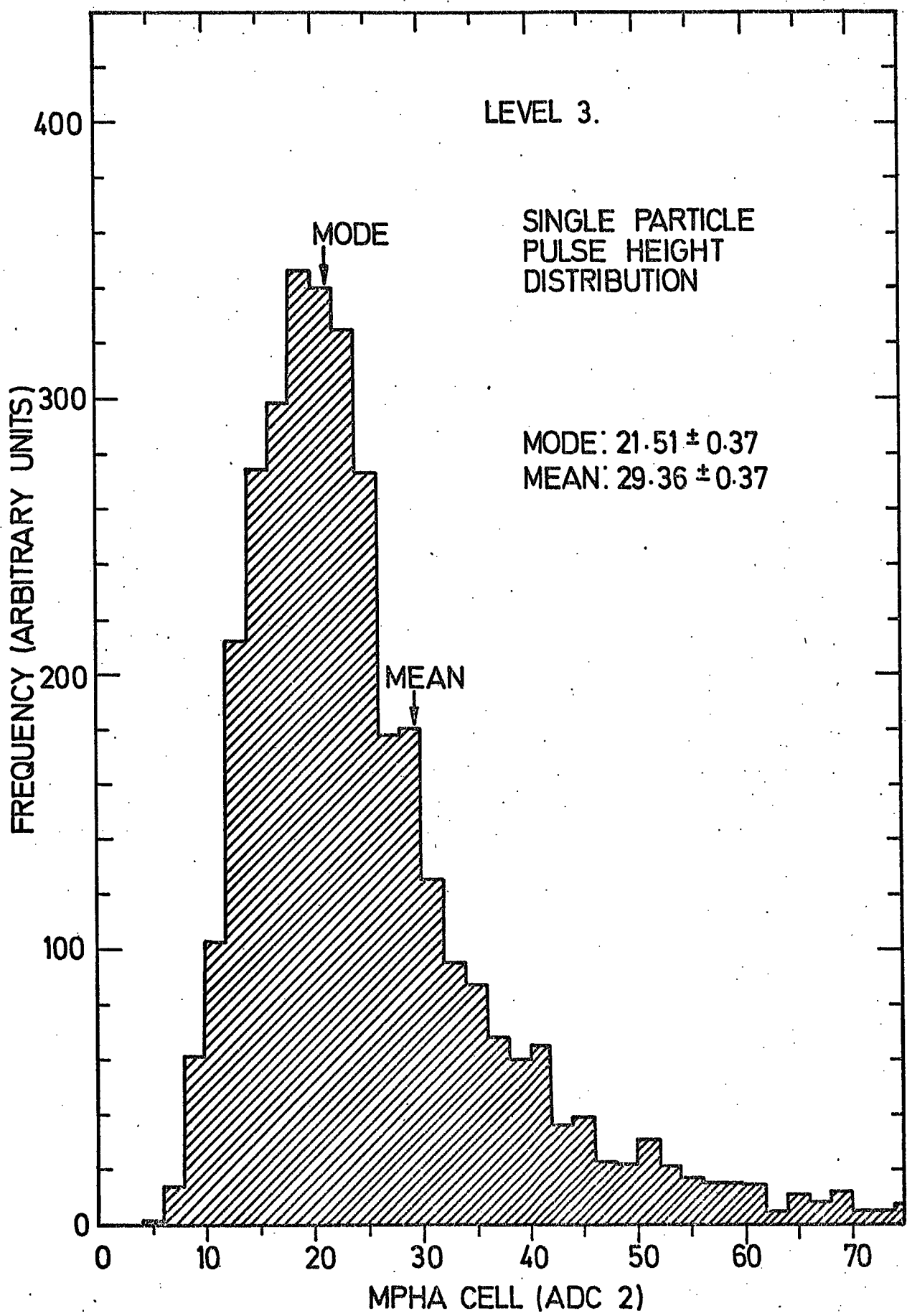


FIGURE 4.11. The single particle pulse height distribution at level 3.

It has been assumed that every particle which passes through a scintillator will produce identical pulse height distributions. This implies that the N particle distribution is the same as folding N single particle distributions together. It follows that the mean of the N particle distribution will be N multiplied by the single particle mean.

The result of this calibration can be seen in Figures 4.12 and 4.13. By using a weighted least squares fitting procedure a linear equation of the form

$$ax + b = y \quad (4.14)$$

has been fitted. Each point was weighted inversely as the square of its errors. The result of the fit is:

$$\text{For Level 1: } y = 1.08x - 0.46 \quad (4.15)$$

$$\text{For Level 3: } y = 1.59x - 0.24 \quad (4.16)$$

where

y is the predicted number of particles in the burst (excluding the muon)

x is the number as determined by the flash tubes.

These curves are also presented in the figures.

As can be observed the flash tube method provided good results for level 1 and underestimated the numbers by ~ 60% at level 3. The discrepancy between the two levels is not unexpected. The rejection efficiencies for a single muon are different for each tray. Monte Carlo calculations predict ~ 5 flash tubes per track on average. Figure 4.14 contains plots of the average number of discharged tubes per track for the two trays. Level 1, as might be expected, is close to the theoretical value, while level 3 is

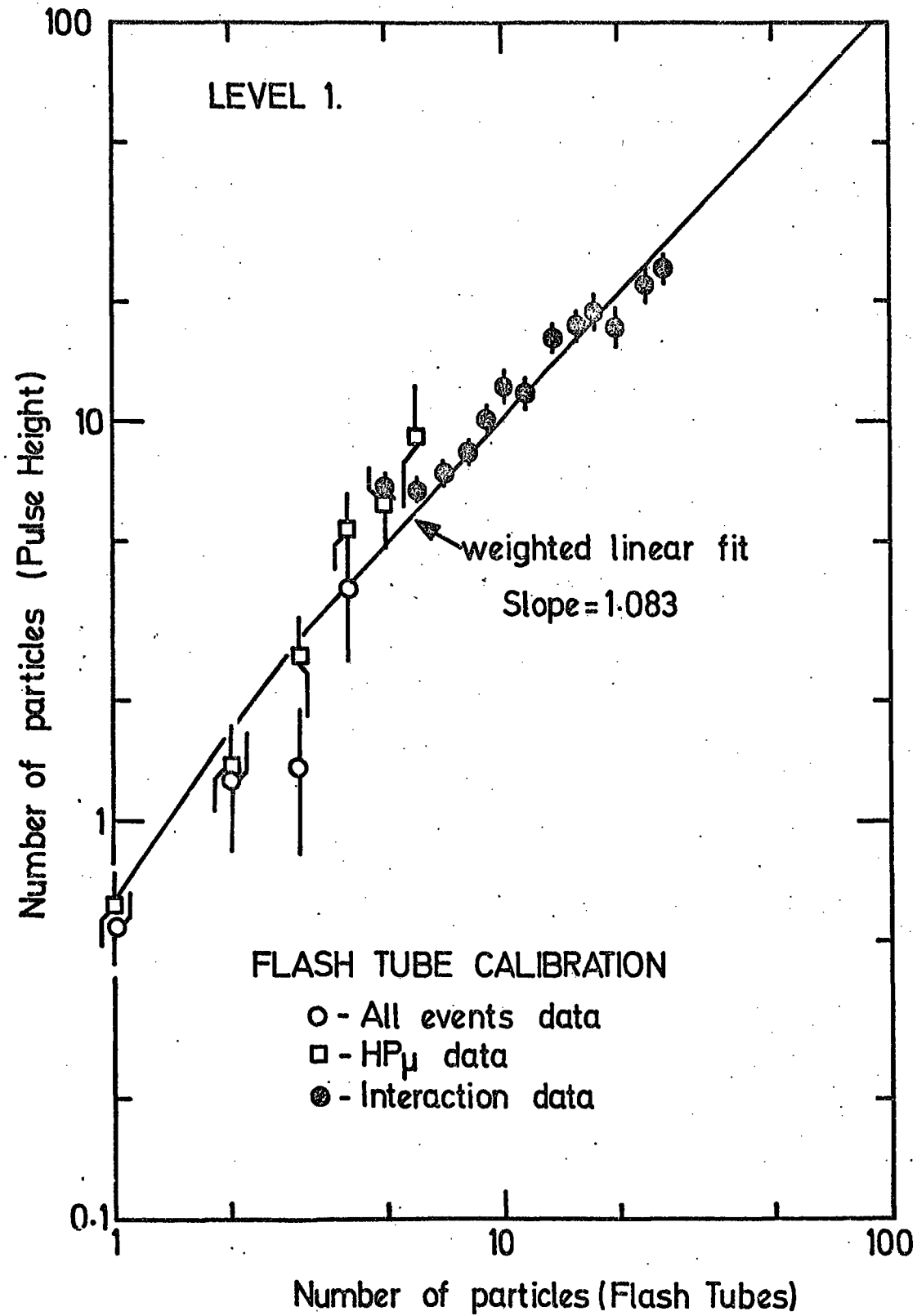


FIGURE 4.12. The flash tube particle number calibration data with weighted linear fit.

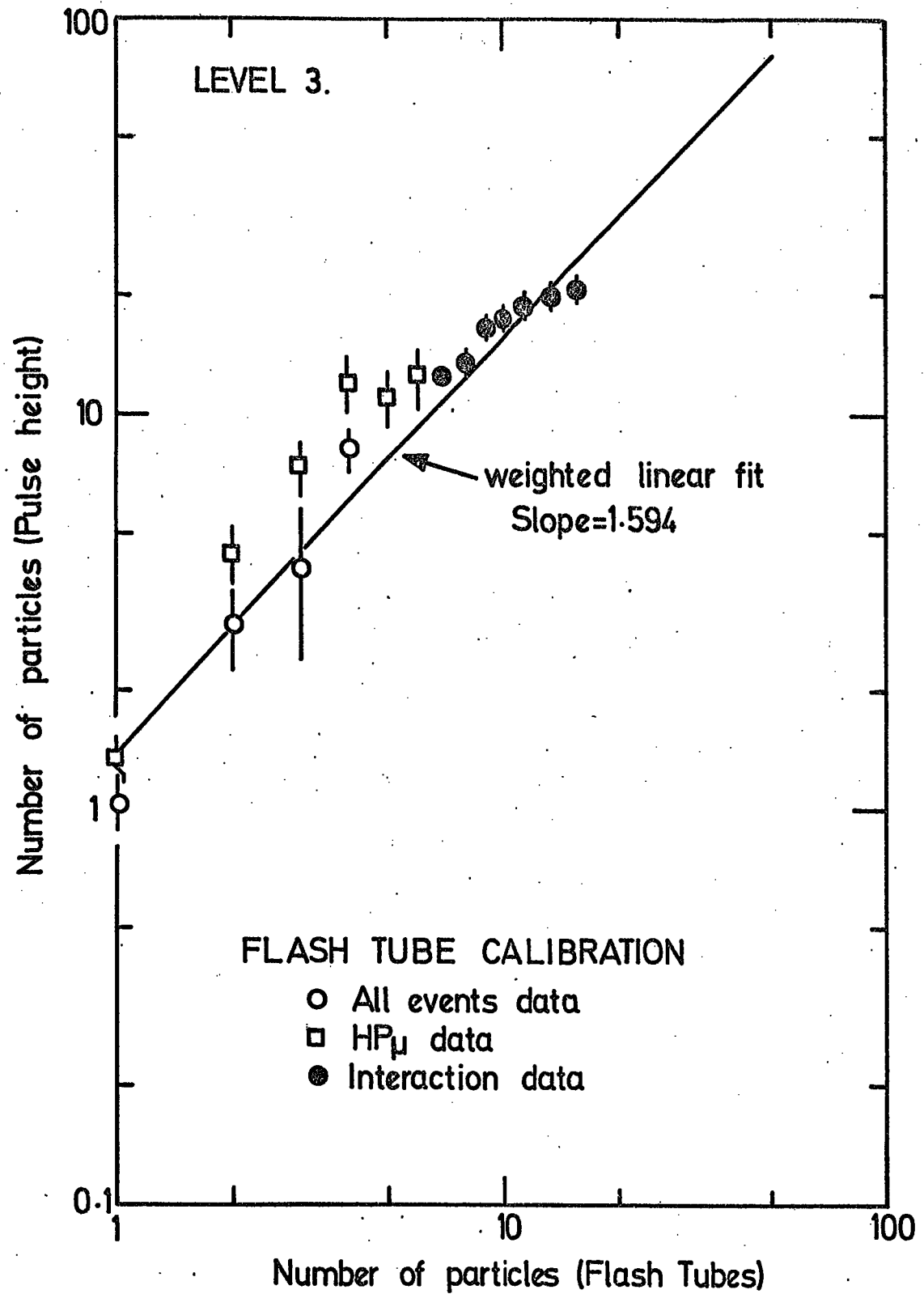


FIGURE 4.13. The flash tube particle number calibration data with weighted linear fit.

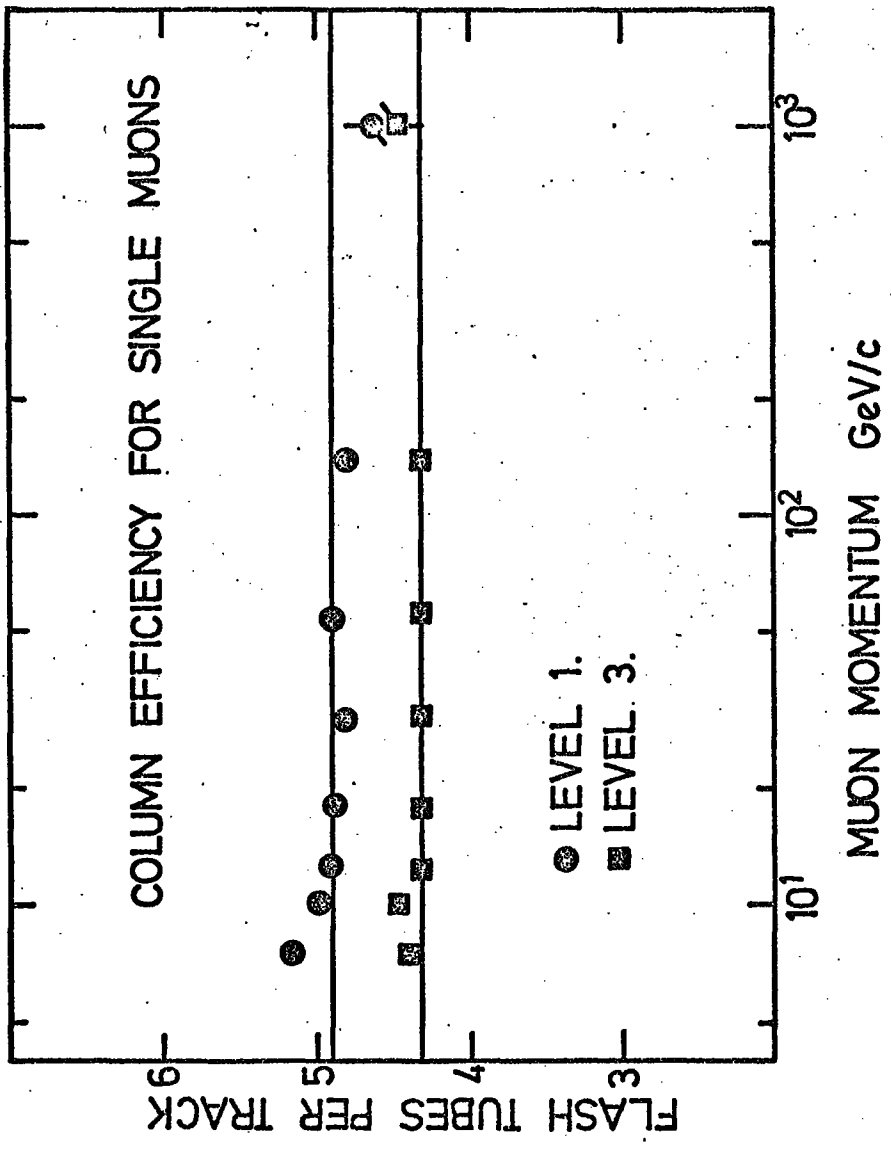


FIGURE 4.14. The average number of flash tubes per single muon track as a function of muon momentum.

low. This inefficiency is visually observable in EAS and large burst events. For example, layers 3 and 5 in the burst at level 3 in Figure 4.2 show marked inefficiencies.

Within the experimental errors the fits seem to be good. The error in the fit has been estimated at $\sim 50\%$ at 1 particle to $< 10\%$ at > 8 particles.

TABLE 4.2

CALIBRATED BURST SIZE

Flash Tube Determined Burst Size	Corrected Burst Size Level 1	Corrected Burst Size Level 3
1	0.62	1.36
2	1.71	2.95
3	2.79	4.55
4	3.87	6.14
5	4.96	7.73
6	6.04	9.33
7	7.12	10.92
8	8.20	12.52
9	9.29	14.11
10	10.37	15.70
11	11.46	17.30
12	12.54	18.89
13	13.62	20.48
14	14.70	22.08
15	15.79	23.67
20	21.20	31.64
25	26.62	39.61
30	32.04	47.58

CHAPTER 5

THE INTERACTION CHARGE ASYMMETRY

5.1 INTRODUCTION

The interaction charge asymmetry has been studied as a function of muon incident energy and the burst size at both levels 1 and 3. Three techniques have been employed. The first has been the conventional method of simply counting the number of events of a given burst size and comparing the charge ratio with that for incident muons. The second method has been to estimate the ratio of the means of the pulse height distributions for positive and negative muon events as a function of burst size and to compare them with the expected result of unity. The third method has been to study the pulse height distributions in detail by dividing them into six sections. An excess of positive or negative events has been looked for in each section.

5.2 METHOD 1: THE INTERACTION CHARGE RATIO

All of the events have been divided into four energy bins (7-14 GeV, 14-54 GeV, 54-204 GeV, > 204 GeV) and into five burst size cells as determined by the flash tubes (0, 1, 2-4, 5-10, > 10 particles). For each of these energy-burst size bins a charge ratio has been found by using equation (5.1).

$$R = N_+ / N_- \quad (5.1)$$

where:

R is the charge ratio

N_+, N_- are the number of positive and negative events respectively for each bin.

The error on the charge ratio can be shown to be

$$dR = R \left(\frac{1}{N_+} + \frac{1}{N_-} \right)^{\frac{1}{2}} \quad (5.2)$$

The data and the numerical results of this analysis are given in tabular form in Tables 5.1a,b,c,d,e,f. In Figure 5.1 are the graphical results as a function of burst size, incident muon energy and level. These results are compared with the charge ratio for all muon events observed in the spectrograph (1.254 ± 0.014). (This charge ratio appears low because of the momentum selector contamination. The charge ratio excluding the high momentum data is 1.292 ± 0.018 .) The errors presented are statistical.

There is no evidence in the results from this method that would support an interaction charge asymmetry either positive or negative. The only oddity occurs in the single muon plot (Figure 5.1a) where there appear to be too few positive muons of energy > 204 GeV. Although the point is low by about two standard deviations, it is considered to be statistical.

5.3 METHOD 2: THE RATIO OF MEAN PULSE HEIGHTS FOR POSITIVE AND NEGATIVE EVENTS

This method of analysis has been to look at the ratio of mean pulse heights for positive and negative events as a function of burst size and muon energy. If muons of different charges interact

All Events Data. Mean Energy = 11.12 ± 0.04 GeV					
	Burst Size	Number of Positive Events	Number of Negative Events	Charge Ratio R = N ₊ /N ₋	Mean Pulse Height of Positive Events
					Mean Pulse Height of Negative Events
Level: 1	0	769	573	1.34 ± 0.07	33.49 ± 0.85
	1	30	29	1.03 ± 0.27	42.17 ± 3.25
	2-4	5	2	3.00 ± 2.45	32.83 ± 8.73
AII	805	605	1.33 ± 0.07	33.80 ± 0.83	36.28 ± 1.49
Level: 3	0	559	559	1.34 ± 0.07	31.15 ± 0.70
	1-2	51	329	1.76 ± 0.41	48.88 ± 5.25
	3-6	9	3	3.00 ± 2.00	123.20 ± 33.61
AII	810	591	1.37 ± 0.07	33.78 ± 1.02	33.02 ± 1.04
All Events Data. Mean Energy = 24.18 ± 0.20 GeV					
Level: 1	0	1136	908	1.25 ± 0.06	35.12 ± 0.76
	1	75	54	1.39 ± 0.25	53.81 ± 5.46
	2-4	24	20	1.20 ± 0.36	79.29 ± 17.48
	5-10	1	2	0.50 ± 0.61	174.00 ± 196.00
AII	1236	984	1.26 ± 0.05	37.22 ± 0.88	37.33 ± 1.33
Level: 3	0	1098	855	1.28 ± 0.06	31.39 ± 0.76
	1-2	58	48	1.21 ± 0.24	59.28 ± 7.18
	3-6	10	5	2.00 ± 1.01	127.40 ± 22.82
	7-16	1	2	0.50 ± 0.61	436.00 ± 800.00
AII	1167	910	1.28 ± 0.06	33.95 ± 0.95	35.63 ± 1.56
All Events Data. Mean Energy = 86.37 ± 2.02 GeV					
Level: 1	0	125	95	1.32 ± 0.18	37.06 ± 2.38
	1	8	9	0.89 ± 0.43	70.75 ± 14.24
	2-4	5	6	0.83 ± 0.50	102.60 ± 30.41
AII	138	110	1.26 ± 0.16	41.38 ± 2.83	40.95 ± 4.50
Level: 3	0	132	98	1.35 ± 0.18	33.89 ± 2.17
	1-2	3	8	0.38 ± 0.25	179.30 ± 100.04
AII	137	106	1.29 ± 0.17	37.92 ± 3.65	34.06 ± 2.74

All Events Data. Mean Energy = 789 ± 314 GeV					
	Burst Size	Number of Positive Events	Number of Negative Events	Charge Ratio R = N ₊ /N ₋	Mean Pulse Height of Positive Events
					Mean Pulse Height of Negative Events
Level: 1	0	769	573	1.34 ± 0.07	33.49 ± 0.85
	1	30	29	1.03 ± 0.27	42.17 ± 3.25
	2-4	5	2	3.00 ± 2.45	32.83 ± 8.73
AII	805	605	1.33 ± 0.07	33.80 ± 0.83	36.28 ± 1.49
Level: 3	0	559	559	1.34 ± 0.07	31.15 ± 0.70
	1-2	51	329	1.76 ± 0.41	48.88 ± 5.25
	3-6	9	3	3.00 ± 2.00	123.20 ± 33.61
AII	810	591	1.37 ± 0.07	33.78 ± 1.02	33.02 ± 1.04
All Events Data. Mean Energy = 27.13 ± 1.82 GeV					
Level: 1	0	559	559	1.34 ± 0.07	31.15 ± 0.70
	1-2	51	329	1.76 ± 0.41	48.88 ± 5.25
	3-6	9	3	3.00 ± 2.00	123.20 ± 33.61
AII	810	591	1.37 ± 0.07	33.78 ± 1.02	33.02 ± 1.04
Level: 3	0	559	559	1.34 ± 0.07	31.15 ± 0.70
	1-2	51	329	1.76 ± 0.41	48.88 ± 5.25
	3-6	9	3	3.00 ± 2.00	123.20 ± 33.61
AII	810	591	1.37 ± 0.07	33.78 ± 1.02	33.02 ± 1.04
All Events Data. Mean Energy = 27.13 ± 1.82 GeV					
Level: 1	0	1966	1525	1.30 ± 0.04	31.62 ± 0.53
	1-2	112	85	1.32 ± 0.19	57.76 ± 5.53
	3-6	21	8	2.63 ± 1.09	122.20 ± 18.70
AII	2187	1712	2	1.00 ± 1.00	430.00 ± 42.00
Level: 3	0	1966	1525	1.30 ± 0.04	31.62 ± 0.53
	1-2	112	85	1.32 ± 0.19	57.76 ± 5.53
	3-6	21	8	2.63 ± 1.09	122.20 ± 18.70
AII	2121	1620	2	1.00 ± 1.00	430.00 ± 42.00
All Events Data. Mean Energy = 11.51 ± 0.04 GeV					
High Momentum Data. Mean Energy = 11.51 ± 0.04 GeV					
Level: 1	0	1966	1525	1.30 ± 0.04	31.62 ± 0.53
	1-2	112	85	1.32 ± 0.19	57.76 ± 5.53
	3-6	21	8	2.63 ± 1.09	122.20 ± 18.70
AII	2121	1620	2	1.00 ± 1.00	430.00 ± 42.00
Level: 3	0	1966	1525	1.30 ± 0.04	31.62 ± 0.53
	1-2	112	85	1.32 ± 0.19	57.76 ± 5.53
	3-6	21	8	2.63 ± 1.09	122.20 ± 18.70
AII	2121	1620	2	1.00 ± 1.00	430.00 ± 42.00

(b)

TABLE 5.1. Data and results from the charge asymmetry data for method 1 and method 2.

(a)

Interaction Run Data.		Mean Energy = 25.46 ± 0.11 GeV		Mean Energy = 803 ± 241 GeV		Mean Energy = 40.82 ± 3.56 GeV	
Burst Size	Number of Positive Events	Number of Negative Events	Charge Ratio R = N ₊ /N ₋	Mean Pulse Height of Positive Events	Pulse Height of Negative Events	Ratio of Means R' = M ₊ /M ₋	Ratio of Means R' = M ₊ /M ₋
Level: 1							
0	2255	1734	1.30 ± 0.04	151.60 ± 1.30	151.30 ± 1.40	1.00 ± 0.01	0.83 ± 0.50
1	421	364	1.16 ± 0.08	172.70 ± 4.20	176.20 ± 4.60	0.98 ± 0.03	0.86 ± 0.48
2-4	601	460	1.31 ± 0.08	207.6	200.40 ± 5.50	1.04 ± 0.04	1.15 ± 0.44
5-10	255	206	1.24 ± 0.12	286.50 ± 11.10	257.30 ± 11.50	1.11 ± 0.07	0.80 ± 0.54
>10	80	76	1.05 ± 0.17	497.00 ± 26.00	466.00 ± 27.00	1.07 ± 0.08	4.00 ± 4.47
All	3612	2840	1.27 ± 0.03	180.50 ± 1.90	178.60 ± 2.10	1.01 ± 0.02	338.40 ± 40.60
Level: 3							
0	239	205	1.17 ± 0.11	175.30 ± 4.50	179.20 ± 5.60	0.98 ± 0.04	0
1-2	220	151	1.46 ± 0.15	207.10 ± 5.50	193.40 ± 6.80	1.07 ± 0.05	1-2
3-6	357	282	1.27 ± 0.10	266.20 ± 6.11	276.20 ± 7.20	0.96 ± 0.03	3-6
7-16	155	114	1.36 ± 0.17	426.20 ± 15.20	465.80 ± 18.10	0.92 ± 0.05	7-16
>16	41	45	0.91 ± 0.20	716.70 ± 22.60	716.70 ± 20.30	0.93 ± 0.04	>16
All	1012	797	1.27 ± 0.06	274.60 ± 5.30	290.60 ± 6.80	0.94 ± 0.03	All
Interaction Run Data.							
Level: 1							
0	259	194	1.34 ± 0.13	157.70 ± 3.30	11.44 ± 5.00	1.02 ± 0.04	0
1	70	53	1.32 ± 0.24	178.60 ± 13.70	130.90 ± 11.80	0.99 ± 0.10	1-2
2-4	147	89	1.65 ± 0.22	196.20 ± 10.10	10.10 ± 18.50	0.88 ± 0.09	3-6
5-10	63	67	1.02 ± 0.17	317.10 ± 25.40	299.20 ± 19.10	1.06 ± 0.11	7-16
>10	46	28	1.64 ± 0.39	643.00 ± 35.00	670.00 ± 40.00	0.96 ± 0.08	>16
All	590	431	1.37 ± 0.87	226.50 ± 7.50	228.10 ± 8.70	0.99 ± 0.05	All
Level: 3							
0	56	37	1.51 ± 0.32	184.00 ± 9.20	203.80 ± 14.40	0.90 ± 0.08	0
1-2	42	39	1.08 ± 0.24	211.20 ± 14.70	211.10 ± 14.60	1.00 ± 0.10	1-2
3-6	102	62	1.65 ± 0.26	294.10 ± 11.00	265.60 ± 12.40	1.05 ± 0.07	3-6
7-16	36	26	1.39 ± 0.35	486.10 ± 36.30	448.30 ± 32.40	1.08 ± 0.11	7-16
>16	16	9	1.78 ± 0.74	78.07 ± 24.30	78.30 ± 44.70	0.99 ± 0.06	>16
All	252	173	1.46 ± 0.14	310.10 ± 12.90	296.20 ± 13.60	1.05 ± 0.06	All
Interaction Run Data.							
Level: 1							
0	22	16	1.38 ± 0.45	171.60 ± 20.80	158.00 ± 18.80	1.09 ± 0.18	0
1	9	6	1.50 ± 0.79	219.80 ± 23.20	156.20 ± 31.70	1.41 ± 0.33	1
2-4	20	18	1.11 ± 0.36	217.80 ± 34.00	236.60 ± 26.20	0.92 ± 0.18	2-4
5-10	15	8	2.00 ± 0.87	318.30 ± 49.20	245.60 ± 60.30	1.30 ± 0.38	5-10
>10	11	10	1.10 ± 0.48	564.80 ± 61.10	668.10 ± 70.90	0.84 ± 0.13	>10
All	78	58	1.35 ± 0.23	274.50 ± 22.50	282.20 ± 29.70	0.97 ± 0.13	All
Level: 3							
Burst Size	Number of Positive Events	Number of Negative Events	Charge Ratio R = N ₊ /N ₋	Mean Pulse Height of Positive Events	Pulse Height of Negative Events	Ratio of Means R' = M ₊ /M ₋	Ratio of Means R' = M ₊ /M ₋
Burst Size	Number of Positive Events	Number of Negative Events	Charge Ratio R = N ₊ /N ₋	Mean Pulse Height of Positive Events	Pulse Height of Negative Events	Ratio of Means R' = M ₊ /M ₋	Ratio of Means R' = M ₊ /M ₋
Burst Size	Number of Positive Events	Number of Negative Events	Charge Ratio R = N ₊ /N ₋	Mean Pulse Height of Positive Events	Pulse Height of Negative Events	Ratio of Means R' = M ₊ /M ₋	Ratio of Means R' = M ₊ /M ₋

(d)

TABLE 5.1. Data and results from the charge asymmetry data for method 1 and method 2.

(c)

High Momentum Data.		Mean Energy = 24.43 ± 0.19 GeV		High Momentum Data.		Mean Energy = 501 ± 38 GeV		High Momentum Data.		Mean Energy = 43.5 ± 1.88 GeV		High Momentum Data.		Mean Energy = 11.27 ± 0.28 GeV								
Burst Size	Number of Positive Events	Number of Negative Events	Charge Ratio R = N ₊ /N ₋	Pulse Height of Positive Events	Mean Pulse Height of Negative Events	Burst Size	Number of Positive Events	Number of Negative Events	Charge Ratio R = N ₊ /N ₋	Pulse Height of Positive Events	Mean Pulse Height of Negative Events	Burst Size	Number of Positive Events	Number of Negative Events	Charge Ratio R = N ₊ /N ₋	Pulse Height of Positive Events	Mean Pulse Height of Negative Events					
Level: 1																						
0	128	1086	1.12 ± 0.05	41.88 ± 1.03	38.38 ± 1.21	1.09 ± 0.04	0	67	72	0.93 ± 0.16	36.51 ± 2.89	43.35 ± 5.01	0.85 ± 0.12	0	123	78	1.58 ± 0.23	170.70 ± 6.30	180.30 ± 7.40	0.95 ± 0.05		
1	98	87	1.12 ± 0.16	71.26 ± 1.18	55.85 ± 7.22	1.25 ± 0.26	1-2	9	13	0.69 ± 0.30	141.90 ± 62.10	72.30 ± 13.20	1.96 ± 0.93	1-2	123	51	1.45 ± 0.26	194.00 ± 9.20	195.20 ± 9.80	0.97 ± 0.07		
2-4	23	31	0.74 ± 0.20	122.70 ± 24.20	106.00 ± 15.10	1.16 ± 0.28	3-6	6	3	2.00 ± 0.14	283.00 ± 73.00	608.00 ± 156.00	0.47 ± 0.17	3-6	123	91	1.35 ± 0.19	258.00 ± 9.00	288.90 ± 11.60	0.89 ± 0.60		
5-10	3	5	0.60 ± 0.43	462.00 ± 154.00	352.00 ± 130.00	1.31 ± 0.65	A11	85	89	0.96 ± 0.14	84.94 ± 16.28	77.07 ± 16.33	1.10 ± 0.31	7-16	26	37	0.94 ± 0.33	403.10 ± 47.40	365.20 ± 40.50	1.10 ± 0.18		
>10	1	2	0.50 ± 0.61	742.00 ± 742.00	855.00 ± 855.00	0.87 ± 0.87	A11	1211	1211	44.09 ± 1.61	1.79 ± 1.79	1.06 ± 0.06	High Momentum Data. Mean Energy = 501 ± 38 GeV		High Momentum Data. Mean Energy = 43.5 ± 1.88 GeV		High Momentum Data. Mean Energy = 11.27 ± 0.28 GeV					
Level: 3																						
0	1169	1045	1.12 ± 0.05	39.39 ± 0.91	38.33 ± 1.00	1.03 ± 0.03	0	0	2328	2002	1.16 ± 0.04	41.70 ± 0.72	38.63 ± 0.93	1.08 ± 0.03	0	2328	1943	1.15 ± 0.04	39.76 ± 0.67	38.42 ± 0.73	1.04 ± 0.03	
1-2	64	64	1.00 ± 0.18	88.27 ± 14.50	89.83 ± 10.95	0.98 ± 0.20	1	177	170	1.04 ± 0.11	56.76 ± 8.07	60.36 ± 4.99	1.10 ± 0.16	1-2	138	134	1.03 ± 0.12	88.87 ± 8.89	86.21 ± 7.76	1.05 ± 0.14		
3-6	21	27	0.78 ± 0.23	185.10 ± 24.30	223.70 ± 30.40	0.83 ± 0.16	2-4	55	63	0.87 ± 0.16	144.60 ± 16.70	119.70 ± 19.60	1.21 ± 0.24	3-6	42	57	0.74 ± 0.15	271.30 ± 28.50	254.30 ± 28.30	1.07 ± 0.16		
7-16	8	3	2.67 ± 1.80	456.40 ± 37.70	698.30 ± 97.60	0.67 ± 0.11	5-10	11	16	0.69 ± 0.27	440.00 ± 81.00	261.00 ± 52.00	1.68 ± 0.46	5-10	10	3	0.50 ± 0.35	717.00 ± 60.00	684.00 ± 133.00	1.04 ± 0.22		
>16	1	1	1.00 ± 1.41	926.00 ± 88.00	887.00 ± 1.04 ±	2.05 ± 0.99 ± 0.05	A11	1140	1140	48.09 ± 1.79	1.79 ± 1.79	1.06 ± 0.06	High Momentum Data. Mean Energy = 96.17 ± 1.83 GeV		High Momentum Data. Mean Energy = 43.5 ± 1.88 GeV		High Momentum Data. Mean Energy = 11.27 ± 0.28 GeV					
Level: 3																						
0	201	162	1.24 ± 0.13	43.04 ± 1.93	45.00 ± 6.37	0.96 ± 0.14	1-2	0	2242	1943	1.15 ± 0.04	39.76 ± 0.67	38.42 ± 0.73	1.04 ± 0.03	1-2	138	134	1.03 ± 0.12	88.87 ± 8.89	86.21 ± 7.76	1.05 ± 0.14	
1	22	21	1.05 ± 0.32	88.50 ± 29.48	57.50 ± 7.71	1.53 ± 0.55	3-6	42	57	0.74 ± 0.15	271.30 ± 28.50	254.30 ± 28.30	1.07 ± 0.16	3-6	18	8	2.25 ± 0.96	570.80 ± 47.10	501.10 ± 81.10	1.14 ± 0.21		
2-4	14	13	1.08 ± 0.41	215.10 ± 32.90	140.60 ± 51.00	1.53 ± 0.60	>16	4	4	1.00 ± 0.71	935.00 ± 129.00	771.00 ± 93.00	1.21 ± 0.16	>16	141	244	1.14 ± 0.03	52.00 ± 1.66	50.23 ± 1.67	1.04 ± 0.05		
5-10	6	5	1.20 ± 0.73	463.00 ± 120.00	299.60 ± 72.30	1.55 ± 0.55	A11	244	203	411.00 ± 289.00	1.41 ± 0.99	1.12 ± 0.18	High Momentum Data. Mean Energy = 96.17 ± 1.83 GeV		High Momentum Data. Mean Energy = 43.5 ± 1.88 GeV		High Momentum Data. Mean Energy = 11.27 ± 0.28 GeV					
>10	1	2	0.50 ± 0.61	580.00 ± 120.00	411.00 ± 289.00	1.41 ± 0.99	A11	1	1	69.56 ± 7.03	62.23 ± 8.02	1.12 ± 0.18	High Momentum Data. Mean Energy = 96.17 ± 1.83 GeV		High Momentum Data. Mean Energy = 43.5 ± 1.88 GeV		High Momentum Data. Mean Energy = 11.27 ± 0.28 GeV					
Level: 3																						
0	192	149	1.29 ± 0.14	45.73 ± 2.94	43.97 ± 3.27	1.04 ± 0.10	1-2	0	1406	1076	1.31 ± 0.05	147.60 ± 1.60	149.00 ± 1.60	1.04 ± 0.03	1-2	141	78	1.23 ± 0.15	170.20 ± 5.00	163.40 ± 5.80	1.05 ± 0.05	
1-2	22	20	1.10 ± 0.34	103.10 ± 15.00	107.50 ± 23.70	0.96 ± 0.25	3-6	1	141	141	1.23 ± 0.15	199.50 ± 11.50	198.10 ± 11.70	1.01 ± 0.05	3-6	95	78	1.22 ± 0.18	244.00 ± 44.00	244.00 ± 51.10	1.01 ± 0.08	
3-6	10	14	0.71 ± 0.30	428.50 ± 66.40	271.18 ± 49.00	1.58 ± 0.37	5-10	2	2-4	15	2.50 ± 1.21	244.00 ± 5.00	244.00 ± 5.00	1.01 ± 0.05	5-10	15	6	2.50 ± 1.21	244.00 ± 44.00	244.00 ± 51.10	1.01 ± 0.08	
7-16	5	2	2.50 ± 2.09	763.00 ± 80.00	519.00 ± 105.00	1.47 ± 0.34	A11	232	187	939.00 ± 17.00	621.00 ± 91.00	1.53 ± 0.23	A11	1659	1275	1.30 ± 0.05	153.60 ± 1.68	154.10 ± 1.68	1.00 ± 0.02			
>16	3	2	1.50 ± 1.37	94.58 ± 11.38	78.97 ± 8.76	1.20 ± 0.20	A11	1	1	123	78	1.58 ± 0.23	170.70 ± 6.30	180.30 ± 7.40	0.95 ± 0.05	123	74	1.45 ± 0.26	194.00 ± 9.20	195.20 ± 9.80	0.97 ± 0.07	
A11	232	187	1.24 ± 0.12	94.58 ± 11.38	78.97 ± 8.76	1.20 ± 0.20	A11	89	90	64.81 ± 8.16	90.76 ± 17.08	0.71 ± 0.16	High Momentum Data. Mean Energy = 501 ± 38 GeV		High Momentum Data. Mean Energy = 43.5 ± 1.88 GeV		High Momentum Data. Mean Energy = 11.27 ± 0.28 GeV					
Level: 1																						
0	68	67	1.02 ± 0.17	46.69 ± 5.04	43.75 ± 6.87	1.07 ± 0.20	1-2	0	123	78	1.58 ± 0.23	170.70 ± 6.30	180.30 ± 7.40	0.95 ± 0.05	1-2	74	51	1.45 ± 0.26	194.00 ± 9.20	195.20 ± 9.80	0.97 ± 0.07	
1	9	7	1.29 ± 0.65	61.00 ± 7.05	55.70 ± 4.49	0.51 ± 0.15	3-6	1	123	91	1.35 ± 0.19	258.00 ± 9.00	288.90 ± 11.60	0.89 ± 0.60	3-6	26	37	0.94 ± 0.33	403.10 ± 47.40	365.20 ± 40.50	1.10 ± 0.18	
2-4	10	9	1.11 ± 0.51	137.20 ± 38.90	90.90 ± 23.00	1.09 ± 0.29	5-10	2	2	17	4	1.21 ± 0.21	365.20 ± 40.50	365.20 ± 40.50	1.10 ± 0.18	5-10	4	6	0.67 ± 0.43	784.00 ± 78.00	697.00 ± 80.00	1.13 ± 0.17
5-10	2	5	0.40 ± 0.33	336.00 ± 91.00	140.00 ± 32.00	2.39 ± 0.85	A11	89	90	64.81 ± 8.16	90.76 ± 17.08	0.71 ± 0.16	High Momentum Data. Mean Energy = 501 ± 38 GeV		High Momentum Data. Mean Energy = 43.5 ± 1.88 GeV		High Momentum Data. Mean Energy = 11.27 ± 0.28 GeV					

(f)

TABLE 5.1. Data and results from the charge asymmetry data for method 1 and method 2.

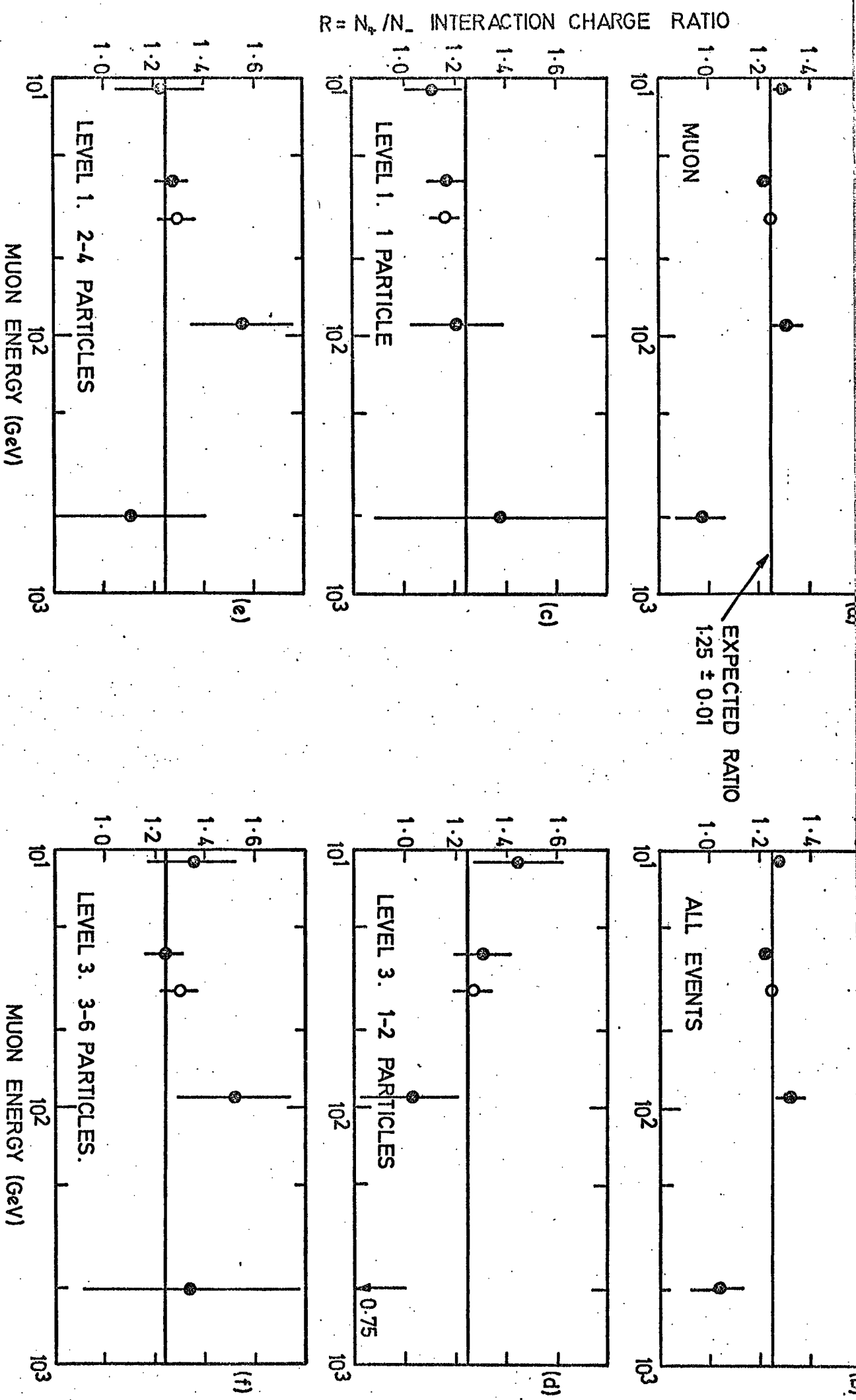


FIGURE 5.1. The interaction charge ratio (method 1) results. Open circles (\circ) are the mean ratio of the burst size cell.

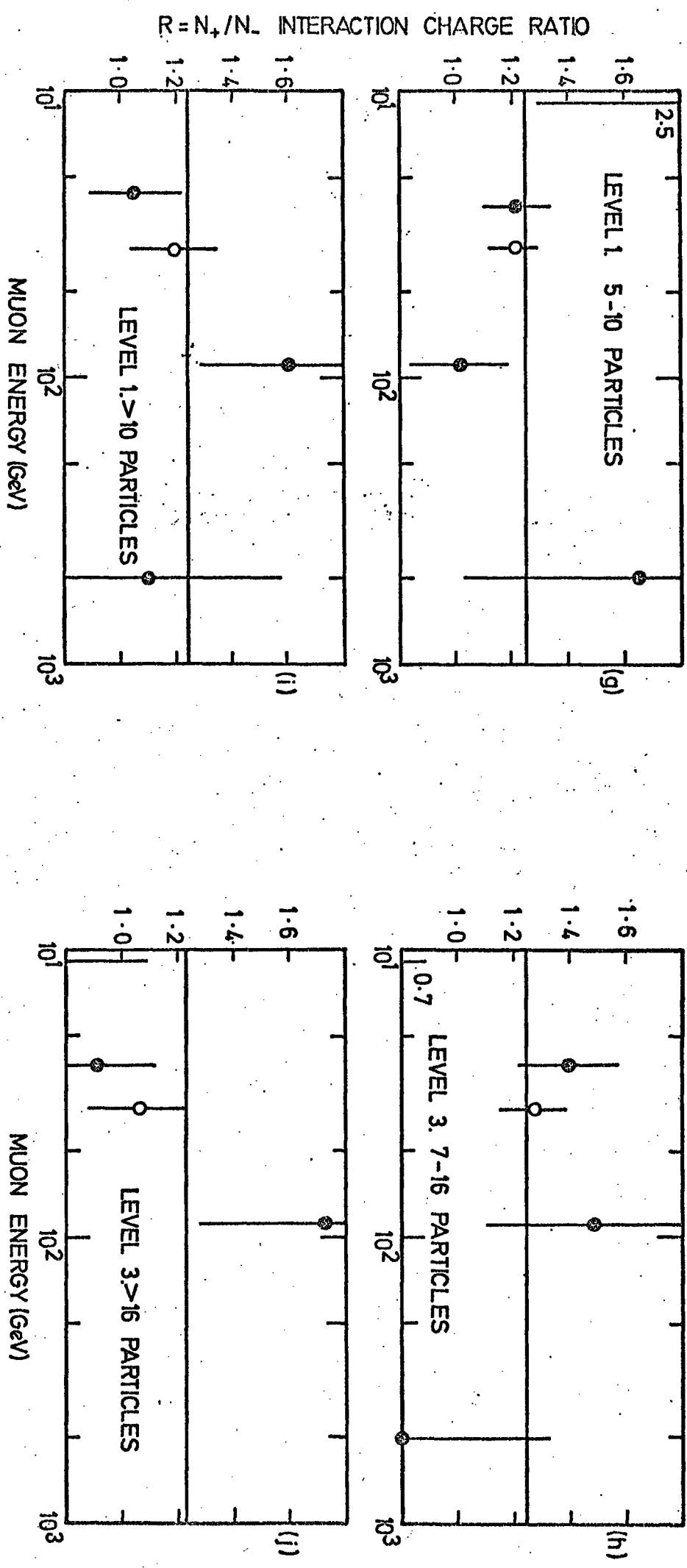


FIGURE 5.1. The interaction charge ratio (method I) results. Open circles (O) are the mean ratio of the burst size cell.

differently, it would be expected that the corresponding pulse height distributions would be of different shapes, producing different means for the same classification of events.

The data have been divided into the same bins as for Method 1 (four energy bins and five burst size bins). For each bin at each experimental level the pulse height distributions have been determined separately for positive events and for negative events.

A ratio R' has been defined as

$$R' = M_+ / M_- \quad (5.3)$$

where M_+ , M_- are the mean pulse heights for positive and negative events respectively. The error dR' can be shown to be

$$dR' = R' \left[\left(\frac{dM_+}{M_+} \right)^2 + \left(\frac{dM_-}{M_-} \right)^2 \right]^{\frac{1}{2}}. \quad (5.4)$$

dM_+ , dM_- are the statistically determined error on the mean pulse heights for positive and negative events respectively.

The data and the numerical results of this analysis are given in tabular form in Tables 5.1a,b,c,d,e,f. In Figure 5.2 are the graphical results as a function of burst size, incident muon energy and level. The errors presented are statistical.

From this analysis, as with the previous analysis, there is no evidence which would support either a positive or a negative interaction charge asymmetry.

5.4 METHOD 3: COMPARISON OF THE PULSE HEIGHT DISTRIBUTIONS FOR POSITIVE AND NEGATIVE EVENTS

As a basis for this method of analysis it has been assumed that if positive or negative muons interacted differently from one

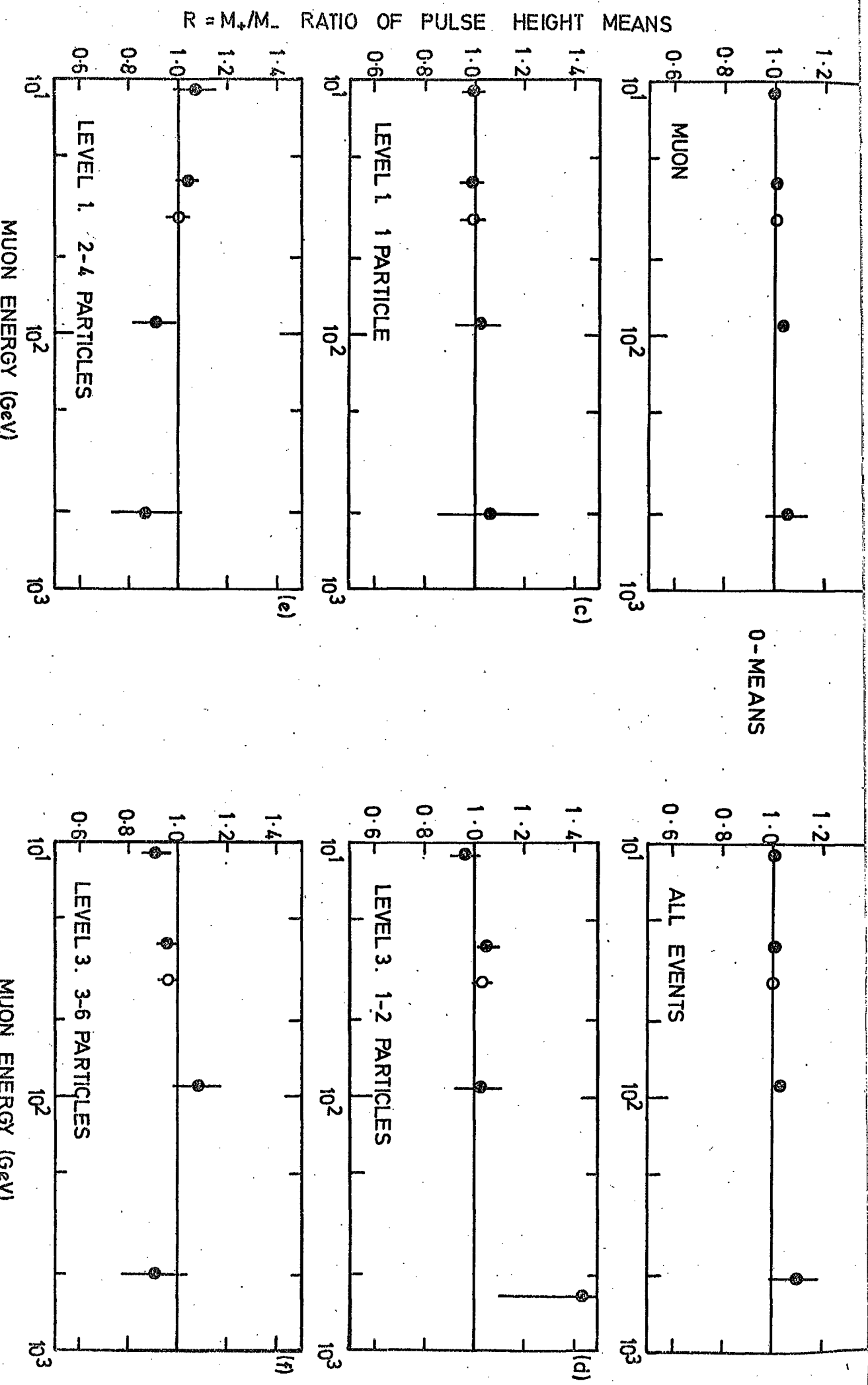


FIGURE 5.2. The interaction charge asymmetry ratio of the mean pulse heights for positive and negative events (method 2).

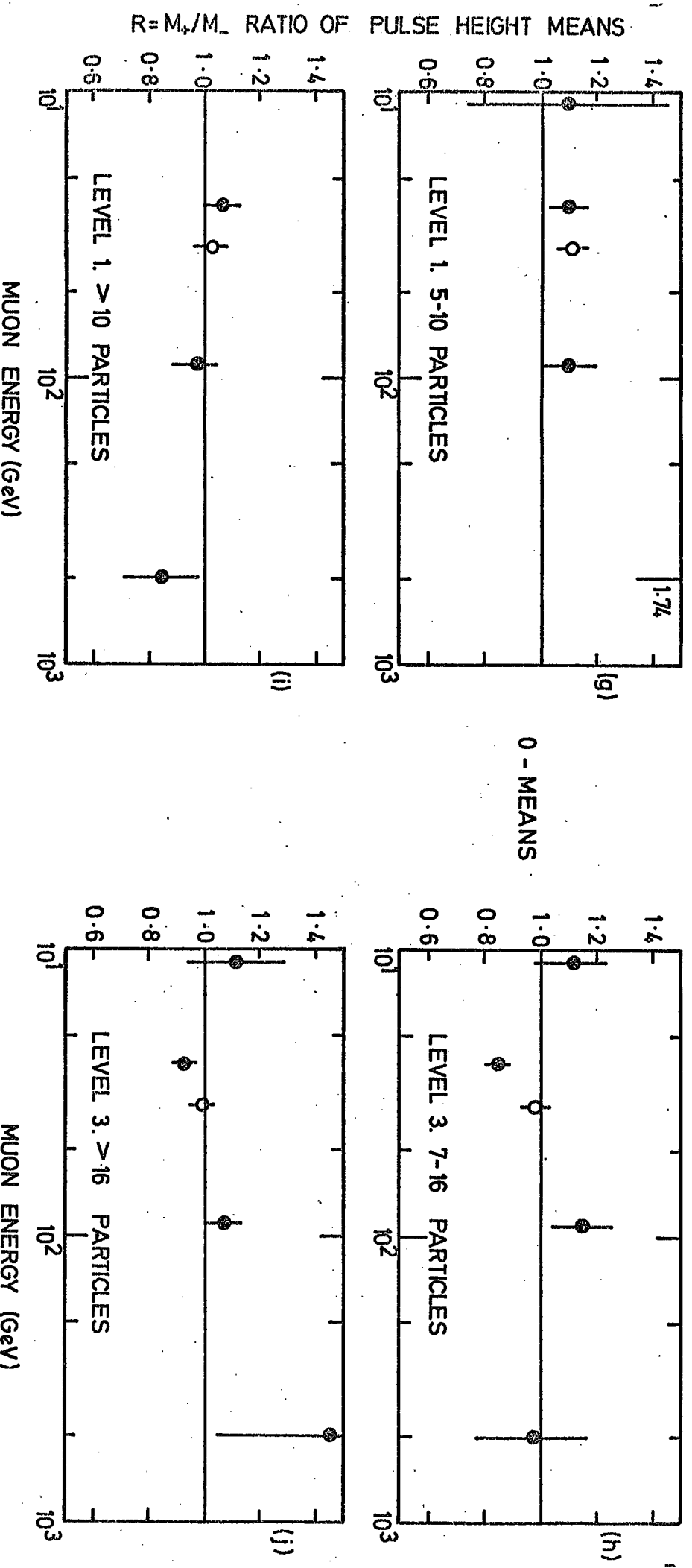


FIGURE 5.2. The interaction charge asymmetry ratio of the mean pulse heights for positive and negative events (method 2).

another, this difference would be reflected in the shape of the pulse height distributions. For this analysis the data has been divided into four energy bins (7-14 GeV, 14-24 GeV, 24-54 GeV, > 54 GeV) and into four flash tube burst size cells (0, 1, 2-5, > 5 particles). To improve the statistics the data from both experimental levels have been combined. This means that due to the different calibration curves at levels 1 and 3, the burst cells overlap slightly (the burst size cells are 0, 1-2, 2-7, > 5 particles). The pulse height distribution ~~s~~ for positive and negative events ~~has~~ ^{HAVE} been determined; the area of the positive distributions has been normalized to the negative distributions, and both distributions were divided into six sections (1-20, 21-50, 51-100, 101-200, 201-400, 401-1000 MPHA cells). For each section a charge excess Q has been calculated using equation (5.5)

$$Q = \frac{CN_+ - N_-}{CN_+ + N_-} \quad (5.5)$$

where:

N_+ , N_- are the number of events in the section of positive and negative events respectively,

C is the inverse charge ratio for the entire distribution.

This normalizes the positive distribution to the negative distribution.

The error on the excess, dQ , can be shown to be approximately

$$dQ = \left(\frac{1 + Q^2}{N_+ + N_-} \right)^{\frac{1}{2}} \quad (5.6)$$

The results of this analysis are presented in Figure 5.3-5.8. Figure 5.3 gives the results for the all events data as a function of magnetic field. It can be seen that there is no magnetic field effect. Figures 5.4-5.7 present the results as a function of burst

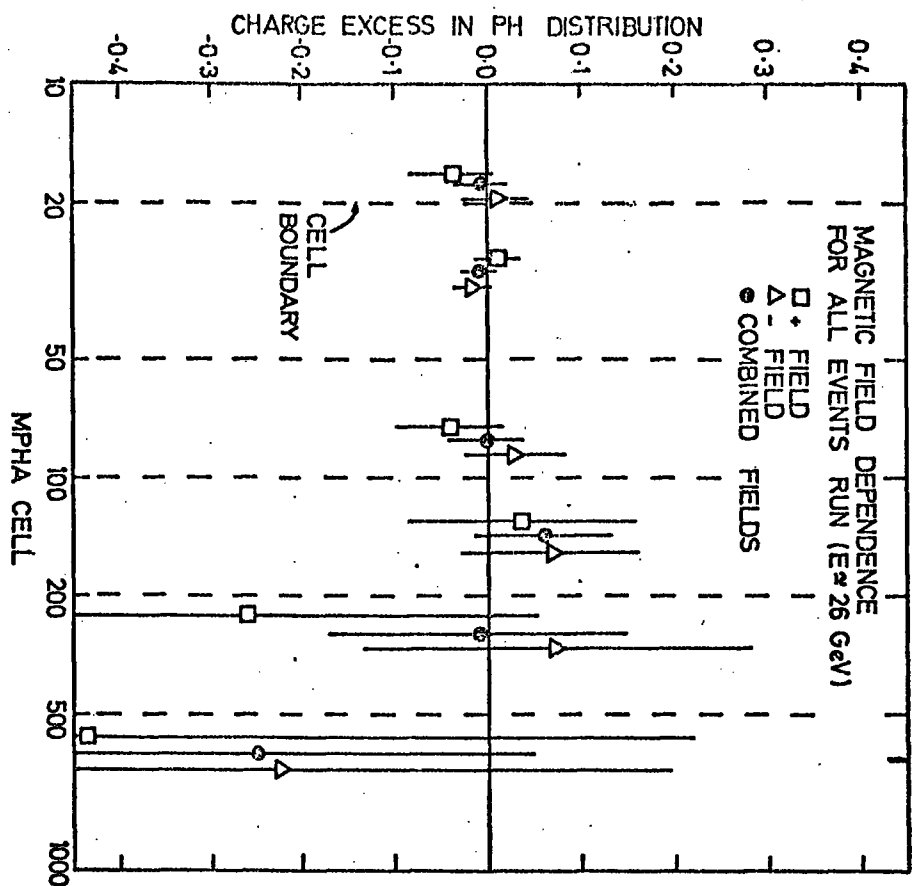


FIGURE 5.3. The magnetic field dependence of the charge excess of the pulse height distribution as a function of muon incident energy and pulse height.

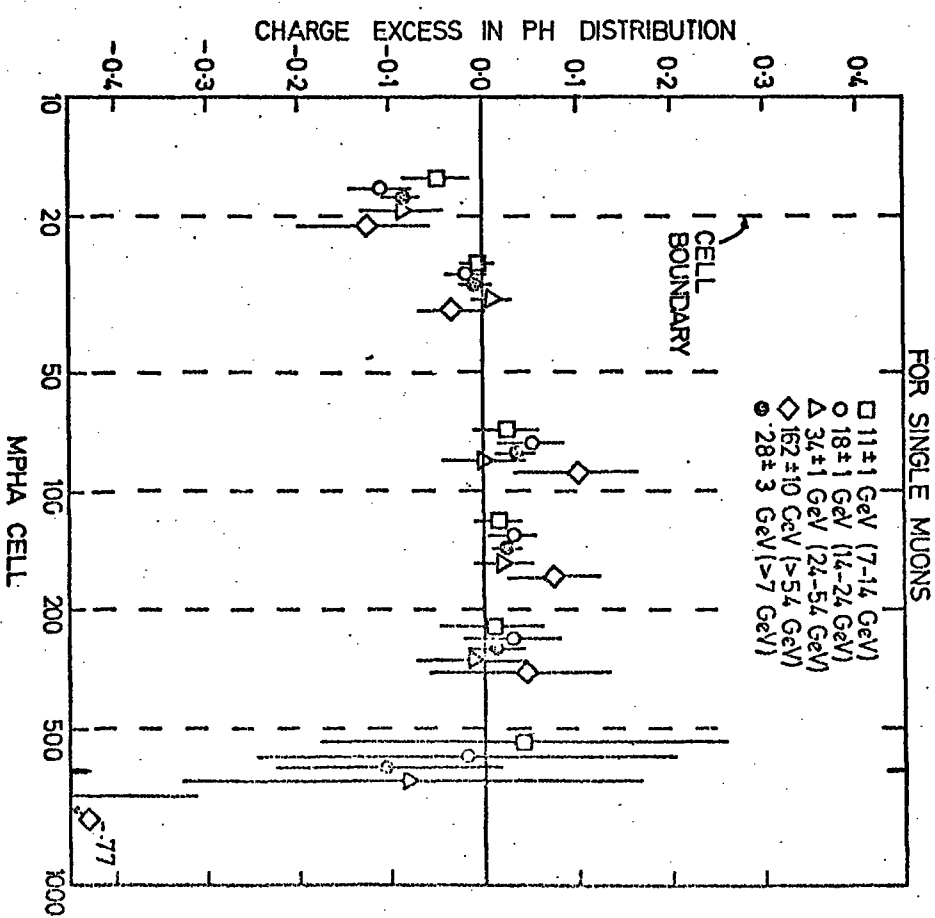


FIGURE 5.4. The charge excess of the single muon pulse height distribution as a function of muon incident energy and pulse height.

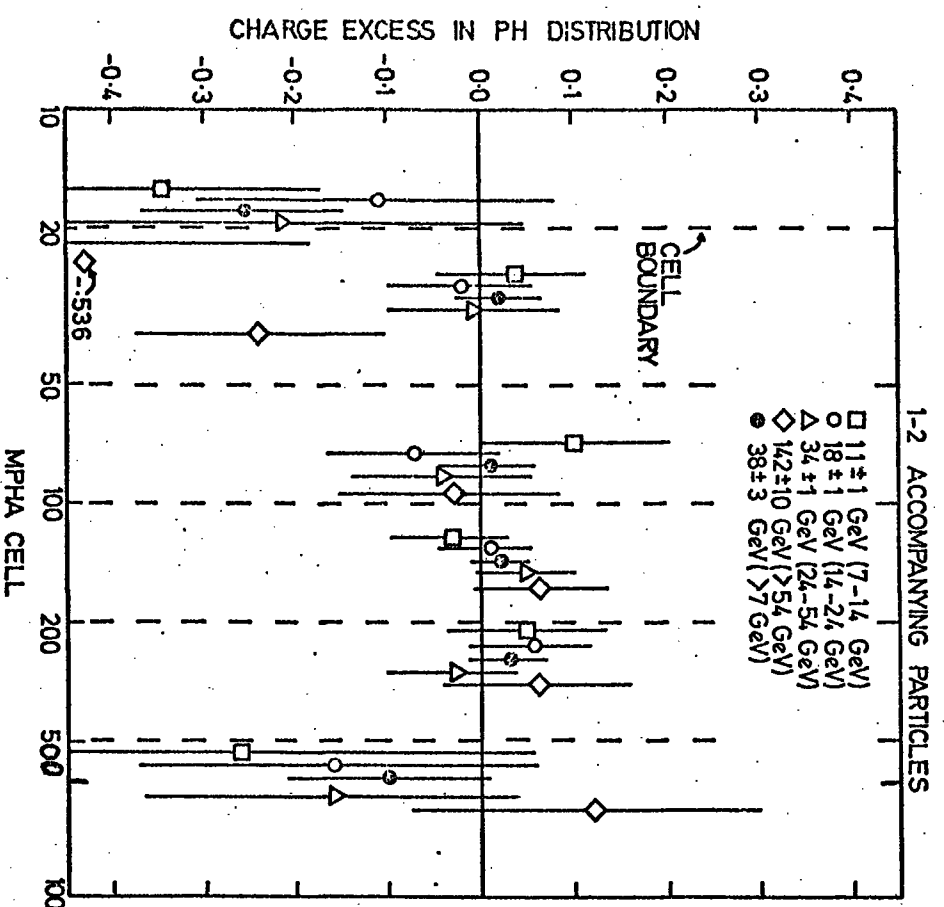


FIGURE 5.5. The charge excesses of the pulse height distribution for bursts of 1-2 particles as a function of muon incident energy and pulse height.

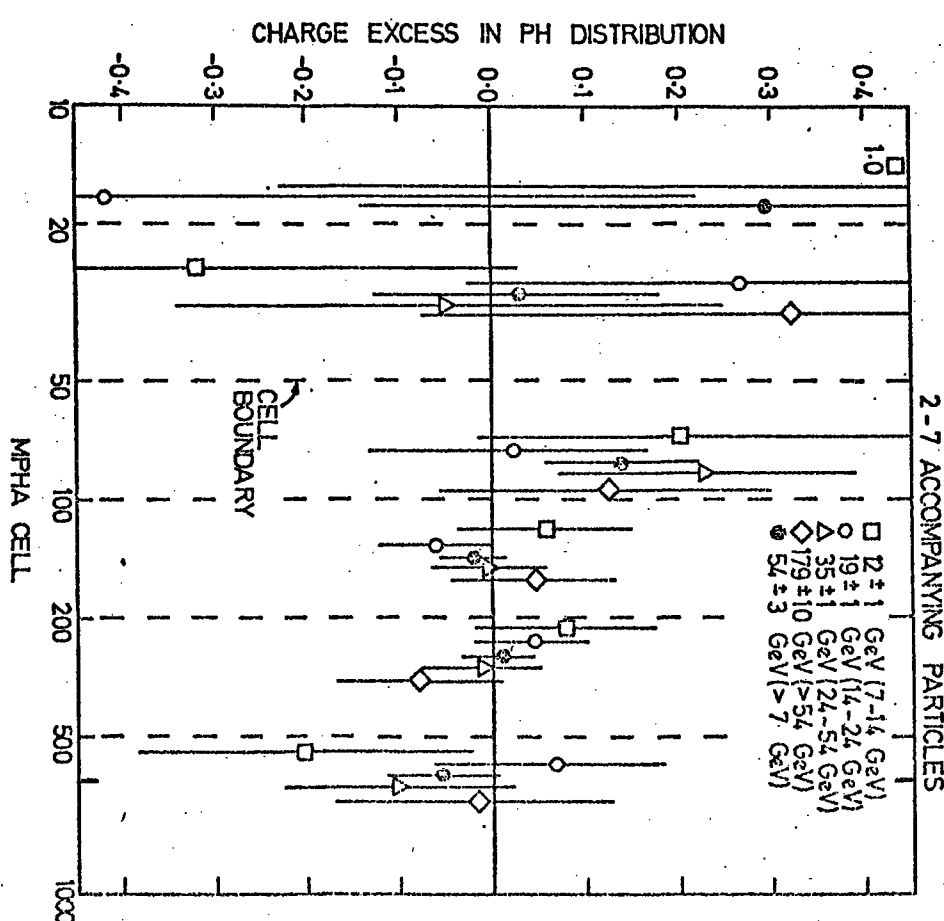


FIGURE 5.6. The charge excess of the pulse height distribution for bursts of 2-7 particles as a function of muon incident energy and pulse height.

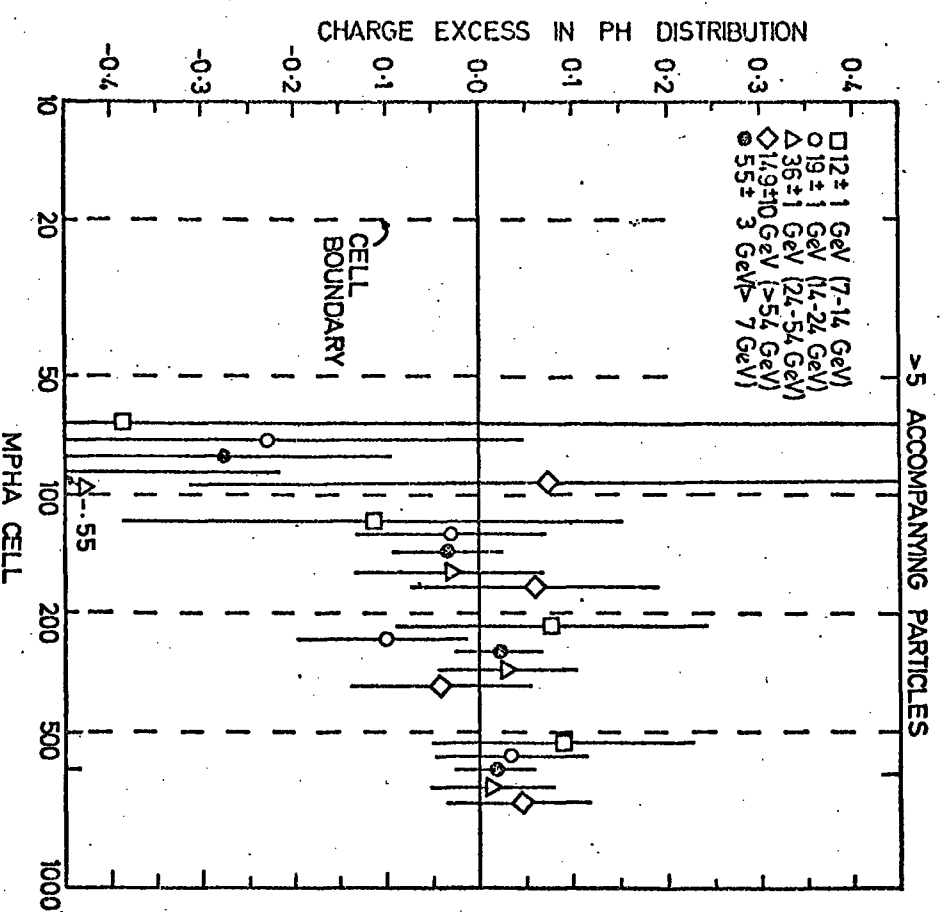


FIGURE 5.7. The charge excess of the pulse height distribution for bursts of > 5 particles as a function of muon incident energy and pulse height.

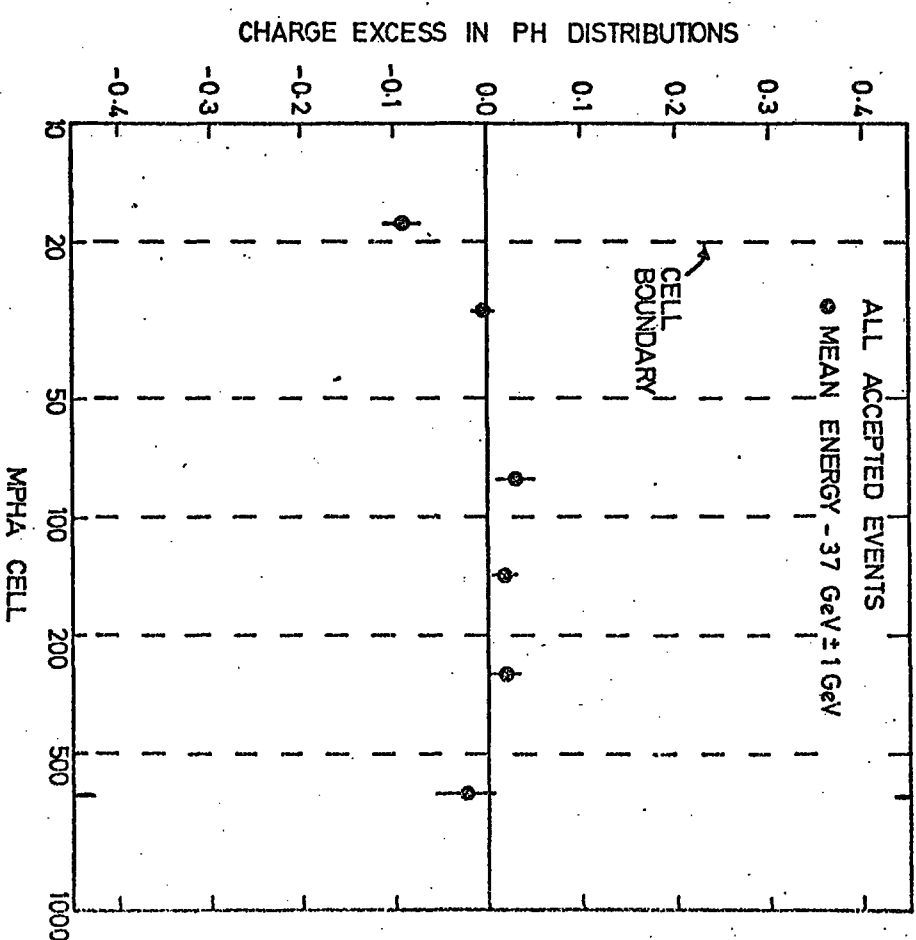


FIGURE 5.8. The charge excess of the pulse height distribution for all the spectrograph events as a function of muon incident energy and pulse height.

size, incident muon energy and MPHA section. The solid circles (●) are plotted at the mean of the MPHA section. Figure 5.8 contains the results for all the data over all energy ranges.

The plot of all accepted events (Figure 5.8) shows a marked structuring as would be expected if there were a charge asymmetry. Section 1 (MPHA cells 1-20) has too few pulse heights for positive events by about four standard deviations. This implies that positive events tend to produce larger pulse heights (i.e. more bursts). This positive effect can be seen in MPHA sections 3, 4 and 5.

However, from inspection of Figures 5.3-5.7 two observations can be made. First, the only other figures which also show this asymmetry are the single muon one (Figure 5.4) and the 1-2 accompanying particle one (Figure 5.5), which itself will contain a high percentage of single muons with knock-on electrons in the flash tube trays. Second, Figure 5.3, the plot of the field dependence of the excess for the all events data, does not show any structuring, or any tendency for structuring. In fact, the high momentum data is the only set of data to contain this structuring. This strongly suggests that there is a systematic effect produced by the momentum selector.

It has become apparent upon investigation that not only is such a systematic effect possible, but it is strongly supported by the pulse height data. The first MPHA section (cells 1-20) was made to end approximately at the mode of the single particle pulse height distribution (see Figures 4.10 and 4.11). If, for some reason, the pulse height distribution or a component of the distribution were to shift to the right (towards larger pulse heights) by an amount of about 10-20% (possibly due to an increase in path length in the scintillators), the excess in this section could be great due to

the fast rising edge of the distribution. A small shift could result in the loss of a large percentage of the particles. It would be expected, however, that positive and negative events would be shifted by the same amount, except if there were a bias on the basis of charge. The momentum selector has such a bias. The contamination from the 'zero' bit lining up with other cells (see Section 3.2.2.2) is such that it only accepts negative contamination in a negative field and positive contamination in a positive field. Based on the accepted charge ratio, the data shows that the momentum selector accepts ^{4.4} ~~5.4~~ times the expected number of positive events in a positive field and negative events in a negative field.

It is reasonable to expect that the contamination particles will tend to pass through the trays and scintillators in localized directions and localized areas, either ^{or} ~~of~~ both of which could superimpose a shifted distribution on top of the expected one with ~ 1.7 times the number of events. Comparing the 'all events' pulse height distributions and the 'high momentum' pulse height distribution, it was found that the means of the 'high momentum' distributions were high by $\sim 15\text{--}25\%$.

Using the single particle distributions corresponding to the high momentum data and the all events data, and the above percentages, the expected possible charge excesses in cells 1-20 have been calculated. The extreme cases correspond to an excess between -0.17 to -0.26. The actual measured excesses for the high momentum data were -0.19 ± 0.04 at level 1 and -0.22 ± 0.05 at level 3.

It is, therefore, believed that there is no anomalous energy loss effect by single muons, but that the effect observed is symptomatic of the high momentum data only. There is no evidence among

the burst distributions (Figures 5.6 and 5.7) to support an interaction charge asymmetry.

5.5 CONCLUSIONS

Three methods have been employed to study the data in the search for any evidence to support an interaction charge asymmetry. Two of the methods have not been previously employed. Although the results of the third method showed some structuring, it is considered to be due to a specific class of single muons and has been shown to be systematic.

It is concluded, based on the results of the three methods, that there is no evidence to support a charge asymmetry in the interaction cross-sections of muons.

5.5.1 COMPARISON WITH PREVIOUS RESULTS

The two experimental methods using the pulse height distributions cannot be compared directly with previous results, except in so far as they do not support the charge asymmetry found by Neddermeyer et al. (1961, 1965, 1967), Allkofer et al. (1971), Ayre et al. (1970) and Sheldon et al. (1973).

The first method using the charge ratio of interaction events can be compared. In this experiment observations have been made under a very thick iron absorber. It, therefore, has not been possible to determine the energy transferred to the shower which is observed. It is only possible to say (as per calculations done in Section 6.3.1) that the mean shower age is about shower maximum and the mean energy per observed particle is, very loosely speaking,

about 1 GeV per particle. Using this result, the energy transferred per burst size cell has been roughly estimated in an attempt to provide a method of direct comparison with previous results.

TABLE 5.2

THE INTERACTION CHARGE ASYMMETRY (METHOD 1) AS A FUNCTION OF
BURST SIZE AND APPROXIMATE ENERGY TRANSFER

Burst Size	Approximate Mean Energy Transfer (GeV)	Asymmetry
0 (Muon)	-	1.002 ± 0.018
1	1	0.969 ± 0.039
2-7	4	1.047 ± 0.041
5-16	7	0.988 ± 0.061
> 10	10	0.924 ± 0.094

Table 5.2 presents the combined results from both experimental levels. The overall asymmetry for bursts of greater than 2 particles is 1.020 ± 0.032 . In Figure 5.9 are the previous results along with the results from the first method of this experiment.

It is useful to present ideas as to why some experiments have found such marked asymmetries. The first results of the MARS spectrograph (Ayre et al. 1970) have been largely attributed to poor statistics and a possible misalignment of the spectrograph. This view is supported by the second results from the spectrograph (Grupen et al. 1972) which do not support an interaction charge asymmetry.

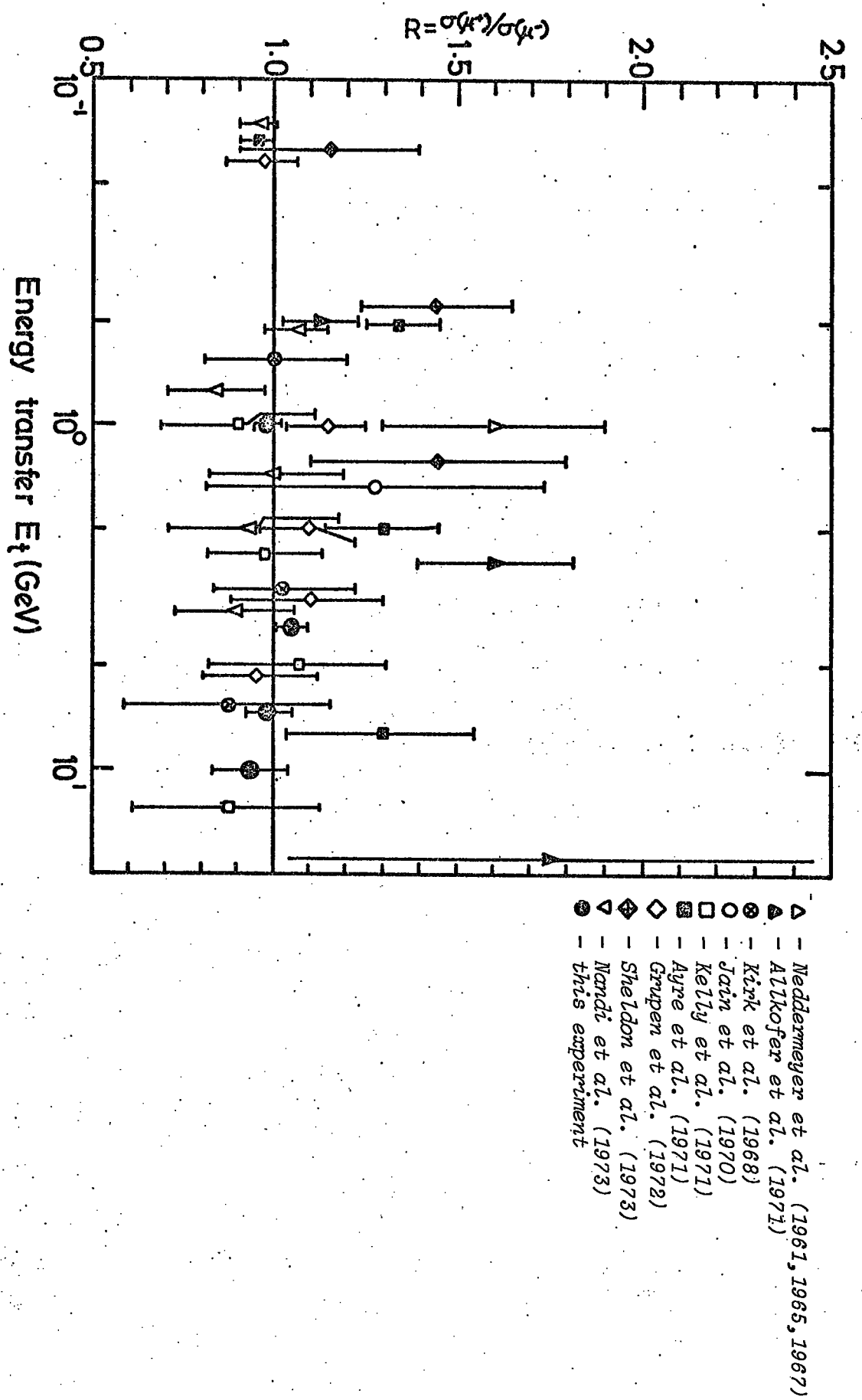


FIGURE 5.9. A comparison of the interaction charge asymmetry results of this experiment with previous experiments.

Grupen (1974) suggests that a possible explanation for the asymmetry in some experiments, particularly those of Neddermeyer et al. (1961,1965,1967) and Sheldon et al. (1973), may be due to proton contamination. Most experimenters assume the proton flux at ground level to be negligible. This is not the case if one compares the fact that only about 2% of muons interact while about 100% of protons will interact if they can get into the apparatus. Neddermeyer et al. have $\sim 400 \text{ g cm}^{-2}$ of lead shielding and Sheldon et al. have no shielding. Grupen has shown by using the proton flux at ground level that it is possible to obtain an interaction charge ratio of 1.40. All experiments showing no asymmetry have $\sim 1000 \text{ g cm}^{-2}$ or more of shielding or are accelerator experiments.

The only experiment for which it is hard to provide any plausible explanation is the result (1.23 ± 0.11) of Allkofer et al. (1971). Their apparatus was in the horizontal with $\sim 2400 \text{ g cm}^{-2}$ of shielding. However, this result may be attributable to statistics in the light of the most recent Allkofer experiment (Allkofer et al. 1974) which obtained an asymmetry ratio of 1.00 ± 0.04 .

CHAPTER 6

THE THEORETICAL BURST SPECTRUM

6.1 INTRODUCTION

The discussion in this chapter will concern itself with the calculation of the theoretical burst spectrum expected at the bottom of the magnet blocks at levels 1 and 3, the experimental levels.

Each magnet block contains $969 \pm 40 \text{ g cm}^{-2}$ of iron (Well 1972), i.e. 69.7 ± 2.9 radiation lengths. To muons of energy in excess of 10 TeV each, the magnet appears as an infinite iron target (neglecting energy loss). Although the treatment given here is not complete, it is considered adequate. Three assumptions have been made.

1. For the numerical integrations performed the blocks have been divided into 70 thicknesses of 1 radiation length. For each radiation length the cross-sections for the processes occurring have been considered to remain constant. The effect of this, if any, will make the result slightly low.
2. It has been assumed that the particle detectors being considered are immediately below the magnet block. This is not the case, see Figures 3.1 and 3.2. This assumption implies that the matter between the detector and the magnet block is assumed to behave as if it were iron.
3. Transition effects have been ignored.

6.2 CONSIDERATIONS IN THE CALCULATION OF THE BURST SPECTRUM

6.2.1 SHOWER DEVELOPMENT

The shower curves used here were taken from work done by Ivanenko and Samosudov (1959, 1967). Figure 6.1 presents the family of cascade curves for iron (critical energy $E_c = 21$ MeV), for minimum electron energy of 3.21 MeV, for various energies (E_t) of the initial particle (electron or photon). Two useful properties can be observed by comparing the series of curves presented in Ivanenko and Samosudov (1967). First, if the families of curves for minimum electron energies of 3.21 MeV and 32.1 MeV (a factor of 10) are compared, it can be noted that the energy transferred curves shift by a factor $\approx 10^{0.5}$. If $N(E_t, t, E_{MIN})$ represents the family of curves in Figure 6.1 (i.e. N particles of $> E_{MIN}$ are observed at a depth t from an energy transfer of E_t), then this observation says that $N(E_t, t, 32.1 \text{ MeV}) = N(10^{-0.5} E_t, t, 3.21 \text{ MeV})$. Assuming that this property holds for any E_{MIN} ($3.21 \text{ MeV} \leq E_{MIN} \leq 32.1 \text{ MeV}$), it is possible to define any family of curves from the 3.21 MeV family.

$$N(E_t, t, E_{MIN}) = N(AE_t, t, 3.21 \text{ MeV}) \quad (6.1)$$

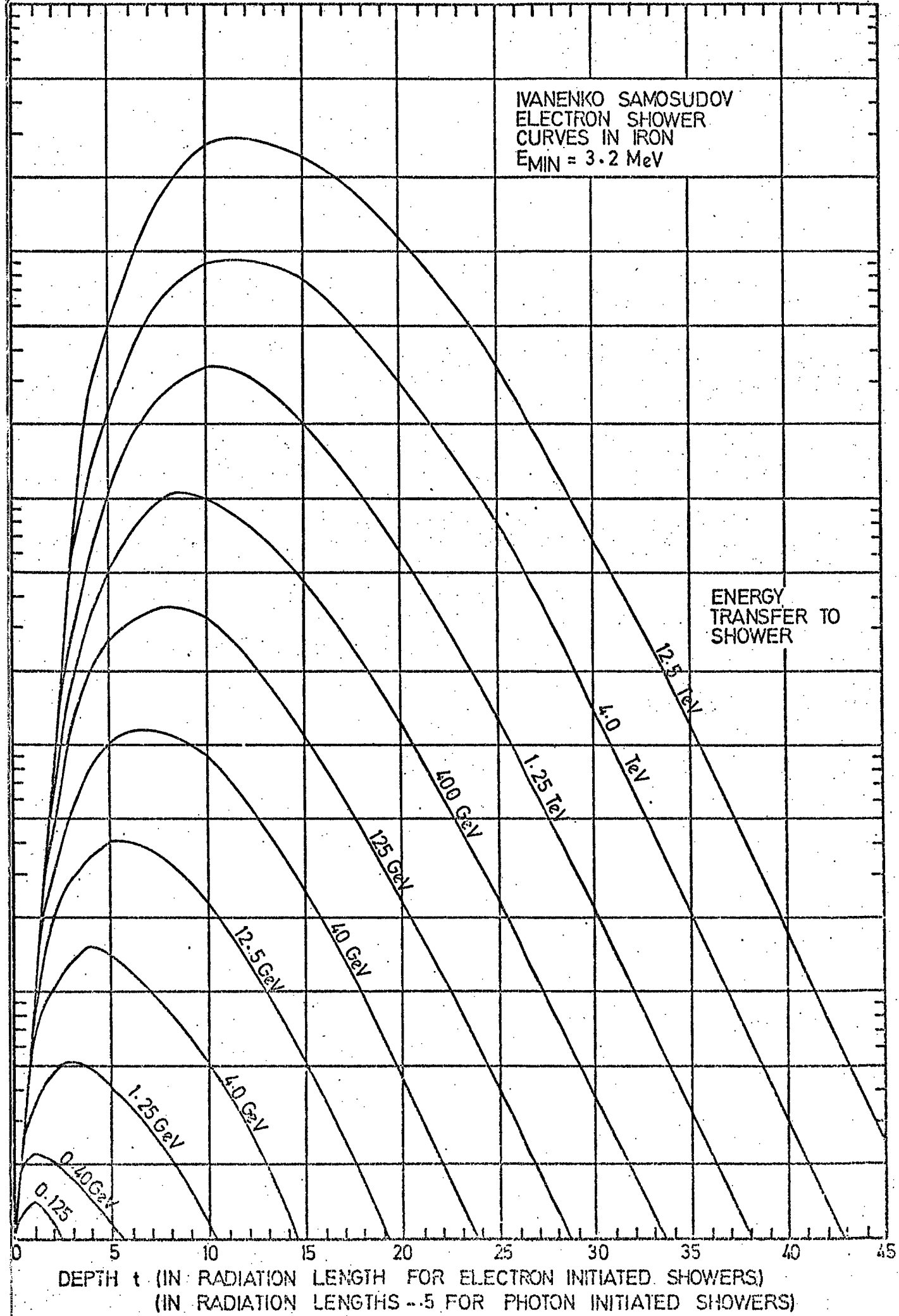
where

$$A = \left(\frac{E_{MIN}}{3.21}\right)^{-0.5} \approx e^{-1.151 \log_{10}(E_{MIN}/3.21)} \quad (6.2)$$

Second, the difference between a photon and an electron initiated shower is that on average the photon initiated shower begins to develop ~ 0.5 radiation lengths later than the electron initiated one. From this observation, if an electron initiated shower is given by $N(E_t, t, E_{MIN})$, then the photon initiated one is given by $N(E_t, t-0.5, E_{MIN})$ where t is in radiation lengths.

IVANENKO SAMOSUDOV
ELECTRON SHOWER
CURVES IN IRON
 $E_{MIN} = 3.2$ MeV

ENERGY
TRANSFER TO
SHOWER



DEPTH t (IN RADIATION LENGTH FOR ELECTRON INITIATED SHOWERS)
(IN RADIATION LENGTHS ≈ 5 FOR PHOTON INITIATED SHOWERS)

FIGURE 6.1. Shower development curves.

Because of the method used it is not important to know how many particles are produced, but what size energy transfer (E_t) is required at a depth t from the bottom of the magnet block to produce N particles. Once the Ivanenko-Samosudov shower curves have been stored on file in the computer, the inverse function determining the energy transfer required (E_t) to produce N particles at a depth t can be found numerically.

$$E_t(N, t, E_{\text{MIN}}) \quad (6.3)$$

for electron initiated showers and

$$E_t(N, t-0.5, E_{\text{MIN}}) \quad (6.4)$$

for photon initiated showers.

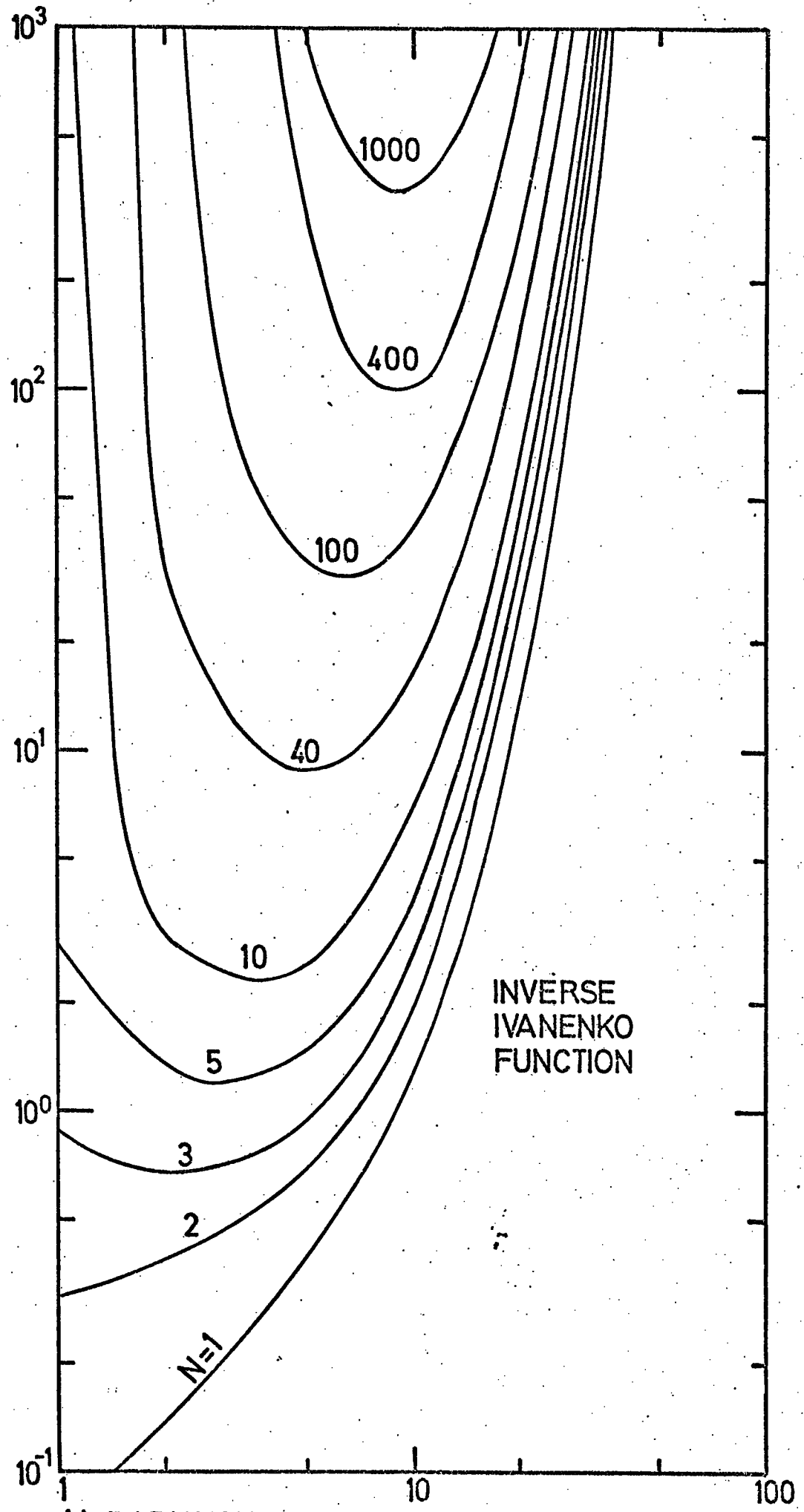
Figure 6.2 presents these inverse functions for various shower sizes.

6.2.2 ENERGY LOSS IN IRON

Since MARS consists of $3876 \pm 20 \text{ g cm}^{-2}$ of iron (Wells 1972), energy loss must be taken into account in order to produce an accurate burst spectrum. The energy loss curves used here are all numerical integrations of the cross-sections discussed and presented in Chapter 2 and Appendix A. Because the ionization (knock-on) cross-section was only calculated from energy transfers of 1 MeV this curve was normalized to CERN results (Serre 1967) at a muon energy of 1 GeV.

The bremsstrahlung energy loss is likely to be slightly low; energy transfers less than 1 MeV have been ignored. Direct pair production is likewise likely to be low. It has been assumed the

E_t (N,t, 3.21 MeV) ENERGY TRANSFER REQUIRED (GeV) TO PRODUCE N PARTICLES
OF MINIMUM ENERGY 3.21 MeV AT t RADIATION LENGTHS



(t) RADIATION LENGTHS FROM SHOWER INITIATION
(t+.5) FOR PHOTON INDUCED SHOWER.

FIGURE 6.2. The energy transfer required to produce a shower of size N as a function of depth from shower initiation.

lowest energy transfer to the pair is 10 MeV. In the calculation of energy loss due to photo-production the resonance peak has been ignored; it is expected to be low by 50-100%, but loss due to this process is negligible.

Figure 6.3 is a graphical presentation of the energy loss by each of the four processes and of the total energy loss. A table of the contribution by each process is given in Table 6.1. These results have been compared to the results of various authors as compiled by Hayman, Palmer and Wolfendale (1963) by a conversion to standard rock. There is general agreement for all processes.

If $EL(E)$ represents the energy loss in iron, then the energy (E) of a muon (of incident energy E_0) as a function of depth (X) can be implicitly defined by

$$\int_{E_0}^E \frac{dE'}{EL(E')} = \int_0^X dX = X . \quad (6.5)$$

To solve for E requires some iterative process. If, over short depth (ΔX) the energy loss is considered constant then it is possible to find $E(E_0, X)$ using a recursive function

$$\begin{aligned} E(E_0, \Delta X) &= E_0 - EL(E_0) \Delta X \\ E(E_0, 2\Delta X) &= E(E_0, \Delta X) - EL(E(E_0, \Delta X)) \Delta X \\ E(E_0, 3\Delta X) &= E(E_0, 2\Delta X) - EL(E(E_0, 2\Delta X)) \Delta X \\ \vdots &\vdots \\ E(E_0, X) = E(E_0, N\Delta X) &= E(E_0, (N-1)\Delta X) - EL(E(E_0, (N-1)\Delta X)) \Delta X \end{aligned} \quad (6.6)$$

where

$$X = N\Delta X .$$

Note also that for convenience, the energy can be defined in terms of depth from the bottom of a magnet block, i.e. ($X = 70 - t$)

TABLE 6.1

CALCULATED ENERGY LOSS IN IRON BY MUONS

$$-\frac{dE}{dt} \text{ (MeV g}^{-1} \text{ cm}^2\text{)}$$

Energy GeV	Knock-On	Brems- strahlung	Direct Pair Prod.	Photo- Nuclear	Total
1.0	1.577	0.000	0.000	0.000	1.577
2.0	1.664	0.001	0.000	0.000	1.665
4.0	1.755	0.004	0.002	0.000	1.762
7.0	1.817	0.008	0.006	0.001	1.832
10.0	1.860	0.013	0.010	0.002	1.885
20.0	1.932	0.022	0.032	0.003	1.989
40.0	2.002	0.061	0.086	0.009	2.158
70.0	2.051	0.125	0.180	0.017	2.373
100.0	2.081	0.192	0.282	0.025	2.580
200.0	2.112	0.269	0.650	0.038	3.069
400.0	2.178	0.757	1.439	0.094	4.468
700.0	2.223	1.508	2.669	0.176	6.576
1000.0	2.250	2.272	3.931	0.261	8.714
2000.0	2.277	2.285	8.154	0.391	13.107
4000.0	2.342	8.056	16.798	0.950	28.146
7000.0	2.387	15.877	29.812	1.779	49.855
10000.0	2.413	23.741	42.884	2.623	71.661

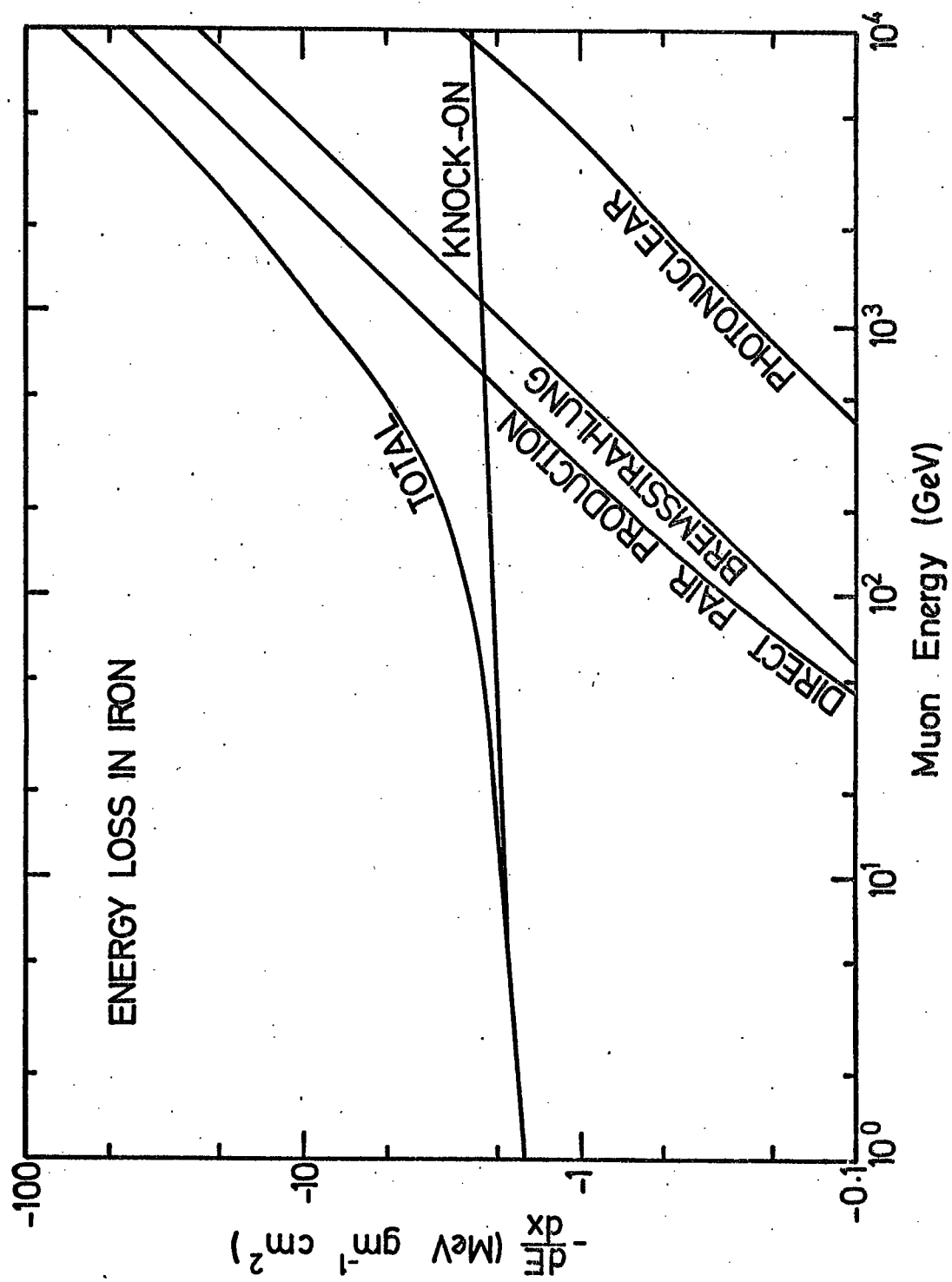


FIGURE 6.3. Energy loss by muons in iron as a function of muon energy.

$$E'(E_o, t) = E(E_o, 70-X) . \quad (6.7)$$

6.2.3 THE PARTICLE PROBABILITIES

It is now possible with the information given to find the probability of N particles of minimum energy E_{MIN} being detected at the bottom of a magnet block from a muon of incident energy E_o . The probability (Φ) of obtaining an energy transfer E_t anywhere in a magnet block is given by

$$\Phi(E_o, E_t) dE_t = \int_{block} \sigma(E', E_t, t) dE_t dt \quad (6.8)$$

where σ is the cross-section of the process (KO, BREM, DPP or photo-production) and E' is the energy of the muon at the depth of the energy transfer. Substituting equation (6.3) (assume for now that the shower is electron initiated) and also substitute equation (6.7)

$$\Phi(E_o, N) dE_t = \int_{block} \sigma[E'(E_o, t), E_t(N, t, E_{MIN}), t] dE_t(N, t, E_{MIN}) dt. \quad (6.9)$$

To finish the transformation multiply by dN/dN to obtain

$$\Phi(E_o, N) dN = \int_{block} \sigma[E'(E_o, t), E_t(N, t, E_{MIN}), t] \frac{dE_t(N, t, E_{MIN})}{dN} dt dN . \quad (6.10)$$

Re-define

$$\phi(E_o, N, t) = \sigma[E'(E_o, t), E_t(N, t, E_{MIN}), t] \frac{dE_t(N, t, E_{MIN})}{dN} . \quad (6.11)$$

Therefore,

$$\Phi(E_o, N) dN = \int_{block} \phi(E_o, N, t) dt dN . \quad (6.12)$$

Equation (6.12) is the probability of obtaining N particles out of a magnet block of MARS from an incident muon of energy E_0 .

ϕ besides being the complex function stated in equation (6.11) is also

$$\phi = \sigma_{KO} \frac{dE_t}{dN} + \sigma_{BREM} \frac{dE_t}{dN} + \sigma_{DPP} \frac{dE_t}{dN} + \sigma_{PN} \frac{dE_t}{dN} . \quad (6.13)$$

In the calculation of the probabilities each one of the above cross-sections had to be considered separately.

1. The knock-on (KO) cross-section was straightforward. One electron is produced, and is assumed to initiate a shower.
2. The bremsstrahlung process (BREM) is assumed to produce a single photon and then after travelling 0.5 radiation lengths a shower is initiated as per the observation in Section 6.2.1.
3. The direct pair production (DPP) process produces two electrons. As can be seen in Figures 2.11a,b,c,d, the distribution of energy to the pair varies with the muon energy E and the energy transferred (E_t). For simplicity the generalization was made that for $E_t > 0.1E$ the production is completely asymmetric. One particle receives the entire energy transfer and initiates a single shower. If $E_t < 0.1E$, the production is assumed to be symmetric. Each particle receives $0.5E_t$ and two showers develop.
4. It was assumed that the contribution from photo-production (PN) is very small. It was not included in the calculation.

In the calculations, the minimum electron energy was assumed to be the energy required for an electron to traverse 0.5 of one of the measuring trays ($3.76 \pm 0.49 \text{ g cm}^{-2}$, Wells 1972). This minimum energy

has been calculated using equation (6.14) obtained from Evans (1971)

$$E(\text{MeV}) = \frac{R(\text{mg cm}^{-2}) + 106}{530} \quad (6.14)$$

R is the range in the material, and E is the energy required.

$$E_{\text{MIN}} \approx 7 \text{ MeV} \quad (6.15)$$

The results of this calculation of particle probabilities out of a magnet block of MARS are presented in Figures 6.4, 6.5, 6.6, 6.7 and 6.8. Figure 6.4 shows the contribution to the particle probabilities of the three interaction processes for a 100 GeV muon. Figure 6.5 also uses a 100 GeV muon to illustrate the probability of producing N particles as a function of depth in the magnet block. The differential probability of obtaining N particles out of a magnet block as a function of incident muon energy is shown in Figure 6.6. Figure 6.7 presents the integral probability of producing $\geq N$ particles at the bottom of a block as a function of energy. Figure 6.8 is a plot of the areas where a particular process is dominant with respect to muon energy and the number of particles observed.

6.2.4 THE VERTICAL MUON SPECTRUM

The spectrum used ($S(E)dE$ muons $s^{-1} \text{ cm}^{-2} \text{ sr}^{-1} \text{ GeV}^{-1}$) was the result of experimental and theoretical work done by Whalley (1974). He conducted an experiment to determine the vertical spectrum between 20 GeV and 500 GeV. He did a least squares fit to his data, see equation (6.20).

Below and above his spectrum, he extrapolated using a derivation from the kaon and pion spectra using the method of Bull et al. (1965). He derived an equation of the form

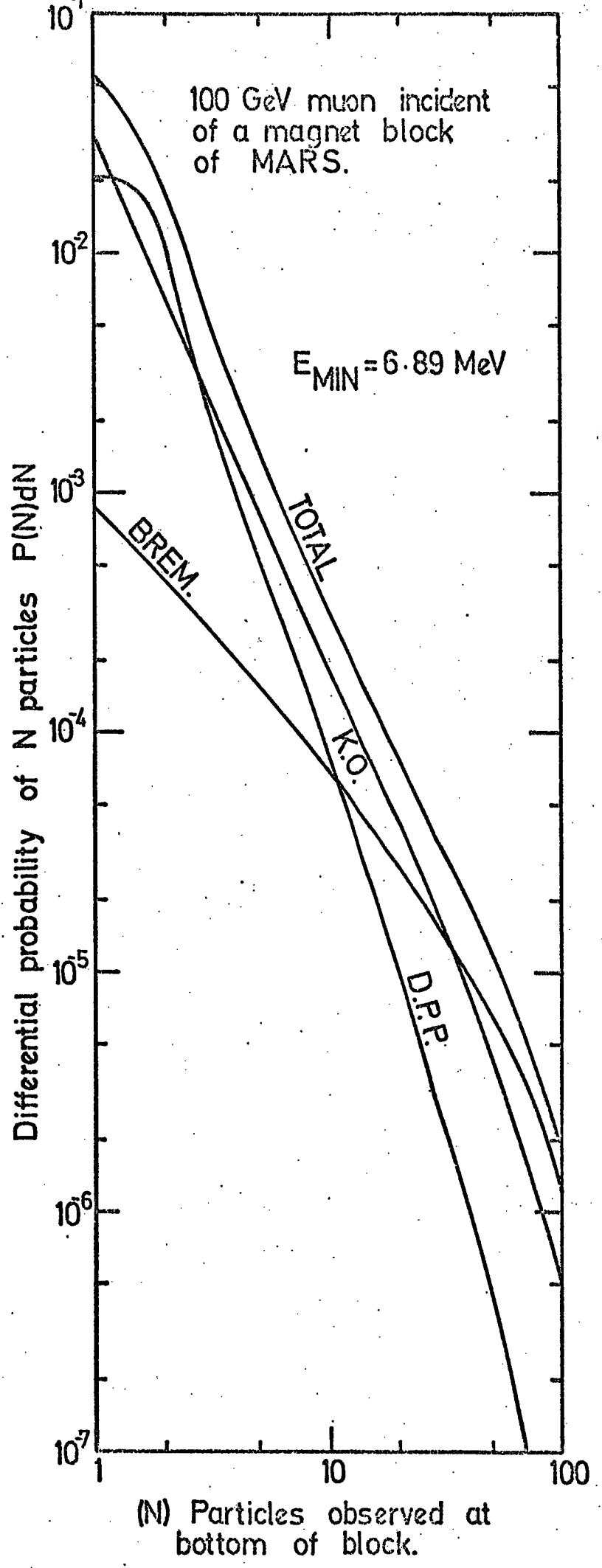


FIGURE 6.4. The differential probability of producing a burst of N particles for a 100 GeV muon.

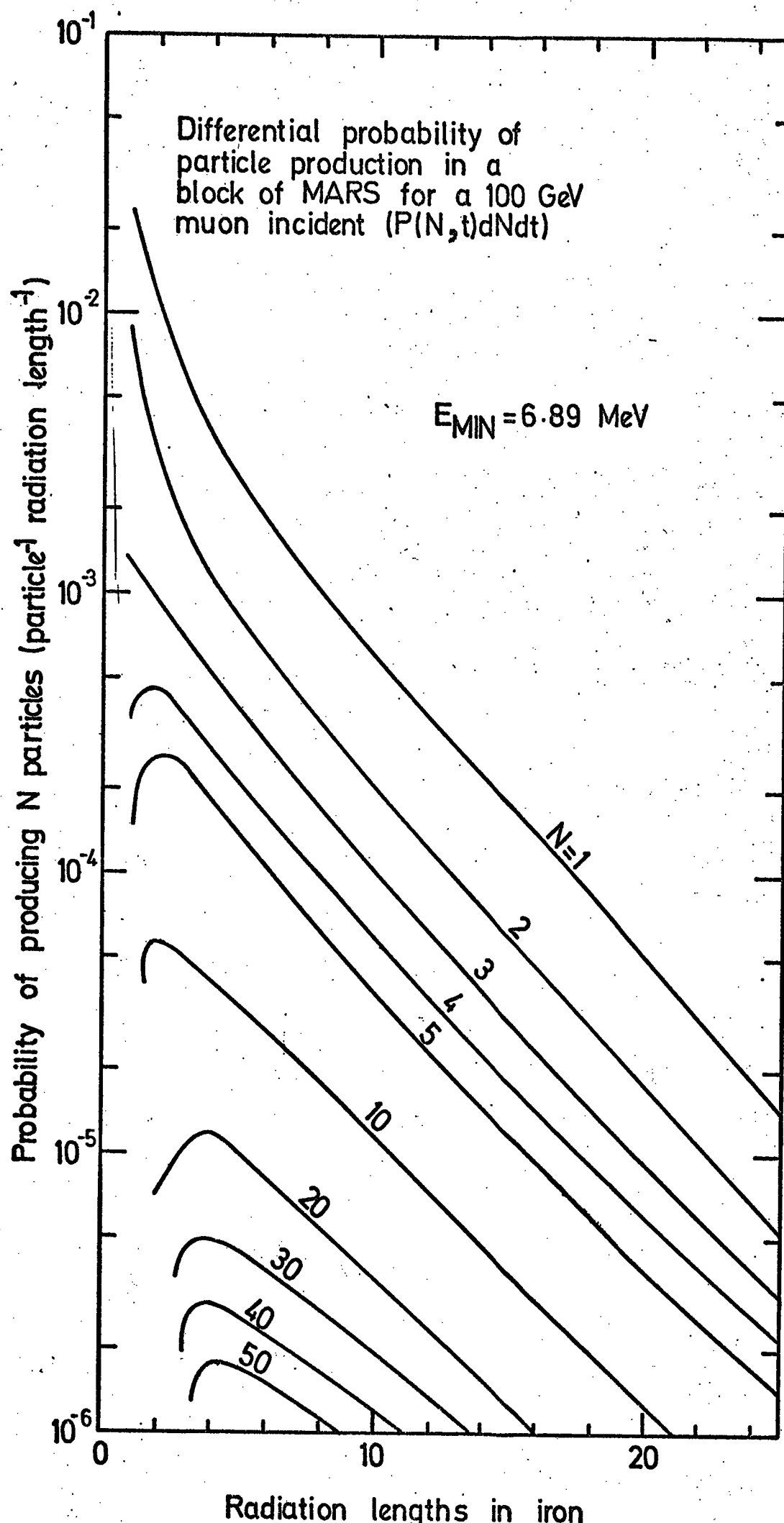


FIGURE 6.5. The differential probability of producing a burst on N particles for a 100 GeV muon as a function of depth from the bottom of a magnet block.

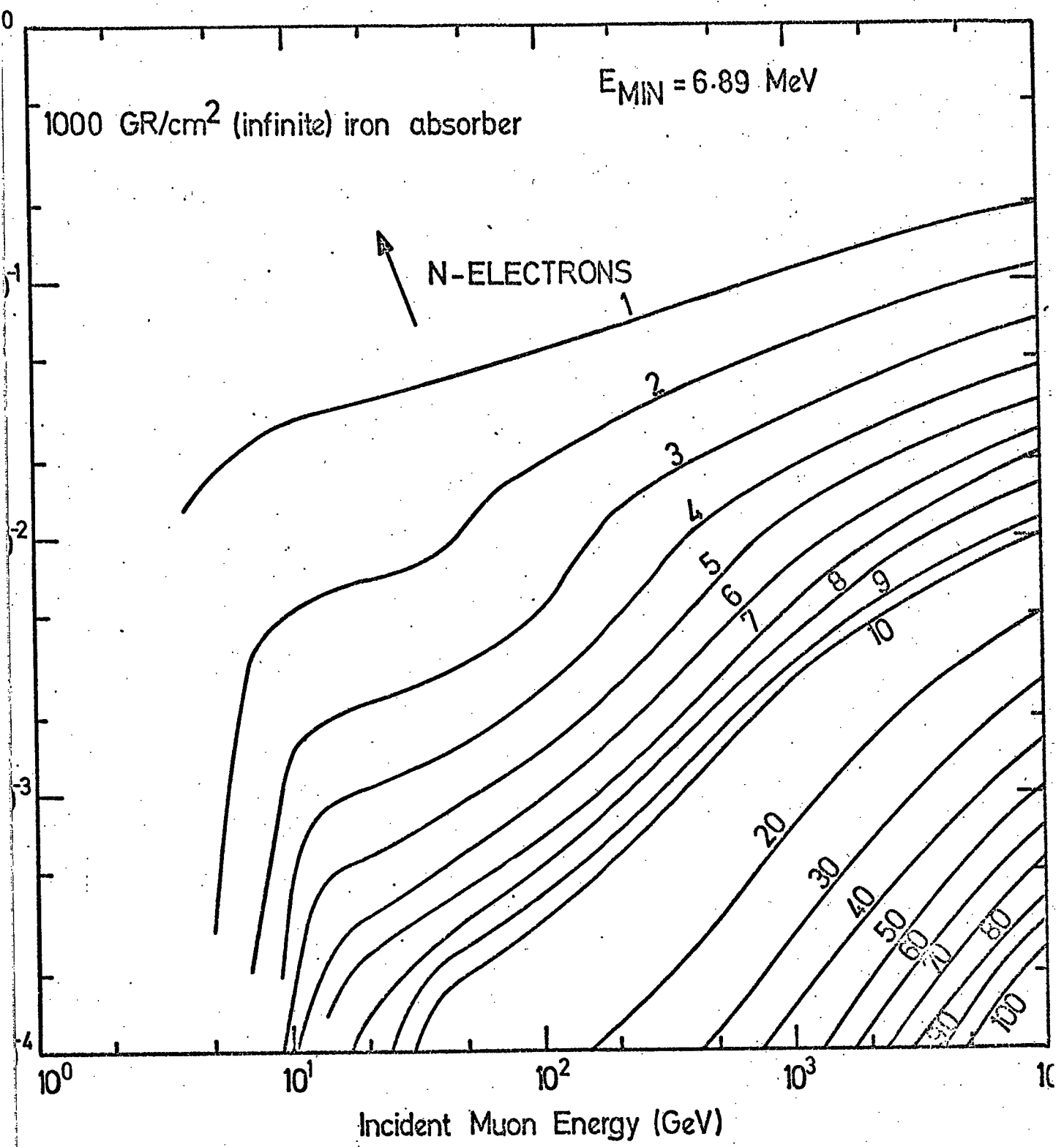


FIGURE 6.6. The differential probability of observing N particles at the bottom of a magnet block as a function of incident muon energy (unfluctuated).

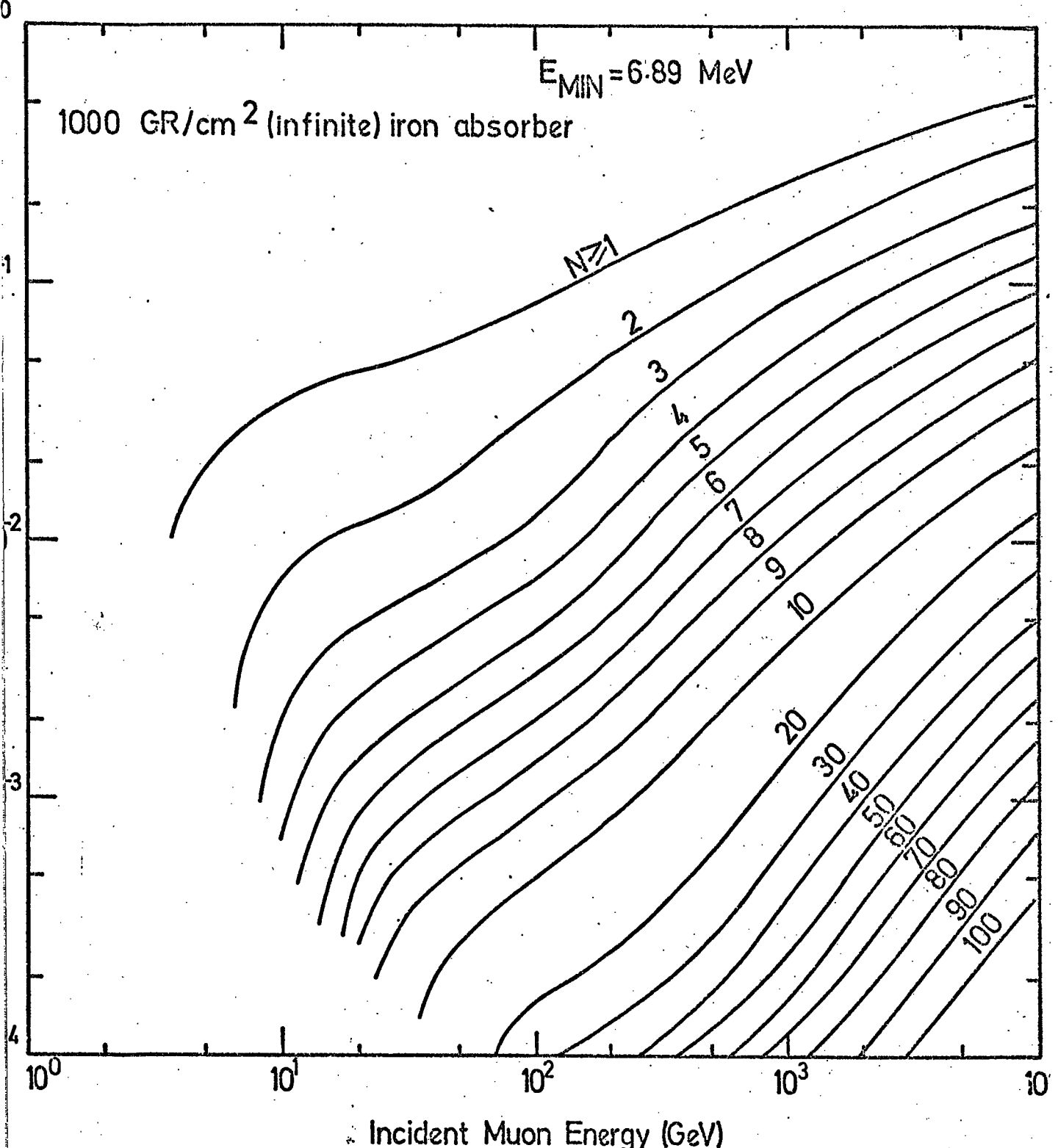


FIGURE 6.7. The integral probability of observing $> N$ particles at the bottom of a magnet block as a function of incident muon energy (unfluctuated).

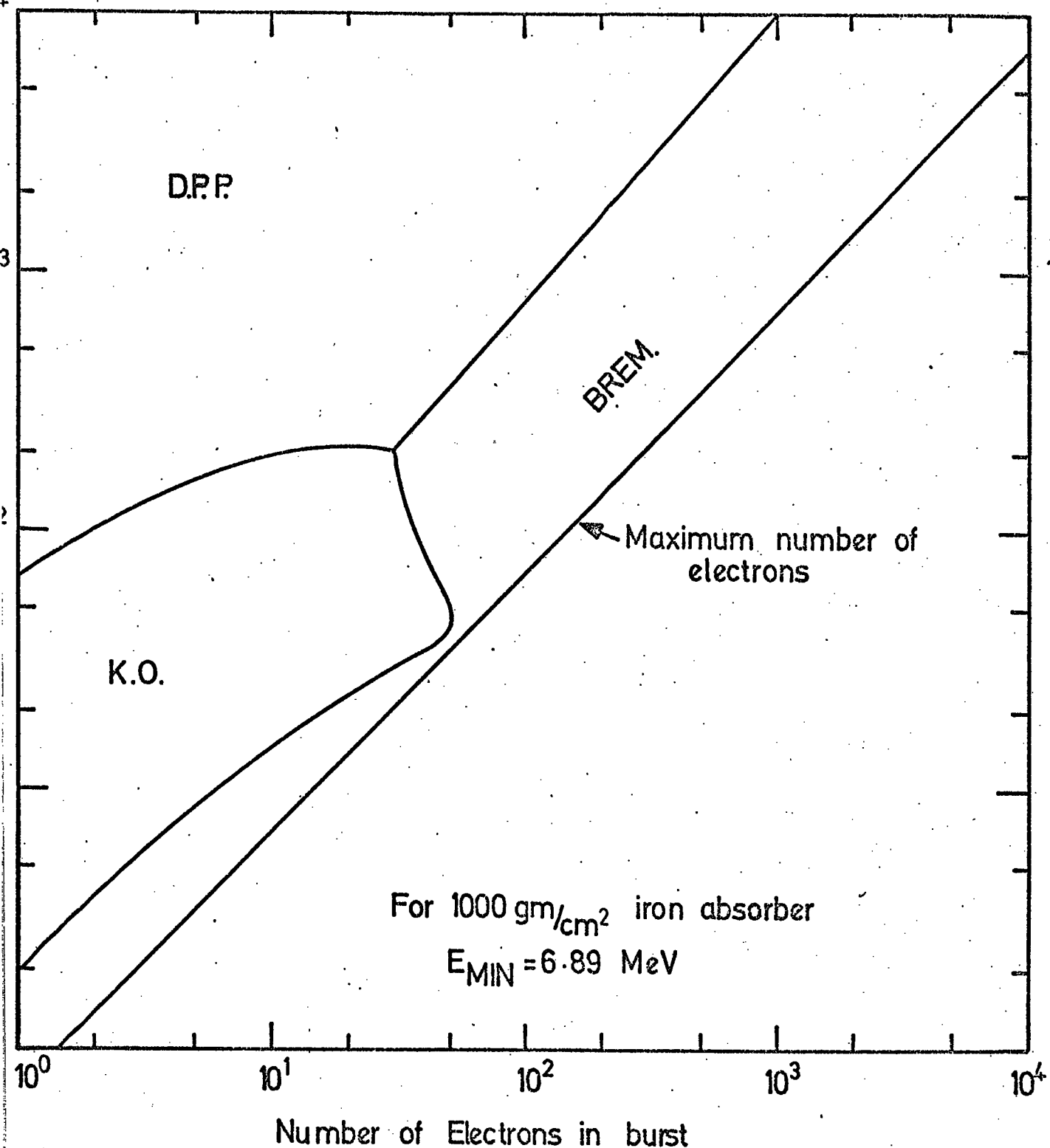


FIGURE 6.8. Regions of dominant interaction processes as a function of burst size and muon energy (unfluctuated).

$$S(E)dE = AP_{\mu}(E + \Delta E)^{\gamma} \left[\frac{r_{\pi}^{\gamma-1} B_{\pi}}{E + \Delta E + B_{\pi}} + \frac{K r_K^{\gamma-1} B_K}{E + \Delta E + B_K} \right] \quad (6.16)$$

where

A is the normalization constant

E is the muon energy

$P_{\mu} = \left(\frac{y}{y_0} \frac{y_o}{E} \right) (M_{\mu} c^2 / \rho(y) \tau_{\mu} E_{TOP})$, the minimum survival probability

y_o, y are the atmospheric depth at sea-level and the observation point respectively

E_{y_o}, E_y, E_{TOP} are the muon energies at sea-level, observation and top of the atmosphere

$M_{\mu} c^2$ is the muon rest mass, 105.655 MeV

$M_{\pi} c^2$ is the pion rest mass, 140 MeV

$M_K c^2$ is the kaon rest mass

$\rho(y)$ is the atmospheric density at depth y

τ_{μ} is the muon mean life

τ_{π} is the pion mean life, 2.60×10^{-8} s

τ_K is the kaon mean life

γ is the exponent of the kaon, pion spectrum ($AE^{-\gamma}$)

ΔE is the energy lost in production

$\Gamma_{\pi, K}$ is approximately the mean of the pion or kaon energy distribution

$$B_{\pi, K} = \Gamma_{\pi, K} b j_{\pi, K}$$

b = 0.771 - a factor introduced by Smith and Duller (1959)

$$j_{\pi, K} = \frac{M_{\pi, K} c^2 y_o}{\tau_{\pi, K} (y_o)}$$

K is the pion to kaon ratio, ≈ 0.15 .

The resultant analytic spectrum is

For $E < 20$ GeV

$$S(E)dE = 0.1815P_\mu(E + \Delta E)^{-2.645} \left[\frac{57.303}{E + \Delta E + 90} + \frac{23.021}{E + \Delta E + 450} \right] dE \quad (6.17)$$

$$\Delta E = 2.333 + 0.0023E \quad (6.18)$$

$$P_\mu = \left(\frac{0.0968E}{E + \Delta E} \right)^{(1.027/(E + 1.107\Delta E))} \quad (6.19)$$

For $20 \text{ GeV} < E < 500 \text{ GeV}$

$$S(E)dE = \frac{1}{E^2} [-0.5236 + 0.3659 \ln|E| - 0.0445(\ln|E|)^2 + 0.0008(\ln|E|)^3] dE \quad (6.20)$$

For $E > 500$ GeV

$$S(E)dE = 0.1187P_\mu(E + \Delta E)^{-2.56} \left[\frac{58.656}{E + \Delta E + 90} + \frac{24.337}{E + \Delta E + 450} \right] dE \quad (6.21)$$

All units are muon $s^{-1} \text{ cm}^{-2} \text{ sr}^{-1} \text{ GeV}^{-1}$.

To define the spectrum $S'(E)dE$ for the spectrograph the acceptance must be taken into account.

$$S'(E)dE = A(E)S(E)dE \quad (6.22)$$

where $A(E)$ is the acceptance function defined in Section 3.3.2. Figure 6.9 presents the muon spectrum as seen at levels 5, 3 and 1. The mean muon energy incident on the spectrograph is 24 GeV at a rate of $0.321 \text{ muons s}^{-1}$.

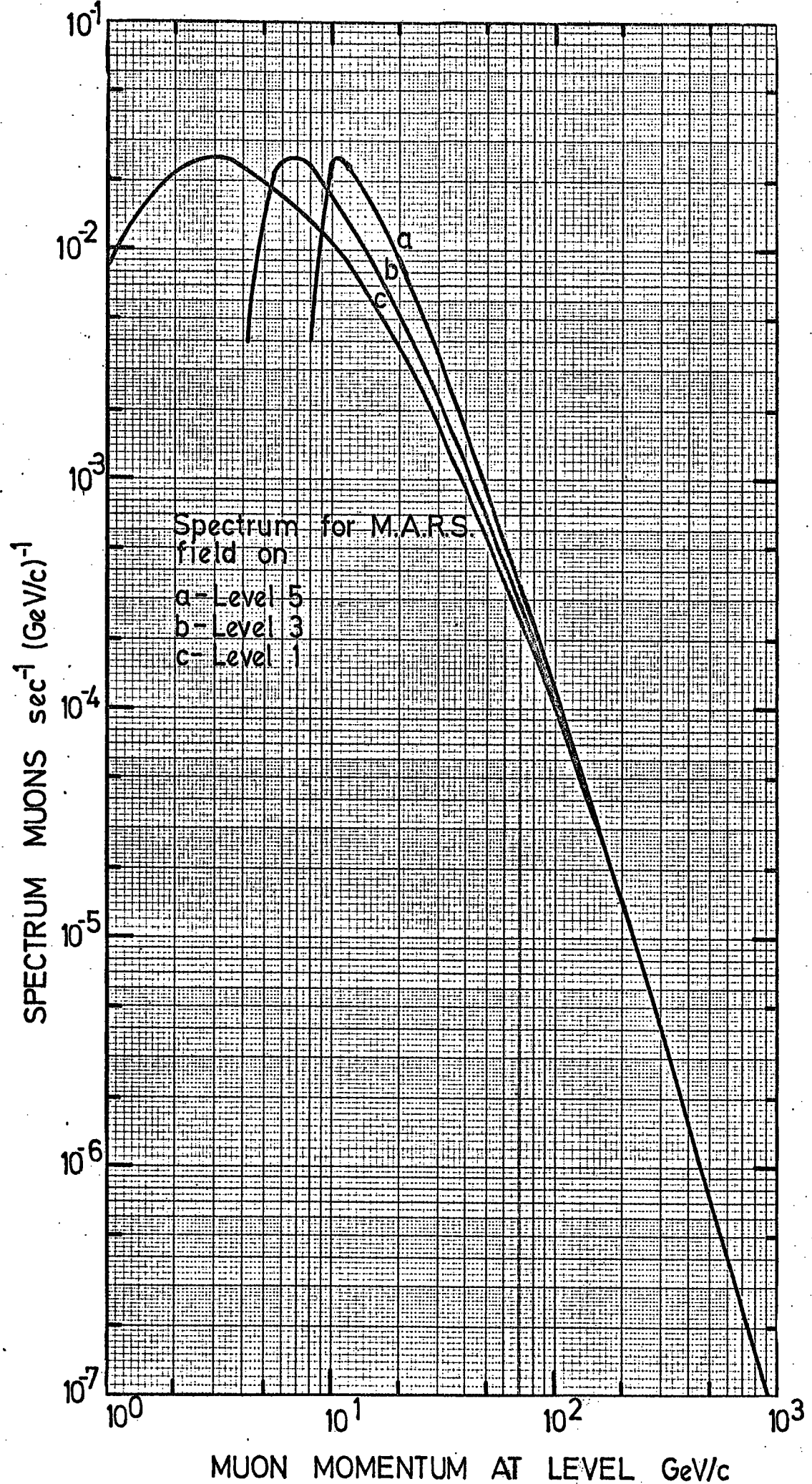


FIGURE 6.9. The muon momentum spectrum at levels 1, 3 and 5 of the MARS spectrograph.

6.3 THE BURST SPECTRUM

Using the results of the last two sections, the rate ($R'_L(N)dN$) of observing bursts of size N at any level (L) in the MARS spectrograph has been calculated using the equation

$$R'_L(N)dN = \int_{E_1}^{E_2} \Phi(E(E_\mu, X_{L-1}), N) S'(E_\mu) dE_\mu dN . \quad (6.23)$$

All functions are as previously stated. X_{L-1} is the depth of iron to the level above the measuring level. E_1, E_2 define the section of the muon energy spectrum of interest.

The burst spectrum was calculated for the following energy ranges which correspond to the energy cells used for the analysis of the data:

1. $7 \text{ GeV} < E_o < 14 \text{ GeV}$	$\bar{E}_o \sim 11$
2. $14 \text{ GeV} < E_o < 54 \text{ GeV}$	$\bar{E}_o \sim 24$
3. $54 \text{ GeV} < E_o < 204 \text{ GeV}$	$\bar{E}_o \sim 86$
4. $204 \text{ GeV} < E_o < 604 \text{ GeV}$	$\bar{E}_o \sim 298$
5. $604 \text{ GeV} < E_o < \text{infinity}$	$\bar{E}_o \sim 1005$
6. $7 \text{ GeV} < E_o < \text{infinity}$	$\bar{E}_o \sim 24$

The results of this calculation are reported in Tables 6.2 and 6.3 and in Figure 6.10. It can be seen that for incident energies $> 54 \text{ GeV}$ the spectra are almost the same (< 5% difference) at the two levels.

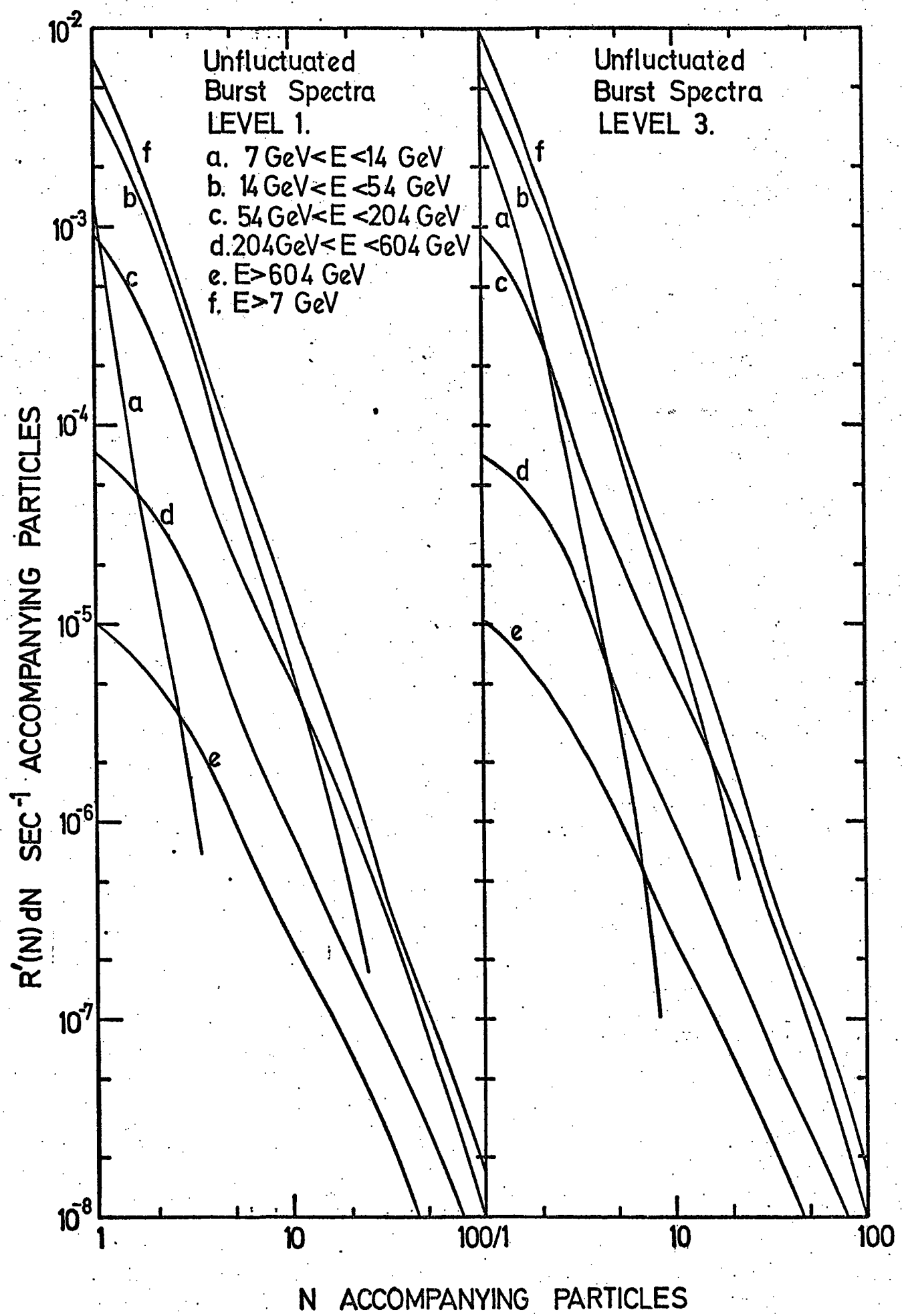


FIGURE 6.10. The unfluctuated burst spectra for levels 1 and 3 of the MARS spectrograph.

TABLE 6.2

LEVEL 1 BURST SPECTRA (UNFLUCTUATED)
 $R'(N)dN \text{ EVENTS } s^{-1} \text{ ACCOMPANYING PARTICLE}^{-1}$

Burst Size	7-14 GeV	14-54 GeV	54-204 GeV	204-604 GeV	> 604 GeV	> 7 GeV
0	1.22×10^{-1}	1.71×10^{-1}	1.72×10^{-2}	9.76×10^{-4}	7.21×10^{-5}	3.11×10^{-1}
1	1.36×10^{-3}	5.41×10^{-3}	9.11×10^{-4}	8.28×10^{-5}	1.01×10^{-5}	7.81×10^{-3}
2	1.70×10^{-6}	9.92×10^{-4}	2.90×10^{-4}	3.77×10^{-5}	5.30×10^{-6}	1.34×10^{-3}
3	7.23×10^{-16}	2.70×10^{-4}	8.32×10^{-5}	1.78×10^{-5}	2.82×10^{-6}	3.75×10^{-4}
4	3.43×10^{-28}	1.08×10^{-4}	3.90×10^{-5}	7.92×10^{-6}	1.67×10^{-6}	1.55×10^{-4}
5		5.90×10^{-5}	2.35×10^{-5}	4.23×10^{-6}	1.11×10^{-6}	8.71×10^{-5}
6		2.80×10^{-5}	1.49×10^{-5}	2.74×10^{-6}	6.61×10^{-7}	4.65×10^{-5}
7		1.94×10^{-5}	1.04×10^{-5}	1.94×10^{-6}	4.68×10^{-7}	3.22×10^{-5}
8		1.35×10^{-5}	7.75×10^{-6}	1.45×10^{-6}	3.63×10^{-7}	2.29×10^{-5}
9		8.41×10^{-6}	6.42×10^{-6}	1.11×10^{-6}	2.95×10^{-7}	1.62×10^{-5}
10		5.41×10^{-6}	5.01×10^{-6}	8.85×10^{-7}	2.44×10^{-7}	1.15×10^{-5}
20		5.13×10^{-7}	1.10×10^{-6}	2.03×10^{-7}	6.90×10^{-8}	1.88×10^{-6}
30		2.85×10^{-10}	3.01×10^{-7}	7.95×10^{-8}	2.69×10^{-8}	4.08×10^{-7}
40		1.78×10^{-12}	1.55×10^{-7}	4.32×10^{-8}	1.41×10^{-8}	2.13×10^{-7}
50		4.63×10^{-13}	8.72×10^{-8}	2.71×10^{-8}	8.19×10^{-9}	1.23×10^{-7}
60		1.30×10^{-13}	5.03×10^{-8}	1.78×10^{-8}	5.39×10^{-9}	7.38×10^{-8}
70			2.54×10^{-8}	1.27×10^{-8}	3.76×10^{-9}	4.19×10^{-8}
80			1.69×10^{-8}	9.74×10^{-9}	2.81×10^{-9}	2.95×10^{-8}
90			1.27×10^{-8}	7.69×10^{-9}	2.14×10^{-9}	2.25×10^{-8}
100			8.63×10^{-9}	5.83×10^{-9}	1.71×10^{-9}	1.62×10^{-8}

TABLE 6.3

LEVEL 3 BURST SPECTRA (UNFLUCTUATED)

 $R'(N) dN \text{ EVENTS } s^{-1} \text{ ACCOMPANYING PARTICLE}^{-1}$

Burst Size	7-14 GeV	14-54 GeV	54-204 GeV	204-604 GeV	> 604 GeV	> 7 GeV
0	1.21×10^{-1}	1.70×10^{-1}	1.72×10^{-1}	9.74×10^{-4}	7.19×10^{-5}	3.08×10^{-1}
1	2.90×10^{-3}	5.95×10^{-3}	9.30×10^{-4}	8.36×10^{-5}	1.02×10^{-5}	9.88×10^{-3}
2	3.54×10^{-4}	1.18×10^{-3}	3.08×10^{-4}	3.82×10^{-5}	5.34×10^{-6}	1.89×10^{-3}
3	4.60×10^{-5}	3.68×10^{-4}	8.74×10^{-5}	1.81×10^{-5}	2.85×10^{-6}	5.23×10^{-4}
4	9.99×10^{-6}	1.55×10^{-4}	4.07×10^{-4}	8.16×10^{-6}	1.69×10^{-6}	2.14×10^{-4}
5	5.18×10^{-6}	8.48×10^{-5}	2.45×10^{-5}	4.34×10^{-6}	1.13×10^{-6}	1.19×10^{-4}
6	1.07×10^{-6}	4.17×10^{-5}	1.56×10^{-6}	2.81×10^{-6}	6.70×10^{-7}	6.17×10^{-5}
7	6.95×10^{-7}	2.90×10^{-5}	1.09×10^{-5}	1.99×10^{-6}	4.75×10^{-7}	4.26×10^{-5}
8	1.34×10^{-7}	2.02×10^{-5}	8.08×10^{-6}	1.50×10^{-6}	3.67×10^{-7}	3.02×10^{-5}
9	7.26×10^{-9}	1.29×10^{-5}	6.69×10^{-6}	1.14×10^{-6}	2.99×10^{-7}	2.10×10^{-5}
10	1.83×10^{-9}	8.35×10^{-6}	5.26×10^{-6}	9.09×10^{-7}	2.48×10^{-5}	1.47×10^{-5}
20		8.21×10^{-7}	1.18×10^{-6}	2.09×10^{-7}	7.03×10^{-8}	2.28×10^{-6}
30		1.28×10^{-9}	3.52×10^{-7}	8.16×10^{-8}	2.75×10^{-8}	4.61×10^{-7}
40		1.72×10^{-11}	1.82×10^{-7}	4.42×10^{-8}	1.44×10^{-8}	2.40×10^{-7}
50		4.93×10^{-12}	1.02×10^{-7}	2.76×10^{-8}	8.35×10^{-9}	1.38×10^{-7}
60		1.44×10^{-12}	5.87×10^{-8}	1.82×10^{-8}	5.49×10^{-9}	6.28×10^{-8}
70			2.94×10^{-8}	1.30×10^{-8}	3.84×10^{-9}	4.64×10^{-8}
80			1.97×10^{-8}	9.94×10^{-9}	2.87×10^{-9}	3.25×10^{-8}
90			1.48×10^{-8}	7.85×10^{-9}	2.18×10^{-9}	2.48×10^{-8}
100			1.01×10^{-8}	5.98×10^{-9}	1.74×10^{-9}	1.78×10^{-8}

6.3.1 FLUCTUATIONS

Thus far the calculations have been performed using average showers. In reality the number of particles at any point in a shower fluctuates from this norm. Due to the decreasing cross-sections as a function of increasing burst size, the fluctuations will alter the shape of the burst spectra. The effects of these fluctuations will be particularly noticeable for small burst sizes and low muon energies. Small showers produced by muons of low energy are very dependent on the points of the first interactions. A late interacting electron (or photon) will tend to produce a smaller shower than an earlier interacting particle. Large fluctuations about the mean might, therefore, be expected with the result that some large showers should be observed from low energy muons.

Fluctuations in shower development are complicated and not well known, most of the theoretical work having been done about the same time as the discovery of penetrating radiation (see Furry 1937, Scott and Uhlenbeck 1942, Rossi and Greisen 1941, and Rossi 1952). Two types of fluctuation have been used in the past. The first and perhaps the most widely used approach assumes that all the shower particles are genetically independent. Based on this assumption the fluctuations in the shower development would be expected to obey Poisson statistics. The probability P of seeing N electrons from a distribution whose mean is m electrons is given by

$$P(N, m) = \frac{e^{-m} m^N}{N!} . \quad (6.24)$$

The assumption of genetic independence will be approximately satisfied for large bursts and for bursts several generations old. However,

for small showers and showers in early development, the Poisson statistics should underestimate the actual fluctuations (Rossi 1952).

The experiment reported here does not only concern itself with relatively large bursts, but also is interested in small showers of less than 10 particles. As a developing shower in which there are 10 particles is just over three generations old, it was therefore thought that the problem of fluctuations should be looked into in more detail.

Furry (1937) considered the problem of fluctuations taking into account the genetic dependence in the shower development. In his treatment, Furry made two major assumptions.

1. Energy loss in the shower was neglected. In order for this assumption to be valid, it is necessary that the total energy transferred to the shower must be large compared to the total ionization loss suffered by all the particles in the shower considered.
2. In solving his set of differential equations he assumed that there must be at least one particle at any point in the shower. If one assumes an electron initiated shower, as Furry did, this assumption does not allow the shower to fluctuate to zero electrons.

At the time when Furry was looking into the problem of fluctuations, penetrating radiation was just being detected experimentally and its implications discussed theoretically (Bhabha 1938, Rossi 1934, Auger et al. 1934, Street et al. 1935). Furry, therefore, did his work for electrons and thin thicknesses of absorber. In order to justify the use of Furry statistics, it must be shown that the assumptions which Furry made are applicable to high energy muon physics and



very thick absorbers. To accomplish this, calculations have been done:

1. to determine the mean energy transferred per observed electron in a burst. (To obtain this the following equation was integrated numerically

$$E_p(E_o, N) = \frac{\int_{\text{block}} E_t(N, t, E_{\text{MIN}}) \phi(E_o, N, t) dt dN}{N \int_{\text{block}} \phi(E_o, N, t) dt dN} \quad (6.25)$$

where E_t and ϕ are as defined earlier. $E_p(E_o, N)$ is the mean energy per electron in a shower of size N as a function of muon energy E_o .

For representative numerical results see Table 6.4);

2. to determine the mean depth (t_p) of the interaction which produces a shower of size N . (This was calculated using the following equation

$$t_p(E_o, N) = \frac{\int_{\text{block}} t \phi(E_o, N, t) dt dN}{\int_{\text{block}} \phi(E_o, N, t) dt dN} \quad (6.26)$$

For representative numerical results see Table 6.4);

3. to determine the mean age of the observed shower as a function of muon energy and shower size. The shower age has been estimated by combining an equation obtained by Rossi (1952) from approximation A and an equation obtained by Baruch (1973), and normalizing it to the Ivanenko-Samosudov shower curves. The estimated shower age (S) as a function of the shower size N and the depth of interaction t is given by

$$S(N, t) = \frac{3t}{t + 2.02[B(N, t) - 1]} \quad (6.27)$$

$$B(N, t) = \frac{E_t(N, t, E_{\text{MIN}})}{E_c} \quad (6.28)$$

TABLE 6.4

A TABLE OF THE MEAN ENERGY TRANSFERRED PER OBSERVED SHOWER PARTICLE,
MEAN DEPTHS OF INTERACTION AND MEAN SHOWER AGE OF
SHOWERS OBSERVED OUT OF A THICK IRON ABSORBER (70 r.i.)

		Muon Energy				
		11 GeV	24 GeV	86 GeV	300 GeV	1000 GeV
Mean Energy Transferred Per Observed Particle (GeV)	Minimum	0.4	0.5	0.8	0.7	0.9
	Maximum	0.8	0.9	1.3	1.3	2.5
	Mean	0.7	0.8	1.1	1.1	1.4
Mean Depth of Interaction (Radiation Lengths)	Minimum	2.1	2.5	2.8	2.9	3.4
	Maximum	4.3	4.6	7.0	8.8	9.3
	Mean	3.6	3.9	5.6	5.9	7.1
Mean Shower Age	Minimum	0.7	0.9	0.8	0.8	0.8
	Maximum	1.1	1.1	1.2	1.2	1.3
	Mean	0.9	0.9	1.0	1.0	1.0

where S is the shower age defined such that $S = 1$ at shower maximum, t is the depth from the point of initiation, E_t is the energy transferred to the shower and E_c is the critical energy of the material.

The mean age (S_p) has been determined as follows:

$$S_p(E_0, N) = \frac{\int_{\text{block}} S(N, t) \phi(E_0, N, t) dN dt}{\int_{\text{block}} \phi(E_0, N, t) dN dt} \quad (6.29)$$

Representative numerical results are presented in Table 6.4.)

These calculations have revealed three important points. First, the average energy transferred per shower particle is, very roughly, $1 \text{ GeV particle}^{-1}$ over all muon energies considered. Second, even in a thick iron absorber the mean point of interaction lies in the last few radiation lengths. Since interaction can occur with a low probability many radiation lengths from the bottom of the absorber, it is apparent that most of the interactions must occur between the mean depth and the bottom of the magnet block. And, third, on average, the showers which are observed tend to be near shower maximum.

Furry's first assumption is that the energy transferred to the total shower must be ~~less~~ ^{GREATER} than the energy loss due to ionization. In traversing one radiation length in iron an electron will lose about 30 MeV to the ionization process. The above calculations show that for the average shower, which is about at shower maximum, the average energy transferred to the shower is much greater than the energy loss due to ionization in depths which are greater than the mean depth of interaction. Based on this result it is believed that Furry's first assumption is satisfied for thick iron absorbers at the muon energies which are relevant to this experiment.

It is possible through the various processes to lose all of the expected electrons and to have a shower fluctuated to a size of zero. The assumption that the initiating electron is always present does not allow this to occur. However, if it is assumed that the shower is not electron initiated but muon initiated, the second Furry assumption is more realistically satisfied. The energy loss of the muon can be considered to be negligible. Since it has no process by which it can be absorbed it will always be present in the shower, and it is reasonable to assume that the muon will not fluctuate to more than one particle. It is believed that the conditions of this experiment satisfy both of the assumptions made by Furry.

The solution to the set of differential equations which Furry obtained can be stated as

$$P(N,m) = (m + 1)^{-1} \left(\frac{m}{m + 1}\right)^N \quad (6.30)$$

where $P(N,m)$ is the probability of obtaining N electrons from a distribution whose mean is m electrons.

It appears, based on the literature and the results obtained here, that Furry statistics should at least be used for small showers and low muon energies, while it appears that Poisson statistics might be valid for large showers and ~~high muon energies~~. To ascertain if the Furry statistics could be used over the entire spectrum, the burst spectra using both types of fluctuations have been calculated and compared. Equation (6.31) was used to fold the fluctuations into the burst spectrum.

$$R(N)dN = \sum_{m=0}^{m=\infty} P(N,m) R'(m) \frac{dm}{dN} dN \quad (6.31)$$

where

R' is the fluctuated burst spectrum

P is the Poisson or the Furry distribution (equation (6.24) or equation (6.30) respectively)

R is the unfluctuated burst spectrum (equation (6.22))

dm/dN is the cell width correction.

The results of these calculations are presented in Figures 6.11, 6.12 and 6.13. It can be seen that at low muon energies (less than about 50 GeV) the Furry fluctuated spectra are flatter than the Poisson fluctuated ones. At high energies the two types of spectra are very similar except at very small burst sizes.

Taking all of this information into account, it appears that the realistic spectra to use are the ones which contain the Furry fluctuations. The numerical values of the spectra containing Furry fluctuations are presented in Tables 6.5 and 6.6 and in Figure 6.14. To present a complete picture, the probabilities of producing N particles out of a magnet block as a function of muon energy have been calculated with fluctuations and are presented in Figure 6.15 and Figure 6.16.

6.4 DISCUSSION OF ERRORS

Because of the nature and complexity of the calculation it is not easy to obtain an exact error on the theoretical burst spectrum. The discussion in this section will attempt to obtain a general idea of the order of the errors.

The electromagnetic interaction cross-sections, as stated in Chapter 2, are considered to be accurate to approximately 3%. In

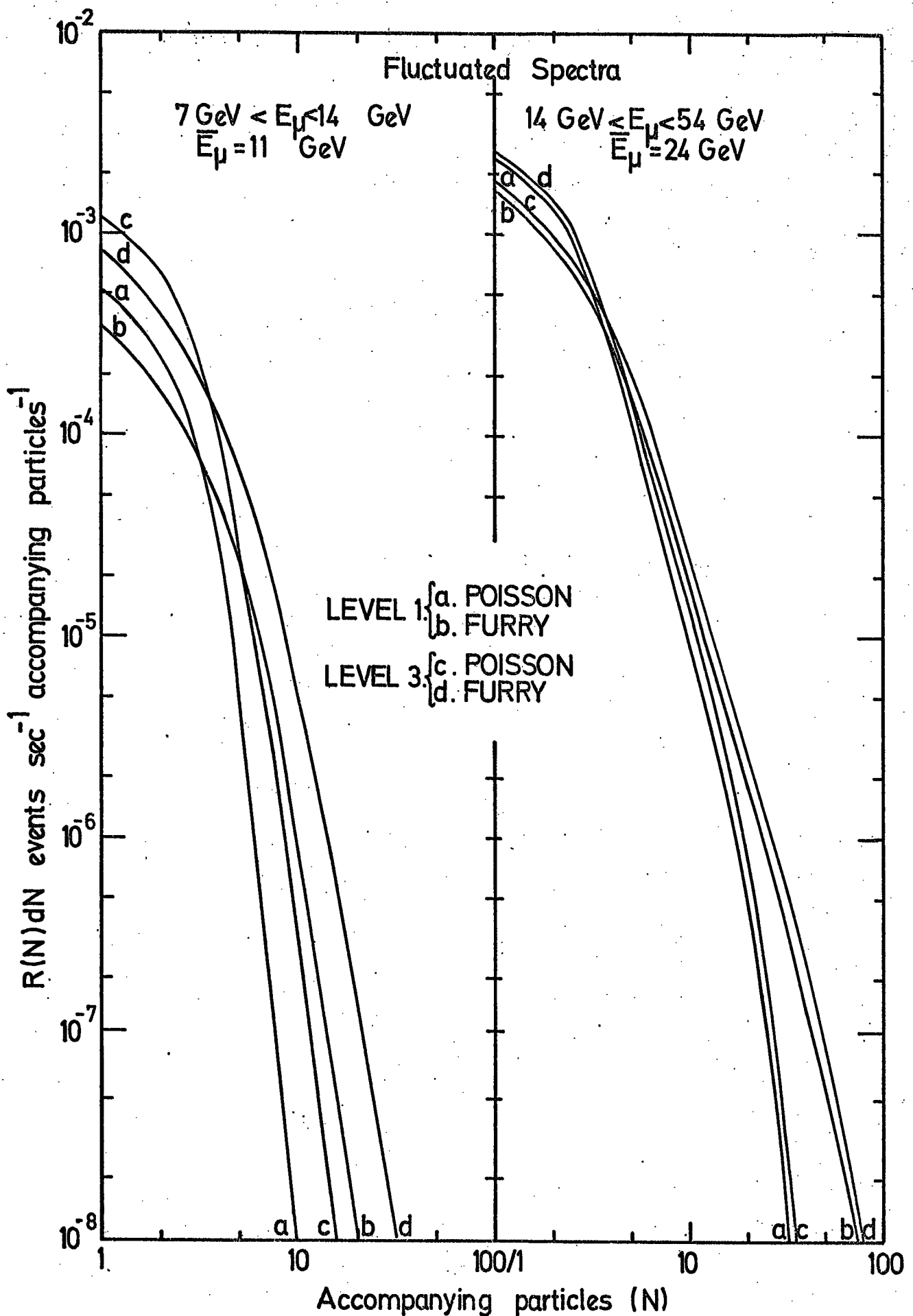


FIGURE 6.11. A comparison between the expected burst spectra in MARS with (a) Poisson fluctuations and (b) Furry fluctuations.

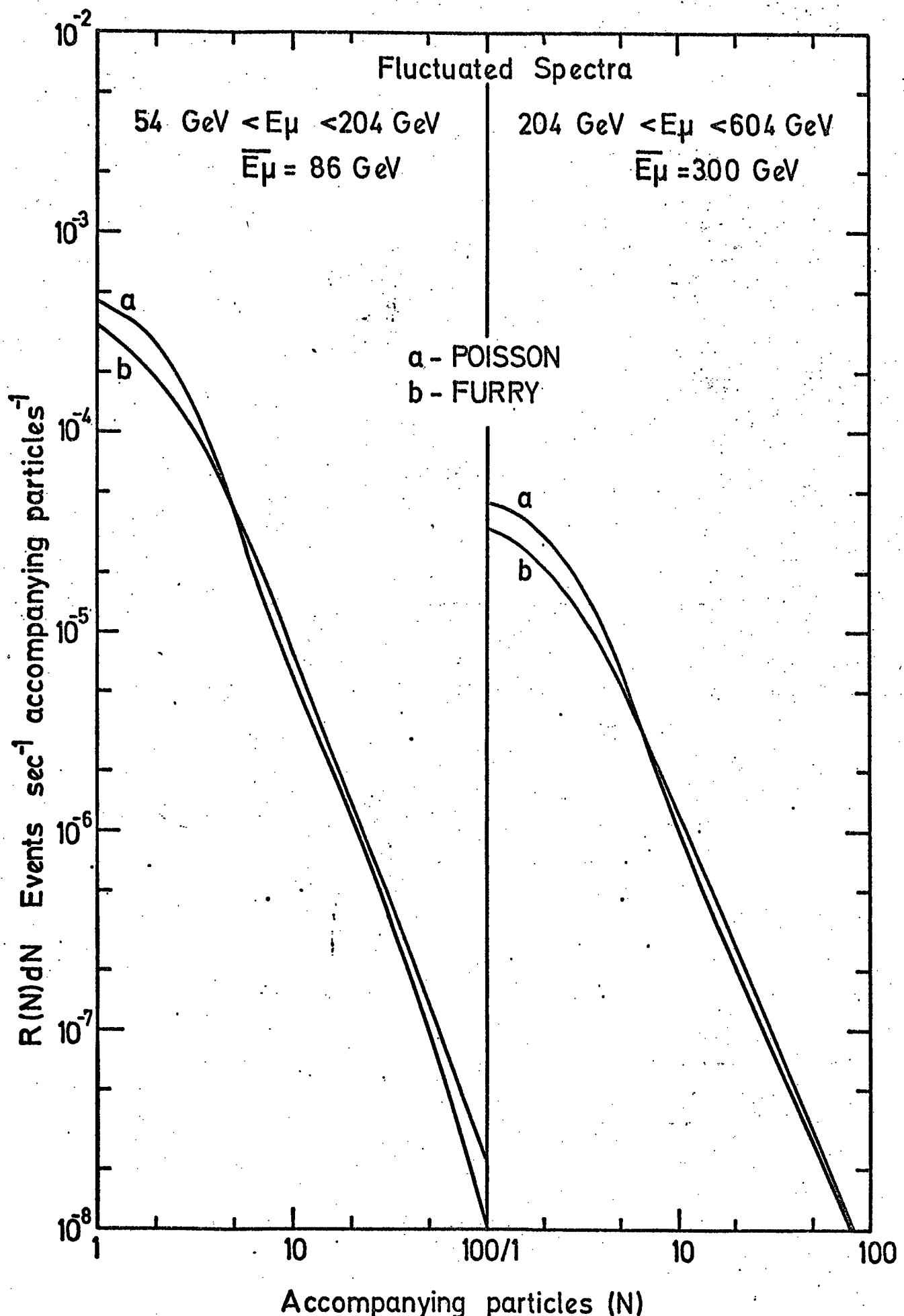


FIGURE 6.12. Comparison between the expected burst spectra containing Poisson (a) and Furry (b) fluctuations.

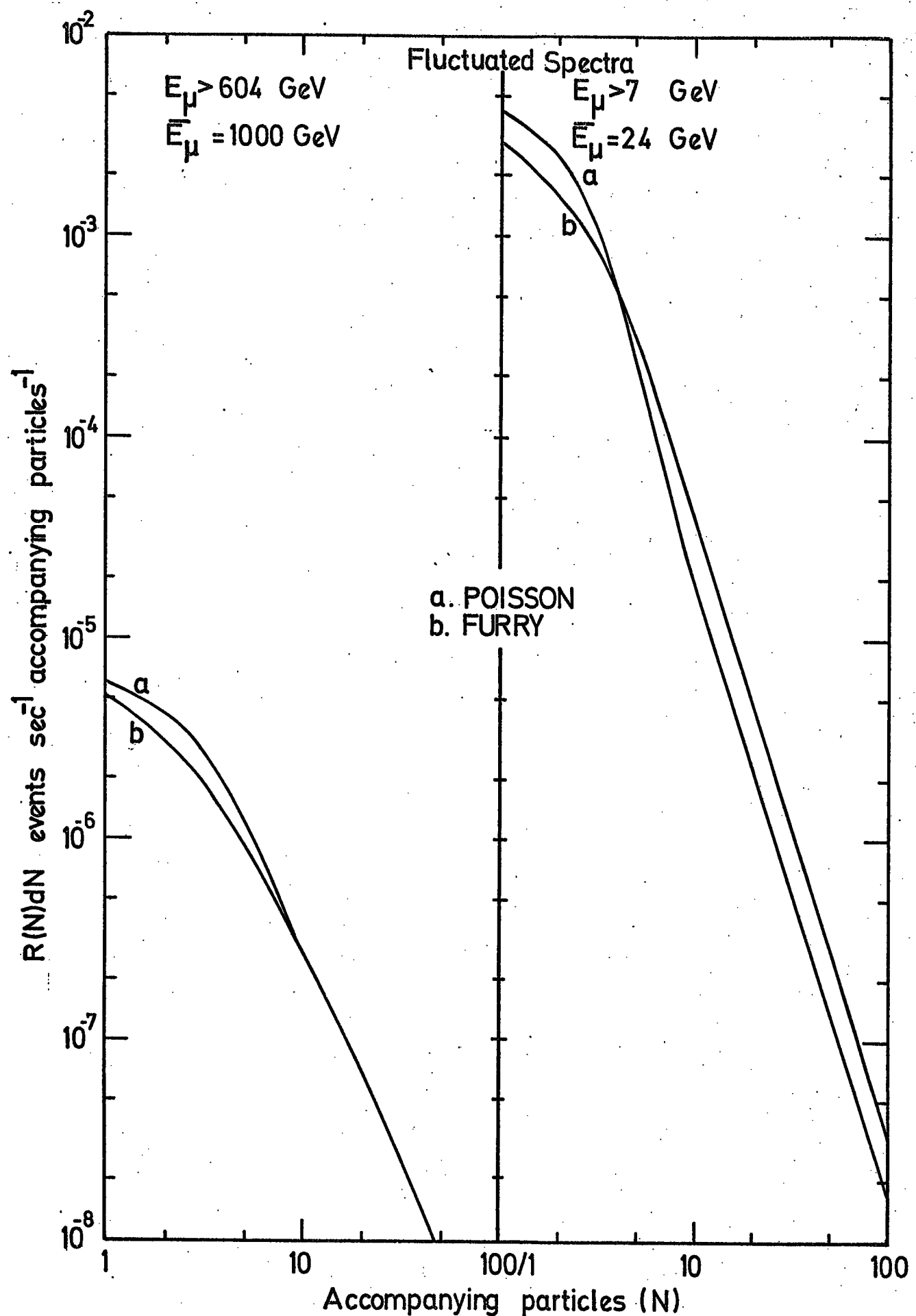


FIGURE 6.13. A comparison between the expected burst spectra in MARS with (a) Poisson fluctuations and (b) Furry fluctuations.

TABLE 6.5

LEVEL 1 BURST SPECTRA (FLUCTUATED)
 $R'(N) dN \text{ EVENTS } s^{-1} \text{ ACCOMPANYING PARTICLE}^{-1}$

Burst Size	7-14 GeV	14-54 GeV	54-204 GeV	204-604 GeV	> 604 GeV	> 7 GeV
0	1.23×10^{-1}	1.74×10^{-1}	1.79×10^{-2}	1.04×10^{-3}	8.05×10^{-5}	3.16×10^{-1}
1	3.43×10^{-4}	1.65×10^{-3}	3.24×10^{-4}	3.55×10^{-5}	4.98×10^{-6}	2.37×10^{-3}
2	1.72×10^{-4}	8.90×10^{-4}	1.82×10^{-4}	2.10×10^{-5}	3.07×10^{-6}	1.27×10^{-3}
3	8.67×10^{-5}	4.88×10^{-4}	1.06×10^{-4}	1.30×10^{-5}	1.99×10^{-6}	6.98×10^{-4}
4	4.37×10^{-5}	2.76×10^{-4}	6.38×10^{-5}	8.32×10^{-6}	1.34×10^{-6}	3.94×10^{-4}
5	2.21×10^{-5}	1.61×10^{-4}	4.01×10^{-5}	5.57×10^{-6}	9.49×10^{-7}	2.30×10^{-4}
6	1.12×10^{-5}	9.71×10^{-5}	2.63×10^{-5}	3.88×10^{-6}	6.96×10^{-7}	1.39×10^{-4}
7	5.70×10^{-6}	6.11×10^{-5}	4.80×10^{-5}	2.80×10^{-6}	5.28×10^{-7}	8.82×10^{-5}
8	2.92×10^{-6}	4.00×10^{-5}	1.28×10^{-5}	2.09×10^{-6}	4.12×10^{-7}	5.82×10^{-5}
9	1.51×10^{-6}	2.71×10^{-5}	9.45×10^{-6}	1.60×10^{-6}	3.28×10^{-7}	4.00×10^{-5}
10	7.88×10^{-7}	1.91×10^{-5}	7.18×10^{-6}	1.25×10^{-6}	2.67×10^{-7}	2.86×10^{-5}
20	3.76×10^{-9}	1.76×10^{-6}	1.23×10^{-6}	2.38×10^{-7}	6.47×10^{-8}	3.31×10^{-6}
30	1.07×10^{-10}	4.05×10^{-7}	4.53×10^{-7}	9.30×10^{-8}	2.77×10^{-8}	9.92×10^{-7}
40	4.81×10^{-12}	1.33×10^{-7}	2.21×10^{-7}	4.85×10^{-8}	1.50×10^{-8}	4.27×10^{-7}
50	2.50×10^{-13}	5.29×10^{-8}	1.23×10^{-7}	2.93×10^{-8}	9.26×10^{-9}	2.21×10^{-7}
60	1.37×10^{-14}	2.35×10^{-8}	7.63×10^{-8}	1.94×10^{-8}	6.18×10^{-9}	1.29×10^{-7}
70	7.67×10^{-16}	1.12×10^{-8}	5.00×10^{-8}	1.37×10^{-8}	4.36×10^{-9}	8.16×10^{-8}
80	4.31×10^{-17}	5.65×10^{-9}	3.44×10^{-8}	1.01×10^{-8}	3.20×10^{-9}	5.48×10^{-8}
90	2.42×10^{-18}	2.95×10^{-9}	2.46×10^{-8}	7.64×10^{-9}	2.43×10^{-9}	3.86×10^{-8}
100	1.36×10^{-19}	1.59×10^{-9}	1.81×10^{-8}	5.97×10^{-9}	1.89×10^{-9}	2.82×10^{-8}

TABLE 6.6

LEVEL 3 BURST SPECTRA (FLUCTUATED)

 $R'(N) dN \text{ EVENTS } s^{-1} \text{ ACCOMPANYING PARTICLE}^{-1}$

Burst Size	7-14 GeV	14-54 GeV	54-204 GeV	204-604 GeV	> 604 GeV	> 7 GeV
0	1.22×10^{-1}	1.74×10^{-1}	1.79×10^{-2}	1.04×10^{-3}	8.03×10^{-5}	3.14×10^{-1}
1	8.14×10^{-4}	1.87×10^{-3}	3.34×10^{-4}	3.59×10^{-5}	5.01×10^{-6}	3.06×10^{-3}
2	4.23×10^{-4}	1.01×10^{-3}	1.88×10^{-4}	2.13×10^{-5}	3.10×10^{-6}	1.65×10^{-3}
3	2.23×10^{-4}	5.62×10^{-4}	1.10×10^{-4}	1.31×10^{-5}	2.00×10^{-6}	9.10×10^{-4}
4	1.19×10^{-4}	3.22×10^{-4}	6.64×10^{-5}	8.45×10^{-6}	1.36×10^{-6}	5.17×10^{-4}
5	6.47×10^{-5}	1.91×10^{-4}	4.19×10^{-5}	5.67×10^{-6}	9.58×10^{-7}	3.04×10^{-4}
6	3.60×10^{-5}	1.18×10^{-4}	2.75×10^{-5}	3.95×10^{-6}	7.03×10^{-7}	1.86×10^{-4}
7	2.05×10^{-5}	7.55×10^{-5}	1.89×10^{-5}	2.86×10^{-6}	5.34×10^{-7}	1.18×10^{-4}
8	1.20×10^{-5}	5.05×10^{-5}	1.35×10^{-5}	2.13×10^{-6}	4.16×10^{-7}	7.85×10^{-4}
9	7.27×10^{-6}	3.50×10^{-5}	9.93×10^{-6}	1.63×10^{-6}	3.32×10^{-7}	5.41×10^{-5}
10	4.52×10^{-6}	2.51×10^{-5}	7.55×10^{-6}	1.28×10^{-6}	2.71×10^{-7}	3.87×10^{-5}
20	1.34×10^{-7}	2.57×10^{-6}	1.30×10^{-6}	2.45×10^{-7}	6.57×10^{-8}	4.33×10^{-6}
30	1.23×10^{-8}	6.13×10^{-7}	4.88×10^{-7}	9.55×10^{-8}	2.81×10^{-8}	1.26×10^{-6}
40	1.87×10^{-9}	2.06×10^{-7}	2.41×10^{-7}	4.98×10^{-8}	1.53×10^{-8}	5.26×10^{-7}
50	3.55×10^{-10}	8.29×10^{-8}	1.37×10^{-7}	3.01×10^{-8}	9.43×10^{-9}	2.68×10^{-7}
60	7.68×10^{-11}	3.72×10^{-8}	8.52×10^{-8}	1.99×10^{-8}	6.30×10^{-9}	1.54×10^{-7}
70	1.81×10^{-11}	1.79×10^{-8}	5.63×10^{-8}	1.40×10^{-8}	4.44×10^{-9}	9.60×10^{-8}
80	4.55×10^{-12}	9.11×10^{-9}	3.90×10^{-8}	1.03×10^{-8}	3.27×10^{-9}	6.38×10^{-8}
90	1.19×10^{-12}	4.80×10^{-9}	2.81×10^{-8}	7.84×10^{-9}	2.48×10^{-9}	4.45×10^{-8}
100	3.25×10^{-13}	2.60×10^{-9}	2.08×10^{-8}	6.12×10^{-9}	1.93×10^{-9}	3.23×10^{-8}

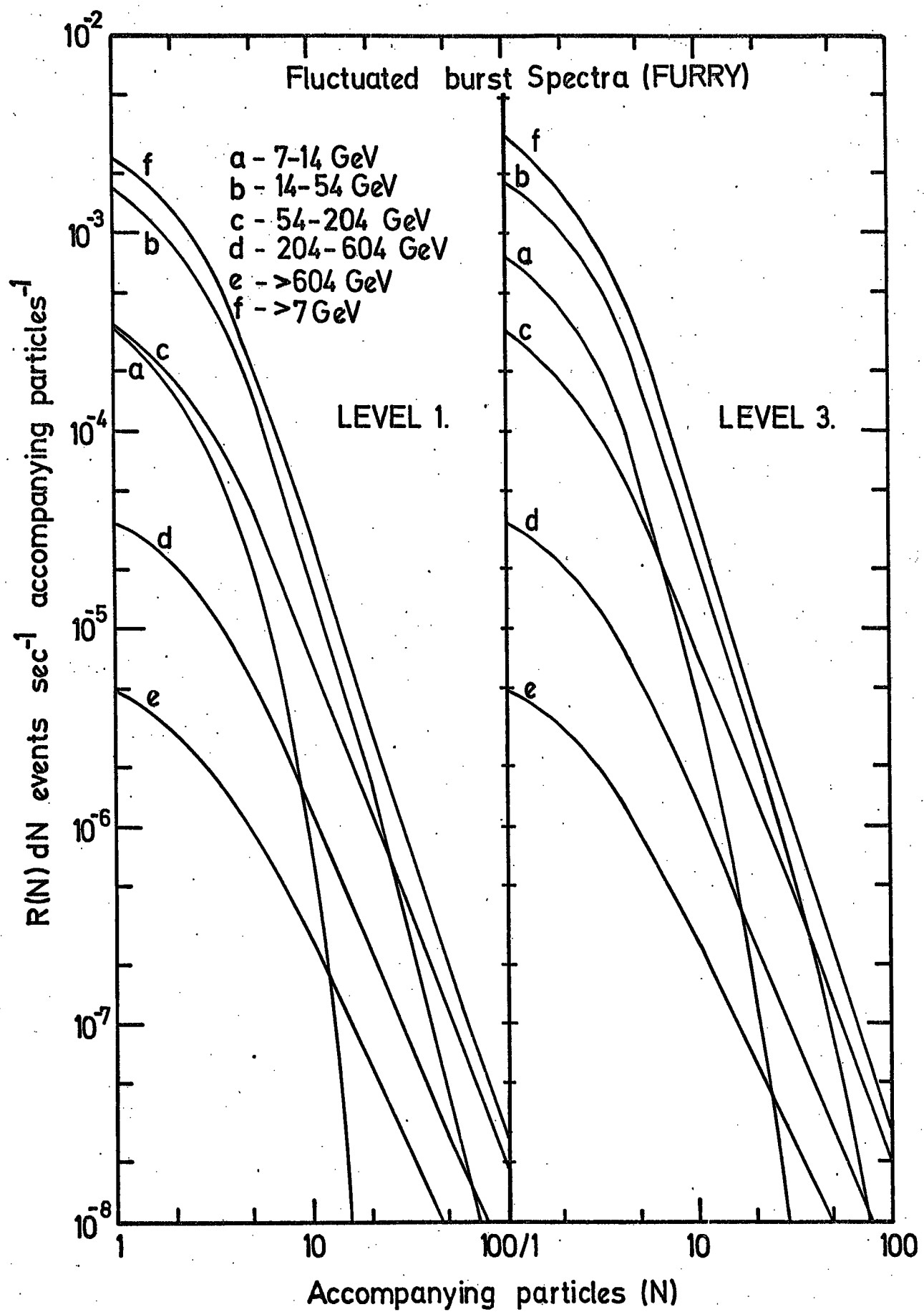


FIGURE 6.14. The expected burst spectra including fluctuations (Furry), for the MARS spectrograph.

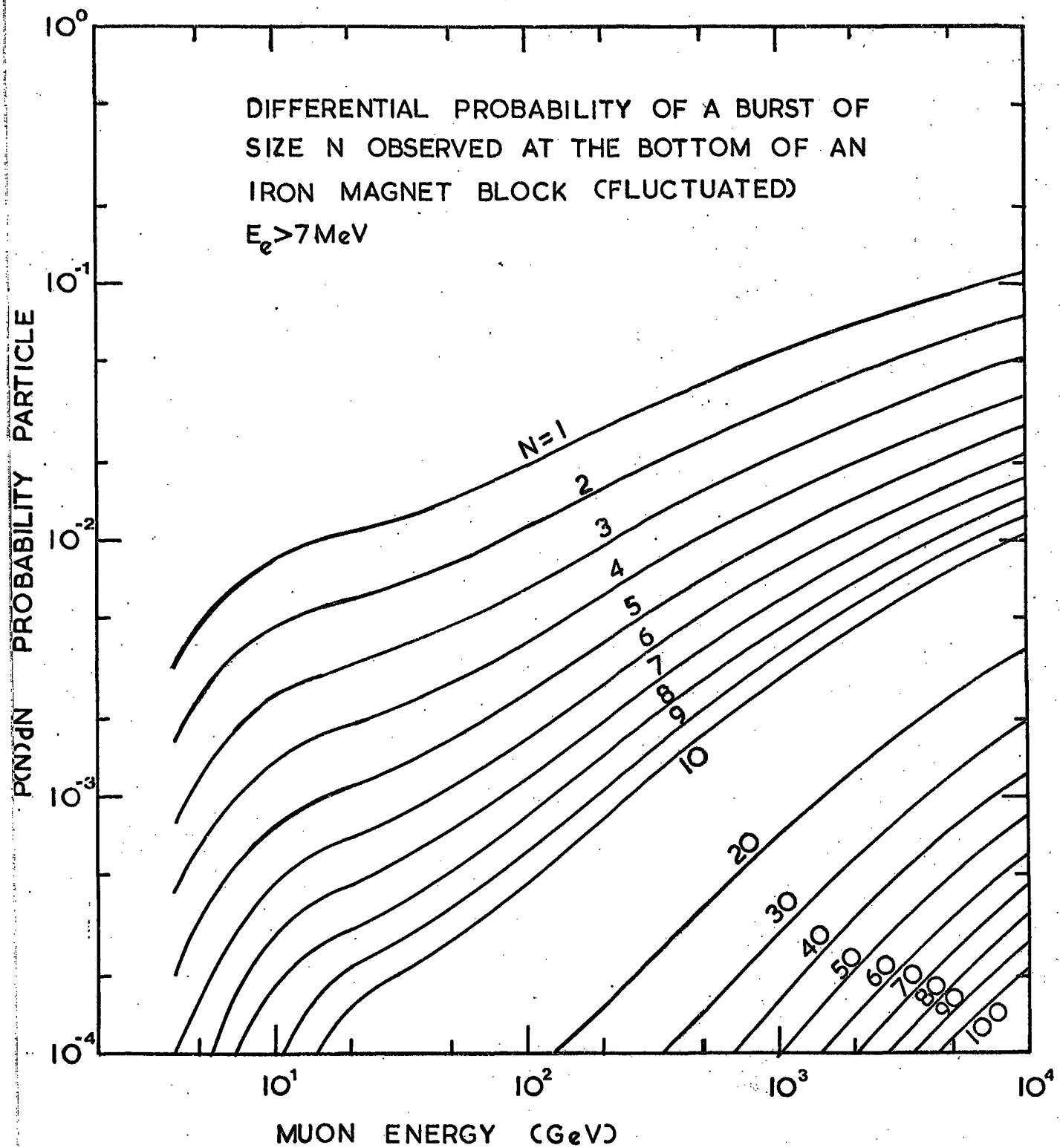


FIGURE 6.15. The differential probability of observing N accompanying particles at the bottom of a 1000 gm cm^{-2} iron absorber as a function of incident energy (fluctuations included).

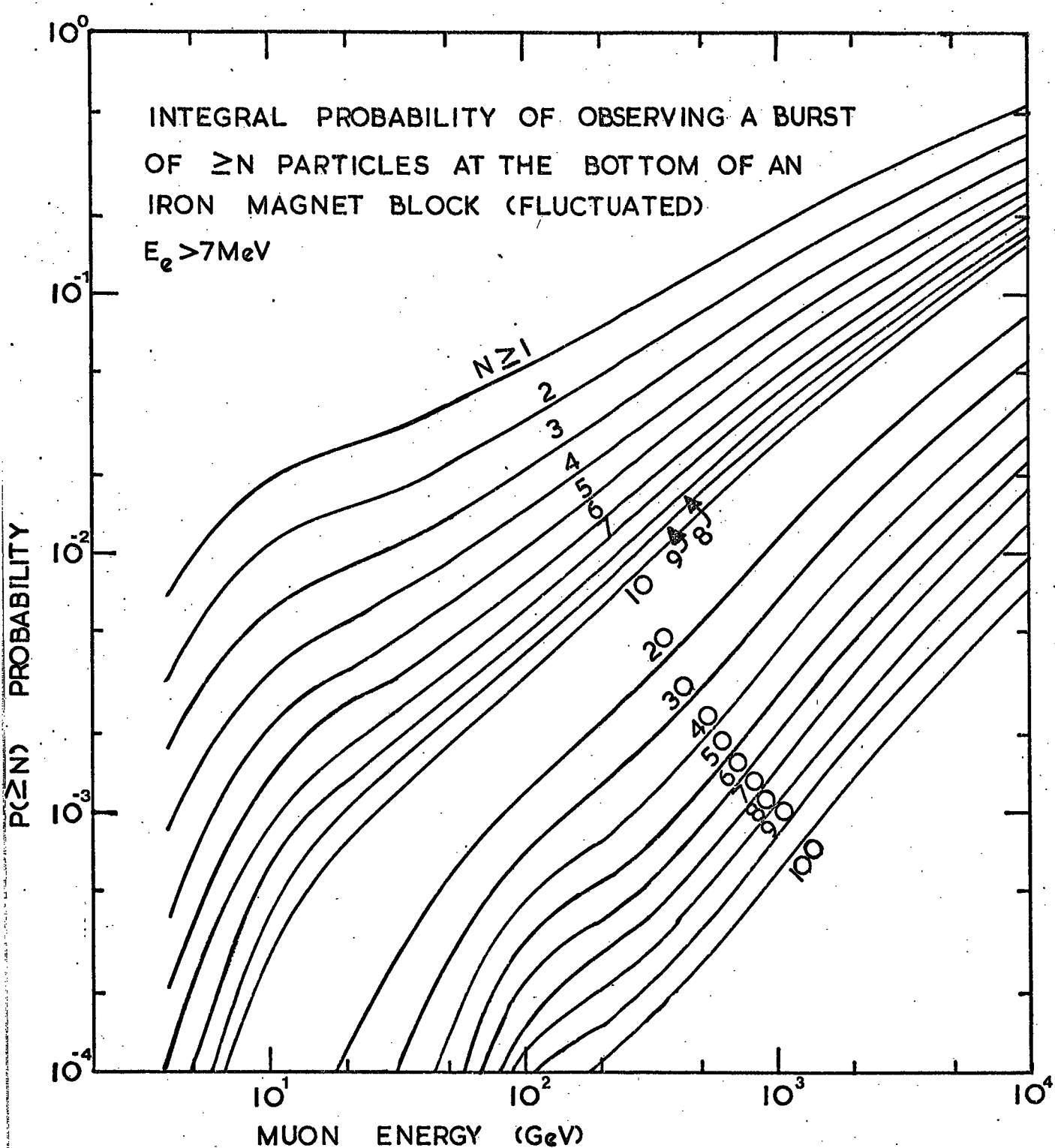


FIGURE 6.16. The integral probability of observing $> N$ accompanying particles at the bottom of a 1000 gm cm^{-2} iron absorber as a function of muon incident energy (fluctuations excluded).

the consideration of the total cross-section, only the error on the dominant cross-section will be important. The maximum error will occur at the point where the three cross-sections are approximately equal ($E_\mu \approx 280$ GeV, $E_t \approx 20$ GeV). At this point the error will be approximately 5%. In the use of these cross-sections in the numerical calculations, the numerical interpolation should introduce errors of $\approx 5\%$ (the interpolation was linear in log-log space. As a consequence the knock-on and bremsstrahlung cross-sections which are linear in log-log space, except at energy transfers near the maximum energy transfer, will be interpolated with almost no error, but for direct pair production, which is curved in log-log space, the straight line interpolation will introduce errors.) The error introduced by the cross-sections should have been approximately 7%.

The shower development curves are estimated by Ivanenko and Samosudov to be accurate to approximately 10%. Again, the interpolation will introduce errors. Due to the nature of the data and the method used, the estimated interpolation error is approximately 10%. This gives a composite error of approximately 14%. When considering the effect of this error on the calculations, it can be seen that this error is magnified by the slope of the cross-section. In general, the steepest cross-section is for the knock-on process where $\sigma_{KO} \propto E_t^{-2}$. The effect of this is that a 14% error in the energy transfer required will cause a 28% error in the cross-section.

The energy loss curves should have errors approximately equal to those for the cross-section (approximately 7%), but because of the criteria on the bremsstrahlung and direct pair production cross-sections, these losses could be low by a small, but unknown, amount. This is unimportant, the effects of error in the energy loss are minimal.

For muon energies > 100 GeV the maximum contribution the energy loss makes to the actual energy is $< 10\%$. In this region the error introduced by energy loss error is $< 1\%$. At muon energies of approximately 7 GeV the error due to energy loss is approximately 7%. The effect this error has on the cross-section can be seen in comparing Figures 2.2, 2.3, 2.13, 2.19-2.23. Since the knock-on and bremsstrahlung processes are essentially *not* energy dependent the error introduced is $\ll 1\%$. Only direct pair production shows a marked energy dependence. DPP only plays an important part in the total cross-section at muon energies > 100 GeV. Consequently the error in energy loss will contribute at most approximately 1%.

The numerical integration through a magnet block assumed that the cross-section was constant over each radiation length. In general, the error introduced should be $\sim 10\%$. This error will be a function of energy, the error will be smaller the higher the muon energy. The most significant contribution to this error will come for 1 or 2 particles produced in the last radiation length where the shower need not develop. The particle numbers may be due to the fastly increasing probability for knock-on and pair production to occur as the bottom of the magnet is approached. It is assumed, however, that this contribution is small when compared to the integral probability from depth > 1 radiation length.

The error, therefore, in Φ , the probability of producing N particles out of a magnet block as a function of energy is $\sim 31\%$.

The muon energy spectrum is estimated by Whalley to be accurate to approximately 2% at 20 GeV and approximately 10% at 500-1000 GeV. This spectrum was used to 10 TeV, well beyond its guaranteed limit. By comparison between the Whalley extrapolation and a best fit of

Ng et al. (1973) (see Whalley 1974) at 10 TeV suggests the Whalley spectrum may be high in this region by 50-100%. The contribution from this area to the total burst spectrum is however small, but should be kept in mind when the comparisons of the experimental results in this region are made. For this error estimation an overall 10% error is assumed.

The acceptance of the spectrograph is accurate to 0.5% (Whalley 1974). The error introduced in this numerical calculation is likely to be $\sim 1\%$ because the method used was similar to the one used to calculate the cross-section of Chapter 2.

Taking all the above errors into account it is believed that the theoretical burst spectrum is accurate to approximately 33%.

CHAPTER 7

THE EXPERIMENTAL BURST SPECTRUM

7.1 INTRODUCTION

In this chapter the determination of the experimental burst spectra is discussed and compared with the theoretical predictions produced in Chapter 6. To produce the experimental burst spectra three corrections have been made ^{to} on the data. First, the rates have been corrected to the real burst sizes from those predicted by the flash tubes. As a consequence there has also been a cell width correction. Second, a correction has been applied to allow for the contamination of the burst size due to knock-on electrons in the flash tube trays. Third, and finally, a correction has been made ^{to} on the interaction run data to correct for the discriminator setting which was used in event selection.

7.2 THE UNCORRECTED BURST SPECTRA

There were 4175 useable events gathered in a run time of 4.0 hours in the all events data and 13349 useable events gathered in a run time of 480.3 hours in the interaction run data. A total of 17524 events have been used in determining the burst spectra. The data have been divided into five energy bins (7-14 GeV, 14-54 GeV, 54-204 GeV, 204-604 GeV, > 604 GeV) and into flash tube determined burst size cells (see Section 4.3.3). The differential uncorrected rate, $R'(N)dN$, has been calculated as follows.

$$R'(N)dN = \frac{M}{t_{\text{eff}}W} \quad (7.1)$$

where

M is the number of events per cell,

N is the burst size cell,

W is the cell width,

t_{eff} is the effective run time.

Due to the scintillation counter efficiencies (E_{sc}) and the probability (R) of rejecting some events at the two experimental levels, the effective run time is different from the measured run time and is given by

$$t_{\text{eff}} = tE_{sc}(1 - R) \quad (7.2)$$

where t is the run time.

Whalley (1974) has measured the scintillation counter efficiencies with the result that the overall efficiency for accepting penetrating muons which traverse the spectrograph is 0.894 ± 0.002 . The event acceptance probability ($1 - R$) at levels 1 and 3 has been obtained from the all events data. The acceptance probabilities are 0.934 ± 0.021 for level 1 and 0.896 ± 0.020 for level 3. The calculated effective run times are given in Table 7.1.

The flash tube burst size cells, cell width, number of events per cell, and uncorrected rate for the two experimental levels are given in columns 1, 2, 4 and 5 respectively of Tables 7.2 to 7.5.

TABLE 7.1

EFFECTIVE RUN TIMES

	Run Time (t)	Effective Run Time t_{eff}
Interaction Run Data		
Level 1	480.3 hr	400.9 ± 9.2 hr
Level 3	480.3 hr	384.6 ± 8.6 hr
All Events Data		
Level 1	4.04 hr	3.37 ± 0.08 hr
Level 3	4.04 hr	3.24 ± 0.07 hr

7.3 CORRECTIONS

7.3.1 PARTICLE NUMBER AND CELL WIDTH CORRECTIONS

The flash tube burst size cell number has been corrected using the calibrations of Section 4.3.5. The corrected burst sizes are given in column 3 of Tables 7.2 to 7.5. The calibration curve is a linear transformation from burst size cell to differential particle number, i.e.

$$ax + b = y . \quad (7.3)$$

Due to the fact that the spectra which have been determined are differential, the cell size changes and a cell width correction is also required. If the burst spectra are given by $R'(y)dy$, the correction yields

$$R(y)dy = R' \left(\frac{y}{a} + \frac{b}{a} \right) \frac{dx}{dy} dy \quad (7.4)$$

where, from equation (7.3),

$$\frac{dx}{dy} = \frac{1}{a} . \quad (7.5)$$

dx/dy is the cell width correction and would be unity if the slope

(a) of the calibration were 1. dx/dy is 0.923 for level 1 and 0.627 for level 3 ($a = 1.08$ and 1.59 for levels 1 and 3 respectively).

The estimated error on the burst size and, therefore, the cell width, is given in Figure 7.1. The cell width corrections are presented in column 7 of Tables 7.2 and 7.3 and in column 8 of Tables 7.4 and 7.5.

7.3.2 THE KNOCK-ON IN THE FLASH TUBE TRAYS CORRECTION

As a muon passes through the flash tube trays it has a probability of producing a knock-on electron of sufficient energy to contaminate the estimated burst size. This contamination will have the most effect on small bursts. Unfortunately, it is hard to estimate. If the flash tube trays were solid iron, a muon would produce a detectable electron about 7% of the time. Due to the different densities and Z of glass and aluminium, the probability would be expected to decrease significantly. The knock-on probability has been estimated to be $4 \pm 2\%$. Kelly et al. (1968) have measured 4% in the flash tubes which they used. The experimental spectra have been corrected by estimating the contamination for each particle number using the theoretical spectra. The correction, C, is given by equation (7.6).

$$C(N) = \frac{R_N}{R_N - 0.04R_N + 0.04R_{N-1}} \quad (7.6)$$

where

R_N is the predicted rate for N particles,

$0.04R_N$ is the rate lost to the R_{N+1} rate due to knock-ons,

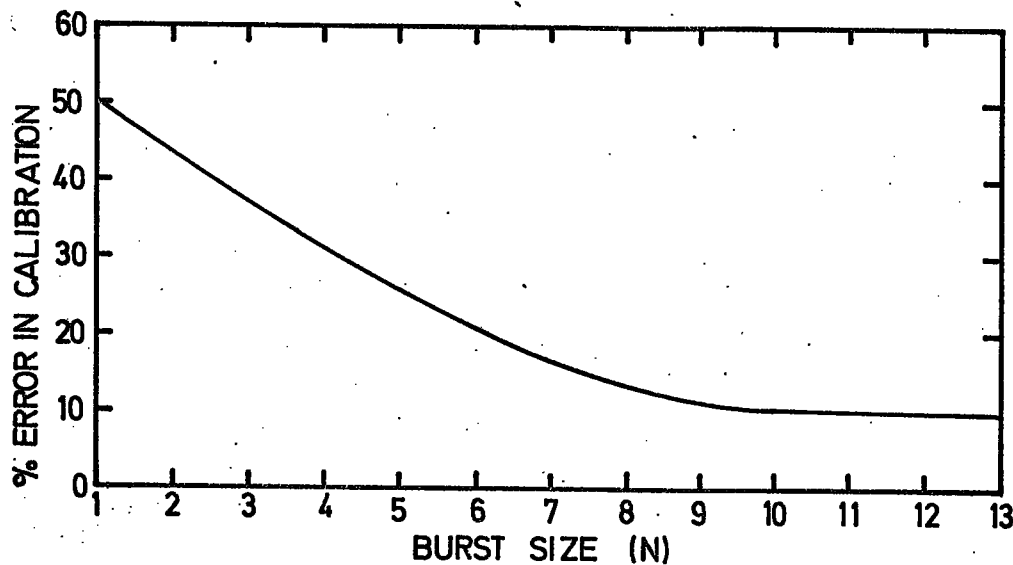


FIGURE 7.1. *The error in the determination of the mean burst size.*

$0.04R_{N-1}$ is the rate gained from the R_{N-1} rate due to knock-ons.

Calculations have shown that this correction has little effect (< 5%) everywhere except for bursts of 1 particle. The estimated errors are about 50% at 1 particle, about 3% at 2 particles, and < 0.5% at 50 particles. The knock-on correction is presented in column 6 in Tables 7.2 and 7.3 and in column 7 in Tables 7.4 and 7.5.

7.3.3 THE INTERACTION RUN DISCRIMINATOR CORRECTION

The interaction run data was collected by triggering the spectrograph on large pulse heights in the scintillation counters at level 1 or at level 3. This was accomplished by using discriminators in coincidence with the main trigger of the spectrograph (see Section 3.4). Due to fluctuations in the pulse height many small bursts have been detected as well as some larger bursts having been lost. Since flash tubes and scintillation counters have been used in conjunction with one another, there has been enough information available to calculate a correction. In Section 4.3.5 the single particle pulse height distributions have been obtained by selecting only pulse heights which were associated with a clear single track in the flash tube tray. It is reasonable to assume that the pulse height distribution for two particles passing through a scintillator is the same as would be obtained by folding two single particle distributions together. Likewise, the Nth particle distribution is equivalent to folding a single particle distribution into itself $N - 1$ times. If P_j^N is the N-particle pulse height distribution, where j is the MPHA cell, and if $\sum_{j=1}^{1000} P_j^1 = 1$, then

the Nth particle distribution is given by the following recursive function.

$$\begin{aligned} p_k^2 &= \sum_{i=1}^{k-1} p_i^1 \cdot p_{k-i}^1 \\ p_k^3 &= \sum_{i=1}^{k-1} p_i^2 \cdot p_{k-i}^1 \\ &\vdots \quad \vdots \quad \vdots \quad \vdots \\ p_k^N &= \sum_{i=1}^{k-1} p_i^{N-1} \cdot p_{k-i}^1 \end{aligned} \tag{7.7}$$

for $k < i$, $p_k^N = 0$.

Figure 7.2 presents the result of folding the single particle distribution (burst size $N = 0$) at level 1 into itself nine times. The discriminator settings used to gather the interaction run data correspond approximately to cell 120 at level 1 (shown in Figure 7.2) and cell 128 at level 3.

The probabilities of obtaining N particles, $B(N)$, are calculated by summing the portion of the distribution above the discriminator cut.

$$B(N) = \sum_{i=\text{cut}}^{1000} p_i^N \tag{7.8}$$

Figure 7.3 gives the acceptance function for both levels 1 and 3 as calculated by this procedure. The estimated errors in this correction are presented in Figure 7.4. The interaction run discriminator correction is presented in column 6 in Tables 7.4 and 7.5.

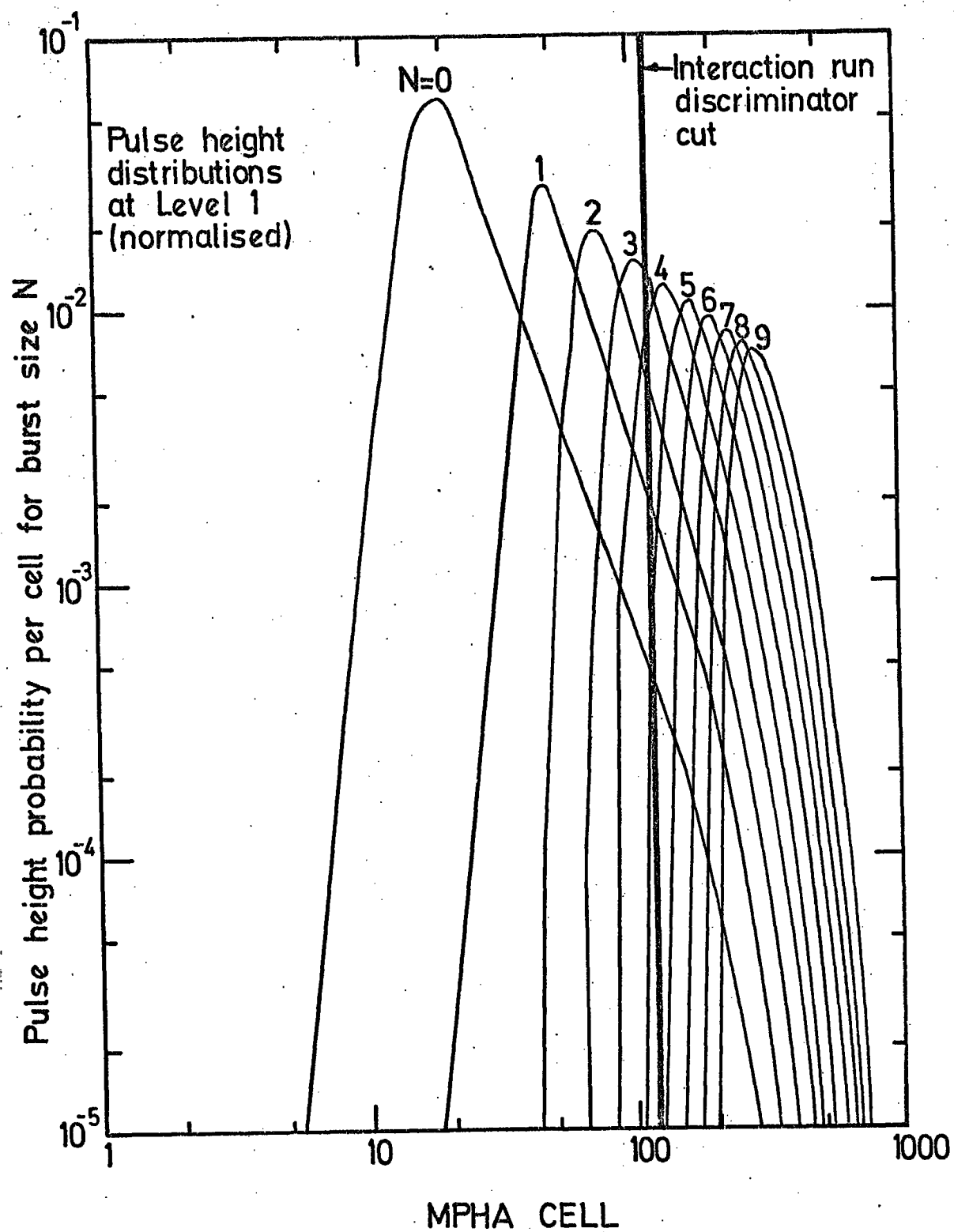


FIGURE 7.2. The calculated pulse height distributions for a burst of N particles ($N = 0$ corresponds to the muon). All areas are normalized to one. The solid line is the interaction run discrimination cut.

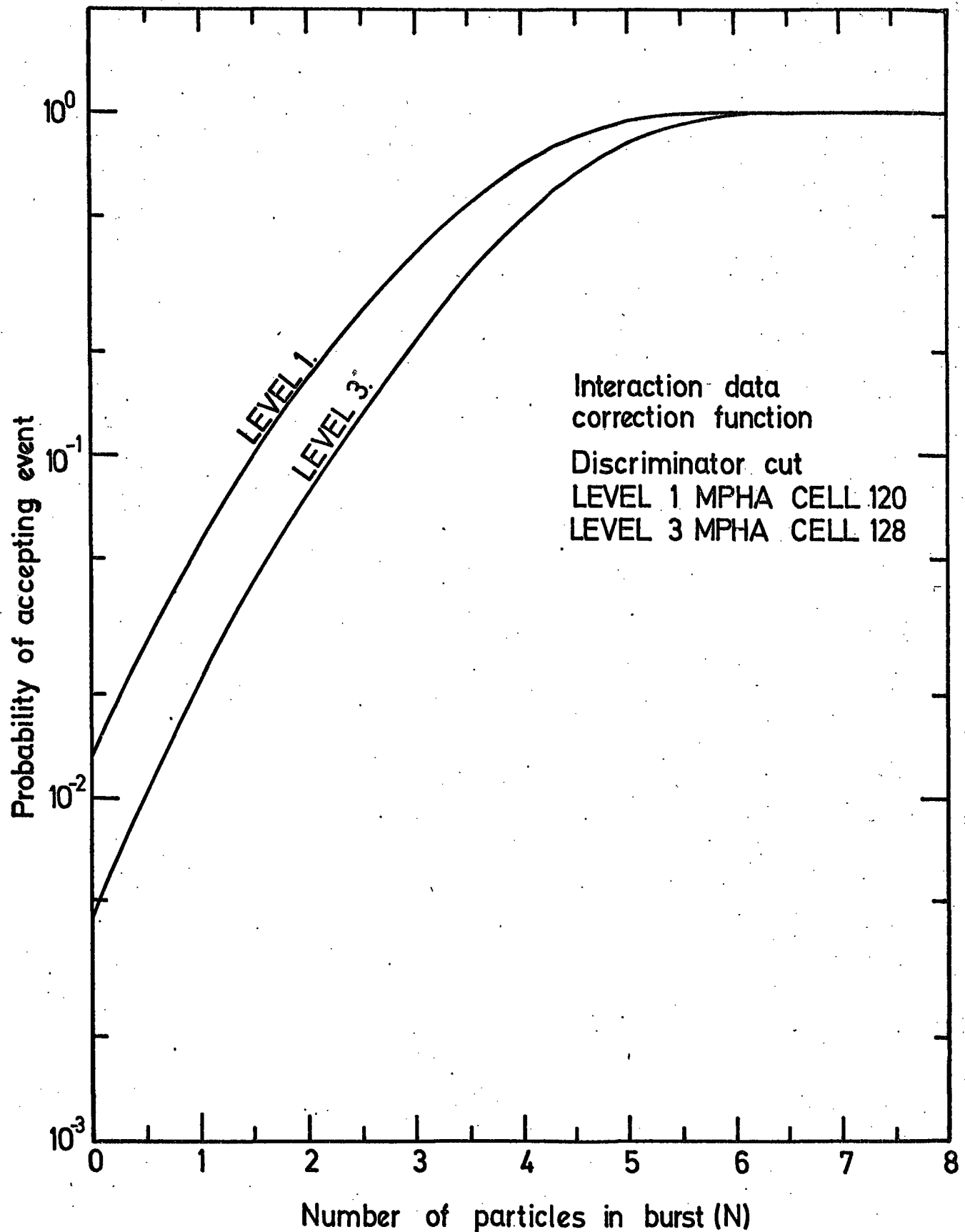


FIGURE 7.3. The interaction run acceptance function.

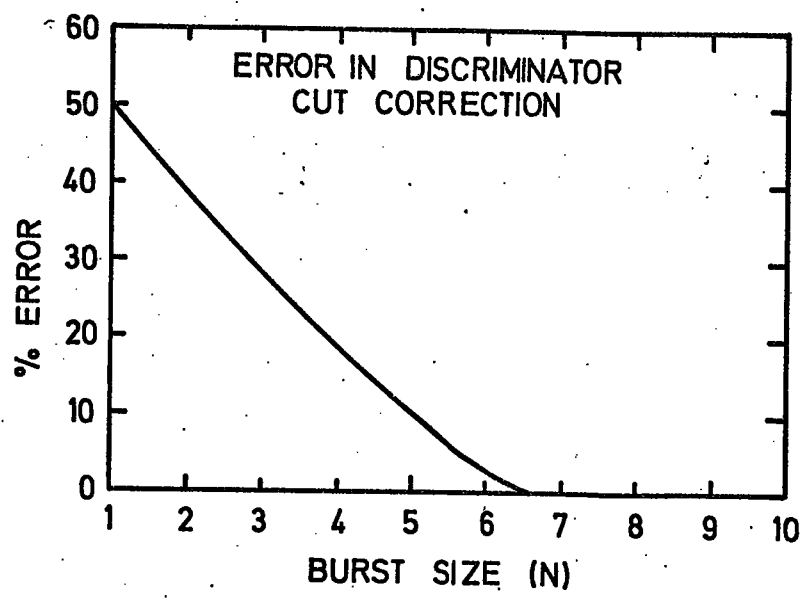


FIGURE 7.4. The estimated error in the interaction run discriminator correction as a function of burst size.

7.4 THE CORRECTED EXPERIMENTAL BURST SPECTRA

The corrected burst spectra at the bottom of the magnet blocks of MARS are given by the following equation.

$$R(N)dN = \frac{R'(N)C(N)}{aB(N)} dN \quad (7.9)$$

where

$R(N)dN$ is the corrected burst spectrum,

$R'(N)dN$ is the uncorrected burst spectrum (see Section 7.2),

$C(N)$ is the knock-on correction,

a is the slope of the burst size calibration curve (see Sections 4.3.5 and 7.3.1),

$B(N)$ is the interaction run discriminator cut correction.

($B(N) = 1$ for the all events data.)

Six burst spectra have been calculated at each experimental level:

1.	$7 \text{ GeV} < E_\mu < 14 \text{ GeV}$	$\bar{E}_\mu \approx 11 \text{ GeV}$
2.	$14 \text{ GeV} < E_\mu < 54 \text{ GeV}$	$\bar{E}_\mu \approx 34 \text{ GeV}$
3.	$54 \text{ GeV} < E_\mu < 204 \text{ GeV}$	$\bar{E}_\mu \approx 86 \text{ GeV}$
4.	$204 \text{ GeV} < E_\mu < 604 \text{ GeV}$	$\bar{E}_\mu \approx 300 \text{ GeV}$
5.	$E_\mu > 604 \text{ GeV}$	$\bar{E}_\mu \approx 1000 \text{ GeV}$
6.	$E_\mu > 7 \text{ GeV}$ (the total Spectrum)	$\bar{E}_\mu \approx 24 \text{ GeV}$.

The uncorrected and corrected burst spectra are presented in Tables 7.2 and 7.3 (the all events data) and Tables 7.4 and 7.5 (the interaction run data). The errors presented in these tables are statistical only.

LEVEL: 1			ENERGY RANGE: > 7 GeV		TYPE: All Events Data		
Flash Tube Burst Size	Cell Width	Corrected Burst Size	Number of Events	Rate in M.A.R.S. (Uncorrected) Events Sec ⁻¹ Particle ⁻¹	4% Knock-On Correction	Cell Width Correction	Rate in M.A.R.S. (Corrected) Events Sec ⁻¹ Particle ⁻¹
1.0	1	0.62	205	$1.68 \pm 0.12 \times 10^{-2}$	0.495	0.923	$7.68 \pm 0.55 \times 10^{-3}$
2.0	1	1.71	45	$3.70 \pm 0.55 \times 10^{-3}$	0.732	0.923	2.50 ± 0.37
3.0	1	2.79	14	1.15 ± 0.31	0.967	0.923	1.03 ± 0.28
4.0	1	3.87	5	$4.12 \pm 1.84 \times 10^{-4}$	0.970	0.923	$3.69 \pm 1.65 \times 10^{-4}$
7.0	5	7.12	3	$8.23 \pm 4.12 \times 10^{-5}$	0.977	0.923	$7.42 \pm 3.72 \times 10^{-5}$
MUONS			3625				
TOTAL			3899				
LEVEL: 1			ENERGY RANGE: 7-14 GeV		TYPE: All Events Data		
1.0	1	0.62	59	$4.85 \pm 0.63 \times 10^{-3}$	0.436	0.923	$1.95 \pm 0.25 \times 10^{-3}$
2.0	1	1.71	7	$5.76 \pm 2.17 \times 10^{-4}$	0.702	0.923	$3.73 \pm 1.41 \times 10^{-4}$
4.5	4	4.41	2	$4.10 \pm 2.90 \times 10^{-5}$	0.962	0.923	$3.64 \pm 2.58 \times 10^{-5}$
MUONS			1342				
TOTAL			1410				
LEVEL: 1			ENERGY RANGE: 14-54 GeV		TYPE: All Events Data		
1.0	1	0.62	129	$1.06 \pm 0.09 \times 10^{-2}$	0.516	0.923	$5.05 \pm 0.43 \times 10^{-3}$
2.0	1	1.71	31	$2.55 \pm 0.46 \times 10^{-3}$	0.742	0.923	1.75 ± 0.32
3.0	1	2.79	10	$8.23 \pm 2.60 \times 10^{-4}$	0.968	0.923	$7.35 \pm 2.32 \times 10^{-4}$
4.0	1	3.87	3	2.46 ± 1.42	0.970	0.923	2.20 ± 1.27
6.5	4	6.58	3	$6.17 \pm 3.56 \times 10^{-5}$	0.976	0.923	$5.56 \pm 3.21 \times 10^{-5}$
MUONS			2044				
TOTAL			2220				
LEVEL: 1			ENERGY RANGE: 54-204 GeV		TYPE: All Events Data		
Flash Tube Burst Size	Cell Width	Corrected Burst Size	Number of Events	Rate in M.A.R.S. (Uncorrected) Events Sec ⁻¹ Particle ⁻¹	4% Knock-On Correction	Cell Width Correction	Rate in M.A.R.S. (Corrected) Events Sec ⁻¹ Particle ⁻¹
1.0	1	0.62	17	$1.40 \pm 0.34 \times 10^{-3}$	0.592	0.923	$7.65 \pm 1.86 \times 10^{-4}$
2.0	1	1.71	6	$4.94 \pm 2.02 \times 10^{-4}$	0.780	0.923	3.56 ± 1.45
3.5	2	3.33	5	2.05 ± 0.92	0.973	0.923	1.84 ± 0.83
MUONS			220				
TOTAL			248				
LEVEL: 1			ENERGY RANGE 204-604 GeV		TYPE: All Events Data		
5.5	8	5.50	2	$2.06 \pm 1.46 \times 10^{-5}$	0.982	0.923	$1.87 \pm 1.32 \times 10^{-5}$
MUONS			15				
TOTAL			17				
LEVEL: 1			ENERGY RANGE: > 604 GeV		TYPE: All Events Data		
TOTAL			4				

TABLE 7.2

LEVEL: 3			ENERGY RANGE: > 7 GeV		TYPE: All Events Data		
Flash Tube Burst Size	Cell Width	Corrected Burst Size	Number of Events	Rate in M.A.R.S. (Uncorrected) Events Sec ⁻¹ Particle ⁻¹	4% Knock-On Correction	Cell Width Correction	Rate in M.A.R.S. (Corrected) Events Sec ⁻¹ Particle ⁻¹
1.0	1	1.36	197	$1.69 \pm 0.12 \times 10^{-2}$	0.474	0.627	$3.02 \pm 0.36 \times 10^{-3}$
2.0	1	2.95	20	$1.71 \pm 0.38 \times 10^{-3}$	0.969	0.627	1.04 ± 0.23
3.0	1	4.55	7	$6.01 \pm 2.27 \times 10^{-4}$	0.971	0.627	$3.66 \pm 1.38 \times 10^{-4}$
5.0	3	7.73	6	1.72 ± 0.70	0.979	0.627	1.06 ± 0.43
MUONS			3511				
TOTAL			3741				
LEVEL: 3			ENERGY RANGE: 7-14 GeV		TYPE: All Events Data		
1.0	1	1.36	80	$6.89 \pm 0.77 \times 10^{-3}$	0.439	0.627	$1.90 \pm 0.21 \times 10^{-3}$
2.0	1	2.95	10	$8.58 \pm 2.71 \times 10^{-4}$	0.965	0.627	$5.19 \pm 1.64 \times 10^{-4}$
4.5	4	6.94	3	$6.43 \pm 3.70 \times 10^{-5}$	0.971	0.627	$3.92 \pm 2.25 \times 10^{-5}$
MUONS			1308				
TOTAL			1401				
LEVEL: 3			ENERGY RANGE: 14-54 GeV		TYPE: All Events Data		
1.0	1	1.36	106	$9.10 \pm 0.88 \times 10^{-3}$	0.485	0.627	$2.77 \pm 0.27 \times 10^{-3}$
2.0	1	2.95	8	$6.86 \pm 2.42 \times 10^{-4}$	0.969	0.627	$4.17 \pm 1.47 \times 10^{-4}$
3.0	1	4.55	5	4.29 ± 1.92	0.972	0.627	2.62 ± 1.17
5.0	3	7.73	5	$8.58 \pm 3.83 \times 10^{-5}$	0.980	0.627	$5.27 \pm 2.35 \times 10^{-5}$
MUONS			1953				
TOTAL			2077				
LEVEL: 3			ENERGY RANGE: 54-204 GeV		TYPE: All Events Data		
Flash Tube Burst Size	Cell Width	Corrected Burst Size	Number of Events	Rate in M.A.R.S. (Uncorrected) Events Sec ⁻¹ Particle ⁻¹	4% Knock-On Correction	Cell Width Correction	Rate in M.A.R.S. (Corrected) Events Sec ⁻¹ Particle ⁻¹
1.0	1	1.36	11	$9.44 \pm 2.85 \times 10^{-4}$	0.653	0.627	$3.86 \pm 1.17 \times 10^{-4}$
2.0	1	2.95	2	1.71 ± 1.21	0.976	0.627	1.05 ± 0.74
MUONS			230				
TOTAL			243				
LEVEL: 3			ENERGY RANGE: 204-604 GeV		TYPE: All Events Data		
TOTAL			16.				
LEVEL: 3			ENERGY RANGE: > 604 GeV		TYPE: All Events Data		
TOTAL			4				

TABLE 7.3

LEVEL: 1 ENERGY RANGE: > 7 GeV TYPE: Interaction Run Data

Flash Tube Burst Size	Cell Width	Corrected Burst Size	Number of Events	Rate in M.A.R.S. (Uncorrected) Events Sec ⁻¹ Particle ⁻¹	Discriminator Correction	4% Knock-On Correction	Cell Width Correction	Rate in M.A.R.S. (Corrected) Events Sec ⁻¹ Particle ⁻¹
1.0	1	0.62	1179	$8.17 \pm 0.24 \times 10^{-4}$	23.95	0.495	0.923	$8.93 \pm 0.26 \times 10^{-3}$
2.0	1	1.71	677	4.69 ± 0.18	7.54	0.732	0.923	2.39 ± 0.09
3.0	1	2.79	486	3.37 ± 0.15	3.00	0.967	0.923	$9.02 \pm 0.40 \times 10^{-4}$
4.0	1	3.87	345	2.39 ± 0.13	1.50	0.970	0.923	3.21 ± 0.17
5.0	1	4.96	212	1.49 ± 0.10	1.06	0.972	0.923	1.42 ± 0.10
6.0	1	6.04	146	1.01 ± 0.08	1.00	0.975	0.923	$9.09 \pm 0.72 \times 10^{-5}$
7.0	1	7.12	115	$7.97 \pm 0.74 \times 10^{-5}$	1.00	0.977	0.923	7.19 ± 0.67
8.0	1	8.21	108	7.48 ± 0.72	1.00	0.980	0.923	6.77 ± 0.65
9.5	2	9.83	115	3.98 ± 0.37	1.00	0.984	0.923	3.62 ± 0.34
15.5	10	16.33	116	1.15 ± 0.09	1.00	0.988	0.923	1.05 ± 0.08
25.5	10	27.16	25	$1.73 \pm 0.34 \times 10^{-6}$	1.00	0.995	0.923	$1.59 \pm 0.32 \times 10^{-6}$
40.5	20	43.41	12	$4.16 \pm 1.20 \times 10^{-7}$	1.00	0.996	0.923	$3.83 \pm 1.10 \times 10^{-7}$
60.5	20	65.08	3	1.04 ± 0.60	1.00	0.990	0.923	$9.49 \pm 5.47 \times 10^{-8}$
MUONS			6962					
TOTAL			10554					

LEVEL: 1 ENERGY RANGE: 7-14 GeV TYPE: Interaction Run Data

Flash Tube Burst Size	Cell Width	Corrected Burst Size	Number of Events	Rate in M.A.R.S. (Uncorrected) Events Sec ⁻¹ Particle ⁻¹	Discriminator Correction	4% Knock-On Correction	Cell Width Correction	Rate in M.A.R.S. (Corrected) Events Sec ⁻¹ Particle ⁻¹
1.0	1	0.62	256	$1.77 \pm 0.11 \times 10^{-4}$	23.95	0.436	0.923	$1.71 \pm 0.11 \times 10^{-3}$
2.0	1	1.71	99	$6.86 \pm 0.69 \times 10^{-5}$	7.54	0.702	0.923	$3.35 \pm 0.34 \times 10^{-4}$
3.0	1	2.79	46	3.19 ± 0.47	3.00	0.962	0.923	$8.50 \pm 1.25 \times 10^{-5}$
4.0	1	3.87	28	1.94 ± 0.37	1.50	0.962	0.923	2.58 ± 0.49
5.0	1	4.96	12	$8.31 \pm 0.24 \times 10^{-6}$	1.06	0.962	0.923	$7.82 \pm 2.26 \times 10^{-6}$
6.5	2	6.58	6	2.08 ± 0.85	1.00	0.963	0.923	1.85 ± 0.76
9.0	3	9.29	4	$9.24 \pm 4.62 \times 10^{-7}$	1.00	0.964	0.923	$8.22 \pm 4.11 \times 10^{-7}$
15.5	10	16.33	1	6.93 ± 6.93	1.00	0.970	0.923	6.20 ± 6.20
MUONS			2482					
TOTAL			2934					

TABLE 7.4

LEVEL: 1

ENERGY RANGE: 14-54 GeV

TYPE: Interaction Run Data

Flash Tube Burst Size	Cell Width	Corrected Burst Size	Number of Events	Rate in M.A.R.S. (Uncorrected) Events Sec ⁻¹ Particle ⁻¹	Discriminator Correction	4% Knock-On Correction	Cell Width Correction	Rate in M.A.R.S. (Corrected) Events Sec ⁻¹ Particle ⁻¹
1.0	1	0.62	785	$5.44 \pm 0.19 \times 10^{-4}$	23.95	0.516	0.923	$6.21 \pm 0.22 \times 10^{-3}$
2.0	1	1.71	482	3.34 ± 0.15	7.54	0.742	0.923	1.73 ± 0.08
3.0	1	2.79	335	2.32 ± 0.13	3.00	0.968	0.923	$4.22 \pm 0.35 \times 10^{-4}$
4.0	1	3.87	244	1.69 ± 0.10	1.50	0.970	0.923	2.27 ± 0.13
5.0	1	4.96	162	1.12 ± 0.09	1.06	0.972	0.923	1.07 ± 0.09
6.0	1	6.04	107	$7.41 \pm 0.72 \times 10^{-5}$	1.00	0.975	0.923	$6.67 \pm 0.65 \times 10^{-5}$
7.0	1	7.12	88	6.10 ± 0.65	1.00	0.977	0.923	5.50 ± 0.59
8.0	1	8.21	70	4.85 ± 0.58	1.00	0.979	0.923	4.38 ± 0.52
9.5	2	9.83	77	2.67 ± 0.30	1.00	0.983	0.923	2.42 ± 0.28
15.5	10	14.33	103	$7.04 \pm 0.70 \times 10^{-6}$	1.00	0.986	0.923	$6.40 \pm 0.64 \times 10^{-6}$
25.5	10	27.16	13	$9.01 \pm 2.50 \times 10^{-7}$	1.00	0.993	0.923	$8.26 \pm 2.29 \times 10^{-7}$
35.5	10	38.00	1	$6.93 \pm 6.93 \times 10^{-8}$	1.00	0.966	0.923	$6.37 \pm 6.37 \times 10^{-8}$
MUONS			3989					
TOTAL			6456					

LEVEL: 1

ENERGY RANGE: 54-204 GeV

TYPE: Interaction Run Data

Flash Tube Burst Size	Cell Width	Corrected Burst Size	Number of Events	Rate in M.A.R.S. (Uncorrected) Events Sec ⁻¹ Particle ⁻¹	Discriminator Correction	4% Knock-On Correction	Cell Width Correction	Rate in M.A.R.S. (Corrected) Events Sec ⁻¹ Particle ⁻¹
1.0	1	0.62	123	$8.52 \pm 0.77 \times 10^{-5}$	23.95	0.592	0.923	$1.11 \pm 0.10 \times 10^{-3}$
2.0	1	1.71	85	5.89 ± 0.64	7.54	0.780	0.923	$3.20 \pm 0.35 \times 10^{-4}$
3.0	1	2.79	88	6.10 ± 0.65	3.00	0.972	0.923	1.64 ± 0.17
4.0	1	3.87	63	4.36 ± 0.55	1.50	0.974	0.923	$5.88 \pm 0.74 \times 10^{-5}$
5.5	2	5.50	66	2.29 ± 0.28	1.02	0.981	0.923	2.12 ± 0.26
7.5	2	7.66	50	1.73 ± 0.25	1.00	0.983	0.923	1.57 ± 0.23
9.5	2	9.83	29	1.00 ± 0.19	1.00	0.988	0.923	$9.12 \pm 1.70 \times 10^{-6}$
15.5	10	16.33	51	$3.53 \pm 0.50 \times 10^{-6}$	1.00	0.992	0.923	3.23 ± 0.46
25.5	10	27.16	10	$6.93 \pm 2.19 \times 10^{-7}$	1.00	0.996	0.923	$6.37 \pm 2.01 \times 10^{-7}$
35.5	10	38.00	5	3.46 ± 1.55	1.00	0.997	0.923	3.18 ± 1.42
45.5	10	48.83	2	1.39 ± 0.98	1.00	0.998	0.923	1.28 ± 0.90
MUONS			453					
TOTAL			1025					

TABLE 7.4 (CONTINUED)

LEVEL: 1 ENERGY RANGE: 204-604 GeV TYPE: Interaction Run Data

Flash Tube Burst Size	Cell Width	Corrected Burst Size	Number of Events	Rate in M.A.R.S. (Uncorrected) Events Sec ⁻¹ Particle ⁻¹	Discriminator Correction	4% Knock-On Correction	Cell Width Correction	Rate in M.A.R.S. (Corrected) Events Sec ⁻¹ Particle ⁻¹
1.0	1	0.62	14	$9.70 \pm 2.59 \times 10^{-6}$	23.95	0.687	0.923	$1.47 \pm 0.39 \times 10^{-4}$
2.0	1	1.71	11	7.62 ± 2.30	7.54	0.827	0.923	$4.40 \pm 1.32 \times 10^{-5}$
3.5	2	3.33	20	6.93 ± 1.55	2.05	0.977	0.923	1.28 ± 0.29
5.5	2	5.50	8	2.77 ± 0.98	1.02	0.982	0.923	$2.56 \pm 0.91 \times 10^{-6}$
8.5	4	8.75	15	2.60 ± 0.67	1.00	0.988	0.923	2.37 ± 0.61
20.5	20	21.75	11	$3.81 \pm 1.15 \times 10^{-7}$	1.00	0.995	0.923	$3.50 \pm 1.05 \times 10^{-7}$
50.5	40	54.25	6	1.21 ± 0.46	1.00	0.998	0.923	1.12 ± 0.42
MUONS			33					
TOTAL			118					

LEVEL: 1 ENERGY RANGE: > 604 GeV TYPE: Interaction Run Data

2.0	3	1.71	7	$1.62 \pm 0.61 \times 10^{-6}$	7.54	0.873	0.923	$9.85 \pm 3.71 \times 10^{-6}$
7.0	7	7.12	6	$5.94 \pm 2.42 \times 10^{-7}$	1.00	0.987	0.923	$5.41 \pm 2.21 \times 10^{-7}$
25.5	30	27.16	3	$6.93 \pm 4.00 \times 10^{-8}$	1.00	0.997	0.923	$6.37 \pm 3.68 \times 10^{-8}$
MUONS			5					
TOTAL			21					

TABLE 7.4 (CONTINUED)

LEVEL: 3

ENERGY RANGE: > 7 GeV

TYPE: Interaction Run Data

Flash Tube Burst Size	Cell Width	Corrected Burst Size	Number of Events	Rate in M.A.R.S. (Uncorrected) Events Sec ⁻¹ Particle ⁻¹	Discriminator Correction	4% Knock-On Correction	Cell Width Correction	Rate in M.A.R.S. (Corrected) Events Sec ⁻¹ Particle ⁻¹
1.0	1	1.36	590	$4.26 \pm 0.18 \times 10^{-4}$	24.78	0.474	0.627	$3.14 \pm 0.13 \times 10^{-3}$
2.0	1	2.95	461	3.33 ± 0.16	4.19	0.969	0.627	$8.48 \pm 0.40 \times 10^{-4}$
3.0	1	4.55	344	2.48 ± 0.13	1.46	0.971	0.627	2.20 ± 0.12
4.0	1	6.14	240	1.73 ± 0.11	1.02	0.975	0.627	1.08 ± 0.07
5.0	1	7.73	147	1.06 ± 0.09	1.00	0.979	0.627	$6.51 \pm 0.55 \times 10^{-5}$
6.0	1	9.33	112	$8.09 \pm 0.76 \times 10^{-5}$	1.00	0.983	0.627	4.99 ± 0.47
7.0	1	10.92	67	4.84 ± 0.59	1.00	0.985	0.627	2.99 ± 0.36
8.0	1	12.52	45	3.25 ± 0.48	1.00	0.987	0.627	2.01 ± 0.30
9.5	2	14.91	66	2.38 ± 0.29	1.00	0.989	0.627	1.48 ± 0.18
15.5	10	24.47	77	$5.56 \pm 0.63 \times 10^{-6}$	1.00	0.994	0.627	$3.47 \pm 0.40 \times 10^{-6}$
25.5	10	40.41	10	$7.72 \pm 2.28 \times 10^{-7}$	1.00	0.997	0.627	$4.52 \pm 1.43 \times 10^{-7}$
40.5	20	64.31	8	2.89 ± 1.02	1.00	0.998	0.627	1.81 ± 0.64
MUONS			749					
TOTAL			2916					

LEVEL: 3

ENERGY RANGE: 7-14 GeV

TYPE: Interaction Run Data

Flash Tube Burst Size	Cell Width	Corrected Burst Size	Number of Events	Rate in M.A.R.S. (Uncorrected) Events Sec ⁻¹ Particle ⁻¹	Discriminator Correction	4% Knock-On Correction	Cell Width Correction	Rate in M.A.R.S. (Corrected) Events Sec ⁻¹ Particle ⁻¹
1.0	1	1.36	125	$9.03 \pm 0.81 \times 10^{-5}$	24.78	0.439	0.627	$6.16 \pm 0.55 \times 10^{-4}$
2.0	1	2.95	92	6.64 ± 0.69	4.83	0.965	0.627	1.94 ± 0.20
3.0	1	4.55	79	5.71 ± 0.64	1.46	0.967	0.627	$5.06 \pm 0.57 \times 10^{-5}$
4.0	1	6.14	43	3.11 ± 0.47	1.02	0.969	0.627	$1.93 \pm 0.29 \times 10^{-5}$
5.0	1	7.73	27	1.95 ± 0.38	1.00	0.972	0.627	1.19 ± 0.23
6.0	1	9.33	15	1.08 ± 0.28	1.00	0.975	0.627	$6.60 \pm 1.71 \times 10^{-6}$
7.0	1	10.92	12	$8.67 \pm 0.25 \times 10^{-6}$	1.00	0.977	0.627	5.31 ± 1.53
9.0	3	14.11	10	2.41 ± 0.76	1.00	0.981	0.627	1.48 ± 0.47
20.5	20	32.44	9	$3.25 \pm 1.08 \times 10^{-7}$	1.00	0.991	0.627	$2.02 \pm 0.67 \times 10^{-7}$
MUONS			201					
TOTAL			613					

TABLE 7.5 ~~cont~~

LEVEL: 3

ENERGY RANGE: 14-54 GeV

TYPE: Interaction Run Data

Flash Tube Burst Size	Cell Width	Corrected Burst Size	Number of Events	Rate in M.A.R.S. (Uncorrected) Events Sec ⁻¹ Particle ⁻¹	Discriminator Correction	4% Knock-On Correction	Cell Width Correction	Rate in M.A.R.S. (Corrected) Events Sec ⁻¹ Particle ⁻¹
1.0	1	1.36	371	$2.86 \pm 0.14 \times 10^{-4}$	24.78	0.485	0.627	$2.16 \pm 0.11 \times 10^{-3}$
2.0	1	2.95	273	1.97 ± 0.12	4.83	0.969	0.627	$5.78 \pm 0.35 \times 10^{-4}$
3.0	1	4.55	216	1.56 ± 0.11	1.46	0.972	0.627	1.39 ± 0.10
4.0	1	6.14	150	1.08 ± 0.09	1.02	0.976	0.627	$4.74 \pm 0.56 \times 10^{-5}$
5.0	1	7.73	96	$6.93 \pm 0.71 \times 10^{-5}$	1.00	0.980	0.627	4.26 ± 0.44
6.0	1	9.33	74	5.34 ± 0.62	1.00	0.983	0.627	3.29 ± 0.38
7.0	1	10.92	47	3.39 ± 0.50	1.00	0.985	0.627	2.09 ± 0.31
8.0	1	12.52	30	2.17 ± 0.40	1.00	0.986	0.627	1.34 ± 0.24
9.5	2	14.91	50	1.81 ± 0.26	1.00	0.988	0.627	1.12 ± 0.16
15.5	10	24.47	53	$3.83 \pm 0.53 \times 10^{-6}$	1.00	0.993	0.627	$2.38 \pm 0.33 \times 10^{-6}$
36.5	20	48.38	7	$2.53 \pm 0.96 \times 10^{-7}$	1.00	0.996	0.627	$1.58 \pm 0.60 \times 10^{-7}$
MUONS			444					
TOTAL			1811					

LEVEL: 3

ENERGY RANGE: 54-204 GeV

TYPE: Interaction Run Data

Flash Tube Burst Size	Cell Width	Corrected Burst Size	Number of Events	Rate in M.A.R.S. (Uncorrected) Events Sec ⁻¹ Particle ⁻¹	Discriminator Correction	4% Knock-On Correction	Cell Width Correction	Rate in M.A.R.S. (Corrected) Events Sec ⁻¹ Particle ⁻¹
1.0	1	1.36	81	$5.85 \pm 0.65 \times 10^{-5}$	24.78	0.556	0.627	$5.05 \pm 0.56 \times 10^{-4}$
2.0	1	2.95	82	5.92 ± 0.65	4.83	0.972	0.627	1.74 ± 0.19
3.0	1	4.55	44	3.18 ± 0.48	1.46	0.976	0.627	$2.84 \pm 0.43 \times 10^{-5}$
4.0	1	6.14	38	2.74 ± 0.45	1.02	0.980	0.627	1.71 ± 0.28
5.5	2	8.53	41	1.48 ± 0.23	1.00	0.985	0.627	$9.14 \pm 1.42 \times 10^{-6}$
7.5	2	11.72	15	$5.42 \pm 1.40 \times 10^{-6}$	1.00	0.989	0.627	3.36 ± 0.87
9.5	2	14.91	11	3.97 ± 1.20	1.00	0.991	0.627	2.47 ± 0.75
15.5	10	24.47	12	$8.67 \pm 2.50 \times 10^{-7}$	1.00	0.996	0.627	$5.41 \pm 1.56 \times 10^{-7}$
25.5	10	40.41	5	3.61 ± 1.61	1.00	0.997	0.627	2.26 ± 1.01
40.5	20	64.31	4	1.44 ± 0.72	1.00	0.998	0.627	$9.01 \pm 4.51 \times 10^{-8}$
MUONS			93					
TOTAL			426					

TABLE 7.5 (CONTINUED)

LEVEL: 3			ENERGY RANGE: 204-604 GeV			TYPE: Interaction Run Data			
Flash Tube Burst Size	Cell Width	Corrected Burst Size	Number of Events	Rate in M.A.R.S. (Uncorrected) Events Sec ⁻¹ Particle ⁻¹	Discriminator Correction	4% Knock-On Correction	Cell Width Correction	Rate in M.A.R.S. (Corrected) Events Sec ⁻¹ Particle ⁻¹	
1.0	1	1.36	10	$7.22 \pm 2.28 \times 10^{-6}$	24.78	0.653	0.627	$7.32 \pm 2.31 \times 10^{-5}$	
2.0	1	2.95	13	9.39 ± 2.60	4.83	0.976	0.627	2.78 ± 0.77	
3.5	2	5.34	10	3.61 ± 1.14	1.13	0.981	0.627	$2.51 \pm 0.79 \times 10^{-6}$	
5.5	2	8.53	5	1.81 ± 0.81	1.00	0.987	0.627	1.12 ± 0.50	
8.5	4	13.31	3	$5.42 \pm 3.13 \times 10^{-7}$	1.00	0.991	0.627	$3.37 \pm 1.95 \times 10^{-7}$	
25.5	30	40.41	5	1.20 ± 0.54	1.00	0.998	0.627	$7.51 \pm 3.37 \times 10^{-8}$	
MUONS			9						
TOTAL			55						
LEVEL: 3			ENERGY RANGE: > 604 GeV			TYPE: Interaction Run Data			
1.0	1	1.36	3	$2.16 \pm 1.25 \times 10^{-6}$	24.78	0.751	0.627	$2.52 \pm 1.46 \times 10^{-5}$	
4.0	4	6.14	9	$8.66 \pm 3.54 \times 10^{-7}$	1.02	0.986	0.627	$5.46 \pm 2.23 \times 10^{-7}$	
MUONS			2						
TOTAL			11						

TABLE 7.5 (CONTINUED)

7.5 THE COMPARISONS OF THE RESULTANT BURST SPECTRA

The experimental burst spectra are presented in Figures 7.5 to 7.10 with the theoretical spectra incorporating Furry fluctuations. The experimental points have been obtained by combining the interaction run data and the all events data by weighting each point by the errors on that point, where the error was a combination of statistical and systematic errors. Neither the experimental points nor the theoretical curves have been normalized. It can be seen that the theoretical and experimental spectra agree over all the energy ranges selected.

In order to compare the experimental results with the various interaction processes ~~one~~ of the experimental points have been divided by the theoretically expected result in various energy ranges and energy transfers where different interaction processes should dominate. The total spectrum ($E_\mu > 7$ GeV) has been used to illustrate the comparison for the knock-on and bremsstrahlung processes. The spectra for muon energies > 204 GeV have been used to illustrate the comparison for the direct pair production process. These results are presented in Figures 7.11 and 7.12. The errors presented incorporate not only the statistical and systematic error on the experimental points but also the estimated error in the theoretical burst spectra ($\sim 33\%$). The dividing line between the processes has been obtained from Figure 6.4 and the result of Section 6.2.3. The approximate mean energy transfers have been taken from calculations performed in Section 6.3.1, i.e. there is on average about 1 GeV energy transferred per observed particle. As can be seen, within the errors of this experiment the experimental results agree with the theoretically predicted ones.

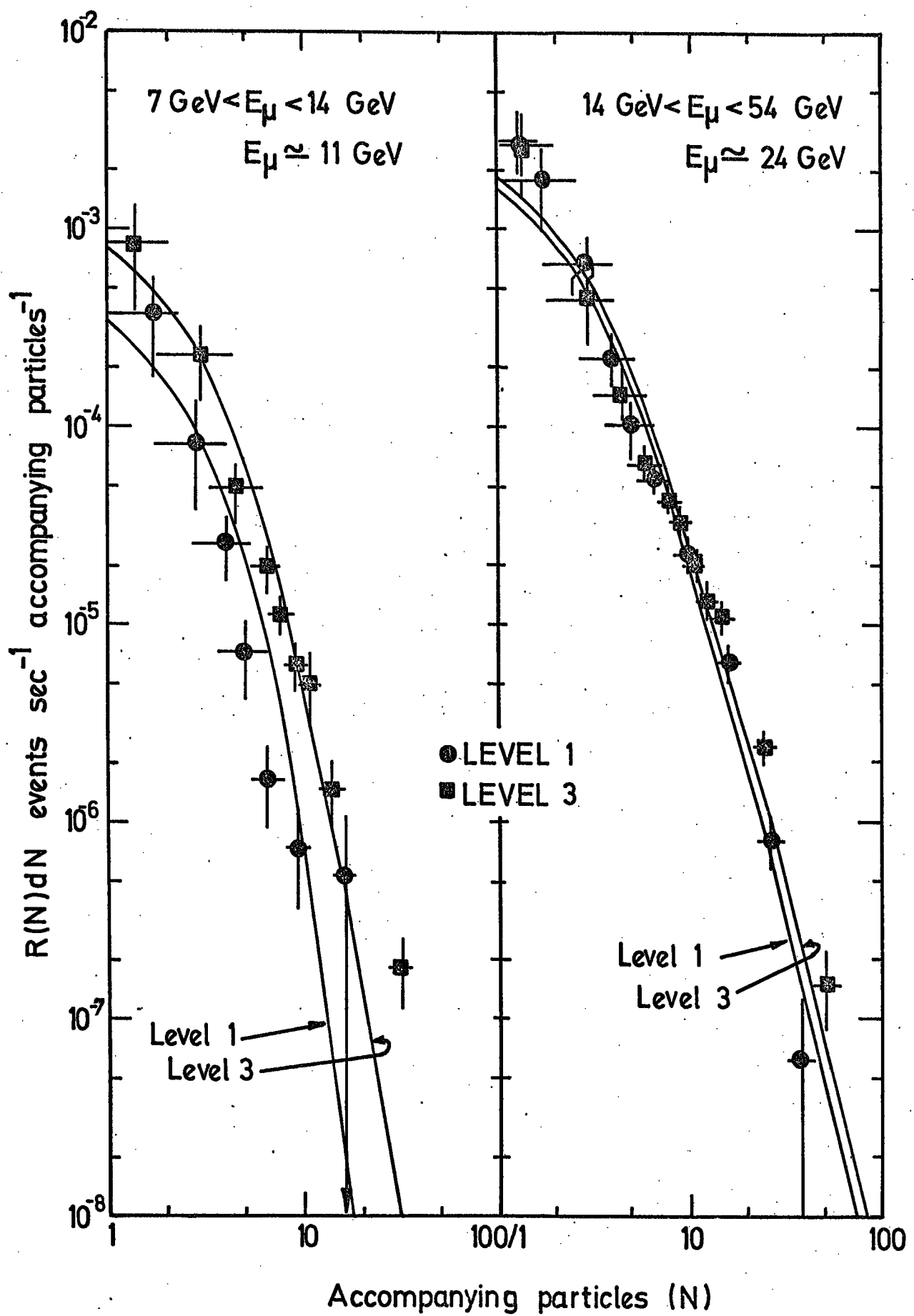


FIGURE 7.5.

FIGURE 7.6

The resultant experimental and theoretical burst spectra as observed at the measuring levels in the MARS spectrograph.

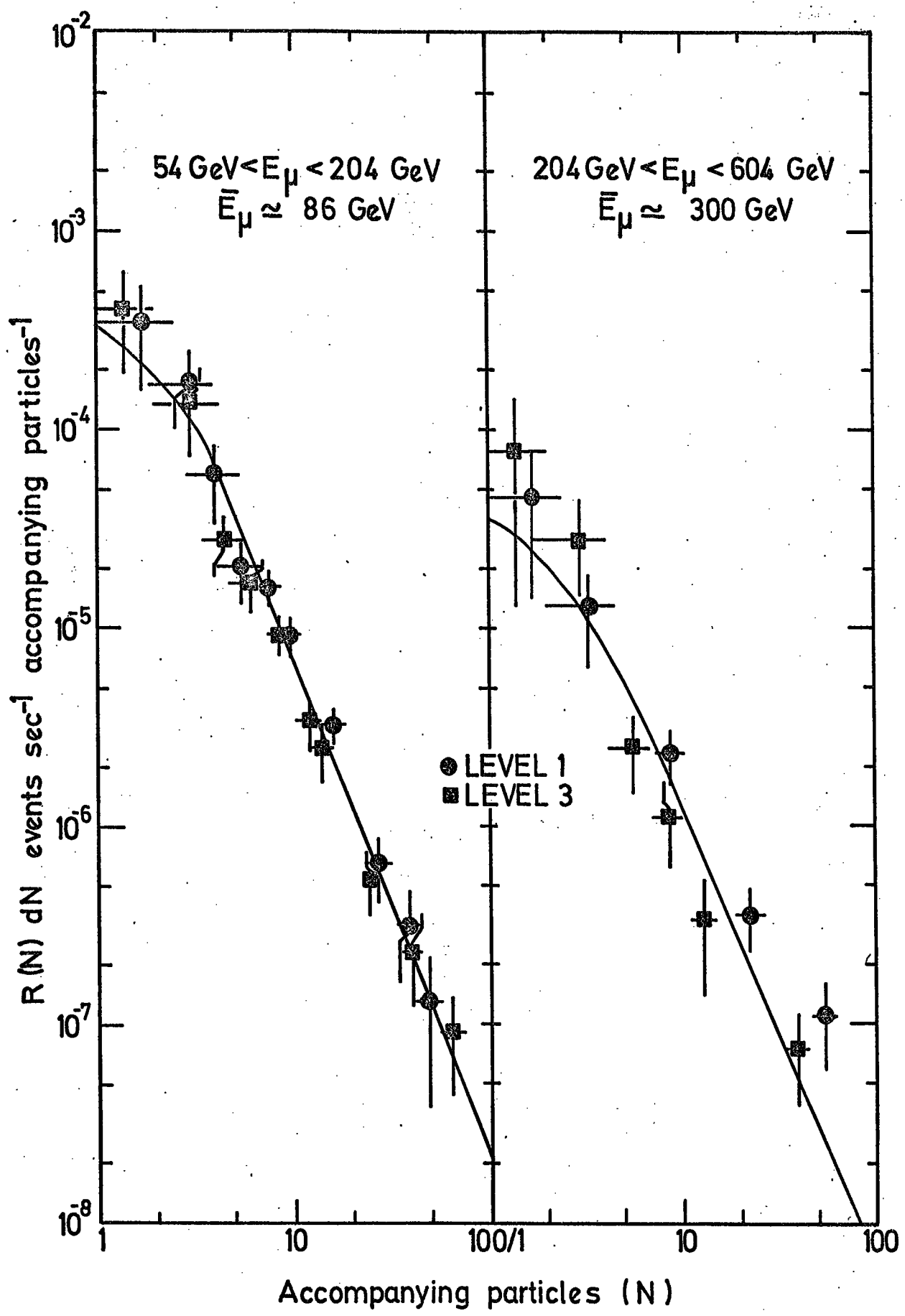


FIGURE 7.7

FIGURE 7.8.

The resultant experimental and theoretical burst spectra as observed at the measuring levels in the MARS spectrograph.

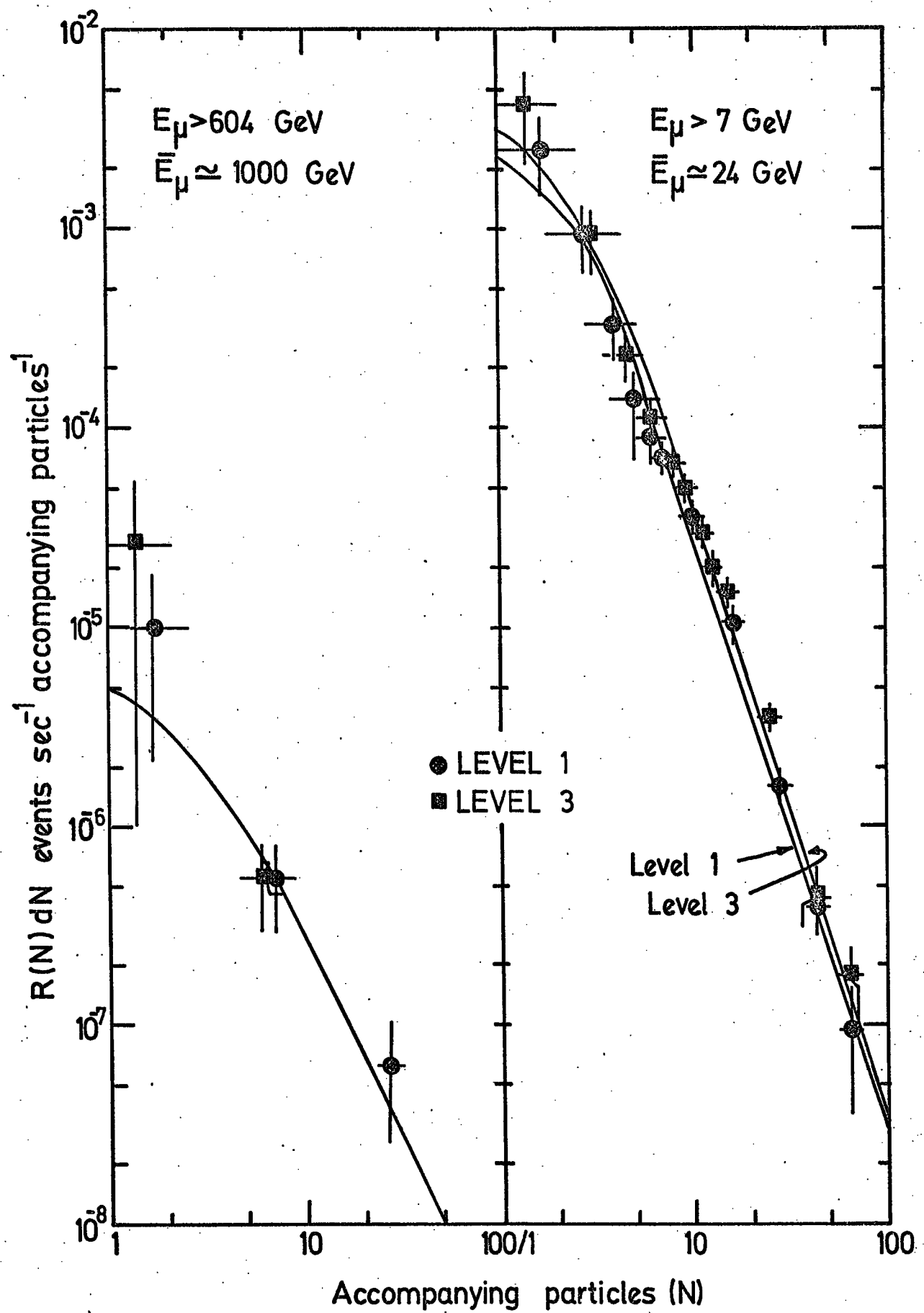


FIGURE 7.9

FIGURE 7.10

The resultant experimental and theoretical burst spectra as observed at the measuring levels in the MARS spectrograph.

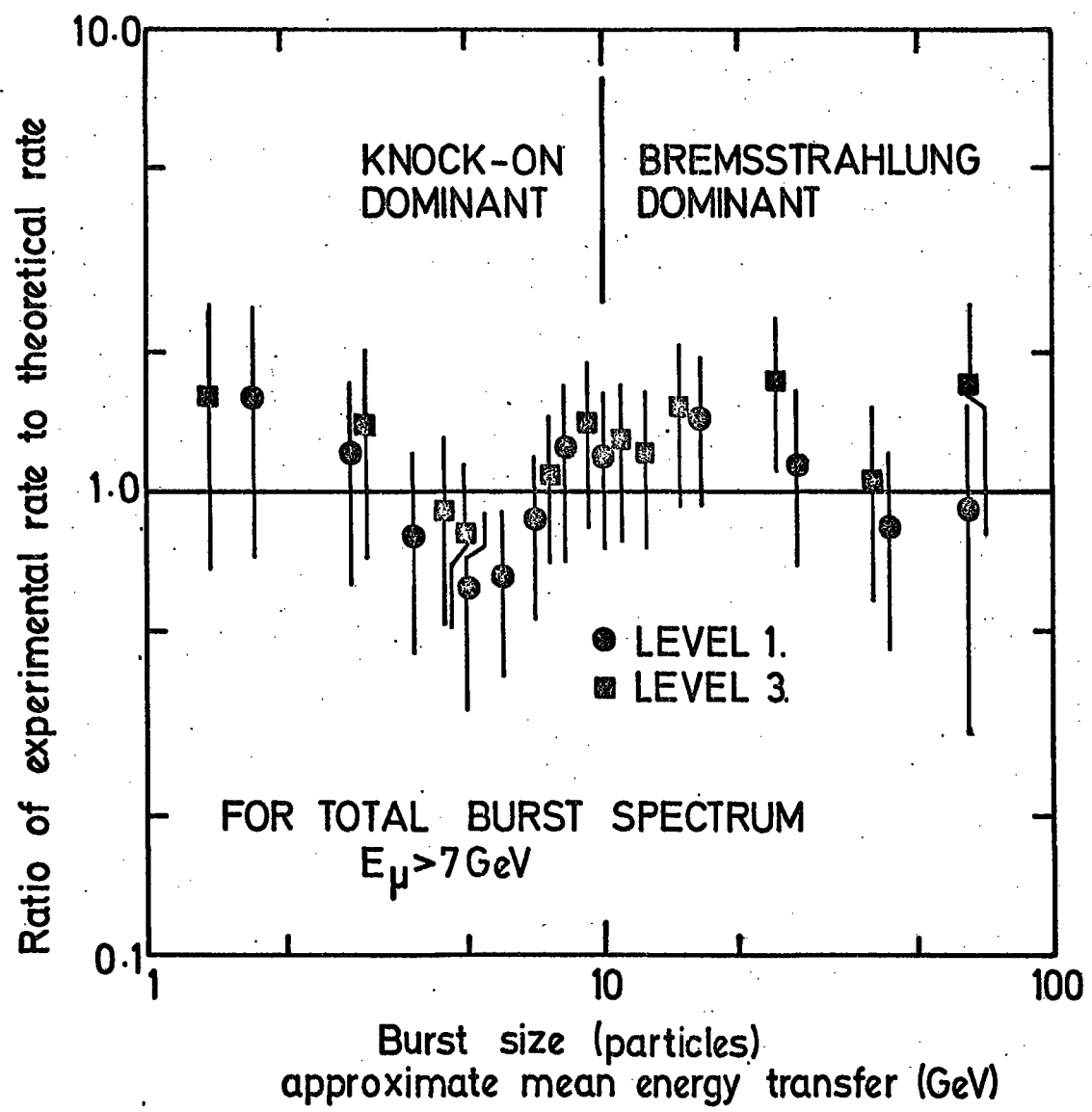


FIGURE 7.11. A comparison between the experimental and theoretical results for muons of energy $> 7 \text{ GeV}$ where the knock-on process and bremsstrahlung processes are dominant. The errors include statistical errors, systematic errors, and errors in the theory.

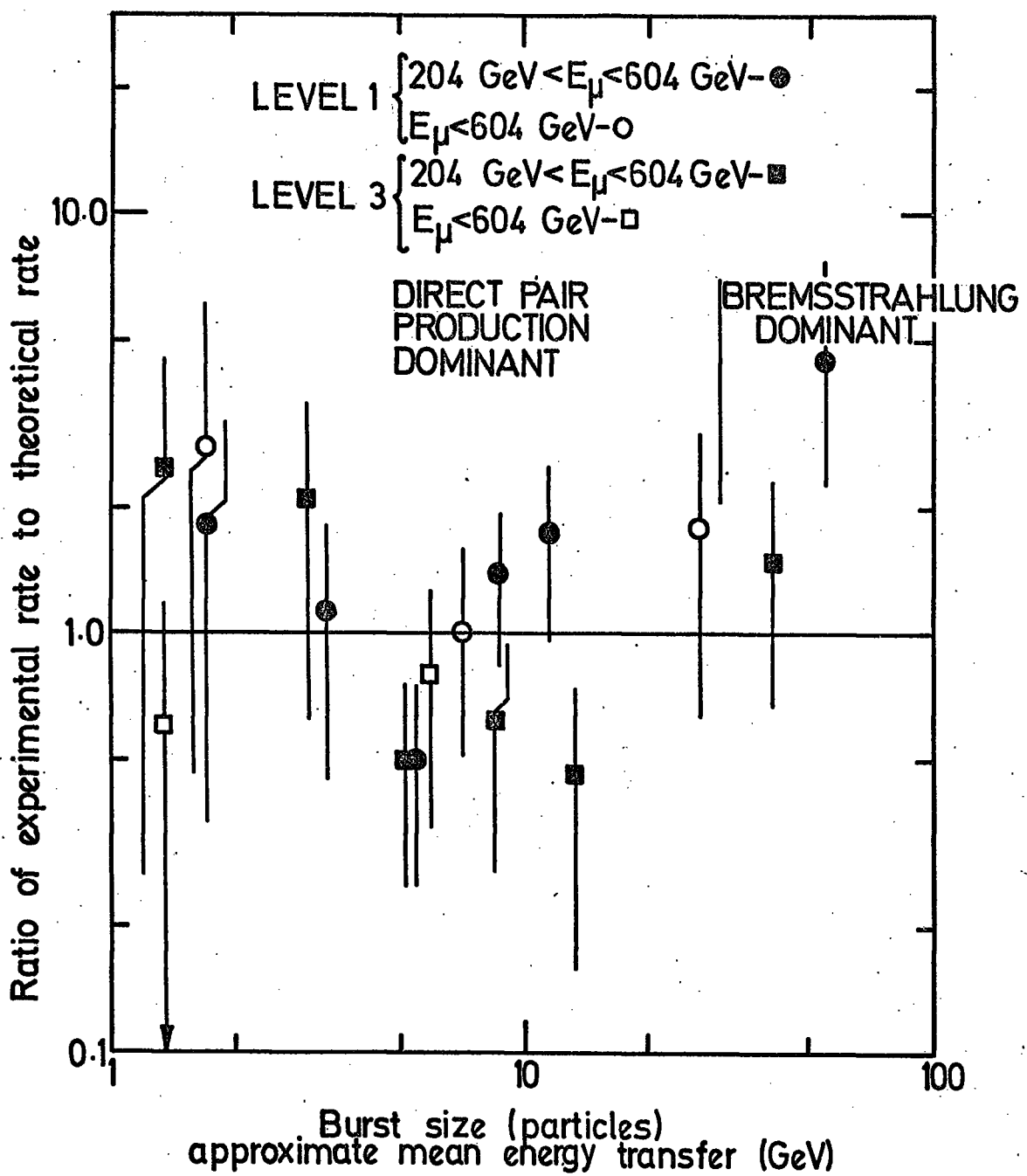


FIGURE 7.12. A comparison between the experimental and theoretical results for muons of energy $> 204 \text{ GeV}$ where the direct pair production and bremsstrahlung processes are dominant. The errors include statistical errors, systematic errors, and errors in the theory.

A brief comparison has been made with previous experiments (see Section 1.3.3 and Figures 1.2, 1.3 and 1.4). The following observations have been made.

1. Some experiments studying the knock-on process have found disagreement with the theory of Bhabha in the region of 1 to 20 GeV energy transfers, particularly those results of Neddermeyer et al. (1961) and Kearney et al. (1965,1972). The results of this experiment which predominantly studies that region of energy transfer disagree with their results and find no significant deviations from the Bhabha theory.

2. While studying the bremsstrahlung process some experimenters have found disagreement with the theory at energy transfers of 100 to 10000 GeV. However, in the region tested by this experiment (energy transfers of 10-60 GeV), all the previous experiments have found no deviation from theory. This experiment supports that conclusion. It can be noted, however, that the 55 GeV point is not inconsistent with an increase in the cross-section as found by Nagano et al. (1970), Matano et al. (1968) and Alexander et al. (1968).

3. Some previous experiments studying the direct pair production process have found the theoretical predictions to be high. In the energy transfer region studied in this experiment, which really covers all previous experiments due to the integral nature of the observations, there is no support for a deviation from the theory as calculated, although the errors presented by this experiment are large.

7.6 CONCLUSIONS FROM THE BURST SPECTRUM STUDY

Based on the results obtained from this analysis, it is concluded that, within the experimental errors of the experiment, the muon cross-sections are as predicted and that the muon behaves as expected using quantum electrodynamics.

An implication is that the cross-sections discussed and calculated in Chapter 2 have not been found to be in disagreement with the experimental results. It is believed that the calculated results given in Appendix A are useable in future experiments studying muons in iron. For example, they should be useful to calculate any burst correction required in the high momentum sea-level spectrum experiment. It is also believed that the energy loss by muons in iron calculated in Section 6.2.2 can be used with confidence.

CHAPTER 8

CONCLUSIONS

The objectives of this experiment have been:

1. to study the interaction probabilities of positive and negative muons to determine the magnitude of an interaction asymmetry, should it be found to exist,

and

2. to produce a set of experimental and theoretical burst spectra in iron over a range of muon energies and to compare them with one another in an attempt to find possible disagreement with the cross-sections as predicted by quantum electrodynamics.

For the production of the theoretical burst spectra, the various theoretical interaction cross-sections have been studied (Chapter 2) and the ones considered to be the best have been calculated and are in tabular form in Appendix A. Based on these cross-sections the energy loss in iron has been calculated (Section 6.2.2). With the use of the Ivanenko-Samusudov shower development curves, a series of theoretical burst spectra have been calculated and are presented in Tables 6.2, 6.3, 6.5 and 6.6.

In the experimental study, the MARS spectrograph which is capable of measuring energies in excess of 5 TeV, has been used to collect a total of 22727 events. The majority of these events contain a burst at one of the experimental levels. These events have been analyzed to see if they support an interaction charge asymmetry using three different methods (Chapter 5). All three methods produce no evidence of a charge asymmetry. The overall charge asymmetry

of the cross-section of positive muons to that of negative muons is 1.020 ± 0.032 , with no disagreement with unity over a large range of energy transfers ($\sim 1\text{-}20$ GeV). The interaction asymmetries seen by Neddermeyer et al. (1961, 1965, 1967), Sheldon et al. (1973), and Ayre et al. (1970) are believed to be systematic. The asymmetry if Allkofer et al. (1971) is very probably statistical in the light of the most recent Allkofer result (Allkofer 1974).

A series of experimental burst spectra over several muon energy ranges have been determined (Chapter 7) and compared with the theoretical spectra. There is agreement over all energy ranges and over all regions where particular cross-sections are dominant. In particular, these results disagree with the results of Neddermeyer et al. (1961) and Kearney et al. (1973) who found disagreement with the knock-on cross-section for energy transfers of 1-20 GeV.

It has been concluded from this study that the electromagnetic cross-sections, as they are now known, are in agreement with the experimental results obtained here. Based on this conclusion the theoretical results (i.e. numerical cross-sections, energy loss and numerical burst spectra) can be used with confidence.

Quantum electrodynamics does not predict an interaction asymmetry, and it is the basis for all the electromagnetic cross-sections used in the theoretical calculations. All of the results obtained in this experiment agree with QED predictions. The muon, therefore, appears to behave as predicted by QED considering it as a 'heavy electron'.

APPENDIX A

TABLES OF THE INTERACTION PROBABILITIES OF MUONS IN IRON

This appendix contains seventeen tables of the differential cross-section for muons in iron ($Z = 26$) calculated using the formulae and other criteria specified in Chapter 2. The cross-sections are of the form $\sigma(E_\mu, E_t) dE_t$, where σ is the cross-section, E_μ is the muon energy, and E_t is the energy transferred in the interaction. The tables extend over the energy range $1 \text{ GeV} \leq E_\mu \leq 10 \text{ TeV}$. Each table contains energy transfers $E_{\text{MIN}} \leq E_t \leq E_{\text{MAX}}$, where E_{MIN} and E_{MAX} are defined as follows.

(a) For the knock-on process:

$$E_{\text{MIN}} = 10 \text{ MeV}$$

$$E_{\text{MAX}} = \text{the maximum transferable energy (see Equation 2.6)}$$

(b) For the bremsstrahlung process:

$$E_{\text{MIN}} = 10 \text{ MeV}$$

$$E_{\text{MAX}} = E_\mu - 0.3870 \text{ GeV. (see Equation 2.14)}$$

(c) For the direct pair production process:

$$E_{\text{MIN}} = 10 \text{ MeV}$$

$$E_{\text{MAX}} = E_\mu - 0.038 \text{ GeV (see Equation 2.27)}$$

(d) For the photonuclear process:

$$E_{\text{MIN}} = \sim 100 \text{ MeV } (\sim \text{ the pion rest mass})$$

$$E_{MAX} = E_\mu - 0.4635 \text{ GeV} \text{ (see equation 2.45)}$$

For each muon energy and energy transfer, data for the following cross-sections are given in columns 3 to 8 of the tables respectively.

1. The knock-on (KO) cross-section, σ_{KO} ,
2. The bremsstrahlung (BREM) cross-section, σ_{BREM} ,
3. The direct pair production (DPP) cross-section, σ_{DPP} ,
4. The photonuclear (PN) cross-section, σ_{PN} ,
5. The total electromagnetic cross-section, i.e. $\sigma_{KO} + \sigma_{BREM} + \sigma_{DPP}$,
6. The total cross-section, i.e. $\sigma_{KO} + \sigma_{BREM} + \sigma_{DPP} + \sigma_{PN}$.

All cross-sections are given in units of 'target particles $\text{gm}^{-1} \text{ cm}^2 \text{ Gev}^{-1}$ '.

DISCUSSION OF UNITS

In general cross-sections are stated in one of two units, either in ' cm^2 ', or in ' $\text{gm}^{-1} \text{ cm}^2$ '. These units are somewhat ambiguous since some of the dimensions are assumed to be implicitly understood, partly because strictly speaking they are not dimensions. When a quantity such as cycle, particle, number, etc. is in the units of a quantity, it is often left out of the physical notation. For example, $\lambda(\lambda)$ is stated in ' cm ' instead of ' cm cycle^{-1} ', (T) is stated in 'sec' instead of 'sec cycle $^{-1}$ ', the muon spectrum is stated in ' $\text{sec}^{-1} \text{ cm}^{-2} \text{ sr}^{-1} \text{ GeV/c}^{-1}$ ', instead of 'muons sec $^{-1} \text{ cm}^{-2} \text{ sr}^{-1} \text{ GeV/c}^{-1}$ '. For the sake of clarity and understanding the complete units have been used in this appendix.

The cross-section in ' cm^2 ', if it appeared, would read ' cm^2 particles atom $^{-1}$ ', i.e. for the knock-on process the units would read ' cm^2 electrons atom $^{-1}$ '. For this reason a cross-section in ' cm^2 ,

is given, often called the atomic cross-section (Rossi, 1952). The cross-section in ' $\text{gm}^{-1} \text{ cm}^2$ ', reads in this appendix as 'target particles $\text{gm}^{-1} \text{ cm}^2$ ' (i.e. for the knock-on process the units are 'electrons $\text{gm}^{-1} \text{ cm}^2$).

The cross-sections have all been calculated in the latter units for ease of use. For example, the probability, ϕ , of a knock-on electron emerging from a material of density, ρ , and thickness, t , is simply

$$\phi = \sigma_{\text{KO}} \rho t , \quad (\text{A.1})$$

If it is required to use the cross-section in ' cm^2 ', instead of ' $\text{gm}^{-1} \text{ cm}^2$ ', the conversion is

$$\sigma(\text{cm}^2 \text{ GeV}^{-1}) = \frac{A}{N_0} \sigma(\text{gm}^{-1} \text{ cm}^2 \text{ GeV}^{-1}) \quad (\text{A.2})$$

where

A is the atomic weight (for iron $A = 55.85$),

N_0 is Avagardo's number (6.02472×10^{23} atom mole $^{-1}$),

$A/N_0 = 9.270 \times 10^{-23}$ gm atom $^{-1}$ (for iron).

INTERACTION PROBABILITIES OF MUONS OF 1.0 GEV IN IRON

ENERGY TRANSFERRED IN GEV	FRACTIONAL ENERGY TRANSFER	BREMSSTRAHLUNG		DIRECT PAIR PRODUCTION		PHOTONICLEAR		TOTAL (EXCEPT PHOTONUCLEAR)		TOTAL	
		CROSS-SECTION IN ELECTRONS PER GM/CM**2	PER GEV	CROSS-SECTION IN NUCLEI PER GM/CM**2	IN NUCLEI PER GEV	CROSS-SECTION IN PARTICLES PER CM/CM**2	IN PARTICLES PER GEV	CROSS-SECTION IN PARTICLES PER GM/CM**2	IN PARTICLES PER GEV	PFR GM/CM**2 PER GEV	PFR GFV
1.0X10-02	1.00X10-02	6.286X10-01	0.0	2.724X10-04	9.964X10-05	0.0	0.0	6.289X10-01	1.361X10-01	1.361X10-01	6.289X10-01
2.0X10-02	2.00X10-02	1.359X10-01	1.200X10-04	7.293X10-05	4.337X10-05	0.0	0.0	5.108X10-02	5.108X10-02	5.108X10-02	5.108X10-02
3.0X10-02	3.00X10-02	5.066X10-02	5.066X10-05	5.076X10-05	2.106X10-05	0.0	0.0	2.343X10-02	2.343X10-02	2.343X10-02	2.343X10-02
4.0X10-02	4.00X10-02	2.366X10-02	2.366X10-05	3.803X10-05	1.145X10-05	0.0	0.0	1.160X10-02	1.160X10-02	1.160X10-02	1.160X10-02
5.0X10-02	5.00X10-02	1.155X10-02	1.155X10-05	2.989X10-05	6.788X10-06	0.0	0.0	5.708X10-03	5.708X10-03	5.708X10-03	5.708X10-03
6.0X10-02	6.00X10-02	5.671X10-03	5.671X10-05	2.427X10-05	4.288X10-06	0.0	0.0	2.466X10-03	2.466X10-03	2.466X10-03	2.466X10-03
7.0X10-02	7.00X10-02	2.439X10-03	2.439X10-05	2.070X10-05	2.845X10-06	0.0	0.0	5.670X10-04	5.670X10-04	5.670X10-04	5.670X10-04
8.0X10-02	8.00X10-02	5.440X10-04	5.440X10-05	1.712X10-05	1.963X10-06	0.0	0.0	1.909X10-05	1.909X10-05	1.909X10-05	1.909X10-05
9.0X10-02	9.00X10-02	0.0	0.0	1.473X10-05	1.326X10-06	2.252X10-06	2.252X10-06	1.613X10-05	1.613X10-05	1.613X10-05	1.613X10-05
1.0X10-01	1.00X10-01	0.0	0.0	5.018X10-06	1.182X10-07	9.257X10-07	5.137X10-06	6.062X10-06	6.062X10-06	6.062X10-06	6.062X10-06
2.0X10-01	2.00X10-01	0.0	0.0	2.382X10-06	2.171X10-08	5.102X10-07	2.404X10-06	2.916X10-06	2.916X10-06	2.916X10-06	2.916X10-06
3.0X10-01	3.00X10-01	0.0	0.0	1.264X10-06	0.0	3.142X10-07	1.264X10-06	1.579X10-06	1.579X10-06	1.579X10-06	1.579X10-06
4.0X10-01	4.00X10-01	0.0	0.0	6.771X10-07	0.0	2.086X10-07	6.771X10-07	8.857X10-07	8.857X10-07	8.857X10-07	8.857X10-07
5.0X10-01	5.00X10-01	0.0	0.0	3.148X10-07	0.0	1.463X10-07	3.148X10-07	4.612X10-07	4.612X10-07	4.612X10-07	4.612X10-07
6.0X10-01	6.00X10-01	0.0	0.0	0.0	0.0	1.079X10-07	0.0	1.079X10-07	1.079X10-07	1.079X10-07	1.079X10-07
7.0X10-01	7.00X10-01	0.0	0.0	0.0	0.0	0.0	0.0	0.0	0.0	0.0	0.0

TABLE A.1

INTERACTION PROBABILITIES OF MUONS OF 2.0 GEV IN IRON

ENERGY TRANSFERRED IN GEV	FRACTIONAL ENERGY TRANSFER	KNOCK-ON CROSS-SECTION		DIRECT PAIR CROSS-SECTION		PHOTONNUCLEAR CROSS-SECTION		TOTAL (EXCEPT PHOTONNUCLEAR) CROSS-SECTION IN PARTICLES PER GM/CM**2		TOTAL CROSS-SECTION IN PARTICLES PER GM/CM**2	
		IN ELECTRONS PER GM/CM**2	PER GEV	IN NUCLEI PER GM/CM**2	PER GEV	IN NUCLEI PER GM/CM**2	PER GEV	IN NUCLEI PER GM/CM**2	PER GEV	PER GM/CM**2	PER GEV
1.0X10-02	5.00X10-03	6.848X10-01	3.180X10-04	0.0	0.0	6.851X10-01	6.851X10-01	1.661X10-01	1.661X10-01	7.135X10-02	7.135X10-02
2.0X10-02	1.00X10-02	1.655X10-01	1.488X10-04	4.600X10-04	0.0	7.135X10-02	7.135X10-02	3.872X10-02	3.872X10-02	2.387X10-02	2.387X10-02
3.0X10-02	1.50X10-02	7.102X10-02	9.399X10-05	2.415X10-04	0.0	3.872X10-02	3.872X10-02	2.387X10-02	2.387X10-02	1.594X10-02	1.594X10-02
4.0X10-02	2.00X10-02	3.452X10-02	6.735X10-05	1.311X10-04	0.0	2.387X10-02	2.387X10-02	1.594X10-02	1.594X10-02	1.125X10-02	1.125X10-02
5.0X10-02	2.50X10-02	2.374X10-02	5.177X10-05	7.702X10-05	0.0	1.594X10-02	1.594X10-02	8.259X10-03	8.259X10-03	6.246X10-03	6.246X10-03
6.0X10-02	3.00X10-02	1.585X10-02	4.162X10-05	4.844X10-05	0.0	6.246X10-03	6.246X10-03	4.832X10-03	4.832X10-03	4.836X10-03	4.836X10-03
7.0X10-02	3.50X10-02	1.118X10-02	3.453X10-05	3.219X10-05	0.0	4.832X10-03	4.832X10-03	6.444X10-04	6.444X10-04	6.460X10-04	6.460X10-04
8.0X10-02	4.00X10-02	8.207X10-03	2.931X10-05	2.235X10-05	0.0	6.444X10-04	6.444X10-04	3.760X10-05	3.760X10-05	3.952X10-05	3.952X10-05
9.0X10-02	4.50X10-02	6.204X10-03	2.533X10-05	1.608X10-05	0.0	3.952X10-05	3.952X10-05	4.005X10-06	4.005X10-06	4.005X10-06	4.005X10-06
1.0X10-01	5.00X10-02	4.798X10-03	2.219X10-05	1.192X10-05	0.0	4.005X10-06	4.005X10-06	3.390X10-06	3.390X10-06	2.332X10-06	2.332X10-06
2.0X10-01	1.00X10-01	6.340X10-04	8.944X10-06	1.476X10-06	0.0	2.332X10-06	2.332X10-06	2.012X10-06	2.012X10-06	1.680X10-06	1.680X10-06
3.0X10-01	1.50X10-01	3.218X10-05	5.028X10-06	3.931X10-07	0.0	1.680X10-06	1.680X10-06	1.259X10-06	1.259X10-06	1.515X10-06	1.515X10-06
4.0X10-01	2.00X10-01	0.0	3.245X10-06	1.449X10-07	0.0	1.259X10-06	1.259X10-06	1.170X10-06	1.170X10-06	9.655X10-07	9.655X10-07
5.0X10-01	2.50X10-01	0.0	2.258X10-06	6.419X10-08	0.0	9.655X10-07	9.655X10-07	7.517X10-07	7.517X10-07	9.166X10-07	9.166X10-07
6.0X10-01	3.00X10-01	0.0	1.648X10-06	3.223X10-08	0.0	7.517X10-07	7.517X10-07	5.898X10-07	5.898X10-07	7.250X10-07	7.250X10-07
7.0X10-01	3.50X10-01	0.0	1.241X10-06	1.777X10-08	0.0	5.898X10-07	5.898X10-07	4.046X10-07	4.046X10-07	2.046X10-07	2.046X10-07
8.0X10-01	4.00X10-01	0.0	9.550X10-07	1.053X10-08	0.0	2.046X10-07	2.046X10-07	1.649X10-07	1.649X10-07	1.170X10-06	1.170X10-06
9.0X10-01	4.50X10-01	0.0	7.451X10-07	6.614X10-09	0.0	1.649X10-07	1.649X10-07	1.170X10-06	1.170X10-06	9.166X10-07	9.166X10-07
1.0X10+00	5.00X10-01	0.0	5.855X10-07	4.338X10-09	0.0	1.352X10-07	1.352X10-07	5.898X10-07	5.898X10-07	7.250X10-07	7.250X10-07

TABLE A.2

INTERACTION PROBABILITIES OF MUONS ON 4.0 GEV IN IRON

ENERGY TRANSFERRED IN GEV	FRACTIONAL ENERGY TRANSFER	BREMSSTRÄHLUNG		DIRECT PAIR PRODUCTION		PHOTONNUCLEAR CROSS-SECTION		TOTAL (EXCEPT PHOTONNUCLEAR) CROSS-SECTION		TOTAL CROSS-SECTION IN PARTICLES	
		CROSS-SECTION IN ELECTRONS PER GM/CM**2	CROSS-SECTION IN NUCLEI PER GM/CM**2	CROSS-SECTION IN NUCLEI PER GM/CM**2	CROSS-SECTION IN NUCLEI PER GM/CM**2	CROSS-SECTION IN NUCLEONS PER GM/CM**2	CROSS-SECTION IN NUCLEONS PER GM/CM**2	CROSS-SECTION IN PARTICLES PER GM/CM**2	CROSS-SECTION IN PARTICLES PER GM/CM**2	CROSS-SECTION IN PARTICLES PER GM/CM**2	CROSS-SECTION IN PARTICLES PER GM/CM**2
1.0X10-02	2.50X10-03	6.996X10-01	3.417X10-04	0.0	0.0	6.999X10-01	6.999X10-01	1.747X10-01	1.747X10-01	6.999X10-01	6.999X10-01
2.0X10-02	5.00X10-03	1.732X10-01	1.662X10-04	1.312X10-03	0.0	1.747X10-01	1.747X10-01	7.722X10-02	7.722X10-02	7.722X10-02	7.722X10-02
3.0X10-02	7.50X10-03	7.627X10-02	1.081X10-04	8.357X10-04	0.0	7.722X10-02	7.722X10-02	4.309X10-02	4.309X10-02	4.309X10-02	4.309X10-02
4.0X10-02	1.00X10-02	4.249X10-02	7.931X10-05	5.197X10-04	0.0	4.309X10-02	4.309X10-02	2.733X10-02	2.733X10-02	2.733X10-02	2.733X10-02
5.0X10-02	1.25X10-02	2.693X10-02	6.216X10-05	3.365X10-04	0.0	2.733X10-02	2.733X10-02	1.880X10-02	1.880X10-02	1.880X10-02	1.880X10-02
6.0X10-02	1.50X10-02	1.852X10-02	5.081X10-05	2.275X10-04	0.0	1.880X10-02	1.880X10-02	1.367X10-02	1.367X10-02	1.367X10-02	1.367X10-02
7.0X10-02	1.75X10-02	1.347X10-02	4.278X10-05	1.597X10-04	0.0	1.367X10-02	1.367X10-02	1.036X10-02	1.036X10-02	1.036X10-02	1.036X10-02
8.0X10-02	2.00X10-02	1.021X10-02	3.680X10-05	1.159X10-04	0.0	1.036X10-02	1.036X10-02	8.107X10-03	8.107X10-03	8.107X10-03	8.107X10-03
9.0X10-02	2.25X10-02	7.980X10-03	3.219X10-05	8.644X10-05	0.0	8.107X10-03	8.107X10-03	6.500X10-03	6.500X10-03	6.500X10-03	6.500X10-03
1.0X10-01	2.50X10-02	6.405X10-03	2.853X10-05	6.601X10-05	4.522X10-05 4.522X10-05 4.522X10-05 4.522X10-05	6.500X10-03	6.500X10-03	4.600X10-03	4.600X10-03	4.600X10-03	4.600X10-03
2.0X10-01	5.00X10-02	1.438X10-03	1.257X10-05	9.795X10-06	2.137X10-06	1.460X10-03	1.460X10-03	1.462X10-03	1.462X10-03	1.462X10-03	1.462X10-03
3.0X10-01	7.50X10-02	5.672X10-04	7.595X10-06	2.949X10-06	1.333X10-06	5.777X10-04	5.777X10-04	5.791X10-04	5.791X10-04	5.791X10-04	5.791X10-04
4.0X10-01	1.00X10-01	2.799X10-04	5.232X10-06	1.216X10-06	9.439X10-07	2.852X10-04	2.852X10-04	2.962X10-04	2.962X10-04	2.962X10-04	2.962X10-04
5.0X10-01	1.25X10-01	1.529X10-04	3.878X10-06	5.993X10-07	7.074X10-07	1.573X10-04	1.573X10-04	1.580X10-04	1.580X10-04	1.580X10-04	1.580X10-04
6.0X10-01	1.50X10-01	8.848X10-05	3.011X10-06	3.309X10-07	5.532X10-07	9.183X10-05	9.183X10-05	9.238X10-05	9.238X10-05	9.238X10-05	9.238X10-05
7.0X10-01	1.75X10-01	5.212X10-05	2.415X10-06	1.980X10-07	4.457X10-07	5.473X10-05	5.473X10-05	5.518X10-05	5.518X10-05	5.518X10-05	5.518X10-05
8.0X10-01	2.00X10-01	3.010X10-05	1.984X10-06	1.256X10-07	3.671X10-07	3.221X10-05	3.221X10-05	3.258X10-05	3.258X10-05	3.258X10-05	3.258X10-05
9.0X10-01	2.25X10-01	1.609X10-05	1.660X10-06	8.355X10-08	3.075X10-07	1.784X10-05	1.784X10-05	1.814X10-05	1.814X10-05	1.814X10-05	1.814X10-05
1.0X10+00	2.50X10-01	6.848X10-06	1.409X10-06	5.764X10-08	2.611X10-07	8.316X10-06	8.316X10-06	8.577X10-06	8.577X10-06	8.577X10-06	8.577X10-06
2.0X10+00	5.00X10-01	0.0	4.157X10-07	4.603X10-09	7.815X10-08	4.203X10-07	4.203X10-07	4.394X10-07	4.394X10-07	4.394X10-07	4.394X10-07
3.0X10+00	7.50X10-01	0.0	1.437X10-07	9.457X10-10	3.704X10-09	1.446X10-07	1.446X10-07	1.817X10-07	1.817X10-07	1.817X10-07	1.817X10-07

TABLE A.3

INTERACTION PROBABILITIES OF MUONS ON 7.0 GEV IN IRON

ENERGY TRANSFERRED IN GEV	FRACTIONAL ENERGY TRANSFER	KNOCK-ON CROSS-SECTION IN ELECTRONS PER GM/CM**2		BREMSTRÄHLUNG CROSS-SECTION IN NUCLEI PER GM/CM**2		DIRECT PAIR PRODUCTION CROSS-SECTION IN NUCLEI PER GM/CM**2		PHOTONNUCLEAR CROSS-SECTION IN NUCLEONS PER GM/CM**2		TOTAL (EXCEPT PHOTONNUCLEAR) CROSS-SECTION IN PARTICLES PER GM/CM**2		TOTAL CROSS-SECTION IN PARTICLES PER GEV	
		PFR	GFV	PFR	GFV	PFR	GFV	PFR	GFV	PFR	GFV	PFR	GFV
1.0X10-02	1.42X10-03	7.033X10-01	3.486X10-04	0.0	0.0	0.0	0.0	7.036X10-01	7.036X10-01	1.777X10-01	1.777X10-01	1.777X10-01	1.777X10-01
2.0X10-02	2.85X10-03	1.751X10-01	1.724X10-04	2.395X10-03	0.0	0.0	0.0	7.940X10-02	7.940X10-02	4.473X10-02	4.473X10-02	2.861X10-02	2.861X10-02
3.0X10-02	4.28X10-03	7.757X10-02	1.137X10-04	1.721X10-03	0.0	0.0	0.0	4.983X10-02	4.983X10-02	1.983X10-02	1.983X10-02	1.452X10-02	1.452X10-02
4.0X10-02	5.71X10-03	4.347X10-02	8.449X10-05	1.179X10-03	0.0	0.0	0.0	2.861X10-02	2.861X10-02	1.045X10-02	1.045X10-02	1.045X10-02	1.045X10-02
5.0X10-02	7.14X10-03	2.772X10-02	6.694X10-05	8.274X10-04	0.0	0.0	0.0	1.045X10-02	1.045X10-02	5.108X10-02	5.108X10-02	2.108X10-02	2.108X10-02
6.0X10-02	8.57X10-03	1.917X10-02	5.526X10-05	5.979X10-04	0.0	0.0	0.0	5.108X10-02	5.108X10-02	1.625X10-02	1.625X10-02	1.625X10-02	1.625X10-02
7.0X10-02	1.00X10-02	1.403X10-02	4.694X10-05	4.438X10-04	0.0	0.0	0.0	1.625X10-02	1.625X10-02	1.108X10-02	1.108X10-02	1.108X10-02	1.108X10-02
8.0X10-02	1.14X10-02	1.070X10-02	4.072X10-05	3.374X10-04	0.0	0.0	0.0	8.726X10-03	8.726X10-03	8.726X10-03	8.726X10-03	8.726X10-03	8.726X10-03
9.0X10-02	1.28X10-02	8.428X10-03	3.589X10-05	2.617X10-04	0.0	0.0	0.0	7.040X10-03	7.040X10-03	7.040X10-03	7.040X10-03	7.040X10-03	7.040X10-03
1.0X10-01	1.42X10-02	6.801X10-03	3.203X10-05	2.066X10-04	0.0	0.0	0.0	5.682X10-03	5.682X10-03	1.687X10-03	1.687X10-03	1.687X10-03	1.687X10-03
2.0X10-01	2.85X10-02	1.626X10-03	1.499X10-05	3.651X10-05	0.0	0.0	0.0	2.625X10-06	2.625X10-06	7.219X10-06	7.219X10-06	7.219X10-06	7.219X10-06
3.0X10-01	4.28X10-02	6.989X10-04	9.348X10-06	1.187X10-05	0.0	0.0	0.0	1.666X10-06	1.666X10-06	3.891X10-06	3.891X10-06	3.891X10-06	3.891X10-06
4.0X10-01	5.71X10-02	3.773X10-04	6.648X10-06	5.164X10-06	0.0	0.0	0.0	1.192X10-06	1.192X10-06	2.400X10-06	2.400X10-06	2.391X10-06	2.391X10-06
5.0X10-01	7.14X10-02	2.314X10-04	5.068X10-06	2.659X10-06	0.0	0.0	0.0	1.122X10-06	1.122X10-06	1.593X10-06	1.593X10-06	1.600X10-06	1.600X10-06
6.0X10-01	8.57X10-02	1.537X10-04	4.039X10-06	1.528X10-06	0.0	0.0	0.0	7.278X10-07	7.278X10-07	1.127X10-06	1.127X10-06	1.127X10-06	1.127X10-06
7.0X10-01	1.00X10-01	1.078X10-04	3.320X10-06	9.494X10-07	0.0	0.0	0.0	5.979X10-07	5.979X10-07	1.211X10-06	1.211X10-06	1.211X10-06	1.211X10-06
8.0X10-01	1.14X10-01	7.872X10-05	2.793X10-06	6.244X10-07	0.0	0.0	0.0	5.021X10-07	5.021X10-07	9.213X10-07	9.213X10-07	8.264X10-07	8.264X10-07
9.0X10-01	1.28X10-01	5.915X10-05	2.390X10-06	4.291X10-07	0.0	0.0	0.0	4.287X10-07	4.287X10-07	6.197X10-07	6.197X10-07	6.240X10-07	6.240X10-07
1.0X10+00	1.42X10-01	4.546X10-05	2.075X10-06	3.054X10-07	0.0	0.0	0.0	3.710X10-07	3.710X10-07	4.784X10-07	4.784X10-07	4.922X10-07	4.922X10-07
2.0X10+00	2.85X10-01	5.436X10-06	7.589X10-07	2.908X10-08	0.0	0.0	0.0	1.306X10-07	1.306X10-07	6.224X10-07	6.224X10-07	6.355X10-07	6.355X10-07
3.0X10+00	4.2P10-01	0.0	3.882X10-07	6.831X10-09	0.0	0.0	0.0	6.408X10-08	6.408X10-08	3.950X10-07	3.950X10-07	4.591X10-07	4.591X10-07
4.0X10+00	5.71X10-01	0.0	2.271X10-07	2.474X10-09	0.0	0.0	0.0	3.738X10-08	3.738X10-08	2.296X10-07	2.296X10-07	2.469X10-07	2.469X10-07
5.0X10+00	7.14X10-01	0.0	1.370X10-07	1.131X10-09	0.0	0.0	0.0	2.507X10-08	2.507X10-08	1.382X10-07	1.382X10-07	1.633X10-07	1.633X10-07
6.0X10+00	8.57X10-01	0.0	6.620X10-08	6.620X10-08	0.0	0.0	0.0	2.085X10-08	2.085X10-08	6.620X10-08	6.620X10-08	8.705X10-08	8.705X10-08

TABLE A.4

INTERACTION PROBABILITIES OF MUONS OF 10.0 GEV IN IRON

ENERGY TRANSFERRED IN GEV	FRACTIONAL ENERGY TRANSFER	KNOCK-ON CROSS-SECTION IN FLCTRNS PFR GM/CM**2 PER GEV	BREMSSTRAHLUNG			DIRECT PAIR PRODUCTION			PHOTONNUCLEAR CROSS-SECTION IN NUCLEONS PFR GM/CM**2 PER GEV			TOTAL (EXCEPT PHOTONNUCLEAR) CROSS-SECTION IN PARTICLES PFR GM/CM**2 PER GEV				
			CROSS-SECTION IN NUCLET PER GM/CM**2 PFR GEV	CROSS-SECTION IN NUCLEI PER GM/CM**2 PFR GEV	CROSS-SECTION IN NUCLEI PER GM/CM**2 PFR GEV	CROSS-SECTION IN NUCLEI PER GM/CM**2 PFR GEV	CROSS-SECTION IN NUCLEI PER GM/CM**2 PFR GEV	CROSS-SECTION IN NUCLEI PER GM/CM**2 PFR GEV								
1.0X10-02	1.00X10-03	7.043X10-01	3.505X10-04	0.0	0.0	3.233X10-03	0.0	0.0	7.046X10-01	7.046X10-01	7.046X10-01	7.046X10-01	7.046X10-01	7.046X10-01		
2.0X10-02	2.00X10-03	1.757X10-01	1.742X10-04	1.155X10-04	2.468X10-03	0.0	0.0	1.791X10-01	1.791X10-01	1.791X10-01	1.791X10-01	1.791X10-01	1.791X10-01	1.791X10-01		
3.0X10-02	3.00X10-03	7.793X10-02	7.793X10-02	4.374X10-02	8.616X10-05	1.778X10-03	0.0	0.0	8.051X10-02	8.051X10-02	8.051X10-02	8.051X10-02	8.051X10-02	8.051X10-02	8.051X10-02	
4.0X10-02	4.00X10-03	4.00X10-02	2.793X10-02	6.855X10-05	1.302X10-03	0.0	0.0	4.560X10-02	4.560X10-02	4.560X10-02	4.560X10-02	4.560X10-02	4.560X10-02	4.560X10-02		
5.0X10-02	5.00X10-03	5.00X10-02	1.936X10-02	5.682X10-05	9.769X10-04	0.0	0.0	2.930X10-02	2.930X10-02	2.930X10-02	2.930X10-02	2.930X10-02	2.930X10-02	2.930X10-02		
6.0X10-02	6.00X10-03	6.00X10-02	1.419X10-02	4.844X10-05	7.498X10-04	0.0	0.0	1.449X10-02	1.449X10-02	1.449X10-02	1.449X10-02	1.449X10-02	1.449X10-02	1.449X10-02		
7.0X10-02	7.00X10-03	7.00X10-02	8.90X10-03	1.084X10-02	4.217X10-05	5.871X10-04	0.0	0.0	1.471X10-02	1.471X10-02	1.471X10-02	1.471X10-02	1.471X10-02	1.471X10-02	1.471X10-02	
8.0X10-02	8.00X10-03	8.00X10-02	9.00X10-03	8.550X10-03	3.729X10-05	4.677X10-04	0.0	0.0	9.055X10-03	9.055X10-03	9.055X10-03	9.055X10-03	9.055X10-03	9.055X10-03	9.055X10-03	
9.0X10-02	9.00X10-03	9.00X10-02	1.00X10-02	6.910X10-03	3.339X10-05	3.782X10-04	0.0	0.0	7.322X10-03	7.322X10-03	7.322X10-03	7.322X10-03	7.322X10-03	7.322X10-03	7.322X10-03	
1.0X10-01	1.00X10-02	1.00X10-02	2.00X10-02	1.691X10-03	1.594X10-05	7.681X10-05	0.0	0.0	2.914X10-06	2.914X10-06	2.914X10-06	2.914X10-06	2.914X10-06	2.914X10-06	2.914X10-06	
2.0X10-01	2.00X10-02	2.00X10-02	3.00X10-02	7.353X10-04	1.020X10-05	2.652X10-05	0.0	0.0	1.977X10-06	1.977X10-06	1.977X10-06	1.977X10-06	1.977X10-06	1.977X10-06	1.977X10-06	
3.0X10-01	3.00X10-02	3.00X10-02	4.00X10-02	4.045X10-04	7.372X10-06	1.195X10-05	0.0	0.0	1.353X10-06	1.353X10-06	1.353X10-06	1.353X10-06	1.353X10-06	1.353X10-06	1.353X10-06	
4.0X10-01	4.00X10-02	4.00X10-02	5.00X10-02	2.531X10-04	5.698X10-06	6.312X10-06	0.0	0.0	1.043X10-06	1.043X10-06	1.043X10-06	1.043X10-06	1.043X10-06	1.043X10-06	1.043X10-06	
5.0X10-01	5.00X10-02	5.00X10-02	6.00X10-02	1.717X10-04	4.564X10-06	3.703X10-06	0.0	0.0	8.386X10-07	8.386X10-07	8.386X10-07	8.386X10-07	8.386X10-07	8.386X10-07	8.386X10-07	
6.0X10-01	6.00X10-02	6.00X10-02	7.00X10-02	2.322X10-04	2.341X10-06	2.341X10-06	0.0	0.0	6.942X10-07	6.942X10-07	6.942X10-07	6.942X10-07	6.942X10-07	6.942X10-07	6.942X10-07	
7.0X10-01	7.00X10-02	7.00X10-02	8.00X10-02	9.217X10-05	3.250X10-06	1.564X10-06	0.0	0.0	5.874X10-07	5.874X10-07	5.874X10-07	5.874X10-07	5.874X10-07	5.874X10-07	5.874X10-07	
8.0X10-01	8.00X10-02	8.00X10-02	9.00X10-02	7.107X10-05	2.810X10-06	1.091X10-06	0.0	0.0	5.053X10-07	5.053X10-07	5.053X10-07	5.053X10-07	5.053X10-07	5.053X10-07	5.053X10-07	
9.0X10-01	9.00X10-02	9.00X10-02	1.00X10-01	5.615X10-05	2.462X10-06	7.880X10-07	0.0	0.0	4.401X10-07	4.401X10-07	4.401X10-07	4.401X10-07	4.401X10-07	4.401X10-07	4.401X10-07	
1.0X10-00	1.00X10-01	1.00X10-01	2.00X10-01	1.060X10-05	0.7766X10-07	8.380X10-08	0.0	0.0	1.662X10-07	1.662X10-07	1.662X10-07	1.662X10-07	1.662X10-07	1.662X10-07	1.662X10-07	
2.0X10-00	2.00X10-01	2.00X10-01	3.00X10-01	3.265X10-06	3.269X10-07	2.069X10-08	0.0	0.0	8.741X10-08	8.741X10-08	8.741X10-08	8.741X10-08	8.741X10-08	8.741X10-08	8.741X10-08	
3.0X10-00	3.00X10-01	3.00X10-01	4.00X10-01	1.064X10-06	3.385X10-07	7.464X10-09	0.0	0.0	5.274X10-09	5.274X10-09	5.274X10-09	5.274X10-09	5.274X10-09	5.274X10-09	5.274X10-09	
4.0X10-00	4.00X10-01	4.00X10-01	5.00X10-01	0.0	0.0	2.305X10-07	3.401X10-09	0.0	0.0	3.455X10-08	3.455X10-08	3.455X10-08	3.455X10-08	3.455X10-08	3.455X10-08	3.455X10-08
5.0X10-00	5.00X10-01	5.00X10-01	6.00X10-01	0.0	0.0	1.642X10-07	1.819X10-09	0.0	0.0	2.476X10-08	2.476X10-08	2.476X10-08	2.476X10-08	2.476X10-08	2.476X10-08	2.476X10-08
6.0X10-00	6.00X10-01	6.00X10-01	7.00X10-01	0.0	0.0	1.187X10-07	1.078X10-09	0.0	0.0	1.197X10-07	1.197X10-07	1.197X10-07	1.197X10-07	1.197X10-07	1.197X10-07	1.197X10-07
7.0X10-00	7.00X10-01	7.00X10-01	8.00X10-01	0.0	0.0	8.219X10-08	6.577X10-10	0.0	0.0	1.890X10-08	1.890X10-08	1.890X10-08	1.890X10-08	1.890X10-08	1.890X10-08	1.890X10-08
8.0X10-00	8.00X10-01	8.00X10-01	9.00X10-01	0.0	0.0	4.301X10-08	0.0	0.0	0.0	4.301X10-08	0.0	0.0	4.301X10-08	0.0	4.301X10-08	0.0

TABLE A.5

INTERACTION PROBABILITIES OF MUONS AT 20.0 GEV IN IRON

140 1

ENERGY TRANSFERRED IN GFV	FRACTIONAL ENERGY TRANSFER	KNOCK-ON CROSS-SECTION IN ELECTRONS PER GM/CM**2 PFR GFV	ARMSTRahlUNG CROSS-SECTION IN NUCLEI PER GM/CM**2 PFR GFV	DIRECT PAIR PRODUCTION CROSS-SECTION IN NUCLEI PER GM/CM**2 PFR GFV	PHOTONNUCLEAR CROSS-SECTION IN NUCLEONS PER GM/CM**2 PFR GFV	TOTAL (EXCEPT PHOTONNUCLEAR) CROSS-SECTION IN PARTICLFS PER GM/CM**2 PFR GFV		TOTAL CROSS-SECTION IN PARTICLFS PER GM/CM**2 PFR GFV	
						TOTAL	CROSS-SECTION IN PARTICLFS PER GM/CM**2 PFR GFV	TOTAL	CROSS-SECTION IN PARTICLFS PER GM/CM**2 PFR GFV
1.0X10-02	5.00X10-04	7.052X10-01	3.520X10-04	0.0	0.0	7.055X10-01	1.814X10-01	1.814X10-01	1.814X10-01
2.0X10-02	1.00X10-03	1.761X10-01	1.757X10-04	5.066X10-03	0.0	8.257X10-02	8.257X10-02	8.257X10-02	8.257X10-02
3.0X10-02	1.50X10-03	7.823X10-02	1.169X10-04	4.218X10-03	0.0	4.733X10-02	4.733X10-02	4.733X10-02	4.733X10-02
4.0X10-02	2.00X10-03	4.397X10-02	8.755X10-05	3.269X10-03	0.0	3.074X10-02	3.074X10-02	3.074X10-02	3.074X10-02
5.0X10-02	2.50X10-03	2.812X10-02	6.992X10-05	2.552X10-03	0.0	2.159X10-02	2.159X10-02	2.159X10-02	2.159X10-02
6.0X10-02	3.00X10-03	1.951X10-02	5.817X10-05	2.027X10-03	0.0	1.601X10-02	1.601X10-02	1.601X10-02	1.601X10-02
7.0X10-02	3.50X10-03	1.432X10-02	4.977X10-05	1.638X10-03	0.0	1.234X10-02	1.234X10-02	1.234X10-02	1.234X10-02
8.0X10-02	4.00X10-03	1.065X10-02	4.348X10-05	1.344X10-03	0.0	9.810X10-03	9.810X10-03	9.810X10-03	9.810X10-03
9.0X10-02	4.50X10-03	8.652X10-03	3.858X10-05	1.118X10-03	0.0	7.979X10-03	7.979X10-03	7.979X10-03	7.979X10-03
1.0X10-01	5.00X10-03	7.003X10-03	3.466X10-05	9.420X10-04	7.466X10-06	2.008X10-03	2.008X10-03	2.008X10-03	2.008X10-03
2.0X10-01	1.00X10-02	1.737X10-03	1.705X10-05	2.539X10-04	3.491X10-06	8.794X10-04	8.794X10-04	8.794X10-04	8.794X10-04
3.0X10-01	1.50X10-02	7.660X10-04	1.118X10-05	1.021X10-04	2.258X10-06	4.862X10-04	4.862X10-04	4.862X10-04	4.862X10-04
4.0X10-01	2.00X10-02	4.275X10-04	8.263X10-06	5.046X10-05	1.646X10-06	3.063X10-04	3.063X10-04	3.063X10-04	3.063X10-04
5.0X10-01	2.50X10-02	2.714X10-04	6.513X10-06	2.835X10-05	1.287X10-06	2.097X10-04	2.097X10-04	2.097X10-04	2.097X10-04
6.0X10-01	3.00X10-02	1.870X10-04	5.350X10-06	1.740X10-05	1.041X10-06	2.108X10-04	2.108X10-04	2.108X10-04	2.108X10-04
7.0X10-01	3.50X10-02	1.363X10-04	4.522X10-06	1.140X10-05	8.710X10-07	1.531X10-04	1.531X10-04	1.531X10-04	1.531X10-04
8.0X10-01	4.00X10-02	1.035X10-04	3.902X10-06	7.855X10-06	7.443X10-07	1.152X10-04	1.152X10-04	1.152X10-04	1.152X10-04
9.0X10-01	4.50X10-02	8.115X10-05	3.423X10-06	5.625X10-06	6.467X10-07	9.020X10-05	9.020X10-05	9.020X10-05	9.020X10-05
1.0X10+00	5.00X10-02	6.520X10-05	3.040X10-06	4.156X10-06	5.693X10-07	7.240X10-05	7.240X10-05	7.240X10-05	7.240X10-05
2.0X10+00	1.00X10-01	1.500X10-05	1.349X10-06	5.233X10-07	2.354X10-07	1.687X10-05	1.687X10-05	1.687X10-05	1.687X10-05
3.0X10+00	1.50X10-01	6.110X10-06	8.107X10-07	1.452X10-07	1.343X10-07	7.066X10-06	7.066X10-06	7.066X10-06	7.066X10-06
4.0X10+00	2.00X10-01	3.134X10-06	5.529X10-07	5.644X10-08	8.755X10-08	3.743X10-06	3.743X10-06	3.743X10-06	3.743X10-06
5.0X10+00	2.50X10-01	1.819X10-06	4.048X10-07	2.651X10-08	6.160X10-08	2.250X10-06	2.250X10-06	2.250X10-06	2.250X10-06
6.0X10+00	3.00X10-01	1.138X10-06	3.104X10-07	1.412X10-08	4.555X10-08	1.462X10-06	1.462X10-06	1.462X10-06	1.462X10-06
7.0X10+00	3.50X10-01	7.481X10-07	2.460X10-07	8.231X10-09	3.491X10-08	1.002X10-06	1.002X10-06	1.002X10-06	1.002X10-06
8.0X10+00	4.00X10-01	5.080X10-07	1.998X10-07	5.148X10-09	2.765X10-08	7.129X10-07	7.129X10-07	7.129X10-07	7.129X10-07
9.0X10+00	4.50X10-01	3.523X10-07	1.654X10-07	3.408X10-09	2.226X10-08	5.122X10-07	5.122X10-07	5.122X10-07	5.122X10-07
1.0X10+01	5.00X10-01	2.474X10-07	1.390X10-07	2.366X10-08	1.827X10-08	3.889X10-07	4.071X10-07	4.071X10-07	4.071X10-07

TABLE A.6

INTERACTION PROBABILITIES OF MUONS IN 40.0 GEV IN IRON

ENERGY TRANSFERRED IN GEV	FRACTIONAL ENERGY TRANSFERRED	BREMSSTRAHLUNG				DIRECT PAIR PRODUCTION				PHOTONNUCLEAR				TOTAL (EXCEPT PHOTONNUCLEAR)			
		CROSS-SECTION IN FLFCTRNS PFR GM/CM**2	CROSS-SECTION IN NUCLEI PFR GM/CM**2	TOTAL CROSS-SECTION IN PARTICLFS PFR GM/CM**2	CROSS-SECTION IN PARTICLFS PFR GM/CM**2	TOTAL CROSS-SECTION IN PARTICLFS PFR GM/CM**2	CROSS-SECTION IN PARTICLFS PFR GM/CM**2	TOTAL CROSS-SECTION IN PARTICLFS PFR GM/CM**2	CROSS-SECTION IN PARTICLFS PFR GM/CM**2								
1.0X10-02	2.50X10-04	7.055X10-01	3.524X10-04	0.0	0.0	7.058X10-01	1.835X10-01	1.835X10-01	1.835X10-01	8.464X10-02	8.464X10-02	8.464X10-02	8.464X10-02	8.464X10-02	8.464X10-02		
2.0X10-02	5.00X10-04	1.763X10-01	1.761X10-06	7.040X10-03	0.0	1.835X10-01	8.464X10-02	8.464X10-02	8.464X10-02	9.16X10-02	9.16X10-02	9.16X10-02	9.16X10-02	9.16X10-02	9.16X10-02		
3.0X10-02	7.50X10-04	7.834X10-02	1.173X10-04	6.188X10-03	0.0	4.916X10-02	4.916X10-02	4.916X10-02	4.916X10-02	2.35X10-02	2.35X10-02	2.35X10-02	2.35X10-02	2.35X10-02	2.35X10-02		
4.0X10-02	1.00X10-03	4.405X10-02	8.797X10-05	5.02RX10-03	0.0	3.235X10-02	3.235X10-02	3.235X10-02	3.235X10-02	2.30X10-02	2.30X10-02	2.30X10-02	2.30X10-02	2.30X10-02	2.30X10-02		
5.0X10-02	1.25X10-03	2.818X10-02	7.033X10-05	4.095X10-03	0.0	2.30X10-02	2.30X10-02	2.30X10-02	2.30X10-02	1.725X10-02	1.725X10-02	1.725X10-02	1.725X10-02	1.725X10-02	1.725X10-02		
6.0X10-02	1.50X10-03	1.056X10-02	5.858X10-05	3.380X10-03	0.0	1.725X10-02	1.725X10-02	1.725X10-02	1.725X10-02	1.344X10-02	1.344X10-02	1.344X10-02	1.344X10-02	1.344X10-02	1.344X10-02		
7.0X10-02	1.75X10-03	1.437X10-02	5.018X10-05	2.830X10-03	0.0	1.078X10-02	1.078X10-02	1.078X10-02	1.078X10-02	8.856X10-03	8.856X10-03	8.856X10-03	8.856X10-03	8.856X10-03	8.856X10-03		
8.0X10-02	2.00X10-03	2.00X10-02	4.388X10-05	2.401X10-03	0.0	2.373X10-03	2.373X10-03	2.373X10-03	2.373X10-03	2.373X10-03	2.373X10-03	2.373X10-03	2.373X10-03	2.373X10-03	2.373X10-03		
9.0X10-02	2.25X10-03	8.687X10-03	3.878X10-05	2.061X10-03	0.0	1.077X10-03	1.077X10-03	1.077X10-03	1.077X10-03	1.077X10-03	1.077X10-03	1.077X10-03	1.077X10-03	1.077X10-03	1.077X10-03		
1.0X10-01	2.50X10-03	7.035X10-03	3.507X10-05	1.786X10-03	0.0	4.044X10-06	4.044X10-06	4.044X10-06	4.044X10-06	2.633X10-06	2.633X10-06	2.633X10-06	2.633X10-06	2.633X10-06	2.633X10-06		
2.0X10-01	5.00X10-03	1.753X10-03	1.743X10-05	6.032X10-04	0.0	1.077X10-03	1.077X10-03	1.077X10-03	1.077X10-03	1.077X10-03	1.077X10-03	1.077X10-03	1.077X10-03	1.077X10-03	1.077X10-03		
3.0X10-01	7.50X10-03	7.766X10-04	1.156X10-05	2.835X10-04	0.0	6.079X10-04	6.079X10-04	6.079X10-04	6.079X10-04	3.820X10-04	3.820X10-04	3.820X10-04	3.820X10-04	3.820X10-04	3.820X10-04		
4.0X10-01	1.00X10-02	4.354X10-04	8.623X10-06	1.568X10-04	0.0	1.932X10-06	1.932X10-06	1.932X10-06	1.932X10-06	1.519X10-06	1.519X10-06	1.519X10-06	1.519X10-06	1.519X10-06	1.519X10-06		
5.0X10-01	1.25X10-02	2.778X10-04	6.861X10-06	9.586X10-05	0.0	2.679X10-06	2.679X10-06	2.679X10-06	2.679X10-06	2.400X10-06	2.400X10-06	2.400X10-06	2.400X10-06	2.400X10-06	2.400X10-06		
6.0X10-01	1.923X10-04	5.923X10-06	5.686X10-06	6.276X10-05	0.0	1.043X10-06	1.043X10-06	1.043X10-06	1.043X10-06	1.043X10-06	1.043X10-06	1.043X10-06	1.043X10-06	1.043X10-06	1.043X10-06		
7.0X10-01	1.75X10-02	1.408X10-04	4.848X10-06	4.325X10-05	0.0	1.047X10-04	1.047X10-04	1.047X10-04	1.047X10-04	1.047X10-04	1.047X10-04	1.047X10-04	1.047X10-04	1.047X10-04	1.047X10-04		
8.0X10-01	2.00X10-02	1.074X10-04	4.219X10-06	3.102X10-05	0.0	8.660X10-07	8.660X10-07	8.660X10-07	8.660X10-07	7.826X10-07	7.826X10-07	7.826X10-07	7.826X10-07	7.826X10-07	7.826X10-07		
9.0X10-01	2.25X10-02	8.465X10-05	3.731X10-06	2.297X10-05	0.0	6.926X10-07	6.926X10-07	6.926X10-07	6.926X10-07	8.915X10-05	8.915X10-05	8.915X10-05	8.915X10-05	8.915X10-05	8.915X10-05		
1.0X10+00	2.50X10-02	6.035X10-05	3.340X10-06	1.744X10-05	0.0	2.072X10-05	2.072X10-05	2.072X10-05	2.072X10-05	2.141X10-06	2.141X10-06	2.141X10-06	2.141X10-06	2.141X10-06	2.141X10-06		
2.0X10+00	5.00X10-02	1.654X10-05	1.587X10-06	2.591X10-06	0.0	3.083X10-07	3.083X10-07	3.083X10-07	3.083X10-07	1.796X10-06	1.796X10-06	1.796X10-06	1.796X10-06	1.796X10-06	1.796X10-06		
3.0X10+00	7.50X10-02	1.75X10-02	1.714X10-06	1.005X10-06	0.0	7.905X10-07	7.905X10-07	7.905X10-07	7.905X10-07	4.923X10-06	4.923X10-06	4.923X10-06	4.923X10-06	4.923X10-06	4.923X10-06		
4.0X10+00	1.00X10-01	3.087X10-06	7.217X10-07	3.305X10-07	0.0	1.224X10-07	1.224X10-07	1.224X10-07	1.224X10-07	3.112X10-06	3.112X10-06	3.112X10-06	3.112X10-06	3.112X10-06	3.112X10-06		
5.0X10+00	1.25X10-01	2.395X10-06	5.521X10-07	1.651X10-07	0.0	9.049X10-08	9.049X10-08	9.049X10-08	9.049X10-08	6.967X10-08	6.967X10-08	6.967X10-08	6.967X10-08	6.967X10-08	6.967X10-08		
6.0X10+00	1.50X10-01	1.607X10-06	4.407X10-07	9.249X10-08	0.0	5.545X10-08	5.545X10-08	5.545X10-08	5.545X10-08	1.559X10-06	1.559X10-06	1.559X10-06	1.559X10-06	1.559X10-06	1.559X10-06		
7.0X10+00	1.75X10-01	1.141X10-06	3.623X10-07	7.113X10-08	0.0	8.913X10-06	8.913X10-06	8.913X10-06	8.913X10-06	1.184X10-06	1.184X10-06	1.184X10-06	1.184X10-06	1.184X10-06	1.184X10-06		
8.0X10+00	2.00X10-01	8.438X10-07	3.044X10-07	3.615X10-08	0.0	4.523X10-08	4.523X10-08	4.523X10-08	4.523X10-08	9.282X10-07	9.282X10-07	9.282X10-07	9.282X10-07	9.282X10-07	9.282X10-07		
9.0X10+00	2.25X10-01	6.436X10-07	2.601X10-07	2.438X10-08	0.0	3.761X10-08	3.761X10-08	3.761X10-08	3.761X10-08	7.454X10-07	7.454X10-07	7.454X10-07	7.454X10-07	7.454X10-07	7.454X10-07		
1.0X10+01	2.50X10-01	5.030X10-07	2.253X10-07	1.707X10-08	0.0	3.175X10-08	3.175X10-08	3.175X10-08	3.175X10-08	1.685X10-07	1.685X10-07	1.685X10-07	1.685X10-07	1.685X10-07	1.685X10-07		
2.0X10+01	5.00X10-01	8.606X10-08	8.098X10-08	1.545X10-09	0.0	9.379X10-09	9.379X10-09	9.379X10-09	9.379X10-09	6.669X10-08	6.669X10-08	6.669X10-08	6.669X10-08	6.669X10-08	6.669X10-08		
3.0X10+01	7.50X10-01	2.549X10-08	4.080X10-08	4.113X10-10	0.0	4.724X10-08	4.724X10-08	4.724X10-08	4.724X10-08	7.142X10-08	7.142X10-08	7.142X10-08	7.142X10-08	7.142X10-08	7.142X10-08		

TABLE A.7

INTERACTION PROBABILITIES OF MUONS ON 70.0 GEV IN IRON

ENERGY TRANSFERRED IN GFV	FRACTIONAL ENERGY TRANSFER	KNOCK-ON CROSS-SECTION IN ELFTRANS		BREMSSTRAHLUNG CROSS-SECTION		DIRECT PAIR PRODUCTION		PHOTONNUCLEAR CROSS-SECTION IN NUCLEI		TOTAL (EXCEPT PHOTONNUCLEAR) CROSS-SECTION IN PARTICLES		TOTAL	
		PER GM/CM**2	PER GFV	PER GM/CM**2	PER GFV	PER GM/CM**2	PER GFV	PER GM/CM**2	PER GFV	PER GM/CM**2	PER GFV	PER GM/CM**2	PER GFV
1.0X10-02	1.422X10-04	7.056X10-01		3.525X10-04		0.0		7.059X10-01		7.059X10-01		7.059X10-01	
2.0X10-02	2.85X10-04	1.763X10-01		1.762X10-04		0.0		1.852X10-01		1.852X10-01		1.852X10-01	
3.0X10-02	4.28X10-04	7.837X10-02		1.174X10-04		7.849X10-03		8.634X10-02		8.634X10-02		8.634X10-02	
4.0X10-02	5.71X10-04	4.407X10-02		8.808X10-05		6.539X10-03		5.070X10-02		5.070X10-02		5.070X10-02	
5.0X10-02	6.0X10-04	7.14X10-04		2.820X10-02		7.044X10-05		5.446X10-03		3.372X10-02		3.372X10-02	
6.0X10-02	8.57X10-04	1.958X10-02		5.869X10-05		4.589X10-03		0.0		2.423X10-02		2.423X10-02	
7.0X10-02	1.00X10-03	1.438X10-02		5.029X10-05		3.918X10-03		0.0		1.835X10-02		1.835X10-02	
8.0X10-02	1.14X10-03	1.101X10-02		4.399X10-05		3.386X10-03		0.0		1.444X10-02		1.444X10-02	
9.0X10-02	1.28X10-03	8.699X10-03		3.910X10-05		2.956X10-03		0.0		1.166X10-02		1.166X10-02	
1.0X10-01	1.0X10-01	7.045X10-03		3.518X10-05		2.605X10-03		0.0		9.685X10-03		9.685X10-03	
2.0X10-01	2.85X10-03	1.758X10-03		1.754X10-05		1.003X10-03		4.499X10-06		2.772X10-03		2.784X10-03	
3.0X10-01	4.26X10-03	7.802X10-04		1.167X10-05		5.203X10-04		2.037X10-04		1.312X10-03		1.315X10-03	
4.0X10-01	5.71X10-03	4.381X10-04		8.731X10-06		3.113X10-04		2.161X10-06		7.582X10-04		7.604X10-04	
5.0X10-01	7.14X10-03	2.799X10-04		6.967X10-06		2.031X10-04		1.697X10-06		4.901X10-04		4.918X10-04	
6.0X10-01	8.57X10-03	1.941X10-04		5.792X10-06		1.406X10-04		1.390X10-06		3.405X10-04		3.419X10-04	
7.0X10-01	1.00X10-02	1.423X10-04		4.953X10-06		1.015X10-04		1.173X10-06		2.489X10-04		2.500X10-04	
8.0X10-01	1.14X10-02	1.088X10-04		4.323X10-06		7.586X10-05		1.011X10-06		1.800X10-04		1.900X10-04	
9.0X10-01	1.28X10-02	8.584X10-05		3.833X10-06		5.816X10-05		8.856X10-07		1.478X10-04		1.487X10-04	
1.0X10+00	1.42X10-02	6.941X10-05		3.442X10-06		4.557X10-05		7.861X10-07		1.186X10-04		1.192X10-04	
2.0X10+00	2.85X10-02	1.705X10-05		1.680X10-06		8.001X10-06		3.517X10-07		2.674X10-05		2.710X10-05	
3.0X10+00	4.28X10-02	7.460X10-06		1.004X10-06		2.643X10-06		2.146X10-07		1.119X10-05		1.141X10-05	
4.0X10+00	5.71X10-02	4.126X10-06		8.017X10-07		1.166X10-06		1.495X10-07		6.074X10-06		6.244X10-06	
5.0X10+00	7.14X10-02	2.507X10-06		6.269X10-07		6.078X10-07		1.120X10-07		3.831X10-06		3.943X10-06	
6.0X10+00	8.57X10-02	1.773X10-06		5.107X10-07		3.530X10-07		8.807X10-08		2.637X10-06		2.725X10-06	
7.0X10+00	1.00X10-01	1.280X10-06		4.281X10-07		2.212X10-07		7.147X10-08		1.930X10-06		2.001X10-06	
8.0X10+00	1.14X10-01	9.642X10-07		3.664X10-07		1.467X10-07		5.947X10-08		1.477X10-06		1.536X10-06	
9.0X10+00	1.28X10-01	7.489X10-07		3.187X10-07		1.016X10-07		5.039X10-08		1.166X10-06		1.219X10-06	
1.0X10+01	1.42X10-01	5.963X10-07		2.807X10-07		7.286X10-08		4.332X10-08		9.500X10-07		9.933X10-07	
2.0X10+01	2.85X10-01	1.253X10-07		1.149X10-07		7.372X10-09		1.479X10-08		2.477X10-07		2.624X10-07	
3.0X10+01	4.28X10-01	6.674X10-08		6.449X10-08		1.805X10-09		7.237X10-09		1.130X10-07		1.202X10-07	
4.0X10+01	5.71X10-01	2.215X10-08		4.176X10-08		6.760X10-10		4.254X10-09		6.844X10-08		6.844X10-08	
5.0X10+01	7.14X10-01	1.209X10-08		2.923X10-10		3.303X10-10		2.932X10-09		4.166X10-08		4.459X10-08	
6.0X10+01	8.57X10-01	7.358X10-09		2.029X10-08		1.863X10-10		2.784X10-08		3.047X10-08		3.047X10-08	

TABLE A.8

INTERACTION PROBABILITIES OF MUONS OF 100.0 GEV IN IRON

1 143 1

ENERGY TRANSFERRED IN GEV	FRACTIONAL ENERGY TRANSFERRED	KNOCK-ON CROSS-SECTION - IN ELECTRONS PER GM/CM**2 PFR GFV	BREMSSTRAHLUNG CROSS-SECTION IN NUCLEI		DIRECT PAIR PRODUCTION CROSS-SECTION IN NUCLEI		PHOTONNUCLEAR CROSS-SECTION IN NUCLEONS		TOTAL (EXCEPT PHOTONNUCLEAR) CROSS-SECTION IN PARTICLES PER CM/CM**2 PFR GFV		TOTAL CROSS-SECTION IN PARTICLES PER CM/CM**2 PFR GFV	
			PFR GM/CM**2 PER GEV	PFR GEV	PFR GM/CM**2 PER GEV	PFR GEV	PFR GM/CM**2 PER GEV	PFR GEV	PFR GM/CM**2 PER GEV	PFR GEV	PFR GM/CM**2 PER GEV	PFR GEV
1.0X10-02	1.00X10-04	7.056X10-01	3.526X10-04	0.0	9.728X10-03	0.0	7.060X10-01	0.0	7.060X10-01	0.0	7.060X10-01	0.0
2.0X10-02	2.00X10-04	1.763X10-01	1.762X10-04	0.0	8.923X10-03	0.0	8.743X10-02	0.0	8.743X10-02	0.0	8.743X10-02	0.0
3.0X10-02	3.00X10-04	7.838X10-02	1.175X10-04	0.0	7.522X10-03	0.0	5.169X10-02	0.0	5.169X10-02	0.0	5.169X10-02	0.0
4.0X10-02	4.00X10-04	4.08X10-02	8.811X10-05	0.0	6.331X10-03	0.0	3.461X10-02	0.0	3.461X10-02	0.0	3.461X10-02	0.0
5.0X10-02	5.00X10-04	2.821X10-02	7.048X10-05	0.0	5.387X10-03	0.0	2.503X10-02	0.0	2.503X10-02	0.0	2.503X10-02	0.0
6.0X10-02	6.00X10-04	1.959X10-02	5.872X10-05	0.0	4.642X10-03	0.0	1.908X10-02	0.0	1.908X10-02	0.0	1.908X10-02	0.0
7.0X10-02	7.00X10-04	1.439X10-02	4.403X10-05	0.0	4.045X10-03	0.0	1.510X10-02	0.0	1.510X10-02	0.0	1.510X10-02	0.0
8.0X10-02	8.00X10-04	1.101X10-02	3.913X10-05	0.0	3.561X10-03	0.0	1.230X10-02	0.0	1.230X10-02	0.0	1.230X10-02	0.0
9.0X10-02	9.00X10-04	8.704X10-03	3.521X10-05	0.0	3.162X10-03	0.0	1.024X10-02	0.0	1.024X10-02	0.0	1.024X10-02	0.0
1.0X10-01	1.00X10-03	7.049X10-03	1.760X10-05	0.0	1.299X10-03	0.0	3.077X10-03	0.0	3.077X10-03	0.0	3.077X10-03	0.0
2.0X10-01	2.00X10-03	7.815X10-03	1.170X10-05	0.0	7.079X10-04	0.0	1.501X10-03	0.0	1.501X10-03	0.0	1.501X10-03	0.0
3.0X10-01	3.00X10-03	4.391X10-03	8.764X10-06	0.0	4.411X10-04	0.0	2.307X10-04	0.0	2.307X10-04	0.0	2.307X10-04	0.0
4.0X10-01	4.00X10-03	2.807X10-04	7.000X10-06	0.0	2.980X10-04	0.0	1.815X10-04	0.0	1.815X10-04	0.0	1.815X10-04	0.0
5.0X10-01	5.00X10-03	1.947X10-04	5.825X10-06	0.0	2.127X10-04	0.0	1.488X10-04	0.0	1.488X10-04	0.0	1.488X10-04	0.0
6.0X10-01	6.00X10-03	1.429X10-04	4.085X10-06	0.0	1.577X10-04	0.0	1.084X10-04	0.0	1.084X10-04	0.0	1.084X10-04	0.0
7.0X10-01	7.00X10-03	8.00X10-03	4.355X10-06	0.0	1.208X10-04	0.0	2.345X10-04	0.0	2.345X10-04	0.0	2.345X10-04	0.0
8.0X10-01	8.00X10-03	6.626X10-05	3.856X10-06	0.0	9.472X10-05	0.0	9.514X10-05	0.0	9.514X10-05	0.0	9.514X10-05	0.0
9.0X10-01	9.00X10-03	6.976X10-05	3.474X10-06	0.0	7.571X10-05	0.0	8.456X10-05	0.0	8.456X10-05	0.0	8.456X10-05	0.0
1.0X10+00	1.00X10-02	6.070X10-05	3.121X10-06	0.0	1.504X10-05	0.0	3.814X10-05	0.0	3.814X10-05	0.0	3.814X10-05	0.0
2.0X10+00	2.00X10-05	1.725X10-05	1.711X10-06	0.0	1.124X10-06	0.0	5.273X10-06	0.0	5.273X10-06	0.0	5.273X10-06	0.0
3.0X10+00	3.00X10-07	7.584X10-06	4.546X10-07	0.0	4.904X10-07	0.0	2.363X10-07	0.0	2.363X10-07	0.0	2.363X10-07	0.0
4.0X10+00	4.00X10-07	4.218X10-06	8.309X10-07	0.0	2.414X10-06	0.0	1.661X10-07	0.0	1.661X10-07	0.0	1.661X10-07	0.0
5.0X10+00	5.00X10-07	2.669X10-06	6.551X10-07	0.0	1.293X10-06	0.0	1.253X10-07	0.0	1.253X10-07	0.0	1.253X10-07	0.0
6.0X10+00	6.00X10-07	1.833X10-06	5.380X10-07	0.0	7.680X10-07	0.0	6.055X10-08	0.0	6.055X10-08	0.0	6.055X10-08	0.0
7.0X10+00	7.00X10-07	1.331X10-06	4.546X10-07	0.0	4.904X10-07	0.0	8.149X10-08	0.0	8.149X10-08	0.0	8.149X10-08	0.0
8.0X10+00	8.00X10-07	1.008X10-06	3.921X10-07	0.0	3.306X10-07	0.0	6.812X10-08	0.0	6.812X10-08	0.0	6.812X10-08	0.0
9.0X10+00	9.00X10-07	7.878X10-07	3.436X10-07	0.0	2.325X10-07	0.0	5.834X10-08	0.0	5.834X10-08	0.0	5.834X10-08	0.0
1.0X10+01	1.00X10-07	6.309X10-07	3.049X10-07	0.0	1.690X10-07	0.0	5.055X10-08	0.0	5.055X10-08	0.0	5.055X10-08	0.0
2.0X10+01	2.00X10-07	1.408X10-07	1.330X10-07	0.0	1.890X10-08	0.0	1.847X10-08	0.0	1.847X10-08	0.0	1.847X10-08	0.0
3.0X10+01	3.00X10-07	5.584X10-08	7.826X10-08	0.0	4.831X10-09	0.0	6.144X10-09	0.0	6.144X10-09	0.0	6.144X10-09	0.0
4.0X10+01	4.00X10-07	2.805X10-08	5.240X10-09	0.0	1.783X10-09	0.0	5.774X10-09	0.0	5.774X10-09	0.0	5.774X10-09	0.0
5.0X10+01	5.00X10-07	1.609X10-08	3.789X10-09	0.0	8.249X10-10	0.0	3.837X10-09	0.0	3.837X10-09	0.0	3.837X10-09	0.0
6.0X10+01	6.00X10-07	5.007X10-08	2.888X10-09	0.0	4.476X10-10	0.0	2.748X10-09	0.0	2.748X10-09	0.0	2.748X10-09	0.0
7.0X10+01	7.00X10-07	6.740X10-09	2.276X10-08	0.0	2.737X10-10	0.0	2.131X10-09	0.0	2.131X10-09	0.0	2.131X10-09	0.0
8.0X10+01	8.00X10-07	4.763X10-09	1.812X10-08	0.0	1.849X10-10	0.0	1.849X10-09	0.0	1.849X10-09	0.0	1.849X10-09	0.0
9.0X10+01	9.00X10-07	3.536X10-09	1.231X10-08	0.0	1.231X10-10	0.0	1.231X10-09	0.0	1.231X10-09	0.0	1.231X10-09	0.0

TABLE A.9

INTERACTION PROBABILITIES OF MUONS OF 200.0 GEV IN IRON

ENERGY TRANSFERRED IN GEV	FRACTIONAL ENERGY TRANSFER	KNOCK-ON CROSS-SECTION IN ELECTRONS PER GM/CM ² PFR GFV	BREMSSSTRAHLUNG		DIRECT PAIR PRODUCTION		PHOTONNUCLEAR		TOTAL (EXCEPT PHOTONNUCLEAR)	
			CROSS-SECTION IN NUCLEI	CROSS-SECTION IN NUCLEI	CROSS-SECTION IN NUCLEI	CROSS-SECTION IN NUCLEI	CROSS-SECTION IN PARTICLES PER GM/CM ² PFR GFV			
1.0X10 ⁻⁰²		5.00X10 ⁻⁰⁵	7.057X10 ⁻⁰¹	3.526X10 ⁻⁰⁴	0.0	0.0	7.060X10 ⁻⁰¹	1.863X10 ⁻⁰¹	1.863X10 ⁻⁰¹	1.863X10 ⁻⁰¹
2.0X10 ⁻⁰²		1.00X10 ⁻⁰⁴	1.764X10 ⁻⁰¹	1.763X10 ⁻⁰⁴	1.178X10 ⁻⁰²	0.0	1.883X10 ⁻⁰¹	9.954X10 ⁻⁰²	9.954X10 ⁻⁰²	9.954X10 ⁻⁰²
3.0X10 ⁻⁰²		1.50X10 ⁻⁰⁴	7.840X10 ⁻⁰²	1.175X10 ⁻⁰⁴	1.102X10 ⁻⁰²	0.0	5.363X10 ⁻⁰²	5.363X10 ⁻⁰²	5.363X10 ⁻⁰²	5.363X10 ⁻⁰²
4.0X10 ⁻⁰²		2.00X10 ⁻⁰⁴	4.409X10 ⁻⁰²	8.814X10 ⁻⁰⁵	9.452X10 ⁻⁰³	0.0	3.636X10 ⁻⁰²	3.636X10 ⁻⁰²	3.636X10 ⁻⁰²	3.636X10 ⁻⁰²
5.0X10 ⁻⁰²		2.50X10 ⁻⁰⁴	2.822X10 ⁻⁰²	7.051X10 ⁻⁰⁵	8.075X10 ⁻⁰³	0.0	2.662X10 ⁻⁰²	2.662X10 ⁻⁰²	2.662X10 ⁻⁰²	2.662X10 ⁻⁰²
6.0X10 ⁻⁰²		3.00X10 ⁻⁰⁴	1.450X10 ⁻⁰²	5.875X10 ⁻⁰⁵	6.965X10 ⁻⁰³	0.0	2.052X10 ⁻⁰²	2.052X10 ⁻⁰²	2.052X10 ⁻⁰²	2.052X10 ⁻⁰²
7.0X10 ⁻⁰²		3.50X10 ⁻⁰⁴	1.439X10 ⁻⁰²	5.036X10 ⁻⁰⁵	6.078X10 ⁻⁰³	0.0	1.642X10 ⁻⁰²	1.642X10 ⁻⁰²	1.642X10 ⁻⁰²	1.642X10 ⁻⁰²
8.0X10 ⁻⁰²		4.00X10 ⁻⁰⁴	1.102X10 ⁻⁰²	4.406X10 ⁻⁰⁵	5.360X10 ⁻⁰³	0.0	1.352X10 ⁻⁰²	1.352X10 ⁻⁰²	1.352X10 ⁻⁰²	1.352X10 ⁻⁰²
9.0X10 ⁻⁰²		4.50X10 ⁻⁰⁴	8.708X10 ⁻⁰³	3.916X10 ⁻⁰⁵	4.772X10 ⁻⁰³	0.0	1.137X10 ⁻⁰²	1.137X10 ⁻⁰²	1.137X10 ⁻⁰²	1.137X10 ⁻⁰²
1.0X10 ⁻⁰¹		5.00X10 ⁻⁰⁴	7.053X10 ⁻⁰³	3.524X10 ⁻⁰⁵	4.284X10 ⁻⁰³	0.0	5.326X10 ⁻⁰³	5.326X10 ⁻⁰³	5.326X10 ⁻⁰³	5.326X10 ⁻⁰³
2.0X10 ⁻⁰¹		1.00X10 ⁻⁰³	1.762X10 ⁻⁰³	1.761X10 ⁻⁰⁵	1.928X10 ⁻⁰³	0.0	3.492X10 ⁻⁰³	1.923X10 ⁻⁰³	1.923X10 ⁻⁰³	1.923X10 ⁻⁰³
3.0X10 ⁻⁰¹		1.50X10 ⁻⁰³	7.829X10 ⁻⁰⁴	1.173X10 ⁻⁰⁵	1.128X10 ⁻⁰³	0.0	2.579X10 ⁻⁰³	1.196X10 ⁻⁰³	1.196X10 ⁻⁰³	1.196X10 ⁻⁰³
4.0X10 ⁻⁰¹		2.00X10 ⁻⁰³	4.401X10 ⁻⁰⁴	8.794X10 ⁻⁰⁶	7.475X10 ⁻⁰⁴	0.0	2.033X10 ⁻⁰³	8.211X10 ⁻⁰⁴	8.211X10 ⁻⁰⁴	8.211X10 ⁻⁰⁴
5.0X10 ⁻⁰¹		2.50X10 ⁻⁰³	2.815X10 ⁻⁰⁴	7.031X10 ⁻⁰⁶	5.326X10 ⁻⁰⁴	0.0	5.996X10 ⁻⁰⁴	6.013X10 ⁻⁰⁴	6.013X10 ⁻⁰⁴	6.013X10 ⁻⁰⁴
6.0X10 ⁻⁰¹		3.00X10 ⁻⁰³	1.954X10 ⁻⁰⁴	5.855X10 ⁻⁰⁶	3.983X10 ⁻⁰⁴	0.0	1.672X10 ⁻⁰⁴	4.570X10 ⁻⁰⁴	4.570X10 ⁻⁰⁴	4.570X10 ⁻⁰⁴
7.0X10 ⁻⁰¹		3.50X10 ⁻⁰³	1.434X10 ⁻⁰⁴	5.016X10 ⁻⁰⁶	3.095X10 ⁻⁰⁴	0.0	1.416X10 ⁻⁰⁴	3.095X10 ⁻⁰⁴	3.095X10 ⁻⁰⁴	3.095X10 ⁻⁰⁴
8.0X10 ⁻⁰¹		4.00X10 ⁻⁰³	1.098X10 ⁻⁰⁴	4.386X10 ⁻⁰⁶	2.454X10 ⁻⁰⁴	0.0	1.223X10 ⁻⁰⁴	3.596X10 ⁻⁰⁴	3.596X10 ⁻⁰⁴	3.596X10 ⁻⁰⁴
9.0X10 ⁻⁰¹		4.50X10 ⁻⁰³	8.671X10 ⁻⁰⁵	3.896X10 ⁻⁰⁶	1.994X10 ⁻⁰⁴	0.0	1.075X10 ⁻⁰⁴	2.900X10 ⁻⁰⁴	2.900X10 ⁻⁰⁴	2.900X10 ⁻⁰⁴
1.0X10 ⁺⁰⁰		5.00X10 ⁻⁰³	7.020X10 ⁻⁰⁵	3.504X10 ⁻⁰⁶	1.647X10 ⁻⁰⁴	0.0	9.575X10 ⁻⁰⁵	2.394X10 ⁻⁰⁴	2.394X10 ⁻⁰⁴	2.394X10 ⁻⁰⁴
2.0X10 ⁺⁰⁰		1.00X10 ⁻⁰²	1.745X10 ⁻⁰⁵	1.741X10 ⁻⁰⁶	4.146X10 ⁻⁰⁵	0.0	4.401X10 ⁻⁰⁷	6.066X10 ⁻⁰⁵	6.066X10 ⁻⁰⁵	6.066X10 ⁻⁰⁵
3.0X10 ⁺⁰⁰		1.50X10 ⁻⁰²	7.118X10 ⁻⁰⁶	1.153X10 ⁻⁰⁶	1.661X10 ⁻⁰⁵	0.0	2.752X10 ⁻⁰⁷	5.576X10 ⁻⁰⁵	5.576X10 ⁻⁰⁵	5.576X10 ⁻⁰⁵
4.0X10 ⁺⁰⁰		2.00X10 ⁻⁰²	4.318X10 ⁻⁰⁶	8.599X10 ⁻⁰⁷	8.286X10 ⁻⁰⁶	0.0	1.346X10 ⁻⁰⁵	1.366X10 ⁻⁰⁵	1.366X10 ⁻⁰⁵	1.366X10 ⁻⁰⁵
5.0X10 ⁺⁰⁰		2.50X10 ⁻⁰²	2.749X10 ⁻⁰⁶	6.837X10 ⁻⁰⁷	4.714X10 ⁻⁰⁶	0.0	1.047X10 ⁻⁰⁵	8.277X10 ⁻⁰⁶	8.277X10 ⁻⁰⁶	8.277X10 ⁻⁰⁶
6.0X10 ⁺⁰⁰		3.00X10 ⁻⁰²	1.899X10 ⁻⁰⁶	5.662X10 ⁻⁰⁷	2.931X10 ⁻⁰⁶	0.0	1.203X10 ⁻⁰⁷	5.397X10 ⁻⁰⁶	5.397X10 ⁻⁰⁶	5.397X10 ⁻⁰⁶
7.0X10 ⁺⁰⁰		3.50X10 ⁻⁰²	1.388X10 ⁻⁰⁶	4.823X10 ⁻⁰⁷	1.043X10 ⁻⁰⁶	0.0	9.960X10 ⁻⁰⁸	3.814X10 ⁻⁰⁶	3.913X10 ⁻⁰⁶	3.913X10 ⁻⁰⁶
8.0X10 ⁺⁰⁰		4.00X10 ⁻⁰²	1.057X10 ⁻⁰⁶	4.194X10 ⁻⁰⁷	1.353X10 ⁻⁰⁶	0.0	2.752X10 ⁻⁰⁷	2.914X10 ⁻⁰⁶	2.914X10 ⁻⁰⁶	2.914X10 ⁻⁰⁶
9.0X10 ⁺⁰⁰		4.50X10 ⁻⁰²	8.308X10 ⁻⁰⁷	3.705X10 ⁻⁰⁷	9.787X10 ⁻⁰⁷	0.0	1.960X10 ⁻⁰⁷	1.346X10 ⁻⁰⁵	1.346X10 ⁻⁰⁵	1.346X10 ⁻⁰⁵
1.0X10 ⁺⁰¹		5.00X10 ⁻⁰²	6.694X10 ⁻⁰⁷	3.314X10 ⁻⁰⁷	7.298X10 ⁻⁰⁷	0.0	1.501X10 ⁻⁰⁷	1.047X10 ⁻⁰⁶	1.047X10 ⁻⁰⁶	1.047X10 ⁻⁰⁶
2.0X10 ⁺⁰¹		1.00X10 ⁻⁰¹	1.587X10 ⁻⁰⁷	1.559X10 ⁻⁰⁷	9.753X10 ⁻⁰⁷	0.0	2.564X10 ⁻⁰⁸	4.121X10 ⁻⁰⁷	4.379X10 ⁻⁰⁷	4.379X10 ⁻⁰⁷
3.0X10 ⁺⁰¹		1.50X10 ⁻⁰¹	6.489X10 ⁻⁰⁸	2.799X10 ⁻⁰⁸	1.441X10 ⁻⁰⁸	0.0	1.928X10 ⁻⁰⁸	2.072X10 ⁻⁰⁷	2.072X10 ⁻⁰⁷	2.072X10 ⁻⁰⁷
4.0X10 ⁺⁰¹		2.00X10 ⁻⁰¹	3.568X10 ⁻⁰⁸	6.936X10 ⁻⁰⁸	1.113X10 ⁻⁰⁸	0.0	1.161X10 ⁻⁰⁷	1.255X10 ⁻⁰⁷	1.255X10 ⁻⁰⁷	1.255X10 ⁻⁰⁷
5.0X10 ⁺⁰¹		2.50X10 ⁻⁰¹	2.166X10 ⁻⁰⁸	5.248X10 ⁻⁰⁸	5.325X10 ⁻⁰⁹	0.0	2.180X10 ⁻⁰⁸	2.252X10 ⁻⁰⁸	2.252X10 ⁻⁰⁸	2.252X10 ⁻⁰⁸
6.0X10 ⁺⁰¹		3.00X10 ⁻⁰¹	1.428X10 ⁻⁰⁸	4.147X10 ⁻⁰⁸	2.874X10 ⁻⁰⁹	0.0	1.730X10 ⁻⁰⁸	1.794X10 ⁻⁰⁸	1.794X10 ⁻⁰⁸	1.794X10 ⁻⁰⁸
7.0X10 ⁺⁰¹		3.50X10 ⁻⁰¹	9.967X10 ⁻⁰⁹	3.379X10 ⁻⁰⁸	1.693X10 ⁻⁰⁹	0.0	3.698X10 ⁻⁰⁹	5.463X10 ⁻⁰⁹	5.463X10 ⁻⁰⁹	5.463X10 ⁻⁰⁹
8.0X10 ⁺⁰¹		4.00X10 ⁻⁰¹	7.256X10 ⁻⁰⁹	2.819X10 ⁻⁰⁸	1.067X10 ⁻⁰⁹	0.0	2.910X10 ⁻⁰⁹	3.943X10 ⁻⁰⁹	3.943X10 ⁻⁰⁹	3.943X10 ⁻⁰⁹
9.0X10 ⁺⁰¹		4.50X10 ⁻⁰¹	5.459X10 ⁻⁰⁹	2.396X10 ⁻⁰⁸	7.102X10 ⁻¹⁰	0.0	3.013X10 ⁻⁰⁹	3.249X10 ⁻⁰⁹	3.249X10 ⁻⁰⁹	3.249X10 ⁻⁰⁹

TABLE A.10

INTERACTION PROBABILITIES OF NIONS OF 200.0 GEV IN IRON

ENERGY TRANSFERRED IN GEV	FRACTIONAL ENERGY TRANSFER	KNOCK-ON CROSS-SECTION		DIRECT PAIR PRODUCTION		PHOTONNUCLEAR CROSS-SECTION		TOTAL (EXCEPT PHOTONNUCLEAR) CROSS-SECTION	
		IN ELECTRONS PER GM/CM**2	IN NUCLEI PER GM/CM**2	CROSS-SECTION IN NUCLEONS PER GM/CM**2	CROSS-SECTION IN NUCLEI PER GM/CM**2	TOTAL CROSS-SECTION IN PARTICLES PFR GM/CM**2	TOTAL CROSS-SECTION IN PARTICLES PFR GM/CM**2		
1.0X10+02	5.00X10-01	4.217X10-09	2.069X10-08	4.946X10-10	1.939X10-07	2.540X10-08	2.734X10-08		

TABLE A.10

INTERACTION PROBABILITIES OF MIJONS IN IRON

TOTAL		CROSS-SECTION		IN PARTICLES		PER GM/CM**2		PER GM/CM**2		PER GFV	
BREMSSTRAHLUNG		DIRECT PAIR		PRODUCTION		CROSS-SECTION		IN NUCL.FONS.		CROSS-SECTION	
KNOCK-ON		CROSS-SCTION		CROSS-SECTION		IN NUCLEI		PER GM/CM**2		IN PARTICLES	
ENERGY	TRANSFERRED	IN GEV	PER GFV	PER GM/CM**2	PER GFV						
1.0X10-02	2.50X10-05	7.057X10-01	3.526X10-04	0.0	0.0	7.060X10-01	7.060X10-01	1.904X10-01	1.904X10-01	1.904X10-01	1.904X10-01
2.0X10-02	5.00X10-05	1.764X10-01	1.763X10-04	1.304X10-02	0.0	1.31X10-02	1.31X10-02	1.166X10-02	1.166X10-02	1.166X10-02	1.166X10-02
3.0X10-02	7.50X10-05	7.840X10-02	1.175X10-04	8.115X10-05	1.139X10-02	9.832X10-03	9.832X10-03	5.558X10-02	5.558X10-02	5.558X10-02	5.558X10-02
4.0X10-02	1.00X10-04	4.410X10-02	2.822X10-02	7.052X10-05	9.832X10-03	8.559X10-03	8.559X10-03	3.812X10-02	3.812X10-02	3.812X10-02	3.812X10-02
5.0X10-02	1.25X10-04	1.50X10-02	5.876X10-05	8.559X10-03	8.559X10-03	8.559X10-03	8.559X10-03	2.821X10-02	2.821X10-02	2.821X10-02	2.821X10-02
6.0X10-02	1.50X10-04	1.60X10-02	5.037X10-05	7.532X10-03	0.0	7.532X10-03	0.0	2.198X10-02	2.198X10-02	2.198X10-02	2.198X10-02
7.0X10-02	1.75X10-04	1.440X10-02	5.037X10-05	4.407X10-05	6.695X10-03	0.0	0.0	1.776X10-02	1.776X10-02	1.776X10-02	1.776X10-02
8.0X10-02	2.00X10-04	1.102X10-02	3.917X10-05	6.005X10-03	6.005X10-03	0.0	0.0	1.475X10-02	1.475X10-02	1.475X10-02	1.475X10-02
9.0X10-02	2.25X10-04	8.710X10-03	3.525X10-05	5.428X10-03	5.428X10-03	5.428X10-03	5.428X10-03	1.251X10-02	1.251X10-02	1.251X10-02	1.251X10-02
1.0X10-01	2.50X10-04	7.055X10-03	1.763X10-03	1.762X10-05	2.591X10-03	2.591X10-03	2.591X10-03	4.378X10-03	4.378X10-03	4.378X10-03	4.378X10-03
2.0X10-01	5.00X10-04	2.00X10-04	7.835X10-04	1.174X10-05	1.599X10-03	3.865X10-03	3.865X10-03	2.385X10-03	2.385X10-03	2.385X10-03	2.385X10-03
3.0X10-01	7.50X10-04	4.406X10-04	8.806X10-06	1.096X10-03	2.851X10-06	1.546X10-03	1.546X10-03	1.549X10-03	1.549X10-03	1.549X10-03	1.549X10-03
4.0X10-01	1.00X10-03	2.125X10-03	2.819X10-04	7.043X10-06	8.105X10-04	2.258X10-06	1.090X10-03	1.011X10-03	1.011X10-03	1.011X10-03	1.011X10-03
5.0X10-01	1.25X10-03	1.957X10-04	5.868X10-06	6.267X10-05	1.859X10-04	1.859X10-04	8.283X10-04	8.302X10-04	8.302X10-04	8.302X10-04	8.302X10-04
6.0X10-01	1.50X10-03	1.437X10-04	5.028X10-06	5.005X10-04	1.575X10-06	6.493X10-04	6.493X10-04	6.508X10-04	6.508X10-04	6.508X10-04	6.508X10-04
7.0X10-01	1.75X10-03	1.437X10-04	1.100X10-04	4.398X10-06	4.095X10-04	1.263X10-06	5.240X10-04	5.240X10-04	5.240X10-04	5.240X10-04	5.240X10-04
8.0X10-01	2.00X10-03	8.692X10-05	3.908X10-06	3.416X10-04	1.199X10-04	1.199X10-04	4.324X10-04	4.324X10-04	4.324X10-04	4.324X10-04	4.324X10-04
9.0X10-01	2.25X10-03	7.039X10-05	3.516X10-06	2.893X10-04	1.069X10-04	3.632X10-04	3.632X10-04	3.642X10-04	3.642X10-04	3.642X10-04	3.642X10-04
1.0X10+00	2.50X10-03	5.000X10-05	1.755X10-05	8.796X10-05	4.958X10-05	1.072X10-04	1.072X10-04	1.077X10-04	1.077X10-04	1.077X10-04	1.077X10-04
2.0X10+00	7.50X10-03	2.000X10-03	1.437X10-04	4.090X10-07	4.013X10-05	3.131X10-07	4.908X10-05	4.930X10-05	4.930X10-05	4.930X10-05	4.930X10-05
3.0X10+00	4.0X10-01	1.00X10-03	1.100X10-04	4.398X10-07	2.200X10-05	2.744X10-07	2.744X10-05	2.744X10-05	2.744X10-05	2.744X10-05	2.744X10-05
4.0X10+00	2.25X10-03	8.692X10-05	4.090X10-06	6.955X10-07	1.344X10-05	1.741X10-07	1.741X10-05	1.692X10-05	1.692X10-05	1.692X10-05	1.692X10-05
5.0X10+00	5.000X10-03	7.039X10-05	3.516X10-06	5.779X10-07	8.836X10-06	1.405X10-07	1.134X10-05	1.134X10-05	1.134X10-05	1.134X10-05	1.134X10-05
6.0X10+00	7.00X10+00	2.000X10-03	1.437X10-04	4.940X10-07	6.124X10-06	1.170X10-07	8.032X10-06	8.032X10-06	8.032X10-06	8.032X10-06	8.032X10-06
7.0X10+00	3.0X10+01	1.00X10+00	1.00X10-03	4.310X10-07	4.421X10-06	9.978X10-07	5.932X10-06	5.932X10-06	5.932X10-06	5.932X10-06	5.932X10-06
8.0X10+00	4.0X10+00	2.25X10-02	8.513X10-07	3.821X10-05	3.297X10-06	8.660X10-08	4.530X10-06	4.530X10-06	4.530X10-06	4.530X10-06	4.530X10-06
9.0X10+00	5.0X10+00	6.878X10-07	3.429X10-07	3.429X10-07	2.525X10-06	7.624X10-08	3.555X10-06	3.555X10-06	3.555X10-06	3.555X10-06	3.555X10-06
1.0X10+01	1.00X10+01	5.000X10-02	1.675X10-02	1.667X10-07	3.979X10-07	3.223X10-08	7.322X10-07	7.322X10-07	7.322X10-07	7.322X10-07	7.322X10-07
2.0X10+01	2.00X10+01	7.50X10-02	2.259X10-08	1.081X10-07	1.263X10-07	1.902X10-08	3.071X10-07	3.071X10-07	3.071X10-07	3.071X10-07	3.071X10-07
3.0X10+01	3.0X10+01	9.979X10-08	7.894X10-08	7.894X10-08	5.424X10-08	1.296X10-08	1.731X10-07	1.731X10-07	1.731X10-07	1.731X10-07	1.731X10-07
4.0X10+01	4.0X10+01	2.482X10-08	2.482X10-08	2.482X10-08	2.776X10-08	9.475X10-09	1.140X10-07	1.140X10-07	1.140X10-07	1.140X10-07	1.140X10-07
5.0X10+01	5.0X10+01	1.680X10-08	4.990X10-08	4.990X10-08	1.582X10-08	7.243X10-09	8.253X10-08	8.253X10-08	8.253X10-08	8.253X10-08	8.253X10-08
6.0X10+01	6.0X10+01	1.203X10-08	4.167X10-08	4.167X10-08	9.746X10-09	5.776X10-09	6.345X10-08	6.345X10-08	6.345X10-08	6.345X10-08	6.345X10-08
7.0X10+01	7.0X10+01	8.961X10-09	3.555X10-08	3.555X10-08	6.355X10-09	4.705X10-09	5.088X10-08	5.088X10-08	5.088X10-08	5.088X10-08	5.088X10-08
8.0X10+01	8.0X10+01	2.25X10-01	6.919X10-09	3.082X10-08	3.082X10-08	4.332X10-09	3.907X10-09	4.207X10-08	4.207X10-08	4.207X10-08	4.207X10-08

TABLE A-11

INTERACTION PROBABILITIES OF MUONS OF 400.0 GEV IN IRON

ENERGY TRANSFERRED IN GFV	FRACTIONAL ENERGY TRANSFERRED	KNOCK-ON		BREMSTRÄHLUNG		DIRECT PAIR		PHOTONNUCLEAR		TOTAL (EXCEPT PHOTONNUCLEAR)		CROSS-SECTION IN PARTICLES	
		CROSS-SECTION IN ELECTRONS	CROSS-SECTION IN NUCLEI	CROSS-SECTION IN NUCLEI	CROSS-SECTION IN NUCLEI	CROSS-SECTION IN NUCLEONS	CROSS-SECTION IN NUCLEONS	PFR GM/CM**2	PFR GM/CM**2	PFR GM/CM**2	PFR GM/CM**2	PFR GM/CM**2	PFR GM/CM**2
1.0X10+02	2.50X10-01	5.465X10-09	2.707X10-08	3.061X10-09	3.295X10-09	9.723X10-10	9.887X10-10	1.02X10-08	2.887X10-10	3.559X10-08	3.889X10-08	1.230X10-08	1.336X10-08
2.0X10+02	5.00X10-01	1.078X10-09	1.102X10-08	1.137X10-09	1.162X10-09	1.786X10-10	1.851X10-10	1.423X10-09	3.772X10-11	4.965X10-10	5.901X10-09	6.901X10-09	7.397X10-09
3.0X10+02	7.50X10-01	4.004X10-10	6.423X10-09	7.786X10-10	8.188X10-10	1.223X10-10	1.313X10-10	8.415X10-10	2.158X10-11	3.055X10-10	3.478X10-10	1.188X10-10	1.308X10-10

TABLE A.11

INTERACTION PROBABILITIES OF MUONS OF 700.0 GEV IN IRON

ENERGY TRANSFERRED IN GFV	FRACTIONAL ENERGY TRANSFER	KNOCK-ON CROSS-SECTION IN ELECTRONS PFR GM/CM**2 PER GFV	BREMSSTRAHLUNG			DIRECT PAIR PRODUCTION			PHOTONNUCLEAR			TOTAL (EXCEPT PHOTONNUCLEAR)		
			CROSS-SECTION IN NUCLEI PFR GM/CM**2 PER GEV	CROSS-SECTION IN NUCLEI PFR GM/CM**2 PER GEV	CROSS-SECTION IN NUCLEI PFR GM/CM**2 PER GEV	CROSS-SECTION IN NUCLIONS PFR GM/CM**2 PER GEV	CROSS-SECTION IN NUCLIONS PFR GM/CM**2 PER GEV	CROSS-SECTION IN NUCLIONS PFR GM/CM**2 PER GEV	CROSS-SECTION IN PARTICLES PFR GM/CM**2 PER GEV	CROSS-SECTION IN PARTICLES PFR GM/CM**2 PER GEV	CROSS-SECTION IN PARTICLES PFR GM/CM**2 PER GEV	TOTAL CROSS-SECTION IN PARTICLES PFR GM/CM**2 PER GEV		
1.0X10-02	1.42X10-05	7.057X10-01	3.526X10-04	0.0	0.0	7.060X10-01	1.921X10-01	1.921X10-01	9.337X10-02	5.715X10-02	3.955X10-02	7.060X10-01		
2.0X10-02	2.85X10-05	1.764X10-01	1.763X10-04	1.551X10-02	0.0	1.484X10-02	1.484X10-02	0.0	5.715X10-02	5.715X10-02	2.951X10-02	1.921X10-01		
3.0X10-02	4.28X10-05	7.841X10-02	1.175X10-04	1.296X10-02	0.0	1.296X10-05	1.296X10-05	0.0	1.984X10-02	1.984X10-02	1.984X10-02	9.337X10-02		
4.0X10-02	5.71X10-05	4.410X10-02	8.816X10-05	1.125X10-02	0.0	1.125X10-05	1.125X10-05	0.0	3.955X10-02	3.955X10-02	2.951X10-02	5.715X10-02		
5.0X10-02	7.14X10-05	2.822X10-02	7.052X10-05	9.851X10-03	0.0	9.851X10-05	9.851X10-05	0.0	2.951X10-02	2.951X10-02	2.951X10-02	1.921X10-01		
6.0X10-02	8.57X10-05	1.060X10-02	5.877X10-05	5.037X10-05	0.0	5.037X10-05	5.037X10-05	0.0	2.316X10-02	2.316X10-02	2.316X10-02	7.060X10-01		
7.0X10-02	1.00X10-04	1.440X10-02	1.102X10-02	4.407X10-05	0.0	4.407X10-05	4.407X10-05	0.0	1.984X10-02	1.984X10-02	1.984X10-02	1.984X10-02		
8.0X10-02	1.14X10-04	8.711X10-03	3.918X10-05	7.006X10-03	0.0	7.006X10-03	7.006X10-03	0.0	1.575X10-02	1.575X10-02	1.575X10-02	1.575X10-02		
9.0X10-02	1.28X10-04	7.056X10-03	3.526X10-05	6.358X10-03	0.0	6.358X10-03	6.358X10-03	0.0	1.345X10-02	1.345X10-02	1.345X10-02	1.345X10-02		
1.0X10-01	1.42X10-04	7.057X10-03	1.762X10-05	3.135X10-03	0.0	3.135X10-03	3.135X10-03	0.0	4.917X10-03	4.917X10-03	4.917X10-03	4.917X10-03		
2.0X10-01	2.85X10-04	1.763X10-03	1.762X10-05	1.974X10-03	0.0	1.974X10-03	1.974X10-03	0.0	2.769X10-03	2.769X10-03	2.769X10-03	2.769X10-03		
3.0X10-01	4.28X10-04	7.838X10-04	1.175X10-05	1.392X10-03	0.0	1.392X10-06	1.392X10-06	0.0	1.845X10-03	1.845X10-03	1.845X10-03	1.845X10-03		
4.0X10-01	5.71X10-04	4.08X10-04	8.811X10-06	1.050X10-03	0.0	1.050X10-03	1.050X10-03	0.0	2.429X10-06	2.429X10-06	2.429X10-06	2.429X10-06		
5.0X10-01	7.14X10-04	2.820X10-04	7.048X10-06	8.272X10-04	0.0	8.272X10-06	8.272X10-06	0.0	2.022X10-06	2.022X10-06	2.022X10-06	2.022X10-06		
6.0X10-01	8.57X10-04	1.959X10-04	5.872X10-06	6.721X10-04	0.0	6.721X10-06	6.721X10-06	0.0	1.699X10-06	1.699X10-06	1.699X10-06	1.699X10-06		
7.0X10-01	1.00X10-03	1.438X10-04	5.032X10-06	6.721X10-04	0.0	6.721X10-06	6.721X10-06	0.0	1.472X10-06	1.472X10-06	1.472X10-06	1.472X10-06		
8.0X10-01	1.14X10-03	1.101X10-04	4.403X10-06	5.590X10-05	0.0	5.590X10-05	5.590X10-05	0.0	1.299X10-06	1.299X10-06	1.299X10-06	1.299X10-06		
9.0X10-01	1.28X10-03	8.701X10-05	3.913X10-06	4.734X10-05	0.0	4.734X10-05	4.734X10-05	0.0	1.157X10-06	1.157X10-06	1.157X10-06	1.157X10-06		
1.0X10+00	1.42X10-03	7.047X10-05	3.521X10-06	4.068X10-04	0.0	4.068X10-04	4.068X10-04	0.0	1.389X10-06	1.389X10-06	1.389X10-06	1.389X10-06		
2.0X10+00	2.85X10-03	1.759X10-05	1.757X10-06	5.415X10-07	0.0	5.415X10-07	5.415X10-07	0.0	1.592X10-06	1.592X10-06	1.592X10-06	1.592X10-06		
3.0X10+00	4.28X10-03	7.807X10-06	1.170X10-06	6.890X10-05	0.0	6.890X10-05	6.890X10-05	0.0	3.436X10-07	3.436X10-07	3.436X10-07	3.436X10-07		
4.0X10+00	5.71X10-03	4.385X10-06	8.763X10-07	4.064X10-05	0.0	4.064X10-05	4.064X10-05	0.0	2.479X10-07	2.479X10-07	2.479X10-07	2.479X10-07		
5.0X10+00	7.14X10-03	2.802X10-06	6.999X10-07	2.611X10-05	0.0	2.611X10-05	2.611X10-05	0.0	2.964X10-05	2.964X10-05	2.964X10-05	2.964X10-05		
6.0X10+00	8.57X10-03	1.943X10-06	5.824X10-07	1.800X10-05	0.0	1.800X10-05	1.800X10-05	0.0	2.057X10-05	2.057X10-05	2.057X10-05	2.057X10-05		
7.0X10+00	1.00X10-02	1.425X10-06	4.984X10-07	1.298X10-05	0.0	1.298X10-05	1.298X10-05	0.0	1.301X10-07	1.301X10-07	1.301X10-07	1.301X10-07		
8.0X10+00	1.14X10-02	1.089X10-06	4.354X10-07	9.697X10-06	0.0	9.697X10-06	9.697X10-06	0.0	1.113X10-07	1.113X10-07	1.113X10-07	1.113X10-07		
9.0X10+00	1.28X10-02	8.599X10-07	3.865X10-07	7.445X10-06	0.0	7.445X10-06	7.445X10-06	0.0	9.699X10-08	9.699X10-08	9.699X10-08	9.699X10-08		
1.0X10+01	1.42X10-02	6.955X10-07	3.473X10-07	5.846X10-06	0.0	5.846X10-06	5.846X10-06	0.0	8.567X10-08	8.567X10-08	8.567X10-08	8.567X10-08		
2.0X10+01	2.85X10-02	1.713X10-07	1.063X10-07	1.063X10-07	0.0	1.063X10-07	1.063X10-07	0.0	3.734X10-08	3.734X10-08	3.734X10-08	3.734X10-08		
3.0X10+01	4.28X10-02	7.507X10-08	1.123X10-07	3.636X10-08	0.0	3.636X10-08	3.636X10-08	0.0	2.254X10-08	2.254X10-08	2.254X10-08	2.254X10-08		
4.0X10+01	5.71X10-02	4.162X10-08	8.259X10-08	1.649X10-07	0.0	1.649X10-07	1.649X10-07	0.0	2.895X10-07	2.895X10-07	2.895X10-07	2.895X10-07		
5.0X10+01	7.14X10-02	2.625X10-08	6.541X10-08	8.796X10-08	0.0	8.796X10-08	8.796X10-08	0.0	1.796X10-07	1.796X10-07	1.796X10-07	1.796X10-07		
6.0X10+01	8.57X10-02	1.796X10-08	5.371X10-08	5.207X10-08	0.0	5.207X10-08	5.207X10-08	0.0	1.328X10-07	1.328X10-07	1.328X10-07	1.328X10-07		
7.0X10+01	1.00X10-01	1.301X10-08	4.536X10-08	3.317X10-08	0.0	3.317X10-08	3.317X10-08	0.0	7.398X10-09	7.398X10-09	7.398X10-09	7.398X10-09		
8.0X10+01	1.14X10-01	9.819X10-09	3.912X10-08	2.231X10-08	0.0	2.231X10-08	2.231X10-08	0.0	6.142X10-08	6.142X10-08	6.142X10-08	6.142X10-08		
9.0X10+01	1.28X10-01	7.647X10-09	3.428X10-08	1.564X10-08	0.0	1.564X10-08	1.564X10-08	0.0	5.757X10-08	5.757X10-08	5.757X10-08	5.757X10-08		

TABLE A.12

INTERACTION PROBABILITIES OF MUONS OF 700.0 GEV IN IRON

ENERGY TRANSFERRED IN GEV	FRACTIONAL ENERGY TRANSFER	KNOCK-ON CROSS-SECTION IN ELECTRONS		BREMSSTRAHLUNG CROSS-SECTION		DIRECT PAIR PRODUCTION CROSS-SECTION		PHOTONUCLEAR CROSS-SECTION IN NUCLEONS		TOTAL (EXCFPT PHOTONUCLEAR) CROSS-SECTION IN PARTICLES PER GM/CM**2	
		PER GM/CM**2	PER PEP GEV	PER GM/CM**2	PER PEP GEV	PER GM/CM**2	PER PEP GEV	PER GM/CM**2	PER PEP GEV	PER GM/CM**2	PER PEP GEV
1.0X10+02	1.42X10-01	6.105X10-09	3.041X10-08	1.134X10-08	4.462X10-09	4.796X10-08	5.233X10-08				
2.0X10+02	2.85X10-01	1.324X10-09	1.335X10-08	1.230X10-09	1.515X10-09	1.587X10-08	1.739X10-08				
3.0X10+02	4.28X10-01	5.149X10-10	7.955X10-09	3.103X10-10	7.398X10-10	8.780X10-09	9.520X10-09				
4.0X10+02	5.71X10-01	2.570X10-10	5.500X10-09	1.172X10-10	4.361X10-10	5.875X10-09	6.311X10-09				
5.0X10+02	7.14X10-01	1.495X10-10	4.161X10-09	5.753X10-11	3.023X10-10	4.368X10-09	4.671X10-09				
6.0X10+02	8.57X10-01	9.737X10-11	3.257X10-09	3.371X10-11	2.754X10-10	3.389X10-09	3.664X10-09				

TABLE A.12

INTERACTION PROBABILITIES OF MUONS OF 1000.0 GEV IN IRON

ENERGY TRANSFERRED IN GEV	FRACTIONAL ENERGY TRANSFER	KNOCK-ON CROSS-SECTION IN ELECTRONS PER GM/CMM**2 PER GEV	BREMSSTRAHLUNG			DIRECT PAIR PRODUCTION			PHOTONNUCLEAR CROSS-SECTION IN NUCLEONS PER GM/CM**2 PER GEV			TOTAL (EXCEPT PHOTONNUCLEAR) CROSS-SECTION IN PARTICLES PER GM/CM**2 PER GEV		
			CROSS-SECTION IN NUCLEI PER GM/CM**2 PER GEV	CROSS-SECTION IN NUCLEI PER GM/CM**2 PER GEV	CROSS-SECTION IN NUCLEI PER GM/CM**2 PER GEV	CROSS-SECTION IN NUCLEI PER GM/CM**2 PER GEV								
1.0X10-02	7.057X10-01	3.526X10-04	0.0	0.0	0.0	7.060X10-01	7.060X10-01	7.060X10-01	1.031X10-01	1.031X10-01	1.031X10-01	1.031X10-01		
2.0X10-02	1.764X10-01	1.763X10-04	1.657X10-02	0.0	0.0	9.446X10-02	9.446X10-02	9.446X10-02	5.816X10-02	5.816X10-02	5.816X10-02	5.816X10-02		
3.0X10-02	3.000X10-05	7.841X10-02	1.175X10-04	1.593X10-02	0.0	5.046X10-02	5.046X10-02	5.046X10-02	4.046X10-02	4.046X10-02	4.046X10-02	4.046X10-02		
4.0X10-02	4.000X10-05	4.410X10-02	B.816X10-05	1.395X10-02	0.0	3.033X10-02	3.033X10-02	3.033X10-02	2.391X10-02	2.391X10-02	2.391X10-02	2.391X10-02		
5.0X10-02	5.000X10-05	2.822X10-02	7.053X10-05	1.216X10-02	0.0	1.953X10-02	1.953X10-02	1.953X10-02	1.639X10-02	1.639X10-02	1.639X10-02	1.639X10-02		
6.0X10-02	6.000X10-05	1.960X10-02	5.877X10-05	1.067X10-02	0.0	1.404X10-02	1.404X10-02	1.404X10-02	1.405X10-02	1.405X10-02	1.405X10-02	1.405X10-02		
7.0X10-02	7.000X10-05	1.440X10-02	5.037X10-05	9.462X10-03	0.0	3.017X10-03	3.017X10-03	3.017X10-03	3.021X10-03	3.021X10-03	3.021X10-03	3.021X10-03		
8.0X10-02	8.000X10-05	1.107X10-02	4.409X10-05	8.469X10-03	0.0	2.034X10-03	2.034X10-03	2.034X10-03	2.037X10-03	2.037X10-03	2.037X10-03	2.037X10-03		
9.0X10-02	9.000X10-05	8.712X10-03	3.919X10-05	7.644X10-03	0.0	1.495X10-03	1.495X10-03	1.495X10-03	1.495X10-03	1.495X10-03	1.495X10-03	1.495X10-03		
1.0X10-01	1.000X10-03	7.056X10-03	3.526X10-05	6.952X10-03	0.0	5.272X10-03	5.272X10-03	5.272X10-03	5.272X10-03	5.272X10-03	5.272X10-03	5.272X10-03		
2.0X10-01	2.000X10-04	1.764X10-03	1.763X10-05	3.484X10-03	0.0	5.265X10-03	5.265X10-03	5.265X10-03	5.265X10-03	5.265X10-03	5.265X10-03	5.265X10-03		
3.0X10-01	3.000X10-04	7.830X10-04	1.175X10-05	2.221X10-03	0.0	4.342X10-03	4.342X10-03	4.342X10-03	3.017X10-03	3.017X10-03	3.017X10-03	3.017X10-03		
4.0X10-01	4.000X10-04	4.409X10-04	8.813X10-06	1.584X10-03	0.0	3.217X10-03	3.217X10-03	3.217X10-03	2.034X10-03	2.034X10-03	2.034X10-03	2.034X10-03		
5.0X10-01	5.000X10-04	2.821X10-04	7.049X10-06	1.206X10-03	0.0	2.544X10-03	2.544X10-03	2.544X10-03	1.495X10-03	1.495X10-03	1.495X10-03	1.495X10-03		
6.0X10-01	6.000X10-04	1.959X10-04	5.034X10-06	9.586X10-04	0.0	2.097X10-03	2.097X10-03	2.097X10-03	1.160X10-03	1.160X10-03	1.160X10-03	1.160X10-03		
7.0X10-01	7.000X10-04	1.439X10-04	5.034X10-06	7.854X10-04	0.0	1.790X10-03	1.790X10-03	1.790X10-03	9.361X10-04	9.361X10-04	9.361X10-04	9.361X10-04		
8.0X10-01	8.000X10-04	1.101X10-04	4.404X10-06	6.583X10-04	0.0	1.543X10-03	1.543X10-03	1.543X10-03	7.745X10-04	7.745X10-04	7.745X10-04	7.745X10-04		
9.0X10-01	9.000X10-04	8.704X10-05	3.014X10-06	5.617X10-04	0.0	1.359X10-03	1.359X10-03	1.359X10-03	6.541X10-04	6.541X10-04	6.541X10-04	6.541X10-04		
1.0X10+00	1.000X10-03	7.050X10-05	3.523X10-06	4.862X10-04	0.0	1.213X10-03	1.213X10-03	1.213X10-03	5.602X10-04	5.602X10-04	5.602X10-04	5.602X10-04		
2.0X10+00	2.000X10-03	1.760X10-05	1.759X10-06	1.760X10-04	0.0	5.689X10-03	5.689X10-03	5.689X10-03	1.054X10-04	1.054X10-04	1.054X10-04	1.054X10-04		
3.0X10+00	3.000X10-03	7.817X10-06	1.171X10-06	9.141X10-05	0.0	3.637X10-03	3.637X10-03	3.637X10-03	1.004X10-04	1.004X10-04	1.004X10-04	1.004X10-04		
4.0X10+00	4.000X10-03	4.392X10-06	8.779X10-07	5.558X10-05	0.0	2.662X10-03	2.662X10-03	2.662X10-03	6.085X10-05	6.085X10-05	6.085X10-05	6.085X10-05		
5.0X10+00	5.000X10-03	2.808X10-06	7.016X10-07	3.703X10-05	0.0	2.039X10-03	2.039X10-03	2.039X10-03	4.054X10-05	4.054X10-05	4.054X10-05	4.054X10-05		
6.0X10+00	6.000X10-03	1.948X10-06	5.841X10-07	2.619X10-05	0.0	1.654X10-03	1.654X10-03	1.654X10-03	2.872X10-05	2.872X10-05	2.872X10-05	2.872X10-05		
7.0X10+00	7.000X10-03	1.430X10-06	5.001X10-07	1.934X10-05	0.0	1.385X10-03	1.385X10-03	1.385X10-03	2.141X10-05	2.141X10-05	2.141X10-05	2.141X10-05		
8.0X10+00	8.000X10-03	1.093X10-06	4.371X10-07	1.475X10-05	0.0	1.187X10-03	1.187X10-03	1.187X10-03	1.628X10-05	1.628X10-05	1.628X10-05	1.628X10-05		
9.0X10+00	9.000X10-03	8.633X10-07	3.881X10-07	1.154X10-05	0.0	1.036X10-03	1.036X10-03	1.036X10-03	1.279X10-05	1.279X10-05	1.279X10-05	1.279X10-05		
1.0X10+01	1.000X10-02	6.986X10-07	3.490X10-07	9.224X10-06	0.0	9.164X10-03	9.164X10-03	9.164X10-03	1.077X10-05	1.077X10-05	1.077X10-05	1.077X10-05		
2.0X10+01	2.000X10-02	1.726X10-07	1.726X10-07	1.726X10-06	0.0	4.033X10-03	4.033X10-03	4.033X10-03	2.207X10-06	2.207X10-06	2.207X10-06	2.207X10-06		
3.0X10+01	3.000X10-02	7.607X10-08	1.139X10-07	6.687X10-07	0.0	2.473X10-03	2.473X10-03	2.473X10-03	8.834X10-07	8.834X10-07	8.834X10-07	8.834X10-07		
4.0X10+01	4.000X10-02	4.236X10-08	8.457X10-08	3.131X10-07	0.0	1.729X10-03	1.729X10-03	1.729X10-03	4.573X10-07	4.573X10-07	4.573X10-07	4.573X10-07		
5.0X10+01	5.000X10-02	2.683X10-08	6.696X10-08	1.719X10-07	0.0	1.302X10-03	1.302X10-03	1.302X10-03	2.778X10-07	2.778X10-07	2.778X10-07	2.778X10-07		
6.0X10+01	6.000X10-02	1.845X10-08	5.523X10-08	1.033X10-07	0.0	1.028X10-03	1.028X10-03	1.028X10-03	1.873X10-07	1.873X10-07	1.873X10-07	1.873X10-07		
7.0X10+01	7.000X10-02	1.341X10-08	4.686X10-08	6.702X10-08	0.0	8.403X10-03	8.403X10-03	8.403X10-03	1.357X10-07	1.357X10-07	1.357X10-07	1.357X10-07		
8.0X10+01	8.000X10-02	1.017X10-08	4.059X10-08	4.581X10-08	0.0	7.033X10-03	7.033X10-03	7.033X10-03	1.036X10-07	1.036X10-07	1.036X10-07	1.036X10-07		
9.0X10+01	9.000X10-02	7.955X10-09	3.572X10-08	3.261X10-08	0.0	5.997X10-03	5.997X10-03	5.997X10-03	8.229X10-08	8.229X10-08	8.229X10-08	8.229X10-08		

TABLE A.13

INTERACTION PROBABILITIES OF MUONS OF 1000.0 GEV IN IRON

ENERGY TRANSFERRED IN GFV	FRACTIONAL ENERGY TRANSFER	BREMSSTRAHLUNG		DIRECT PAIR PRODUCTION		TOTAL (FXCFPT PHOTONNUCL.FAR)	
		CROSS-SECTION IN ELECTRONS	CROSS-SECTION IN NUCLEI	CROSS-SECTION IN NUCLEI	CROSS-SECTION IN NUCLEI	TOTAL CROSS-SECTION IN PARTICLES PER GM/CM**2 PFR GEV	
		PFR GM/CM**2 PER GFV	PFR GM/CM**2 PER GFV	PFR GM/CM**2 PER GFV	PFR GM/CM**2 PER GFV	TOTAL CROSS-SECTION IN PARTICLES PER GM/CM**2 PFR GEV	
1.0X10+02	1.00X10-01	6.379X10-09	3.183X10-08	2.398X10-08	5.190X10-09	6.210X10-08	
2.0X10+02	2.00X10-01	1.442X10-09	1.446X10-08	2.892X10-09	1.845X10-09	2.068X10-08	
3.0X10+02	3.00X10-01	5.816X10-10	8.841X10-09	7.699X10-10	9.791X10-10	1.117X10-08	
4.0X10+02	4.00X10-01	2.980X10-10	6.157X10-09	2.910X10-10	5.892X10-10	7.335X10-09	
5.0X10+02	5.00X10-01	1.748X10-10	4.640X10-09	1.362X10-10	3.907X10-10	5.341X10-09	
6.0X10+02	6.00X10-01	1.124X10-10	3.699X10-09	7.427X10-11	2.802X10-10	3.885X10-09	
7.0X10+02	7.00X10-01	7.738X10-11	3.073X10-09	4.558X10-11	2.179X10-10	3.196X10-09	
8.0X10+02	8.00X10-01	5.637X10-11	2.618X10-09	3.067X10-11	1.901X10-10	2.805X10-09	
9.0X10+02	9.00X10-01	4.313X10-11	2.199X10-09	2.188X10-11	0.0	2.479X10-09	

TABLE A.13

INTRACTION PROBABILITIES OF MUONS OF 2000.0 GEV IN IRON

FRACTIONAL ENERGY TRANSFERRED IN GEV	KNACK-ON CROSS-SECTION IN ELECTRONS PER GM/CM**2 PER GEV	BREMSSTRAHLUNG		DIRECT PAIR PRODUCTION		PHOTONICLAR		TOTAL (EXCEPT PHOTONICLAR)		CROSS-SECTION IN PARTICLES PER GM/CM**2 PER GEV	
		CROSS-SECTION IN NUCLEI	CROSS-SECTION IN NUCLEI	CROSS-SECTION IN NUCLEI	CROSS-SECTION IN NUCLEI	CROSS-SECTION IN NUCLEONS	CROSS-SECTION IN NUCLEONS	TOTAL	CROSS-SECTION IN PARTICLES PER GM/CM**2 PER GEV	CROSS-SECTION IN PARTICLES PER GM/CM**2 PER GEV	TOTAL
1.0X10-02	5.00X10-06	7.057X10-01	3.526X10-04	0.0	0.0	7.060X10-01	1.052X10-01	1.052X10-01	9.659X10-02	9.659X10-02	7.060X10-01
2.0X10-02	1.00X10-05	1.764X10-01	1.763X10-04	1.844X10-02	0.0	1.763X10-01	1.844X10-02	1.844X10-02	1.844X10-02	1.844X10-02	1.763X10-01
3.0X10-02	1.50X10-05	7.841X10-02	1.175X10-04	1.805X10-02	0.0	7.841X10-02	1.175X10-04	1.175X10-04	1.175X10-04	1.175X10-04	7.841X10-02
4.0X10-02	2.00X10-05	4.410X10-02	8.816X10-05	1.591X10-02	0.0	4.410X10-02	8.816X10-05	8.816X10-05	8.816X10-05	8.816X10-05	4.410X10-02
5.0X10-02	2.50X10-05	2.822X10-02	7.053X10-05	1.392X10-02	0.0	2.822X10-02	7.053X10-05	7.053X10-05	7.053X10-05	7.053X10-05	2.822X10-02
6.0X10-02	3.00X10-05	1.960X10-02	5.877X10-05	1.227X10-02	0.0	1.960X10-02	5.877X10-05	5.877X10-05	5.877X10-05	5.877X10-05	1.960X10-02
7.0X10-02	3.50X10-05	1.440X10-02	5.038X10-05	1.092X10-02	0.0	1.440X10-02	5.038X10-05	5.038X10-05	5.038X10-05	5.038X10-05	1.440X10-02
8.0X10-02	4.00X10-05	1.102X10-02	4.408X10-05	9.812X10-03	0.0	1.102X10-02	4.408X10-05	4.408X10-05	4.408X10-05	4.408X10-05	9.812X10-03
9.0X10-02	4.50X10-05	8.712X10-03	3.918X10-05	8.866X10-03	0.0	8.712X10-03	3.918X10-05	3.918X10-05	3.918X10-05	3.918X10-05	8.712X10-03
1.0X10-01	5.00X10-05	7.057X10-03	3.526X10-05	8.107X10-03	0.0	7.057X10-03	3.526X10-05	3.526X10-05	3.526X10-05	3.526X10-05	7.057X10-03
1.1X10-01	5.60X10-05	1.763X10-03	4.163X10-05	7.133X10-06	0.0	1.763X10-03	4.163X10-05	4.163X10-05	4.163X10-05	4.163X10-05	1.763X10-03
1.2X10-01	6.00X10-05	7.840X10-03	1.175X10-05	2.703X10-03	0.0	7.840X10-03	1.175X10-05	1.175X10-05	1.175X10-05	1.175X10-05	7.840X10-03
1.3X10-01	6.50X10-05	2.003X10-04	8.815X10-06	1.958X10-03	0.0	2.003X10-04	8.815X10-06	8.815X10-06	8.815X10-06	8.815X10-06	2.003X10-04
1.4X10-01	7.00X10-05	2.500X10-04	2.822X10-06	1.512X10-03	0.0	2.500X10-04	2.822X10-06	2.822X10-06	2.822X10-06	2.822X10-06	2.500X10-05
1.5X10-01	7.50X10-05	3.000X10-04	1.959X10-06	5.876X10-06	0.0	3.000X10-04	1.959X10-06	1.959X10-06	1.959X10-06	1.959X10-06	3.000X10-05
1.6X10-01	8.00X10-05	3.500X10-04	1.439X10-06	1.009X10-03	0.0	3.500X10-04	1.439X10-06	1.439X10-06	1.439X10-06	1.439X10-06	3.500X10-05
1.7X10-01	8.50X10-05	4.000X10-04	1.102X10-06	8.555X10-04	0.0	4.000X10-04	1.102X10-06	1.102X10-06	1.102X10-06	1.102X10-06	4.000X10-05
1.8X10-01	9.00X10-05	4.500X10-04	8.708X10-06	7.378X10-04	0.0	4.500X10-04	8.708X10-06	8.708X10-06	8.708X10-06	8.708X10-06	4.500X10-05
1.9X10-01	9.50X10-05	5.000X10-04	7.053X10-06	6.450X10-04	0.0	5.000X10-04	7.053X10-06	7.053X10-06	7.053X10-06	7.053X10-06	5.000X10-05
2.0X10-00	1.00X10+00	2.000X10-03	4.022X10-06	8.798X10-07	0.0	2.000X10-03	4.022X10-06	4.022X10-06	4.022X10-06	4.022X10-06	2.000X10-03
2.1X10-00	2.0X10+00	2.500X10-03	2.815X10-06	7.035X10-07	0.0	2.500X10-03	2.815X10-06	2.815X10-06	2.815X10-06	2.815X10-06	2.500X10-03
2.2X10-00	2.50X10+00	3.000X10-03	1.954X10-06	5.859X10-07	0.0	3.000X10-03	1.954X10-06	1.954X10-06	1.954X10-06	1.954X10-06	3.000X10-03
2.3X10-00	3.00X10+00	1.00X10-03	1.762X10-06	2.542X10-06	0.0	1.00X10-03	1.762X10-06	1.762X10-06	1.762X10-06	1.762X10-06	2.000X10-03
2.4X10-00	3.50X10-04	7.057X10-03	7.829X10-06	1.173X10-06	0.0	7.057X10-03	7.829X10-06	7.829X10-06	7.829X10-06	7.829X10-06	7.057X10-03
2.5X10-00	4.00X10-04	8.0X10-04	4.408X10-06	8.798X10-07	0.0	4.00X10-04	8.0X10-04	8.0X10-04	8.0X10-04	8.0X10-04	4.00X10-04
2.6X10-00	4.50X10-04	9.0X10-04	9.161X10-06	7.378X10-07	0.0	4.50X10-04	9.0X10-04	9.0X10-04	9.0X10-04	9.0X10-04	4.50X10-04
2.7X10-00	5.00X10-04	1.00X10-04	7.053X10-06	6.450X10-07	0.0	5.00X10-04	7.053X10-06	7.053X10-06	7.053X10-06	7.053X10-06	5.00X10-04
2.8X10-00	5.50X10-04	1.10X10-04	1.50X10-06	5.020X10-07	0.0	5.50X10-04	1.10X10-04	1.10X10-04	1.10X10-04	1.10X10-04	5.50X10-04
2.9X10-00	6.0X10-04	1.20X10-04	1.439X10-06	4.411X10-07	0.0	6.0X10-04	1.20X10-04	1.20X10-04	1.20X10-04	1.20X10-04	6.0X10-04
3.0X10-00	6.50X10-04	1.30X10-04	1.844X10-06	3.998X10-07	0.0	6.50X10-04	1.30X10-04	1.30X10-04	1.30X10-04	1.30X10-04	6.50X10-04
3.1X10-00	7.00X10-04	1.40X10-04	2.425X10-06	2.99X10-07	0.0	7.00X10-04	1.40X10-04	1.40X10-04	1.40X10-04	1.40X10-04	7.00X10-04
3.2X10-00	7.50X10-04	1.50X10-04	3.089X10-06	2.299X10-07	0.0	7.50X10-04	1.50X10-04	1.50X10-04	1.50X10-04	1.50X10-04	7.50X10-04
3.3X10-00	8.0X10-04	1.60X10-04	3.745X10-06	1.838X10-07	0.0	8.0X10-04	1.60X10-04	1.60X10-04	1.60X10-04	1.60X10-04	8.0X10-04
3.4X10-00	8.50X10-04	1.70X10-04	4.411X10-06	1.411X10-07	0.0	8.50X10-04	1.70X10-04	1.70X10-04	1.70X10-04	1.70X10-04	8.50X10-04
3.5X10-00	9.00X10-04	1.80X10-04	5.086X10-06	1.028X10-07	0.0	9.00X10-04	1.80X10-04	1.80X10-04	1.80X10-04	1.80X10-04	9.00X10-04
3.6X10-00	9.50X10-04	1.90X10-04	5.761X10-06	6.876X10-08	0.0	9.50X10-04	1.90X10-04	1.90X10-04	1.90X10-04	1.90X10-04	9.50X10-04
3.7X10-00	1.00X10-04	2.00X10-04	6.456X10-06	5.465X10-07	0.0	1.00X10-04	2.00X10-04	2.00X10-04	2.00X10-04	2.00X10-04	1.00X10-04
3.8X10-00	1.10X10-04	2.10X10-04	7.137X10-06	4.862X10-07	0.0	1.10X10-04	2.10X10-04	2.10X10-04	2.10X10-04	2.10X10-04	1.10X10-04
3.9X10-00	1.20X10-04	2.20X10-04	7.812X10-06	4.295X10-07	0.0	1.20X10-04	2.20X10-04	2.20X10-04	2.20X10-04	2.20X10-04	1.20X10-04
4.0X10-00	1.30X10-04	2.30X10-04	8.489X10-06	3.649X10-07	0.0	1.30X10-04	2.30X10-04	2.30X10-04	2.30X10-04	2.30X10-04	1.30X10-04
4.1X10-00	1.40X10-04	2.40X10-04	9.165X10-06	3.043X10-07	0.0	1.40X10-04	2.40X10-04	2.40X10-04	2.40X10-04	2.40X10-04	1.40X10-04
4.2X10-00	1.50X10-04	2.50X10-04	9.841X10-06	2.425X10-07	0.0	1.50X10-04	2.50X10-04	2.50X10-04	2.50X10-04	2.50X10-04	1.50X10-04
4.3X10-00	1.60X10-04	2.60X10-04	1.052X10-06	1.971X10-07	0.0	1.60X10-04	2.60X10-04	2.60X10-04	2.60X10-04	2.60X10-04	1.60X10-04
4.4X10-00	1.70X10-04	2.70X10-04	1.120X10-06	1.547X10-07	0.0	1.70X10-04	2.70X10-04	2.70X10-04	2.70X10-04	2.70X10-04	1.70X10-04
4.5X10-00	1.80X10-04	2.80X10-04	1.188X10-06	1.237X10-07	0.0	1.80X10-04	2.80X10-04	2.80X10-04	2.80X10-04	2.80X10-04	1.80X10-04
4.6X10-00	1.90X10-04	2.90X10-04	1.256X10-06	1.022X10-07	0.0	1.90X10-04	2.90X10-04	2.90X10-04	2.90X10-04	2.90X10-04	1.90X10-04
4.7X10-00	2.00X10-04	3.00X10-04	1.323X10-06	8.639X10-08	0.0	2.00X10-04	3.00X10-04	3.00X10-04	3.00X10-04	3.00X10-04	2.00X10-04
4.8X10-00	2.10X10-04	3.10X10-04	1.391X10-06	7.011X10-08	0.0	2.10X10-04	3.10X10-04	3.10X10-04	3.10X10-04	3.10X10-04	2.10X10-04
4.9X10-00	2.20X10-04	3.20X10-04	1.459X10-06	5.457X10-08	0.0	2.20X10-04	3.20X10-04	3.20X10-04	3.20X10-04	3.20X10-04	2.20X10-04
5.0X10-00	2.30X10-04	3.30X10-04	1.527X10-06	4.089X10-08	0.0	2.30X10-04	3.30X10-04	3.30X10-04	3.30X10-04	3.30X10-04	2.30X10-04
5.1X10-00	2.40X10-04	3.40X10-04	1.595X10-06	2.821X10-08	0.0	2.40X10-04	3.40X10-04	3.40X10-04	3.40X10-04	3.40X10-04	2.40X10-04
5.2X10-00	2.50X10-04	3.50X10-04	1.663X10-06	1.621X10-08	0.0	2.50X10-04	3.50X10-04	3.50X10-04	3.50X10-04	3.50X10-04	2.50X10-04
5.3X10-00	2.60X10-04	3.60X10-04	1.731X10-06	1.227X10-08	0.0	2.60X10-04	3.60X10-04	3.60X10-04	3.60X10-04	3.60X10-04	2.60X10-04
5.4X10-00	2.70X10-04	3.70X10-04	1.799X10-06	8.462X10-09	0.0	2.70X10-04	3.70X10-04	3.70X10-04	3.70X10-04	3.70X10-04	2.70X10-04
5.5X10-00	2.80X10-04	3.80X10-04	1.867X10-06	4.223X10-09	0.0	2.80X10-04	3.80X10-04	3.80X10-04	3.80X10-04	3.80X10-04	2.80X10-04
5.6X10-00	2.90X10-04	3.90X10-04	1.935X10-06	2.863X10-09	0.0	2.90X10-04	3.90X10-04	3.90X10-04	3.90X10-04	3.90X10-04	2.90X10-04
5.7X10-00	3.00X10-04	4.00X10-04	2.003X10-06	1.601X10-09	0.0	3.00X10-04	4.00X				

INTERACTION PROBABILITIES OF MUONS OF 2000.0 GEV IN IRON

ENERGY TRANSFERRED IN GFV	FRACTIONAL ENERGY TRANSFER	KNOCK-ON CROSS-SECTION IN ELECTRONS		BREMSTRÄHLUNG CROSS-SECTION IN NUCLEON		DIRECT PAIR PRODUCTION CROSS-SECTION IN NUCLEON		PHOTONNUCLEAR CROSS-SECTION IN NUCLEON		TOTAL (EXCEPT PHOTONNUCLEAR) CROSS-SECTION IN PARTICLES PER GM/CM**2 PFR GFV	
		PFR GM/CM**2 PER GFV	PER GFV	PFR GM/CM**2 PER GFV	PER GFV	PFR GM/CM**2 PER GFV	PER GFV	PFR GM/CM**2 PER GFV	PER GFV	PFR GM/CM**2 PER GFV	PER GFV
1.0X10+02	5.00X10-02	6.711X10-09	3.352X10-08	8.832X10-08	6.517X10-09	1.285X10-07	1.350X10-07	3.271X10-08	3.271X10-08	1.604X10-08	1.604X10-08
2.0X10+02	1.00X10-01	1.595X10-09	1.595X10-08	1.255X10-08	2.605X10-08	3.011X10-08	3.011X10-08	1.461X10-09	1.461X10-09	1.012X10-09	1.012X10-09
3.0X10+02	1.50X10-01	6.747X10-10	1.014X10-08	3.762X10-09	1.461X10-09	1.458X10-09	1.458X10-09	9.179X10-10	9.179X10-10	7.714X10-10	7.714X10-10
4.0X10+02	2.00X10-01	3.612X10-10	7.273X10-09	1.544X10-09	9.450X10-10	6.620X10-10	6.552X10-10	6.620X10-10	6.552X10-10	5.515X10-09	5.515X10-09
5.0X10+02	2.50X10-01	2.201X10-10	5.575X10-09	7.574X10-10	7.574X10-10	4.169X10-10	4.893X10-10	5.027X10-09	5.027X10-09	4.414X10-09	4.414X10-09
6.0X10+02	3.00X10-01	1.457X10-10	4.464X10-09	4.169X10-10	4.893X10-10	3.737X10-10	4.041X10-09	3.653X10-09	3.653X10-09	3.357X10-09	3.357X10-09
7.0X10+02	3.50X10-01	1.021X10-10	3.689X10-09	2.494X10-10	3.737X10-10	2.958X10-10	2.958X10-10	2.383X10-10	2.383X10-10	2.860X10-09	2.860X10-09
8.0X10+02	4.00X10-01	7.474X10-11	3.123X10-09	1.590X10-10	1.590X10-10	1.068X10-10	1.068X10-10	7.492X10-11	7.492X10-11	2.487X10-09	2.487X10-09
9.0X10+02	4.50X10-01	5.652X10-11	2.697X10-09	2.368X10-10	2.368X10-10	1.959X10-10	1.959X10-10	2.683X10-09	2.683X10-09	2.683X10-09	2.683X10-09
1.0X10+03	5.00X10-01	4.391X10-11									

TABLE A.14

INTERFRACTION PROBABILITIES OF MUONS OF 4000.0 GEV IN IRON

FRACTIONAL ENERGY TRANSFERRED IN GEV.	KNOCK-ON CROSS-SECTION IN ELECTRONS PFR GM/CM**2 PER GEV	BRFMSS STRAHLUNG CROSS-SECTION IN NUCLEI PFR GM/CM**2 PER GEV	DIRECT PAIR PRODUCTION CROSS-SECTION IN NUCLEI PFR GM/CM**2 PER GEV	PHOTONUCLEAR CROSS-SECTION IN NUCLEONS PFR GM/CM**2 PER GFV	TOTAL (EXCEPT PHOTONUCLEAR) CROSS-SECTION IN PARTICLFS PFR GM/CM**2 PER GFV	TOTAL CROSS-SECTION IN PARTICLFS PFR GM/CM**2 PER GEV
1.0X10-02	2.50X10-06	7.057X10-01	3.526X10-04	0.0	7.060X10-01	7.060X10-01
2.0X10-02	5.00X10-06	1.764X10-01	1.763X10-04	2.070X10-02	1.973X10-01	1.973X10-01
3.0X10-02	7.50X10-06	7.841X10-02	1.175X10-04	2.017X10-02	0.970X10-02	0.970X10-02
4.0X10-02	1.00X10-05	4.410X10-02	8.816X10-05	1.786X10-02	6.206X10-02	6.206X10-02
5.0X10-02	1.25X10-05	2.822X10-02	7.053X10-05	1.569X10-02	4.399X10-02	4.399X10-02
6.0X10-02	1.50X10-05	1.960X10-02	5.877X10-05	1.387X10-02	3.354X10-02	3.354X10-02
7.0X10-02	1.75X10-05	1.440X10-02	5.038X10-05	1.238X10-02	2.684X10-02	2.684X10-02
8.0X10-02	2.00X10-05	1.102X10-02	4.408X10-05	1.115X10-02	2.222X10-02	2.222X10-02
9.0X10-02	2.25X10-05	8.712X10-03	3.918X10-05	1.012X10-02	1.988X10-02	1.988X10-02
1.0X10-01	2.50X10-05	7.057X10-03	3.262X10-05	9.262X10-03	1.635X10-02	1.635X10-02
2.0X10-01	5.00X10-05	1.764X10-03	1.763X10-05	4.842X10-03	7.669X10-06	6.632X10-03
3.0X10-01	7.50X10-05	7.840X10-04	1.175X10-05	3.187X10-03	5.057X10-06	3.983X10-03
4.0X10-01	1.00X10-04	4.410X10-04	8.816X10-06	2.334X10-03	2.784X10-06	2.784X10-03
5.0X10-01	1.25X10-04	2.822X10-04	7.052X10-06	1.819X10-03	2.991X10-06	2.112X10-03
6.0X10-01	1.50X10-04	1.960X10-04	5.877X10-06	1.477X10-03	2.462X10-06	1.679X10-03
7.0X10-01	1.75X10-04	1.440X10-04	5.037X10-06	1.235X10-03	2.092X10-06	1.386X10-03
8.0X10-01	2.00X10-04	1.102X10-04	4.407X10-06	1.054X10-03	1.816X10-06	1.171X10-03
9.0X10-01	2.25X10-04	8.712X10-05	3.917X10-06	9.161X10-04	1.602X10-06	1.007X10-03
1.0X10+00	2.50X10-04	7.055X10-05	3.525X10-06	8.064X10-04	1.432X10-06	8.805X10-04
2.0X10+00	5.00X10-04	1.763X10-05	1.762X10-06	3.362X10-04	6.783X10-07	3.563X10-04
3.0X10+00	7.50X10-04	7.835X10-06	1.174X10-06	1.953X10-04	4.354X10-07	2.043X10-04
4.0X10+00	1.00X10-03	4.406X10-06	8.807X10-07	1.306X10-04	1.71X10-07	1.362X10-04
5.0X10+00	1.25X10-03	2.810X10-06	7.044X10-07	9.463X10-05	2.482X10-07	9.815X10-05
6.0X10+00	1.50X10-03	1.957X10-06	5.029X10-07	7.214X10-05	2.025X10-07	7.468X10-05
7.0X10+00	1.75X10-03	1.437X10-06	5.029X10-07	5.700X10-05	1.704X10-07	5.804X10-05
8.0X10+00	2.00X10-03	1.100X10-06	4.399X10-07	4.627X10-05	1.467X10-07	4.781X10-05
9.0X10+00	2.25X10-03	8.693X10-07	3.909X10-07	3.834X10-05	1.285X10-07	3.960X10-05
1.0X10+01	2.50X10-03	7.039X10-07	3.517X10-07	3.230X10-05	1.140X10-07	3.335X10-05
2.0X10+01	5.00X10-03	1.755X10-07	1.754X10-07	9.589X10-06	5.181X10-09	9.940X10-06
3.0X10+01	7.50X10-03	7.782X10-08	1.166X10-07	4.32RX10-06	4.543X10-06	4.575X10-06
4.0X10+01	1.00X10-02	4.366X10-08	8.728X10-08	2.219X10-08	2.512X10-06	2.535X10-06
5.0X10+01	1.25X10-02	2.787X10-08	6.965X10-08	1.456X10-08	1.553X10-06	1.571X10-06
6.0X10+01	1.50X10-02	1.931X10-08	5.789X10-07	1.439X10-08	1.035X10-06	1.050X10-06
7.0X10+01	1.75X10-02	1.415X10-08	4.950X10-07	6.664X10-08	7.300X10-07	7.420X10-07
8.0X10+01	2.00X10-02	1.080X10-08	4.320X10-08	4.825X10-07	1.019X10-07	5.365X10-07
9.0X10+01	2.25X10-02	8.518X10-09	3.830X10-08	3.609X10-07	4.077X10-07	4.166X10-07

INTERACTION PROBABILITIES OF MUONS OF 4000.0 GEV IN IRON

FRACTIONAL ENERGY TRANSFERRED IN GEV	KNOCK-ON CROSS-SECTION		BREMSSTRAHLUNG CROSS-SECTION		DIRECT PAIR PRODUCTION CROSS-SECTION		PHOTONNUCLEAR CROSS-SECTION		TOTAL (EXCEPT PHOTONNUCLEAR) CROSS-SECTION	
	IN ELECTRONS PER GM/CM**2	PER GFV	IN NUCLEI PER GM/CM**2	PER GFV	IN NUCLEI PER GM/CM**2	PER GFV	IN NUCLEONS PER GM/CM**2	PER GFV	PFR GM/CM**2	PFR GFV
1.0X10+02	2.50X10-02	6.492X10-09	3.439X10-08	2.772X10-07	7.769X10-09	3.263X10-07	3.195X10-07	3.263X10-07	6.675X10-08	6.675X10-08
2.0X10+02	5.00X10-02	1.678X10-09	1.677X10-08	4.503X10-08	3.266X10-09	6.348X10-08	6.348X10-08	6.348X10-08	8.24X10-08	8.24X10-08
3.0X10+02	7.50X10-02	7.273X10-10	1.091X10-08	1.468X10-08	1.923X10-09	2.632X10-08	2.632X10-08	2.632X10-08	8.45X10-08	8.45X10-08
4.0X10+02	1.00X10-01	3.990X10-10	7.990X10-09	6.462X10-09	1.308X10-09	1.495X10-08	1.495X10-08	1.495X10-08	6.16X10-08	6.16X10-08
5.0X10+02	1.25X10-01	2.491X10-10	6.243X10-09	3.364X10-09	9.557X10-10	9.857X10-09	1.081X10-08	1.081X10-08	1.081X10-08	1.081X10-08
6.0X10+02	1.50X10-01	1.687X10-10	5.084X10-09	1.951X10-09	7.331X10-10	7.204X10-09	7.937X10-09	7.937X10-09	7.937X10-09	7.937X10-09
7.0X10+02	1.75X10-01	1.209X10-10	4.261X10-09	1.220X10-09	5.820X10-10	5.602X10-09	6.184X10-09	6.184X10-09	6.184X10-09	6.184X10-09
8.0X10+02	2.00X10-01	9.036X10-11	3.647X10-09	8.069X10-09	4.739X10-10	4.544X10-09	5.018X10-09	5.018X10-09	5.018X10-09	5.018X10-09
9.0X10+02	2.25X10-01	6.967X10-11	3.174X10-09	5.570X10-09	3.924X10-10	3.801X10-09	4.193X10-09	4.193X10-09	4.193X10-09	4.193X10-09
1.0X10+03	2.50X10-01	5.508X10-11	2.798X10-09	3.980X10-10	3.317X10-10	3.251X10-09	3.583X10-09	3.583X10-09	3.583X10-09	3.583X10-09
2.0X10+03	5.00X10-01	1.100X10-11	1.197X10-09	4.022X10-11	9.782X10-11	1.248X10-09	1.346X10-09	1.346X10-09	1.346X10-09	1.346X10-09
3.0X10+03	7.50X10-01	4.149X10-12	7.634X10-10	1.117X10-11	5.006X10-11	7.787X10-10	8.287X10-10	8.287X10-10	8.287X10-10	8.287X10-10

TABLE A.15

INTERACTION PROBABILITIES OF MUONS ON 7000.0 GEV IN IRON

ENERGY TRANSFERRED IN GEV	FRACTIONAL ENERGY TRANSFERRED	KNOCK-ON CROSS-SECTION IN ELECTRONS PER GM/CM**2	BREMSTRÄHLUNG CROSS-SECTION IN NUCLEI PER GM/CM**2	DIRECT PAIR PRODUCTION CROSS-SECTION IN NUCLEI PER GM/CM**2	PHOTONNUCLEAR CROSS-SECTION IN NUCLEI PER GM/CM**2	TOTAL (FXCEPT PHOTONNUCLEAR) CROSS-SECTION IN PARTICLFS. PER GM/CM**2		TOTAL (FXCEPT PHOTONNUCLEAR) CROSS-SECTION IN PARTICLFS. PER GM/CM**2	
						PER GEV	PER GFV	PER GEV	PER GFV
1.0X10-02	1.42X10-06	7.057X10-01	3.526X10-04	0.0	0.0	7.060X10-01	7.060X10-01	1.989X10-01	1.989X10-01
2.0X10-02	2.85X10-06	1.764X10-01	1.763X10-04	2.237X10-02	0.0	1.004X10-01	1.004X10-01	1.004X10-01	1.004X10-01
3.0X10-02	4.28X10-06	7.841X10-02	1.175X10-04	2.188X10-02	0.0	6.363X10-02	6.363X10-02	6.363X10-02	6.363X10-02
4.0X10-02	5.71X10-06	4.410X10-02	8.816X10-05	1.943X10-02	0.0	4.541X10-02	4.541X10-02	4.541X10-02	4.541X10-02
5.0X10-02	7.14X10-06	2.822X10-02	7.053X10-05	1.711X10-02	0.0	3.483X10-02	3.483X10-02	3.483X10-02	3.483X10-02
6.0X10-02	8.57X10-06	1.960X10-02	5.877X10-05	1.517X10-02	0.0	2.802X10-02	2.802X10-02	2.802X10-02	2.802X10-02
7.0X10-02	1.00X10-05	1.440X10-02	5.039X10-05	1.356X10-02	0.0	2.331X10-02	2.331X10-02	2.331X10-02	2.331X10-02
8.0X10-02	1.14X10-05	1.102X10-02	4.408X10-05	1.224X10-02	0.0	1.988X10-02	1.988X10-02	1.988X10-02	1.988X10-02
9.0X10-02	1.28X10-05	8.712X10-03	3.918X10-05	1.113X10-02	0.0	1.728X10-02	1.728X10-02	1.728X10-02	1.728X10-02
1.0X10-01	1.42X10-05	7.057X10-03	3.526X10-05	1.019X10-02	0.0005	1.730X10-02	1.730X10-02	1.730X10-02	1.730X10-02
2.0X10-01	2.85X10-05	1.764X10-03	1.763X10-05	5.391X10-03	8.116X10-06	7.173X10-03	7.173X10-03	7.173X10-03	7.173X10-03
3.0X10-01	4.28X10-05	7.841X10-04	1.175X10-05	3.577X10-03	5.353X10-06	4.373X10-03	4.373X10-03	4.373X10-03	4.373X10-03
4.0X10-01	5.71X10-05	4.410X10-04	8.816X10-06	2.637X10-03	3.975X10-06	3.097X10-03	3.097X10-03	3.097X10-03	3.097X10-03
5.0X10-01	7.14X10-05	2.822X10-04	7.053X10-06	2.068X10-03	3.152X10-06	2.357X10-03	2.357X10-03	2.357X10-03	2.357X10-03
6.0X10-01	8.57X10-05	1.960X10-04	5.877X10-06	1.688X10-03	2.604X10-06	1.889X10-03	1.889X10-03	1.889X10-03	1.889X10-03
7.0X10-01	1.00X10-04	1.440X10-04	5.037X10-06	1.417X10-03	2.215X10-06	1.566X10-03	1.566X10-03	1.566X10-03	1.566X10-03
8.0X10-01	1.14X10-04	1.102X10-04	4.407X10-06	1.216X10-03	1.924X10-06	1.330X10-03	1.330X10-03	1.330X10-03	1.330X10-03
9.0X10-01	1.28X10-04	8.711X10-05	3.918X10-06	1.060X10-03	1.698X10-06	1.151X10-03	1.151X10-03	1.151X10-03	1.151X10-03
1.0X10+00	1.42X10-04	7.056X10-05	3.526X10-06	9.372X10-04	1.518X10-06	1.011X10-03	1.011X10-03	1.011X10-03	1.011X10-03
2.0X10+00	2.85X10-04	1.960X10-04	5.877X10-06	4.034X10-04	7.229X10-07	4.236X10-04	4.236X10-04	4.236X10-04	4.236X10-04
3.0X10+00	4.28X10-04	7.841X10-04	1.175X10-06	4.203X10-04	4.651X10-07	2.498X10-04	2.498X10-04	2.498X10-04	2.498X10-04
4.0X10+00	5.71X10-04	4.410X10-04	8.816X10-06	4.811X10-04	1.663X10-07	1.699X10-04	1.699X10-04	1.699X10-04	1.699X10-04
5.0X10+00	7.14X10-04	2.822X10-04	7.053X10-06	7.048X10-04	1.213X10-07	1.249X10-04	1.249X10-04	1.249X10-04	1.249X10-04
6.0X10+00	8.57X10-04	1.960X10-04	5.877X10-06	5.872X10-07	9.421X10-05	2.169X10-07	9.676X10-05	9.676X10-05	9.676X10-05
7.0X10+00	1.00X10-04	1.440X10-04	1.763X10-05	1.762X10-06	4.034X10-04	7.571X10-05	7.765X10-05	7.765X10-05	7.765X10-05
8.0X10+00	1.14X10-04	1.102X10-04	6.408X10-06	6.403X10-07	6.243X10-05	6.576X10-07	6.493X10-05	6.493X10-05	6.493X10-05
9.0X10+00	1.28X10-04	8.711X10-05	2.920X10-06	7.048X10-07	3.913X10-07	3.393X10-07	3.377X10-05	3.377X10-05	3.377X10-05
1.0X10+01	1.42X10-04	7.056X10-05	7.056X10-06	5.872X10-07	4.696X10-07	2.653X10-07	4.592X10-05	4.592X10-05	4.592X10-05
2.0X10+01	2.85X10-04	1.960X10-04	1.763X10-05	1.762X10-06	4.034X10-04	7.571X10-05	7.828X10-05	7.828X10-05	7.828X10-05
3.0X10+01	4.28X10-04	7.841X10-04	1.175X10-06	4.403X10-07	6.243X10-05	6.576X10-07	6.493X10-05	6.493X10-05	6.493X10-05
4.0X10+01	5.71X10-04	4.410X10-04	8.816X10-06	4.811X10-07	5.251X10-05	1.382X10-07	5.377X10-05	5.377X10-05	5.377X10-05
5.0X10+01	7.14X10-04	2.822X10-04	7.053X10-06	7.048X10-07	3.521X10-05	1.228X10-07	4.592X10-05	4.592X10-05	4.592X10-05
6.0X10+01	8.57X10-04	1.960X10-04	1.958X10-06	5.872X10-07	4.490X10-05	5.638X10-08	1.525X10-05	1.525X10-05	1.525X10-05
7.0X10+01	1.00X10-04	1.440X10-04	1.438X10-06	5.033X10-07	7.571X10-05	1.828X10-07	7.765X10-05	7.765X10-05	7.765X10-05
8.0X10+01	1.14X10-04	1.102X10-04	1.101X10-06	4.403X10-07	6.243X10-05	6.576X10-07	6.493X10-05	6.493X10-05	6.493X10-05
9.0X10+01	1.28X10-04	8.711X10-05	8.701X10-07	7.048X10-07	5.251X10-05	1.382X10-07	5.377X10-05	5.377X10-05	5.377X10-05
1.0X10+02	1.42X10-04	7.047X10-05	7.047X10-07	3.521X10-07	4.496X10-05	1.228X10-07	4.592X10-05	4.592X10-05	4.592X10-05
2.0X10+02	2.85X10-04	1.759X10-05	1.758X10-07	1.758X10-07	1.490X10-05	5.638X10-08	1.525X10-05	1.525X10-05	1.525X10-05
3.0X10+02	4.28X10-04	4.28X10-05	7.807X10-07	7.807X10-07	7.331X10-06	3.549X10-08	7.552X10-06	7.552X10-06	7.552X10-06
4.0X10+02	5.71X10-04	5.71X10-05	4.101X10-06	4.101X10-06	4.281X10-06	2.548X10-08	4.412X10-06	4.412X10-06	4.412X10-06
5.0X10+02	7.14X10-04	7.14X10-05	3.903X10-07	3.903X10-07	2.759X10-06	1.968X10-08	2.857X10-06	2.857X10-06	2.857X10-06
6.0X10+02	8.57X10-04	8.57X10-05	1.943X10-08	1.943X10-08	5.827X10-07	1.898X10-08	1.976X10-06	1.976X10-06	1.976X10-06
7.0X10+02	1.00X10-04	1.00X10-05	1.428X10-08	1.428X10-08	4.987X10-08	1.368X10-08	1.433X10-06	1.433X10-06	1.433X10-06
8.0X10+02	1.14X10-04	1.14X10-05	1.090X10-08	1.090X10-08	4.358X10-08	1.022X10-08	1.135X10-06	1.135X10-06	1.135X10-06
9.0X10+02	1.28X10-04	1.28X10-05	8.601X10-09	8.601X10-09	3.868X10-07	7.854X10-09	8.426X10-07	8.426X10-07	8.426X10-07

TABLE A.16

INTERACTION PROBABILITIES OF MUONS OF 7000.0 GEV IN IRON

ENERGY TRANSFERRED IN GFV	FRACTIONAL ENERGY TRANSFER	KNOCK-ON CROSS-SECTION IN ELECTRONS		DIRECT PAIR PRODUCTION IN NUCLEI		PHOTONUCLEAR CROSS-SECTION IN NUCLEONS		TOTAL (FXCFPT PHOTONUCLEAR) CROSS-SECTION IN PARTICLFS PER GM/CM**2 PER GEV	
		PFR GM/CM**2	PFR GFV	PFR GM/CM**2	PFR GFV	PFR GM/CM**2	PFR GFV	PFR GM/CM**2	PFR GFV
1.0X10+02	1.42X10-02	6.957X10-09	3.476X10-08	6.176X10-07	8.713X10-09	6.593X10-07	6.680X10-07	1.325X10-07	1.363X10-07
2.0X10+02	2.85X10-02	1.713X10-09	1.713X10-08	1.126X10-07	3.934X10-08	2.276X10-09	5.134X10-09	5.364X10-09	5.364X10-09
3.0X10+02	3.0X10+02	4.28X10-02	7.512X10-10	8.331X10-09	1.006X10-08	1.573X10-09	2.680X10-08	2.838X10-08	2.838X10-08
4.0X10+02	5.71X10-02	4.165X10-10	4.165X10-10	6.573X10-09	9.739X10-09	1.174X10-09	1.657X10-09	1.774X10-09	1.774X10-09
5.0X10+02	7.14X10-02	7.14X10-02	2.628X10-10	5.402X10-09	5.825X10-09	9.193X10-10	1.140X10-09	1.232X10-09	1.232X10-09
6.0X10+02	8.57X10-02	1.799X10-10	4.568X10-09	3.747X10-09	7.444X10-10	8.446X10-09	9.190X10-09	9.190X10-09	9.190X10-09
7.0X10+02	1.00X10-01	1.303X10-10	3.944X10-09	2.543X10-09	6.178X10-10	6.586X10-09	7.204X10-09	7.204X10-09	7.204X10-09
8.0X10+02	1.14X10-01	9.836X10-11	3.459X10-09	1.799X10-09	5.223X10-10	5.335X10-09	5.858X10-09	5.858X10-09	5.858X10-09
9.0X10+02	1.28X10-01	7.662X10-11	3.073X10-09	1.315X10-09	4.485X10-10	4.450X10-09	4.898X10-09	4.898X10-09	4.898X10-09
1.0X10+03	1.42X10-01	6.119X10-11	2.885X10-09	1.520X10-10	1.521X10-10	1.520X10-09	1.681X10-09	1.681X10-09	1.681X10-09
2.0X10+03	2.0X10+03	1.331X10-11	1.363X10-09	1.520X10-10	1.521X10-10	1.520X10-09	1.488X10-10	1.488X10-10	1.488X10-10
3.0X10+03	3.0X10+03	5.195X10-01	8.293X10-12	3.95X10-11	7.435X10-11	8.744X10-10	9.488X10-10	9.488X10-10	9.488X10-10
4.0X10+03	4.0X10+03	5.71X10-01	2.606X10-12	5.883X10-10	1.547X10-11	4.379X10-11	6.063X10-10	6.501X10-10	6.501X10-10
5.0X10+03	7.14X10-01	1.523X10-12	4.634X10-10	7.741X10-12	3.037X10-11	4.727X10-10	5.031X10-10	5.031X10-10	5.031X10-10
6.0X10+03	8.57X10-01	9.975X10-13	3.924X10-10	4.691X10-12	2.773X10-11	3.981X10-10	4.259X10-10	4.259X10-10	4.259X10-10

TABLE A.16

INTERACTION PROBABILITIES OF MUONS OF 10000.0 GEV IN IRON

ENERGY TRANSFERRED IN GEV	FRACTIONAL ENERGY TRANSFER	BREMSTRÄHLUNG CROSS-SECTION IN ELECTRONS		DIRECT PAIR PRODUCTION CROSS-SECTION		PHOTONNUCLEAR CROSS-SECTION IN NUCLEONS		TOTAL (EXCEPT PHOTONNUCLEAR) CROSS-SECTION IN PARTICLES PER GM/CM**2		TOTAL CROSS-SECTION IN PARTICLES PER GM/CM**2	
		PFR GM/CM**2 PER GEV	PFR GM/CM**2 PER GFV	CROSS-SECTION IN NUCLEI	PFR GM/CM**2 PER GFV	CROSS-SECTION IN NUCLEONS	PFR GM/CM**2 PER GFV	CROSS-SECTION IN NUCLEI	PFR GM/CM**2 PER GFV	CROSS-SECTION IN NUCLEONS	PFR GM/CM**2 PER GFV
1.0X10-02	1.00X10-06	7.057X10-01	3.526X10-04	0.0	0.0	7.060X10-01	2.000X10-01	7.060X10-01	2.000X10-01	7.060X10-01	2.000X10-01
2.0X10-02	2.00X10-06	1.764X10-01	1.763X10-04	2.344X10-02	2.297X10-02	0.0	1.015X10-01	1.015X10-01	1.015X10-01	1.015X10-01	1.015X10-01
3.0X10-02	3.00X10-06	7.841X10-02	1.175X10-04	0.0	0.0	8.16X10-05	2.044X10-02	6.463X10-02	6.463X10-02	6.463X10-02	6.463X10-02
4.0X10-02	4.00X10-06	4.410X10-02	7.053X10-05	1.802X10-02	0.0	0.0	4.632X10-02	4.632X10-02	4.632X10-02	4.632X10-02	4.632X10-02
5.0X10-02	5.00X10-06	2.822X10-02	5.877X10-05	1.599X10-02	0.0	0.0	3.566X10-02	3.566X10-02	3.566X10-02	3.566X10-02	3.566X10-02
6.0X10-02	6.00X10-06	1.060X10-02	5.038X10-05	1.432X10-02	0.0	0.0	2.877X10-02	2.877X10-02	2.877X10-02	2.877X10-02	2.877X10-02
7.0X10-02	7.00X10-06	1.440X10-02	4.408X10-05	1.293X10-02	0.0	0.0	2.400X10-02	2.400X10-02	2.400X10-02	2.400X10-02	2.400X10-02
8.0X10-02	8.00X10-06	1.102X10-02	3.913X10-05	1.177X10-02	0.0	0.0	2.052X10-02	2.052X10-02	2.052X10-02	2.052X10-02	2.052X10-02
9.0X10-02	9.00X10-06	8.712X10-03	7.057X10-03	3.526X10-02	4.778X10-02	4.778X10-02	1.789X10-02	1.789X10-02	1.789X10-02	1.789X10-02	1.789X10-02
1.0X10-01	1.00X10-05	1.763X10-03	1.763X10-05	5.740X10-03	8.385X10-03	8.385X10-03	7.522X10-03	7.531X10-03	7.531X10-03	7.531X10-03	7.531X10-03
2.0X10-01	2.00X10-05	7.841X10-04	1.175X10-05	3.825X10-03	5.533X10-06	5.533X10-06	4.621X10-03	4.627X10-03	4.627X10-03	4.627X10-03	4.627X10-03
3.0X10-01	3.00X10-05	4.410X10-04	8.816X10-06	2.831X10-03	4.119X10-06	4.119X10-06	3.281X10-03	3.285X10-03	3.285X10-03	3.285X10-03	3.285X10-03
4.0X10-01	4.00X10-05	2.822X10-04	7.053X10-06	2.226X10-03	3.266X10-06	3.266X10-06	2.515X10-03	2.519X10-03	2.519X10-03	2.519X10-03	2.519X10-03
5.0X10-01	5.00X10-05	1.960X10-04	5.877X10-06	1.822X10-03	2.699X10-06	2.699X10-06	2.024X10-03	2.026X10-03	2.026X10-03	2.026X10-03	2.026X10-03
6.0X10-01	6.00X10-05	1.440X10-04	5.037X10-06	1.543X10-03	2.796X10-06	2.796X10-06	1.683X10-03	1.685X10-03	1.685X10-03	1.685X10-03	1.685X10-03
7.0X10-01	7.00X10-05	1.02X10-04	4.408X10-06	1.319X10-03	1.994X10-06	1.994X10-06	1.433X10-03	1.435X10-03	1.435X10-03	1.435X10-03	1.435X10-03
8.0X10-01	8.00X10-05	9.00X10-05	3.918X10-06	1.152X10-03	1.761X10-06	1.761X10-06	1.243X10-03	1.245X10-03	1.245X10-03	1.245X10-03	1.245X10-03
9.0X10-01	9.00X10-05	7.056X10-05	3.526X10-06	1.020X10-03	1.575X10-06	1.575X10-06	1.044X10-03	1.046X10-03	1.046X10-03	1.046X10-03	1.046X10-03
1.0X10+00	1.00X10-04	7.12X10-05	2.0X10-04	4.464X10-04	7.501X10-07	7.501X10-07	4.658X10-04	4.666X10-04	4.666X10-04	4.666X10-04	4.666X10-04
2.0X10+00	2.00X10-04	1.764X10-05	1.763X10-06	1.175X10-06	2.692X10-04	2.692X10-04	1.319X10-04	1.333X10-04	1.333X10-04	1.333X10-04	1.333X10-04
3.0X10+00	3.00X10-04	7.839X10-06	7.839X10-06	4.408X10-06	8.183X10-07	8.183X10-07	1.960X10-04	1.971X10-04	1.971X10-04	1.971X10-04	1.971X10-04
4.0X10+00	4.00X10-04	4.09X10-06	4.09X10-06	7.049X10-06	7.387X10-07	7.387X10-07	3.073X10-07	3.073X10-07	3.073X10-07	3.073X10-07	3.073X10-07
5.0X10+00	5.00X10-04	5.00X10-06	2.812X10-06	7.049X10-07	7.681X10-07	7.681X10-07	1.422X10-04	1.425X10-04	1.425X10-04	1.425X10-04	1.425X10-04
6.0X10+00	6.00X10-04	1.959X10-06	5.874X10-07	1.086X10-04	2.264X10-07	2.264X10-07	1.112X10-04	1.114X10-04	1.114X10-04	1.114X10-04	1.114X10-04
7.0X10+00	7.00X10-04	5.034X10-06	5.034X10-07	8.804X10-05	1.909X10-07	1.909X10-07	8.98X10-05	9.017X10-05	9.017X10-05	9.017X10-05	9.017X10-05
8.0X10+00	8.00X10-04	1.01X10-06	4.404X10-07	7.315X10-05	1.647X10-07	1.647X10-07	7.486X10-05	7.486X10-05	7.486X10-05	7.486X10-05	7.486X10-05
9.0X10+00	9.00X10-04	8.705X10-07	3.915X10-07	6.198X10-05	1.445X10-07	1.445X10-07	6.324X10-05	6.338X10-05	6.338X10-05	6.338X10-05	6.338X10-05
1.0X10+01	1.00X10-03	7.050X10-07	3.523X10-07	5.333X10-05	1.285X10-07	1.285X10-07	5.439X10-05	5.452X10-05	5.452X10-05	5.452X10-05	5.452X10-05
2.0X10+01	2.00X10-03	1.760X10-07	1.750X10-07	1.876X10-05	5.912X10-08	5.912X10-08	1.911X10-05	1.917X10-05	1.917X10-05	1.917X10-05	1.917X10-05
3.0X10+01	3.00X10-03	7.818X10-08	1.172X10-07	9.640X10-06	3.745X10-08	3.745X10-08	9.873X10-06	9.873X10-06	9.873X10-06	9.873X10-06	9.873X10-06
4.0X10+01	4.00X10-03	4.393X10-08	8.781X10-08	5.831X10-06	2.696X10-08	2.696X10-08	5.963X10-06	5.990X10-06	5.990X10-06	5.990X10-06	5.990X10-06
5.0X10+01	5.00X10-03	2.808X10-08	7.018X10-08	3.872X10-06	2.086X10-08	2.086X10-08	3.971X10-06	3.991X10-06	3.991X10-06	3.991X10-06	3.991X10-06
6.0X10+01	6.00X10-03	1.948X10-08	5.842X10-08	2.734X10-06	1.689X10-08	1.689X10-08	2.812X10-06	2.829X10-06	2.829X10-06	2.829X10-06	2.829X10-06
7.0X10+01	7.00X10-03	1.430X10-08	5.002X10-08	2.017X10-06	1.412X10-08	1.412X10-08	2.081X10-06	2.095X10-06	2.095X10-06	2.095X10-06	2.095X10-06
8.0X10+01	8.00X10-03	1.093X10-08	4.373X10-08	1.537X10-06	1.209X10-08	1.209X10-08	1.597X10-06	1.604X10-06	1.604X10-06	1.604X10-06	1.604X10-06
9.0X10+01	9.00X10-03	8.634X10-09	3.883X10-08	1.202X10-06	1.053X10-08	1.053X10-08	1.250X10-06	1.260X10-06	1.260X10-06	1.260X10-06	1.260X10-06

TABLE A.17

INTERACTION PROBABILITIES OF MUONS OF 10000.0 GEV IN IRON

ENERGY TRANSFER IN GFV	FRACTIONAL ENERGY TRANSFER	KNOCK-ON CROSS-SECTION IN FLFCTRNS		BREMSTRÄHLUNG CROSS-SECTION IN NUCLF1		DIRECT PAIR PRODUCTION CROSS-SECTION IN NUCLEI		PHOTONNUCLEAR CROSS-SECTION IN NUCLEONS		TOTAL (EXCEPT PHOTONNUCLEAR) CROSS-SECTION IN PARTICLES PER GM/CM**2 PER GFV	
		PFR	GM/CM**2	PFR	GM/CM**2	PFR	GM/CM**2	PFR	GM/CM**2	PFR	GM/CM**2
1.0X10+02	1.00X10-02	6.987X10-09		3.491X10-08		9.607X10-07		9.311X10-09		1.002X10-06	
2.0X10+02	2.00X10-02	1.729X10-09		1.728X10-08		1.942X10-07		4.078X10-09		2.139X10-07	
3.0X10+02	3.00X10-02	7.609X10-10		1.140X10-08		7.046X10-08		2.494X10-09		8.263X10-08	
4.0X10+02	4.00X10-02	4.237X10-10		8.473X10-09		3.322X10-08		1.741X10-09		4.212X10-08	
5.0X10+02	5.00X10-02	2.685X10-10		6.712X10-09		1.827X10-08		1.310X10-09		2.525X10-08	
6.0X10+02	6.00X10-02	1.846X10-10		5.532X10-09		1.111X10-08		1.035X10-09		1.683X10-08	
7.0X10+02	7.00X10-02	1.342X10-10		4.702X10-09		7.252X10-09		8.450X10-10		1.208X10-08	
8.0X10+02	8.00X10-02	1.017X10-10		4.075X10-09		4.987X10-09		7.070X10-10		9.164X10-09	
9.0X10+02	9.00X10-02	7.963X10-11		3.587X10-09		3.571X10-09		6.027X10-10		7.238X10-09	
1.0X10+03	1.00X10-01	6.386X10-11		3.198X10-09		2.640X10-09		5.214X10-10		5.903X10-09	
2.0X10+03	2.00X10-01	1.446X10-11		1.461X10-09		3.338X10-10		1.892X10-10		1.810X10-09	
3.0X10+03	3.00X10-01	5.839X10-12		9.003X10-10		9.214X10-11		9.820X10-11		9.983X10-10	
4.0X10+03	4.00X10-01	2.997X10-12		6.327X10-10		3.580X10-11		5.909X10-11		6.715X10-10	
5.0X10+03	5.00X10-01	1.767X10-12		4.825X10-10		1.710X10-11		3.918X10-11		5.014X10-10	
6.0X10+03	6.00X10-01	1.135X10-12		3.909X10-10		9.471X10-12		2.810X10-11		4.015X10-10	
7.0X10+03	7.00X10-01	7.838X10-13		3.325X10-10				2.187X10-11		3.610X10-10	
8.0X10+03	8.00X10-01	5.724X10-13		2.941X10-10				1.910X10-11		3.178X10-10	
9.0X10+03	9.00X10-01	4.391X10-13		2.663X10-10				0.0		2.697X10-10	

TABLE A.17

APPENDIX B

THE FOUR-MOMENTUM TRANSFER SQUARED (q^2 OR t)

The four-momentum transfer squared (referred to as t , where $t = |q^2|$) is a very useful quantity in the description of any interaction process because it is Lorentz invariant. In the bremsstrahlung and direct pair production processes discussed in Chapter 2, the integration over the variable t was performed by the authors of the theories and formulae. However, in the photonuclear process the integration had to be performed numerically by this worker.

Consider Figure B.1 where a muon of momentum P_μ and energy E_μ travelling along the x -axis, interacts with a nucleon via a photon exchange, and is scattered in the $x-y$ plane at an angle θ .

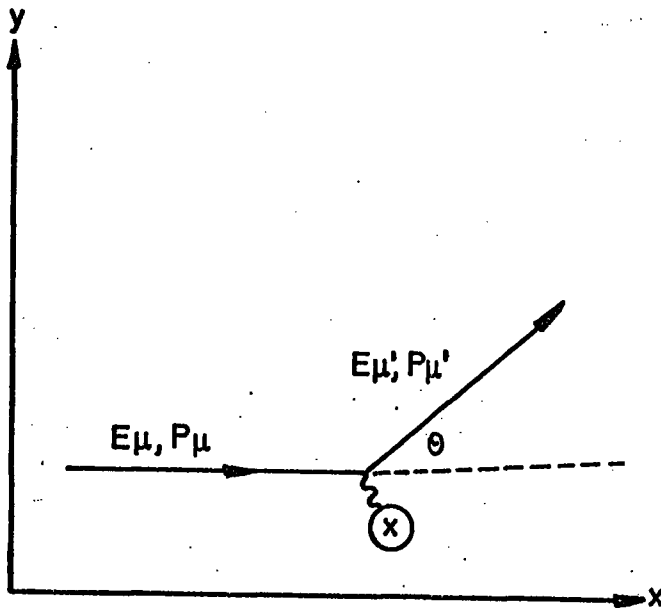


FIGURE B.1. Muon scattering by photoproduction.

The four-momentum (P_4^c) before collision is

$$P_4^c = (P_\mu^c, 0, 0, iE_\mu) \quad (B.1)$$

and the four-momentum (P'_4^c) after the collision is

$$P'_4^c = (P'_\mu^c \cos \theta, P'_\mu^c \sin \theta, 0, iE'_\mu). \quad (B.2)$$

Therefore, the four-momentum transferred is

$$q = P_4^c - P'_4^c = (P_\mu^c - P'_\mu^c \cos \theta, -P'_\mu^c \sin \theta, 0, i(E_\mu - E'_\mu)). \quad (B.3)$$

If Equation B.3 is squared, it gives t or the four-momentum transfer squared.

$$\begin{aligned} t = |q^2| &= |(P_\mu^c - P'_\mu^c \cos \theta)^2 + (P'_\mu^c \sin \theta)^2 \\ &\quad - (E_\mu - E'_\mu)^2| \end{aligned} \quad (B.4)$$

which reduces to

$$t = |q^2| = |2E_\mu E'_\mu - 2M^2 c^4 - 2P_\mu^c P'_\mu^c \cos \theta| \quad (B.5)$$

where $M^2 c^2$ is the muon rest mass.

t is often referred to as the mass of the virtual photon and can be either space-like or time-like. The minimum t will occur when $\theta = 0$, the case of forward scattering. If in Equation B.5, θ is set equal to zero and it is assumed that $(E'/Mc^2) \gg 1$, then it is simple to obtain the minimum t .

$$t_{\text{MIN}} = \frac{M^2 c^4 E_t^2}{E_\mu (E_\mu - E_t)} \quad (B.6)$$

where $E_t = E_\mu - E'_\mu$.

REFERENCES

- Allkofer, O. C., Grupen, C., 1970, VI Interam. Sem. Cosmic Rays, IV, 1085.
- Allkofer, O. C., Grupen, C., Stamm, W., 1971, Phys. Rev. D, 4, 638.
- Allkofer, O. C., Backer, A., Garstensen, K., Dau, W. D., Grupen, C., Jokisch, H., Meyer, H. J., Stamm, W., 1974, Proc. Int. Cosmic Ray Symposium, Tokyo (Tokyo:University of Tokyo), 350.
- Alexander, D., Thompson, M. G., Turner, M. J. L., Wolfendale, A. W., 1970, Acta Phys. Sci. Hung., 29, Suppl. 4, 215.
- Anderson, C. D., 1932, Science, 76, 238.
- Anderson, G. D., Neddermeyer, S. H., 1938, Phys. Rev., 54, 88.
- Anderson, H. H., Sorensen, H., Vadja, P., 1969, Phys. Rev., 180, 373.
- Ashton, F., Coats, R. B., 1965, Proc. Int. Conf. Cosmic Rays, London, 2, 959.
- Ashton, F., Coats, R. B., Holyoak, B., Simpson, D. A., Thompson, M. G., 1965, Nucl. Instr. and Meth., 37, 181.
- Ashton, F., Coats, R. B., Simpson, D. A., 1968, Canad. J. Phys., 46, 363.
- Auger, P., Ehrenfest, P., 1934, C. R. Acad. Sci. Paris, 204, 257.
- Ayre, C. A., Breare, J. M., Holroyd, F. W., Thompson, M. G., Wells, S. C., Wolfendale, A. W., 1970, Acta Physica Academiae Scientiarum Hungaricae, 29, Suppl. 4, 547.
- Ayre, C. A., Thompson, M. G., 1969, Nucl. Instr. and Meth., 69, 106.
- Ayre, C. A., Grupen, C., Hamdan, M. A., Hume, C. J., Thompson, M. G., Wells, S. C., Wolfendale, A. W., 1971, Proc. 12th Int. Conf. on Cosmic Rays, Hobart, 4, 1447.
- Ayre, C. A., 1971, Ph.D. Thesis, University of Durham.
- Ayre, C. A., Thompson, M. G., Whalley, M. R., Young, E. C. M., 1972, Nuc. Instr. and Meth., 103, 49.
- Ayre, C. A., Hamdan, M. A., Hume, S. J., Stubbs, F. W., Thompson, M. G., Wells, S. C., Whalley, M. R., 1972(a), Nuc. Instr. and Meth., 102, 19.
- Ayre, C. A., Hamdan, M. A., Hume, S. J., Stubbs, F. W., Thompson, M. G., Nandi, B. C., 1972 (b), Nuc. Instr. and Meth., 102, 19.
- Backenstross, G., Hyams, B. D., Knop, G., Marin, P. C., Stierlin, U., 1963, Phys. Rev., 129, 2759.

- Baruch, J. E. F., 1973, Ph.D. Thesis, University of Leeds.
- Barton, J. C., Rogers, I. W., Thompson, M. G., 1965, Proc. Int. Conf. Cosmic Rays, London, 2, 970.
- Barton, J. C., Rogers, I. W., Thompson, M. G., 1966, Proc. Roy. Soc., 87, 101.
- Bethe, H., Heitler, W., 1934, Proc. Roy. Soc., 146A, 83.
- Bethe, H., 1934, Proc. Cambridge Phil. Soc., 30, 524.
- Bhabha, H. J., 1935, Proc. Roy. Soc., 152A, 559.
- Bhabha, H. J., 1935, Proc. Roy. Soc., 152A, 394.
- Bhabha, H. J., 1938, Proc. Roy. Soc., 164A, 257.
- Bohm, E., Nagano, M., Van Staa, P., Trumper, J., 1971, Proc. Int. Conf. Cosmic Rays, Hobart, 4, 1438.
- Bohm, E., Nagano, M., 1973, J. Phys. A, 6, 1262.
- Bothe, W., Kolhorster, W., 1929, Zeits Phys., 56, 751.
- Brodsky, S. J., Pumplin, J., 1969, Phys Rev., 182, 1794.
- Bull, R. M., Nash, W. F., Rastin, B. C., 1965, Nuovo Cim., 40A, 365.
- Caldwell, D. O., Elings, V. B., Hesse, W. P., Sahrn, G. E., Morrison, R. J., Murphy, F. B., Yourt, D. E., 1969, Phys. Rev. Letters, 23, 1256.
- Carlson, J. F., Furry, W. H., 1933, Phys. Rev., 44, 237.
- Cassiday, G. L., 1971, Phys. Rev. D, 3, 1109.
- Cassiday, G. L., 1972, 1973, private communication.
- Chaudhuri, N., Sinha, M. S., 1964, Nuovo Cim., 32, 853.
- Chaudhuri, N., Sinha., M. S., 1965, Nuovo Cim., 35, 13.
- Chin, S., Hanayama, Hara, T., Higashi, S., Kitamura, T., Mono, S., Nakahawa, M., Ozaki, S., Tahahashi, T., Tsuji, K., Watse, Y., Kobayakawa, K., Sibata, H., 1968, Canad. J. Phys., 46, s297.
- Christy, R. F., Kusaka, S., 1941, Phys. Rev., 59, 405.
- Christy, R. F., Kusaka, S., 1941, Phys. Rev., 59, 414.
- Clay, J., 1927, Proc. Roy. Acad. of Amsterdam, 30, 115.
- Cone, A. D., Chen, K. W., Dunning, J. R., Hartwig, G., Ramsey, N. F., Walker, J. K., Wilson, R., 1967, Phys. Rev., 156, 1490.
- Conversi, M., Gozzini, A., 1955, Nuovo Cim., 2, 189.

- Daniels, B., 1974, 1975, private communication.
- Das, A. K., Sinha, M. S., 1967, Proc. Phys. Soc., 92, 110.
- Derry, A. R. F., Neddermeyer, S. H., 1961, Phys. Rev., 121, 1803.
- Diayasu, K., Kobayakawa, K., Murota, T., Nakano, T., 1962, Suppl. J. Phys. Soc. Japan., 17, 344.
- Dietreriche, B. D., Graunstein, T., Cox, J., Martin, F., Toner, W. T., Perl, M. L., Zipf, T. F., Lakin, W. L., Bryant, H. C., 1969, Phys. Rev. Letters, 23, 1187.
- Dietreriche, B. C., Braunstein, T., Cos, J., Martin, F., Toner, W. T., Perl, M. L., Zipf, T. F., Lakin, W. L., Bryant, H. C., 1969, Phys. Rev. Letters, 23, 1191.
- Drell, S. D., Walecka, J. D., 1964, Ann. Phys. (USA), 28, 18.
- Engler, J., Horn, K., Konig, J., Monnig, F., Schludelker, P., Schopper, H., Sievers, P., Ullrich, H., Runge, K., 1968, Phys. Letters, 28B, 64.
- Evans, R. D., 1971, 'The Atomic Nucleus', 625.
- F^{EYNMAN}
Feynman, R. F., 1962, 'The Theory of Fundamental Processes', W. A. Benjamin Inc., New York.
- Fowler, G. N., Crossland, A. D., 1964, Nucl. Phys., 53, 273.
- Furry, W. H., 1937, Phys. Rev., 52, S69.
- Gaebler, J. F., Hazen, W. E., Hendel, A. Z., 1961, Nuovo Cim., 19, 265.
- Gottfried, K., Yennie, D. R., 1969, Phys. Rev., 182, 1595.
- Grupen, C., Hamdan, M. A., Hansen, S., Thompson, M. G., Wolfendale, A. W., Young, E. C. M., 1972, J. Phys. A, 5, 1706.
- Grupen, C., Hamdan, M. A., Hansen, S., Thompson, M. G., Wolfendale, A. W., Young, E. C. M., 1972, J. Phys. A, 5, 1713.
- Grupen, C., 1974, 'Elektromagnetische Wechselwirkungen Hohenenergetischer Hohenstrahl-Muonen', unpublished.
- Hamdan, M. A., Ph.D. Thesis, University of Durham.
- Hand, L. N., 1963, Phys. Rev., 129, 1834.
- Hansen, S., Thompson, M. G., 1975, Proc. XIV Int. Cosmic Ray Conf., 6, 1922.
- Harvey, B. G., 1969, 'Introduction to Nuclear Physics and Chemistry', Prentice-Hall Inc., New Jersey, USA.
- Hayakawa, S., 1969, 'Cosmic Ray Physics', John Wiley and Son, New York.

- Hayman, P. J., Palmer, N. S., Wolfendale, A. W., 1963, Proc. Roy. Soc., 275A, 391.
- Haywood, J. K., Bull, R. M., Nash, W. F., 1970, Acta Physica Academiae Scientiarum Hungaricae, 29, Suppl. 4.
- Hess, V. F., 1912, Phys. Zeits., 13, 1084.
- Higashi, S., Kitamura, T., Mishima, Y., Miyamoto, S., Watsase, Y., Shibata, H., 1965, Nuovo Cim., 38, 107.
- Hume, C. J., 1975, Ph.D. Thesis, University of Durham.
- Ivanenko, I. P., Samosudov, B. E., 1959, Soviet Physics JEPT, 35(8), 5, 884.
- Ivanenko, I. P., Samosudov, B. E., 1967, Bull. Acad. Sci. USSR (Phys. Ser.), 30, 10, 1722.
- Jain, P. L., Wixon, N. J., Phillips, D. A., Felteau, J. T., Phys. Rev. D, 1, 813.
- Johnson, H., Street, J. C., 1933, Phys. Rev., 43, 381.
- Kearney, P. D., Hazen, W. E., 1965, Phys. Rev., 138, B173.
- Kearney, P. D., Binns, W. R., 1972, Nucl. Phys., B43, 402.
- Kelly, G. N., MacKeown, P. K., Said, S. S., Wolfendale, A. W., 1968, Canad. J. Phys., 46, S365.
- Kel'ner, S. R., 1967, Sov. J. Nucl. Phys., 5, 778.
- Kel'ner, S. R., Kotov, Yu. D., 1968, Sov. J. Nucl. Phys., 7, 237.
- Kel'ner, S. R., Kotov, Yu. D., 1968, Canad. J. Phys., 46, S387.
- Kessler, D., Kessler, P., 1956, Nuovo Cim., 4, 601.
- Kirk, T. B. W., Neddermeyer, S. H., 1968, Phys. Rev., 171, 1412.
- Kokoulin, R. P., Petrukhin, A. A., 1970, Acta Physica Academiae Scientiarum Hungaricae, 29, Suppl. 4, 277.
- Kokoulin, R. P., Petrukhin, A. A., 1971, Proc. Int. Conf. on Cosmic Rays, Tasmania, 6, 2436.
- Kotzer, P., Neddermeyer, S. H., 1965, Bull. Amer. Phys. Soc., 10, 80.
- Kotzer, P., Neddermeyer, S. H., 1967, Bull. Amer. Phys. Soc., 12, 1916.
- Landau, L., Lifshitz, E., 1934, Phys. Z. Sowjet., 6, 244.
- Lattes, C. M. G., Muirhead, H., Occhialini, G. P. S., Powell, C. F., 1947, Nature, 159, 694.
- Lewis, G. M., 1973, 'Particle Properties', CERN, 57.

- Matano, T., Nagano, M., Shibata, S., Suga, K., Tanahashi, G., Kameda, T., Tayoda, Y., Hasegawa, H., 1968, Canad. J. Phys., 46, S369.
- McDiarmid, I. B., Wilson, M. D., 1962, Canad. J. Phys., 40, 689.
- Murota, T., Ueda, A., Tanaka, H., 1956, Prog. Theor. Phys. (Kyoto), 16, 482.
- Nagano, M., Hara, T., Kawaguchi, S., Mikamo, S., Suga, K., Tanahashi, G., Matano, M., 1970, INS-Report, Tokyo.
- Nandi, B. C., Sinha, M. S., 1973, Int. Conf. Cosmic Rays, Denver, 3, 2051.
- Ng, L. K., Wdowczyk, J., Wolfendale, A. W., 1973, Proc. Int. Conf. Cosmic Rays, Denver, 3, 1781.
- Nishina, Y., Tomonaga, S., Kobayasi, M., 1935, Sci. PAP Inst. Phys. Chem. Res., Tokyo, 27, 137.
- Osborne, J. L., Palmer, N. S., Wolfendale, A. W., 1964, Proc. Phys. Soc., 84, 911.
- Petrukhin, A. A., Shestakov, V. V., 1966, 'Elementary Particle Physics', Atomizdat, Moscow.
- Petrukhin, A. A., Shestakov, V. V., 1968, Canad. J. Phys., 46, S377.
- Racah, G., 1937, Nuovo Cim., 14, 93.
- Rada, W., 1973, private communication.
- Roe, B. P., Ozaki, S., 1959, Phys. Rev., 116, 1022.
- Rogers, I. W., 1965, Ph.D. Thesis, University of Durham.
- Roll, P. G., Wilkinson, P. T., 1967, Ann. Phys. (USA), 44, 289.
- Rossi, B., 1934, Int. Conf. Nucl. Phys., London.
- Rossi, B., Greisen, K., 1941, Rev. Mod. Phys., 13, 240.
- Rossi, B., 1952, 'High Energy Particles', Prentice-Hall Inc., New York.
- Rossi, B., 1964, 'Cosmic Rays', McGraw-Hill Book Co., New York.
- Rosental', I. L., 1968, Soviet Physics USPEKHI, 11, 49.
- Said, S. S., 1966, Ph.D. Thesis, University of Durham.
- Sakurai, J. J., 1969, Phys. Rev. Letters, 22, 981.
- Scott, W. T., Uhlenbeck, G. E., 1972, Phys. Rev., 62, 497.
- Serre, C., 1967, CERN Report, 67, 5.
- Sheldon, W. R., 1973 (see Grupen 1974).
- Smith, J. A., Duller, N. M., 1959, J. Geophys. Res., 64, 2297.

- Stodolsky, L., 1967, Phys. Rev. Letters, 18, 135.
- Stoker, P. H., Bornman, C. H., Van Der Merwe, J. P., 1962, J. Phys. Soc. Japan, 17AIII, 348.
- Stoker, P. H., Bornman, C. H., Van Der Merwe, J. P., 1963, Nucl. Phys., 45, 505.
- Street, J. C., Woodward, R. H., Stevenson, E. C., 1935, Phys. Rev., 47, 891.
- Street, J. C., Stevenson, E. C., 1937, Phys. Rev., 51, 1005.
- Takahashi, T., Honda, K., Osshima, M., Shibata, H., 1971, Proc. Int. Conf. Cosmic Rays, Hobart, 4, 1463.
- Ternovskii, F. F., 1960, Sov. Phys. JETP, 10, 565 (1959, Zh. Eksp. Teor. Fiz., 37, 793).
- Thompson, M. G., Wells, S. C., 1972, Nucl. Instr. and Meth., 102, 35.
- Weizacker, C. F., 1934, Zeit. f. Phys., 88, 412.
- Wells, S. C., 1972, Ph.D. Thesis, University of Durham.
- Whalley, M. R., 1972, 'Multiparameter Pulse Height Analysis System for M.A.R.S.', unpublished.
- Whalley, M. R., 1974, Ph.D. Thesis, University of Durham.
- Williams, C. J., 1935, Kyl. Vid. Selsk., 13, No. 4.
- Wolfendale, A. W., 1963, 'Cosmic Rays', Birchall and Son Ltd., London.
- Wright, A. G., 1973, J. Phys. A, 6, 79.
- Wright, A. G., 1975, J. Phys. G: Nucl. Phys., 1, 362.
- Yuda, T., Jida, S., Mitsui, K., Mizutani, K., Taira, K., 1971, Proc. Int. Conf. Cosmic Rays, Hobart, 4, 1423.
- Yukawa, H., 1935, Proc. Phys. Math. Soc. Japan, 17, 48.

